JAERI-M
84-092

DATA COMPILATION FOR DEPTH DISTRIBUTION OF ION-INDUCED DAMAGE AND ION-IMPLANTED ATOMS

May 1984

Michitaka TERASAWA*, Sigeo NAKAHIGASHI*
and Kunio OZAWA

日本原子力研究所
Japan Atomic Energy Research Institute

JAERI-M レポートは，日本原子力研究所が不定期に公刊している研究報告書です。

入手の問合わせは，日本原子力研究所技術情報部情報資料課（〒319—11 茨城県那珂郡東海村）あて，お申しこしください。なお，このほかに財団法人原子力弘済会資料センター（〒319—11 茨城県那珂郡東海村日本原子力研究所内）で複写による実費頒布をおこなっております。

JAERI-M reports are issued irregularly.

Inquiries about availability of the reports should be addressed to Information Section, Division of Technical Information, Japan Atomic Energy Research Institute, Tokai-mura, Naka-gun, Ibaraki-ken 319—11, Japan.

編集兼発行　日本原子力研究所
印　　刷　日立高速印刷株式会社

JAERI-M 84-092

DATA COMPILATION FOR DEPTH DISTRIBUTION OF ION-INDUCED DAMAGE AND ION-IMPLANTED ATOMS

Michitaka TERASAWA*, Sigeo NAKAHIGASHI*
and Kunio OZAWA
Department of Physics, Tokai Research Establishment, JAERI

(Received April 23, 1984)

In the recent progress of utilizing ion bombardment technique to ion implantation and neutron irradiation simulation, the experimental data have accumulated concerning the depth distribution of deposited atoms and induced damage along ion incident direction. In the ion-induced damage experiments, the density of point defects or void swelling has been investigated as a function of depth. In this study, the data available until the present time are compiled and compared with theoretical prediction represented by E-DEP-1 computer code.

It is recognized in general that the experimentally observed damage peak is deeper than that E-DEP-1 calculated using the LSS electronic stopping parameter, k_{LSS}. Agreement between the observation and calculation can be obtained using a modified electronic stopping parameter $k = 0.8 - 0.9\ k_{LSS}$. With regard to the deposited atoms by ion bombardment, the peak of the observed distribution is deeper in some cases and shallower in other cases than that calculated by E-DEP-1, indicating that the modified electronic stopping parameter k is oscillating relative to k_{LSS}. This oscillatory behavior is not recognized in the damage distribution. It is suggested that future work should be made to determine the distribution of ion-induced damage in relation to that of the deposited atoms, since the defect evolution may directly be related to the implanted atoms.

Keywords: Fusion Reactor, Damage Ion-Implanation, Void Swelling, Point Defect, Cluster, Neutron Irradiation Simulation, Data Base.

---

* Toshiba Nuclear Engineering Laboratory, Kawasaki.
This report was prepared as an account of work supported partly by a research contract of JAERI with Toshiba Corporation in fiscal year 1982.

JAERI－M 84－092

イオン照射損傷及びイオン注入分布のデータ収集

日本原子力研究所東海研究所物理部
寺澤　倫孝*・中東　重雄*・小沢　国夫

（１９８４年４月２３日受理）

イオン注入及び加速器イオン照射による中性子照射効果のシミュレーションなど固体へのイオン衝撃に関連して，固体中でのイオン飛程及び照射損傷の深さ分布などのデータベースが要求されている。本レポートでは，現在迄公表されたイオン照射損傷（スエリング及び欠陥又はクラスター）の深さ分布及び飛程，ストラグリングの実験データを可能な限り広範囲に収集し，Ｅ－ＤＥＰ－１計算コードによる理論計算との比較を行った。データベースとの比較でＬＳＳ理論の電子阻止能パラメータ k_{LSS} に対する補正係数（0.8～0.9）の議論と評価が行っている。尚Appendix として，ボイドスエリング，点欠陥ととそのクラスター及び注入イオンに関する図表とその文献がリストアップされている。

* 東芝原子力技術研究所

CONTENTS

1. INTRODUCTION 1

2. THEORETICAL CALCULATION BY E-DEP-1 1

3. DEPTH DISTRIBUTION OF VOID SWELLING 7

4. DEPTH DISTRIBUTION OF POINT DEFECTS AND THEIR CLUSTERS 12

5. DEPTH DISTRIBUTION OF IMPLANTED ATOMS 15

6. CONCLUSION 21

APPENDIX 1. EXPERIMENTAL DATA AND LITERATURES CONCERNING VOID SWELLING 24

APPENDIX 2. EXPERIMENTAL DATA AND LITERATURES CONCERNING POINT DEFECTS AND THEIR CLUSTERS 51

APPENDIX 3. EXPERIMENTAL DATA AND LITERACTURES CONCERNING IMPLANTED ATOMS 73

目　　次

1. 序　論 1

2. E－DEP－1コードによる理論計算 1

3. ボイド・スエリングの深さ分布 7

4. 点欠陥及びクラスターの深さ分布 12

5. 注入原子の深さ分布 15

6. 結　論 21

附　録 24

1. ボイド・スエリングの実験データとその文献 24

2. 点欠陥とクラスターの実験データとその文献 51

3. 注入原子の実験データとその文献 73

1. INTRODUCTION

In the recent progress of utilizing ion bombardment technique to ion implantation and neutron irradiation simulation, precise experimental data concerning the depth distribution of implanted atoms and induced displacement damage in solid materials have become to be required. Although there are still very limited works to meet the requirement, the experimental data have been accumulated some extent so far. Several calculation methods based on theoretical model have also been developed. The ion species and target materials investigated in the experimental work range widely and also the incident ion energies range from the energy lower than 10 keV to some 10 MeV. Consequently it seems hard to obtain unified relation between the experimental result and the theoretical calculation.

In this work, the experimental data on the depth variation of ion-induced displacement damage in metals, i.e. void swelling and point defects and their clusters, and the data on ion-implanted atom depth distribution are compiled and compared with theoretical calculation. As for implanted atom distribution, though plenty of the experimental works have been made for these several decades, literatures issued after 1975 are surveyed, intending to collect new experimental data. A computer code called E-DEP-1 is widely used for ion-induced displacement damage calculation. Although Brice code, Winterbon's method or Monte Carlo calculation like TRIM code is also available, the E-DEP-1 is rather simple and easy to use, being usefull for parameter survey and designing experiment. In this study, theoretical calculation by the E-DEP-1 is imployed in order to compare with the experimental data.

2. THEORETICAL CALCULATION BY E-DEP-1

Theoretical calculation for the damage energy distribution was developed and made up to a computer code named E-DEP-1 by Manning and Mueller [1]. This code is the one by which one calculates the depth distribution of the energy dissipated to target atoms through elastic atomic collision when projectile ions are incident on the target. The calculation is based on the approximation of Kulcinski et al, which estimates the energy straggling by relating it to the range straggling. The mean range and range straggling are obtained from the theory of Lindhard et al (LSS)

1. INTRODUCTION

In the recent progress of utilizing ion bombardment technique to ion implantation and neutron irradiation simulation, precise experimental data concerning the depth distribution of implanted atoms and induced displacement damage in solid materials have become to be required. Although there are still very limited works to meet the requirement, the experimental data have been accumulated some extent so far. Several calculation methods based on theoretical model have also been developed. The ion species and target materials investigated in the experimental work range widely and also the incident ion energies range from the energy lower than 10 keV to some 10 MeV. Consequently it seems hard to obtain unified relation between the experimental result and the theoretical calculation.

In this work, the experimental data on the depth variation of ion-induced displacement damage in metals, i.e. void swelling and point defects and their clusters, and the data on ion-implanted atom depth distribution are compiled and compared with theoretical calculation. As for implanted atom distribution, though plenty of the experimental works have been made for these several decades, literatures issued after 1975 are surveyed, intending to collect new experimental data. A computer code called E-DEP-1 is widely used for ion-induced displacement damage calculation. Although Brice code, Winterbon's method or Monte Carlo calculation like TRIM code is also available, the E-DEP-1 is rather simple and easy to use, being usefull for parameter survey and designing experiment. In this study, theoretical calculation by the E-DEP-1 is imployed in order to compare with the experimental data.

2. THEORETICAL CALCULATION BY E-DEP-1

Theoretical calculation for the damage energy distribution was developed and made up to a computer code named E-DEP-1 by Manning and Mueller [1]. This code is the one by which one calculates the depth distribution of the energy dissipated to target atoms through elastic atomic collision when projectile ions are incident on the target. The calculation is based on the approximation of Kulcinski et al, which estimates the energy straggling by relating it to the range straggling. The mean range and range straggling are obtained from the theory of Lindhard et al (LSS)

[2]. The calculation is refined by using the Lindhard partition theory to exclude the energy lost to inelastic processes.

The computer code E-DEP-1, since it is based on the LSS theory, has a restriction in use due to the applicability limitation of the theory. The incident ion beam energy E_B should be lower than E_{LIM}, as shown in eq. (1).

$$E_B \lesssim E_{LIM} \tag{1}$$

$$E_{LIM}(\mathrm{MeV}) = 0.024801\ A_1 Z_1^{4/3}$$

This relation is resulted in considering the validity of the assumption that an electronic stopping power S_e can be represented by eq. (2).

$$S_e = \left(-\frac{d\rho}{d\varepsilon}\right)_e = k_{LSS}\ \varepsilon^{1/2} \tag{2}$$

$$k_{LSS} = \xi_e \frac{0.0793\ Z_1^{1/2} Z_2^{1/2} (A_1+A_2)^{3/2}}{(Z_1^{2/3}+Z_2^{2/3})^{3/4} A_1^{3/2} A_2^{1/2}} \tag{3}$$

$$\xi_e \approx Z_1^{1/6}$$

where, Z_i and A_i (i=1 for incident ion and i=2 for target atom) is atomic number and mass number, respectively. And ε and ρ is dimensionless energy and range, respectively, introduced by Lindhard et al.

In the E-DEP-1 code, one makes the assumption that the primary knock-on atom (PKA) ranges are small. A condition for the validity of this assumption is represented by eq. (4).

$$E_B \gg 0.28 \frac{A_1^{1/2} A_2^{1/2}}{A_1+A_2} E_L \tag{4}$$

$$E_L(\mathrm{keV}) = 0.0307358\ Z_1 Z_2 Z^{1/3} (A_1+A_2)/A_2$$

$$Z = (Z_1^{2/3} + Z_2^{2/3})^{3/2}$$

Fig. 1 shows the energy range where the E-DEP-1 calculation can be applied for various ions incident on Si, Ni, Mo and Au. Solid line indicates the upper energy limit given by eq.(1), showing independence on target materials. Broken lines indicate the lower energy limit given by eq.(4)

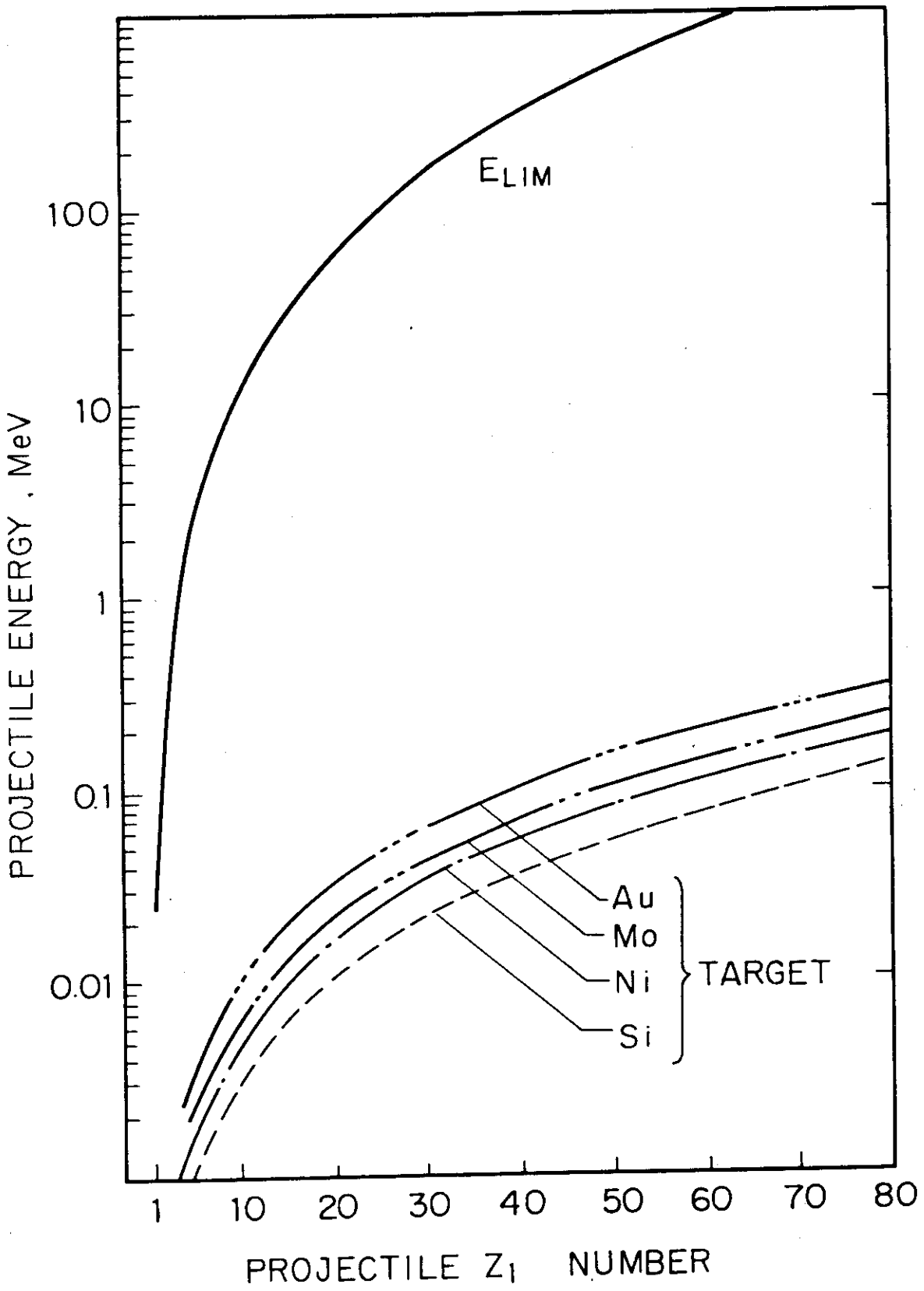

Fig. 1 Upper (solid line) and lower (broken lines) energy limits for projectiles in E-DEP-1 calculation.

for the target materials pointed out. As shown in the figure, there is essentially no high energy limitation to be applied to heavier projectiles, while the limit for light projectiles such as protons and helium ions is in the energies of some 100 keV, above which, because the LSS theory is not relevant, an appropriate correction should be made for the electronic stopping power in the E-DEP-1 calculation. The electronic stopping power extended to higher energies was tabulated by Ziegler or Northcliffe and Schilling by evaluating experimental data [3,4].

In addition, a convenient functional form for the electronic stopping power developed by Brice and the required three parameters tabulated for a number of ion-target combinations [5]. The extended energy region is an intermediate region just below the Bethe-Bloch-Bohr region, where the stopping power has a maximum value and then decreases in proportion to inverse incident energy. Fig. 2 shows electronic stopping power as a function of projectile energy for $Al^{+}\rightarrow Ni$. The LSS theory, Brice calculation, Ziegler's data, and the data by Northcliffe and Schilling are compared in the figure. In the LSS calculation, a modified electronic stopping power S_e' is obtained using modified k as follows:

$$k = \nu\, k_{LSS}\ , \qquad \nu = k/k_{LSS} \tag{5}$$

$$S_e' = k\varepsilon^{1/2} \tag{6}$$

where, k/k_{LSS} $(=\nu)$ = 1.0 is for the original LSS. The LSS-calculated electronic stopping power is higher than the experimental data above the energy around E_{LIM}. It is noted that, even in lower energies, the experimental stopping powers deviate from the LSS (ν=1.0), and the extent of the deviation varies with energy. It is known that the stopping powers show strong quantum oscillations in relation to the electronic shell structure of the projectile and target atoms. The oscillation is not described in the LSS theory. In comparing the experimental data with the E-DEP-1 calculation on depth distribution of induced-damage or implanted atoms in ion bombardment, the influence due to the discrepancy in the stopping power should be considered.

The E-DEP-1 calculation can also be excecuted by modifying it using other electronic stopping power like Brice's three parameter formulation than the LSS.

Fig. 3 shows damage curves calculated for 4 MeV $Ni^{+}\rightarrow Ni$ process by

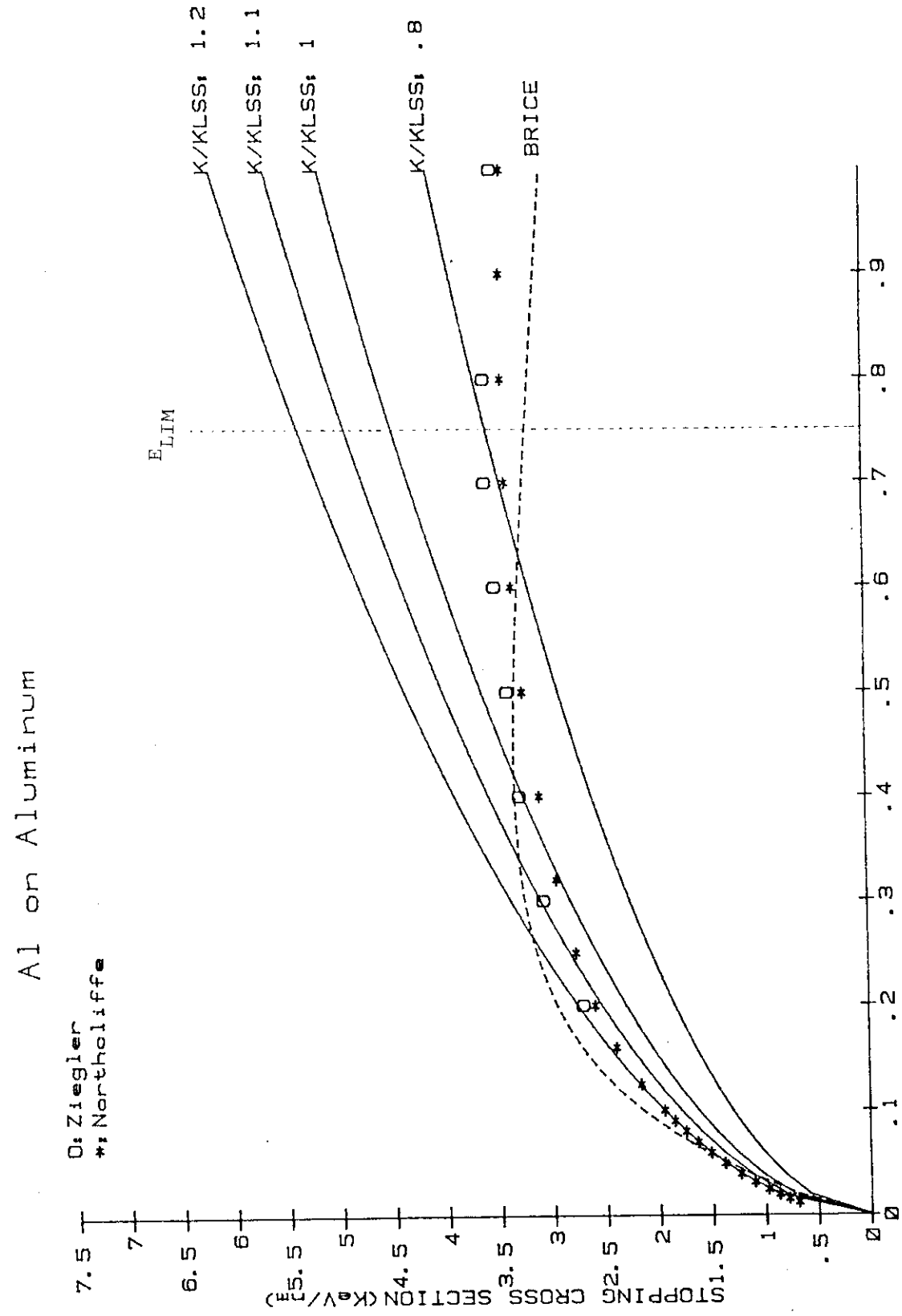

Fig. 2 Electronic stopping power as a function of projectile energy for Al^{+}→Ni.

Ni on Nickel
Incident Energy : 4 MeV

Rp : Projected Range (Micron)
DRp: Standard Deviation
ED : Deposited Energy (MeV)

	E-DEP1	Brice	TRIM
Rp	0.8033	0.9148	0.8512
DRp	0.1157	0.1693	0.1501
ED	0.6926	0.7656	0.5951

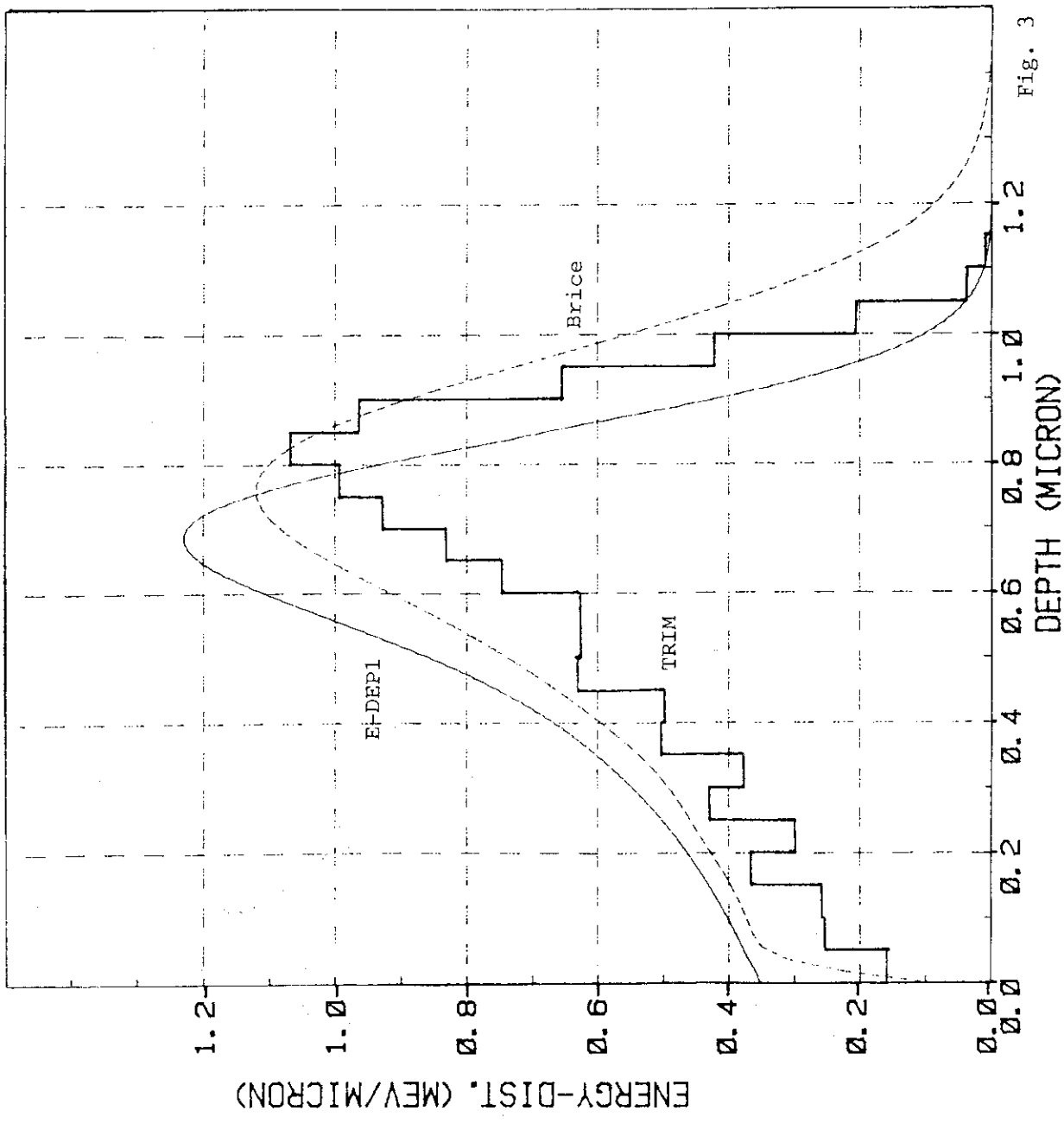

Fig. 3 Damage energy for 4 MeV Ni^{+}→Ni as a function of depth.

E-DEP-1 code, Brice's code and TRIM Monte Carlo program. In the figure, RP means projected range, DRP range straggling, ED total energy dissipated to displacement damage. Peak damage depth obtained by the E-DEP-1 is the shortest, while the peak by TRIM is the deepest. The difference between three calculations seems rather significant.

3. DEPTH DISTRIBUTION OF VOID SWELLING

The experimental studies concerning distribution of void swelling or void number density along projectile incident direction are reviewed. The experimental data of 21 cases (the number of the original papers is 18) are compiled (See Appendix 1). Swelling is an eventual damage phenomena resulted in after diffusion of irradiation-induced point defects under high temperature, and, then, mutual interaction between point defects themselves or interaction between point defects and solutes, dislocations, and precipitates. Although there is a difficulty to compare directly the experimental swelling data with the E-DEP-1 damage curve showing primary displacement damage distribution, the comparison might be valid in elucidating swelling mechanism and supply meaningful informations in designing swelling experiment.

Summaries of the comparison are as follows:

(1) The depth showing swelling maximum (peak depth) tends to be larger than the peak depth in the E-DEP-1 damage curve.

(2) Damaged region width (full width at half maximum in swelling distribution) is generally broader than that predicted by the E-DEP-1 calculation.

(3) Void density distribution shows sometimes better agreement with the E-DEP-1 curve than swelling distribution.

(4) Swelling per deposited energy [%/(MeV/μm)] at near surface is sometimes different from that at around peak depth, implying a surface effect on void formation and growth.

Almost of all swelling experiments have been performed at higher energy than 10 keV/amu, where electronic interaction is dominant energy loss process to decide range and damage depth distribution. The LSS theory, as mentioned above, predicts that electronic stopping power is proportional to a square root of projectile energy, the proportional constant being k_{LSS}. In considering the disagreement between the swelling and the E-DEP-1

E-DEP-1 code, Brice's code and TRIM Monte Carlo program. In the figure, RP means projected range, DRP range straggling, ED total energy dissipated to displacement damage. Peak damage depth obtained by the E-DEP-1 is the shortest, while the peak by TRIM is the deepest. The difference between three calculations seems rather significant.

3. DEPTH DISTRIBUTION OF VOID SWELLING

The experimental studies concerning distribution of void swelling or void number density along projectile incident direction are reviewed. The experimental data of 21 cases (the number of the original papers is 18) are compiled (See Appendix 1). Swelling is an eventual damage phenomena resulted in after diffusion of irradiation-induced point defects under high temperature, and, then, mutual interaction between point defects themselves or interaction between point defects and solutes, dislocations, and precipitates. Although there is a difficulty to compare directly the experimental swelling data with the E-DEP-1 damage curve showing primary displacement damage distribution, the comparison might be valid in elucidating swelling mechanism and supply meaningful informations in designing swelling experiment.

Summaries of the comparison are as follows:

(1) The depth showing swelling maximum (peak depth) tends to be larger than the peak depth in the E-DEP-1 damage curve.

(2) Damaged region width (full width at half maximum in swelling distribution) is generally broader than that predicted by the E-DEP-1 calculation.

(3) Void density distribution shows sometimes better agreement with the E-DEP-1 curve than swelling distribution.

(4) Swelling per deposited energy [%/(MeV/μm)] at near surface is sometimes different from that at around peak depth, implying a surface effect on void formation and growth.

Almost of all swelling experiments have been performed at higher energy than 10 keV/amu, where electronic interaction is dominant energy loss process to decide range and damage depth distribution. The LSS theory, as mentioned above, predicts that electronic stopping power is proportional to a square root of projectile energy, the proportional constant being k_{LSS}. In considering the disagreement between the swelling and the E-DEP-1

damage calculation using k_{LSS}, a modified constant k ($= \nu k_{LSS}$) is selected so that the E-DEP-1 damage peak coincides with the swelling peak. If $\nu < 1$, i.e. $k < k_{LSS}$, the modified stopping power is smaller, and damage peak depth is deeper than the LSS prediction.

Fig. 4 shows the void number density and swelling data in 8.1 MeV $Al^+ \rightarrow Ni$. The damage curves calculated by E-DEP-1 with ν = 0.93 and 1.0 are also shown, indicating that the former agrees well with the experimental data. ν = 0.92 is also obtained in 14 MeV $Ni^+ \rightarrow Ni$, and 19 MeV $Cu^+ \rightarrow Ni$. In the irradiation of austenitic stainless steel with 5 MeV Ni^+, ν = 0.96 for Type 304SS, ν = 0.9 for Type 316SS, and ν = 1.1 for Type 321SS are obtained. In addition, one obtains ν = 0.85 in Type 304SS irradiation with 4 MeV Ni^+, and ν = 1.1 in Type 316SS irradiation with 1.1 MeV N^+, while, in 3.2 MeV $Ni^+ \rightarrow Nb$, the swelling distribution agrees with the LSS (ν = 1.0). Table 1 and Fig. 5 show the value of ν obtained in the best-fit analysis for various combination of projectile and target materials.

Table 1 The value of k/k_{LSS} in void swelling for various projectile-target combination

PROJECTILE	TARGET	k/k_{LSS}	PROJECTILE	TARGET	k/k_{LSS}
8.1 MeV Al^+	Ni	0.93	5 MeV Ni^+	SUS (316)	0.90
18 MeV Ni^+	Ni	0.88	5 MeV Ni^+	SUS (304)	0.96
14 MeV Ni^+	Ni	0.92	5 MeV Ni^+	SUS (321)	1.10
19 MeV Cu^+	Ni	0.92	4 MeV Ni^+	SUS (304)	0.85
0.5 MeV He^+	Ni	0.90	3.5 MeV Ni^+	SUS	1.05
14 MeV Cu^+	Ni	0.89	5 MeV Ni^+	Mo	0.81
5 MeV C^+	Ni	0.93	3.2 MeV Ni^+	Nb	1.00
			1.1 MeV N^+	SUS (316)	1.10

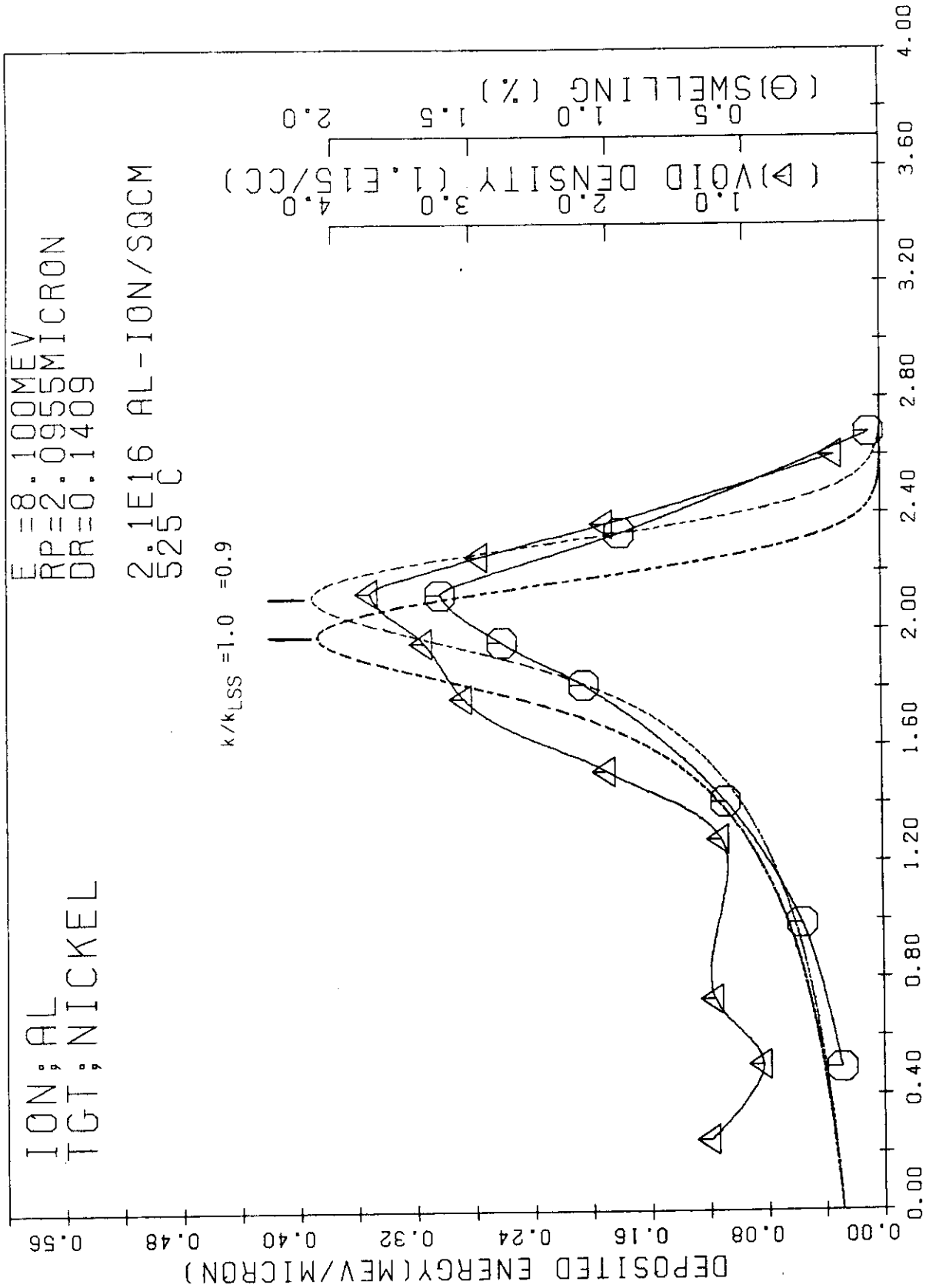

Fig. 4 Void number density and swelling for 8.1 MeV Al^{+}→Ni as a function of depth

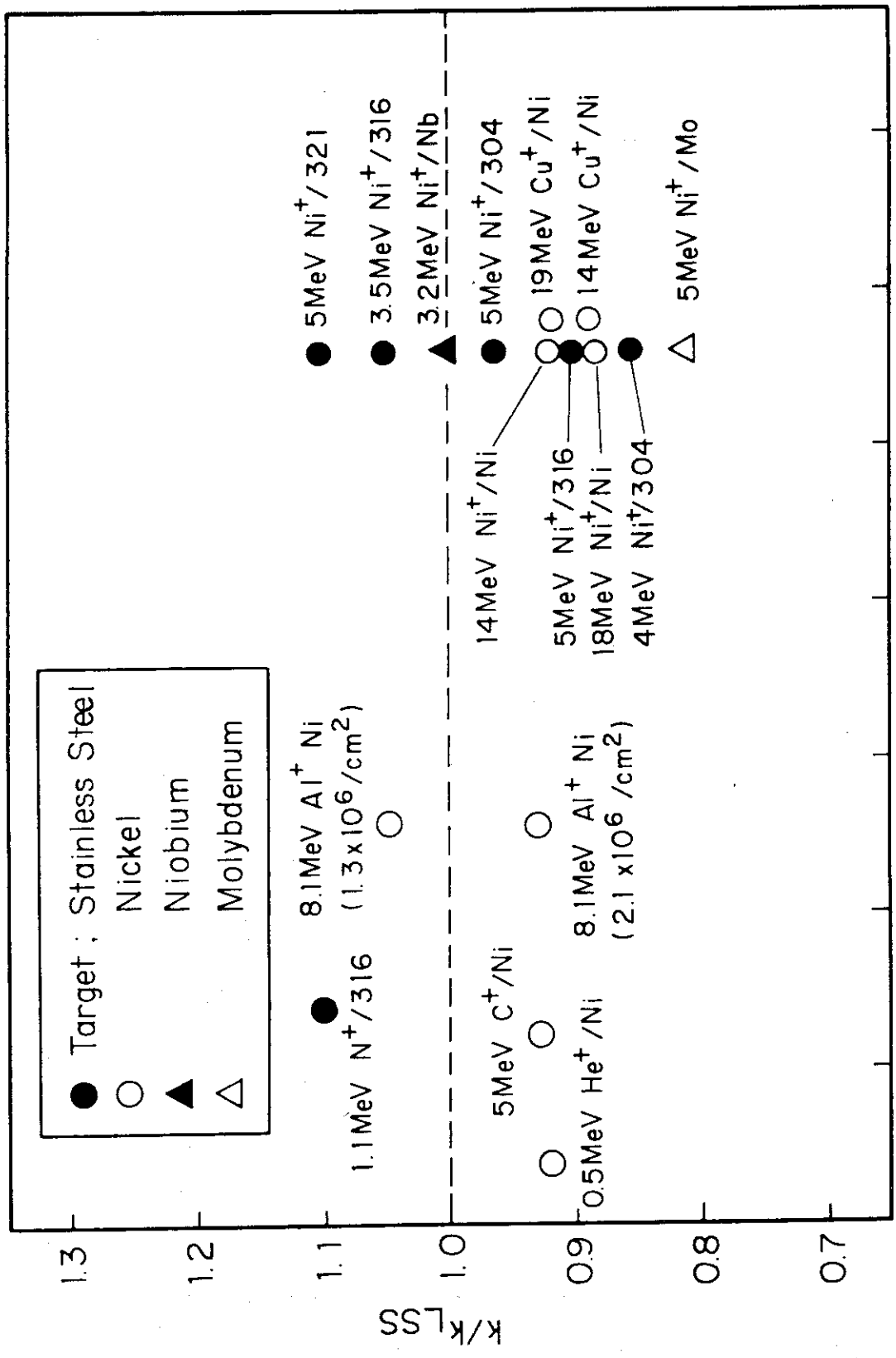

Fig. 5 The value of k/k_{LSS} in void swelling for various projectile-target combination.

Summaries of the analysis are as follows:

(1) In general, k is less than k_{LSS}, i.e. $\nu < 1$. In the cases of Ni target irradiated with the projectiles ranging from Z = 2(He) to 29 (Cu), $\nu = 0.9$ is obtained.

(2) In the irradiation of stainless steel with Ni^+, the values of ν show broad scattering, i.e. $\nu = 0.85 \sim 1.10$.

Although there is a difficulty to evaluate directly electronic stopping power from swelling data, as mentioned preveously, the evidence that ν tends to be less than 1.0 appears even in the point defect distribution, as shown later, suggesting a generic problem in radiation damage study.

It is suggested that, in ion bombardment, the injected interstial atoms deposit around range region in the target materials, and may enhance annihilation of ion-induced defects due to their vacancy trapping and segregation to dislocation networks [6]. There is a possibility that swelling peak may show a shift to surface from the original damage peak due to the reduced void nucleation around range region. The observed data showing $\nu > 1.0$ are considered as examples to show the consequence. However, many experimental data show $\nu \approx 0.9$ and contradict the speculation, being an article to be discussed further.

4. DEPTH DISTRIBUTION OF POINT DEFECTS AND THEIR CLUSTERS

The experimental studies with respect to depth distribution of point defects and their clusters, and disordering and amorphization in single crystal materilas are reviewed. The experimental data of 39 cases (the number of the original papers is 23) are compiled. (See Appendix 2). Since the experiments have been made at lower temperature than room temperature, where primary defect diffusion is substantially limited, one expects meaningful comparison between the experiment and theoretical calculation. Although the data concerning low energy ion implantation are included in the compile, they are only listed in Appendix 2. For low energy region, Brice's or Winterbon's methods would be preferable to calculate depth distribution.

In the comparison between the experimental data and the E-DEP-1 calculation, one obtains summaries as follows:

(1) When projectile ion energy is relatively high, the observed damage depth profile is very similar to the E-DEP-1 calculated damage curve. It is noted, however, that the observed peak is deeper than that calculated.

(2) Width of damaged region is broader than that predicted by the E-DEP-1 calculation, though the difference is not large.

(3) When projectile ions are incident along a low index crystal direction, damage region extends deeper than predicted by E-DEP-1, suggesting the occurrence of ion channeling.

The experimental damage distribution is well understood by the theoretical calculation using the E-DEP-1 code except the peak shift. Modified constant k, as introduced in 3, is chosen so that the E-DEP-1 damage peak coincides with the observed peak. Fig. 6 shows the point defect density data in 4 MeV $Ni^{+}\rightarrow Ni$. The damage curves calculated by E-DEP-1 with $\nu = 0.78$ and 1.0 are also shown, indicating that the former agrees well with the experimental data. Fig. 7 and Table 2 show $\nu = k/k_{LSS}$ obtained in the best-fit analysis for various combination of projectile and target materials.

Summaries of the analysis are as follows:

(1) The E-DEP-1 calculation using $\nu \simeq 0.8$ shows general agreement with the experimental data.

(2) Atomic number oscillation of electronic stopping power or $\nu = k/k_{LSS}$ is not recognized.

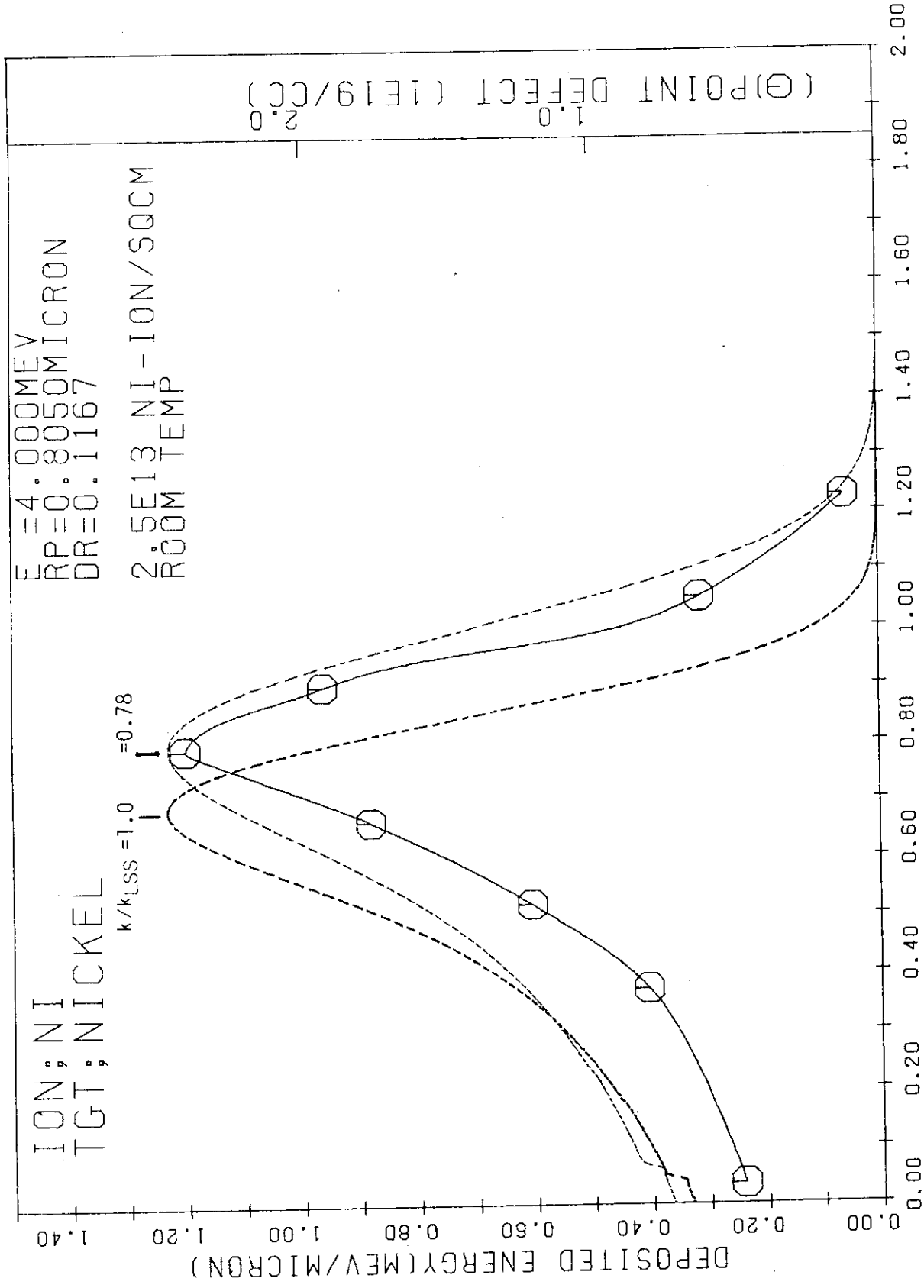

Fig. 6 Point defect density for 4 MeV $Ni^+ \rightarrow Ni$ as a function of depth

Table 2 The value of k/k_{LSS} in point defects and their clusters for various projectile-target combination

PROJECTILE	TARGET	k/k_{LSS}	PROJECTILE	TARGET	k/k_{LSS}
1.0 MeV He^+	Cu	0.84	0.22 MeV Ne^+	Si	0.78
2 MeV N^+	Mo	0.80	0.3 MeV N^+	Si	1.40
4 MeV Ni^+	Ni	0.78	2 MeV Si^+	Si	0.90

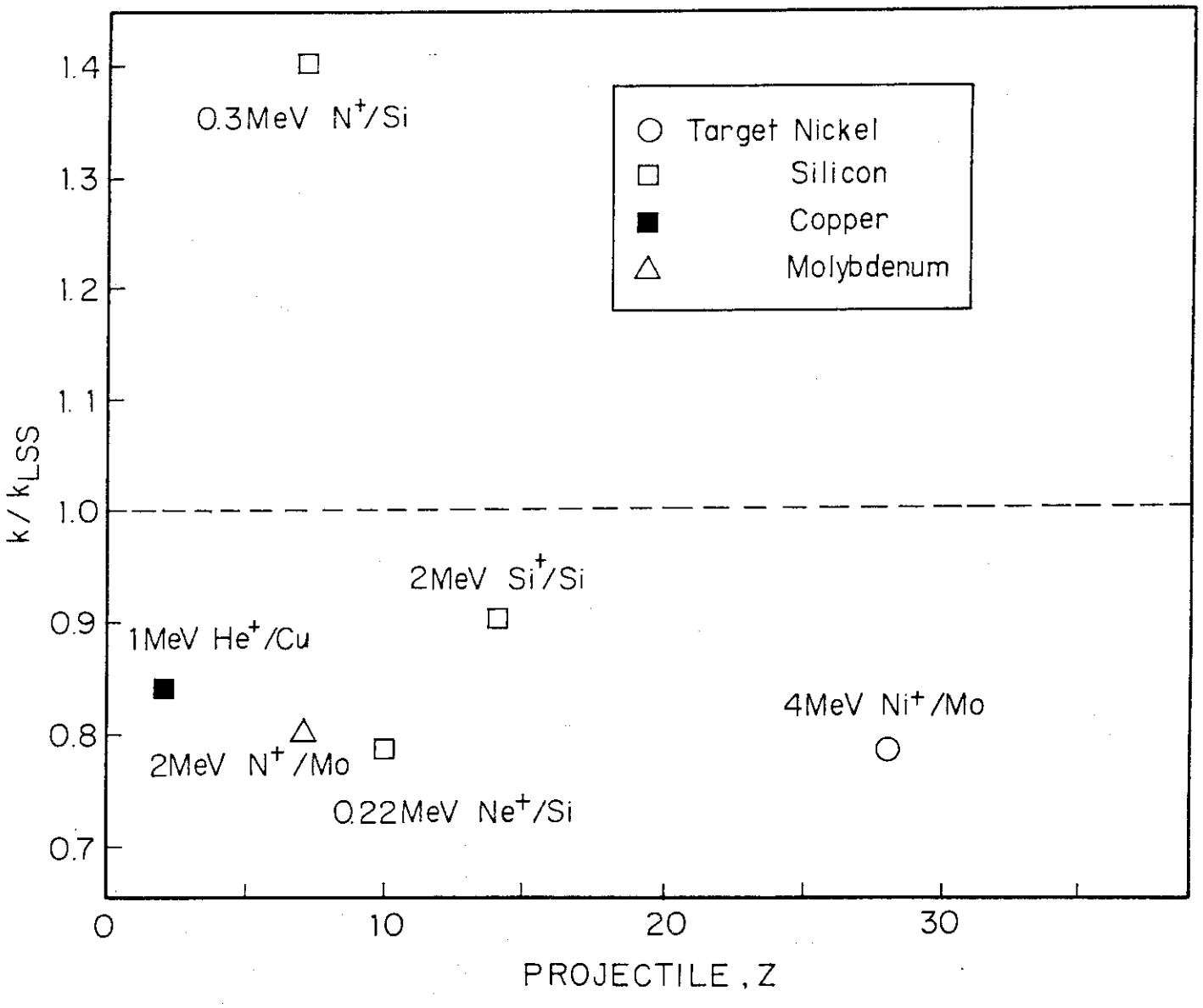

Fig. 7 The value of k/k_{LSS} in point defects and their clusters for various projectile-target combination.

It is noted that the observed damage peak shows systematic displacement against the E-DEP-1 damage peak. Although, as described in 2, the damage peak in Brice's calculation is slightly behind the peak in the E-DEP-1 calculation with $\nu = 1.0$, the peak in the E-DEP-1 with $\nu = 0.8$ is far behind the peak with $\nu = 1.0$. The experimental data agree with the E-DEP-1 calculation using $\nu = 0.8$ for point defects and and their clusters and $\nu = 0.9$ for void density and swelling. This result indicates that the swelling peak appears near to the surface compared to the peak in the primary damage, which may be considered as a consequence of injected interstitial accumulation, mentioned in 3. However, more experimental studies are required in order to obtain more concrete conclusion.

5. DEPTH DISTRIBUTION OF IMPLANTED ATOMS

Distribution of implanted atoms in solid materials in ion implantation is described by projected range R_p or range R and range struggling ΔR. The investigations on the range and stragging have been executed for long from early 1940's. Moreover, recent ion implantation works in semiconductor development have offered a number of experimental data. It is almost impossible to collect all of those data because they are widely distributed. Northcliffe and Schilling (1970) and Ziegler (1980) have already issued the tables of range and stopping power for various projectile-target combinations, generalizing the experimental data [3,4]. Range is considered one of the primary sources causing the discrepancy between the experiment and theoretical calculation on ion-induced damage distribution mentioned in the previous sections. In this work, range and straggling data reported since 1975 are collected. The number of the reports collected are 92, which are mainly issued from 1977 to 1981. Almost of those, however, are concerned with ion implantation of semi-conductor, in which projectile energy is usually low. A few works have been performed at energies $\varepsilon > 1.0$, where many ion irradiation works have been carried out and electronic stopping power is a principal factor to determine projectile range and damage depth. The latter high energy data will be considered in this section. At energies $\varepsilon \lesssim 1.0$, where nuclear stopping is main process of the energy loss, it is known that the range is higher than predicted by the LSS theory [7]. Moreover, at Bethe-Bloch-Bohr energy region ($\varepsilon \gtrsim 10^3$), electronic stopping is not described by the simple LSS theory, as mentioned previously.

It is noted that the observed damage peak shows systematic displacement against the E-DEP-1 damage peak. Although, as described in 2, the damage peak in Brice's calculation is slightly behind the peak in the E-DEP-1 calculation with $\nu = 1.0$, the peak in the E-DEP-1 with $\nu = 0.8$ is far behind the peak with $\nu = 1.0$. The experimental data agree with the E-DEP-1 calculation using $\nu = 0.8$ for point defects and and their clusters and $\nu = 0.9$ for void density and swelling. This result indicates that the swelling peak appears near to the surface compared to the peak in the primary damage, which may be considered as a consequence of injected interstitial accumulation, mentioned in 3. However, more experimental studies are required in order to obtain more concrete conclusion.

5. DEPTH DISTRIBUTION OF IMPLANTED ATOMS

Distribution of implanted atoms in solid materials in ion implantation is described by projected range R_p or range R and range struggling ΔR. The investigations on the range and stragging have been executed for long from early 1940's. Moreover, recent ion implantation works in semiconductor development have offered a number of experimental data. It is almost impossible to collect all of those data because they are widely distributed. Northcliffe and Schilling (1970) and Ziegler (1980) have already issued the tables of range and stopping power for various projectile-target combinations, generalizing the experimental data [3,4]. Range is considered one of the primary sources causing the discrepancy between the experiment and theoretical calculation on ion-induced damage distribution mentioned in the previous sections. In this work, range and straggling data reported since 1975 are collected. The number of the reports collected are 92, which are mainly issued from 1977 to 1981. Almost of those, however, are concerned with ion implantation of semi-conductor, in which projectile energy is usually low. A few works have been performed at energies $\varepsilon > 1.0$, where many ion irradiation works have been carried out and electronic stopping power is a principal factor to determine projectile range and damage depth. The latter high energy data will be considered in this section. At energies $\varepsilon \lesssim 1.0$, where nuclear stopping is main process of the energy loss, it is known that the range is higher than predicted by the LSS theory [7]. Moreover, at Bethe-Bloch-Bohr energy region ($\varepsilon \gtrsim 10^3$), electronic stopping is not described by the simple LSS theory, as mentioned previously.

The experimental range data are compiled for 46 projectile ion-target combinations. (See Fig. RA-1 to Fig. RA-6 in Appendix 3). They show general agreement with LSS calculation ($\nu = 1.0$). In Fig. 8, the ratio of the observed R_p to that predicted by LSS is shown as a function of ε for $X^+ \rightarrow Ta$ and $^{15}N^+ \rightarrow Y$, where X and Y mean various elements as shown in the figure. The ratio to the theoretical calculation by Monte Carlo method are also shown as a reference. At energies $\varepsilon \gtrsim 3$, the ratio is almost unity, indicating good agreement between the experiment and theory. With decreasing energy the ratio tends to increase apart from unity. It is noted that the Monte Carlo calculated ranges are closer to the observed ones than the LSS calculated ones especially at low energies.

The observed range data are more carefully compared with the LSS calculation, examples of which are shown for $^3He^+ \rightarrow Cu$ and $N^+ \rightarrow Be$ in Fig. 9 and Fig. 10, respectively. The LSS calculation is performed for various ν ranging from 0.75 to 1.25 ($\nu = 1.0$ is for the original LSS theory). It is suggested that the ν value chosen so as to fit the observed data varies significantly depending on ion-target combination, while it varies slightly with ion energy. The same comparisons are made for other various ion-target combinations. (See Fig. RB-1 to Fig. RB-46 in Appendix 3) Fig. 11 shows ν ($= k/k_{LSS}$) thus obtained for $^3He^+$, $^{15}N^+$, and Xe^+ projectiles as a function of target atomic number Z_2. There are some data showing the ν values significantly higher or lower than unity. It is seen, though the number of the data compiled is not much, that ν varies periodically against Z_2, suggesting the increase of ν around innert atoms. Fig. 12 shows ν for Be and C targets as a function of projectile atomic number Z_1, indicating again that ν varies periodically against Z_1. The atomic number periodic oscillation, which has been previously recognized in electronic stopping power, is confirmed to be observable in these range data.

As a result of the comparison of the observed range data with the LSS calculation, one obtains summaries as follows:

(1) The observed R_p shows agreement with the LSS calculated one in the energies $\varepsilon \gtrsim 3$, while the former tends to be higher than the latter in the energies $\varepsilon < 1$.

(2) The ν value varies periodically against Z_1 and Z_2.

In relation to the projected range, the straggling showing the spatial distribution of the implanted atoms is also an important physical parameter. The experimental investigations on the straggling are scarce. Moreover,

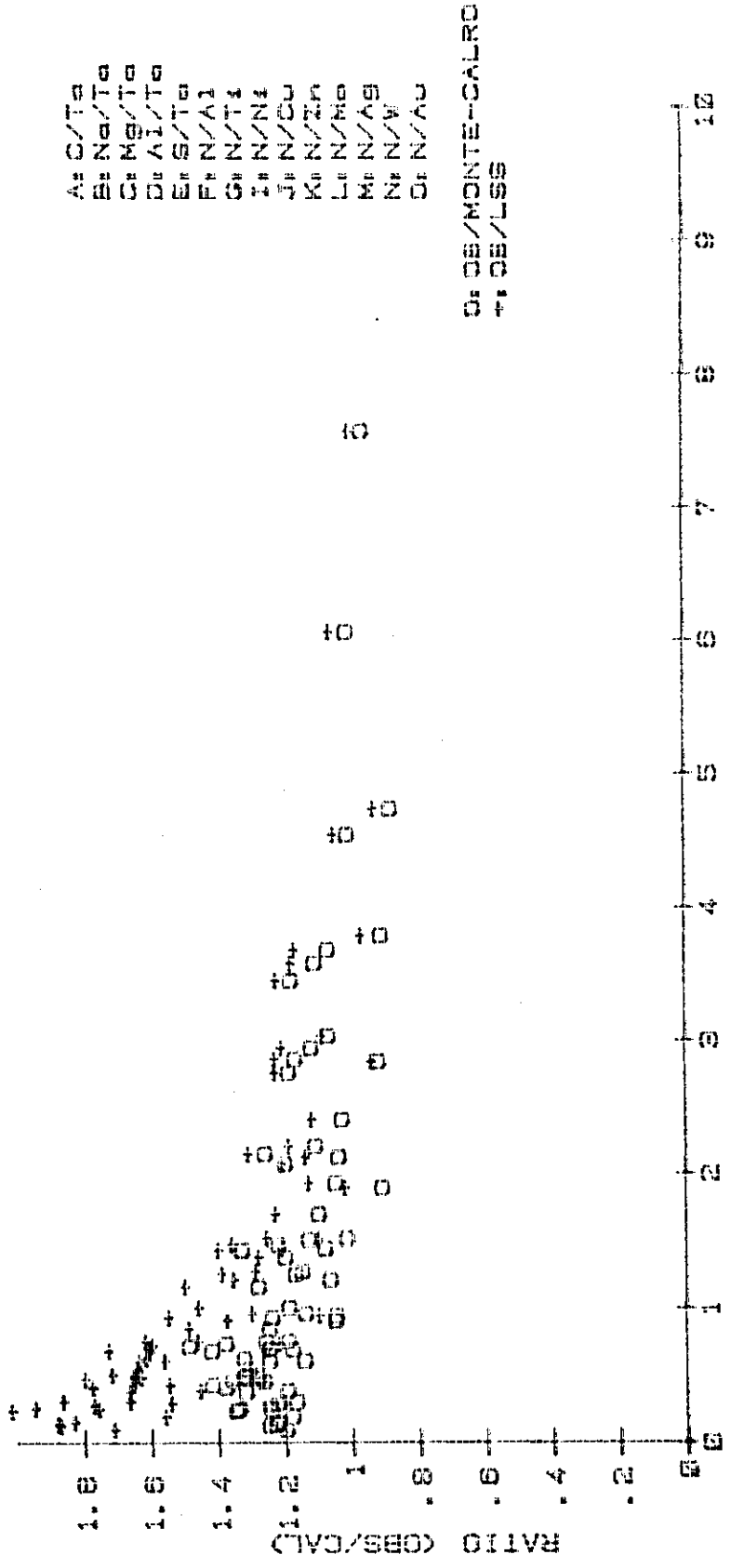

Fig. 8 Observed range relative to theoretical range as a function of dimensionless energy (From Ref. 7).

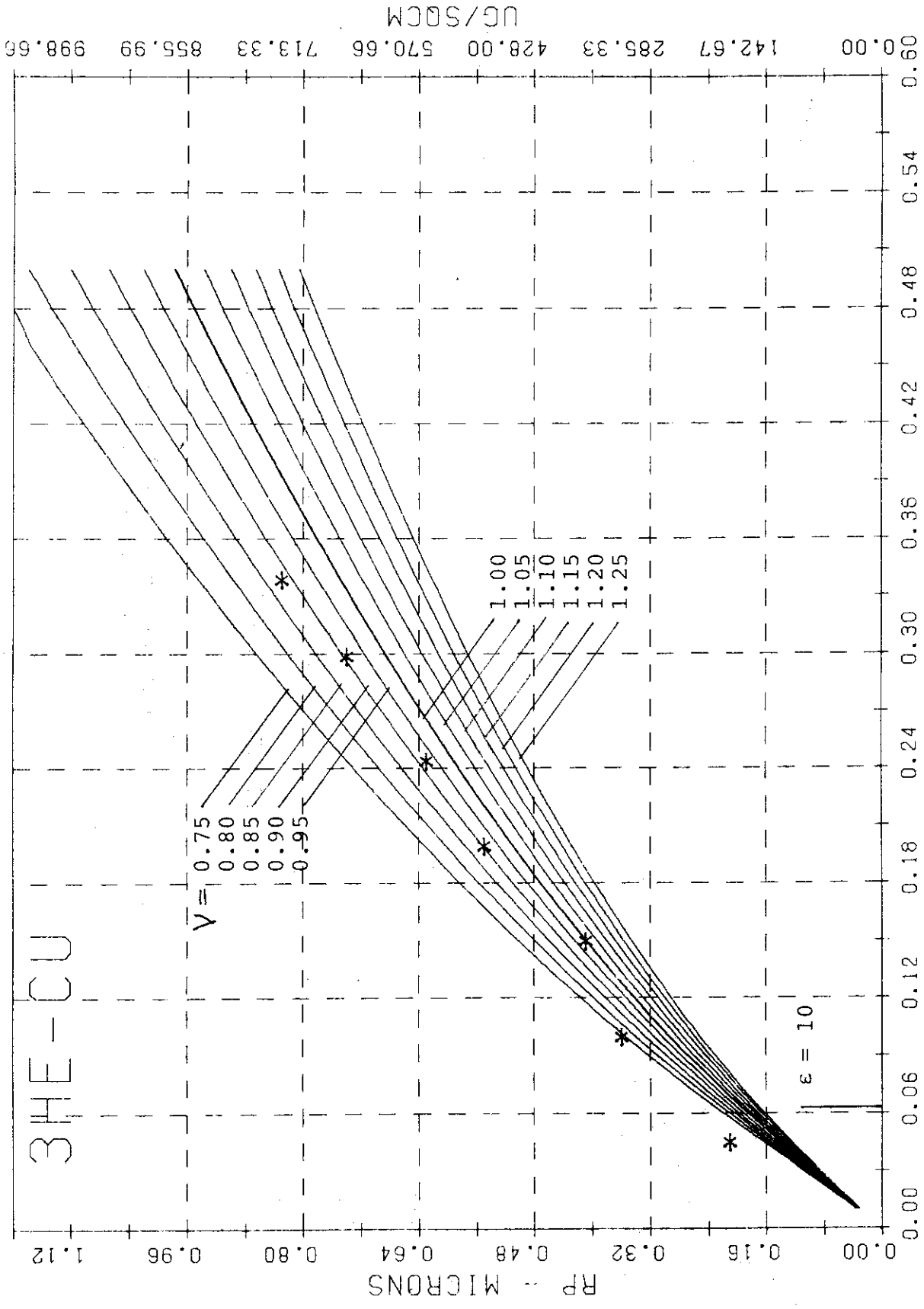

Fig. 9 Range for $^{3}He \rightarrow Cu$ as a function of incident energy.

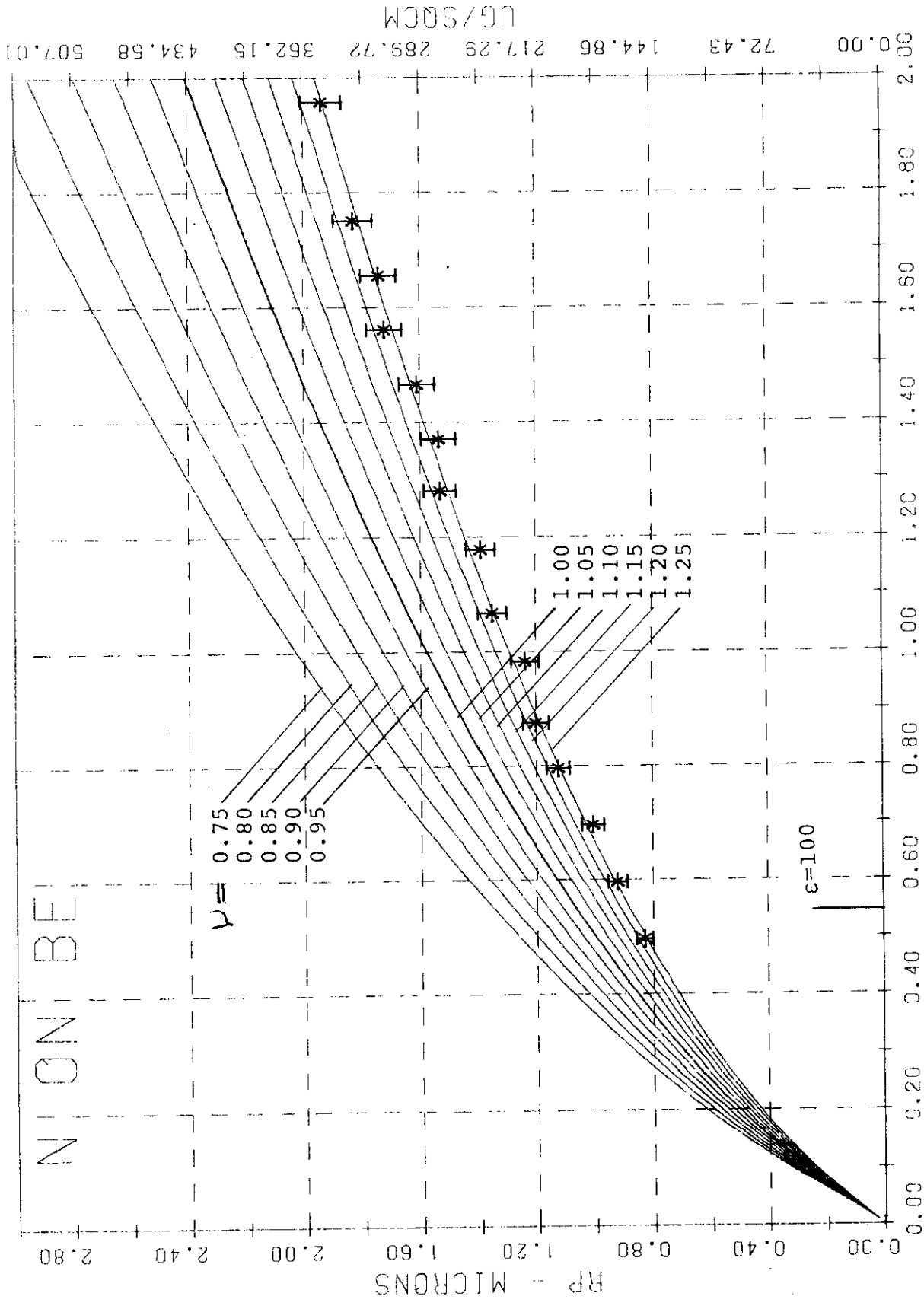

Fig. 10 Range for N^{+}→Be as a function of incident energy.

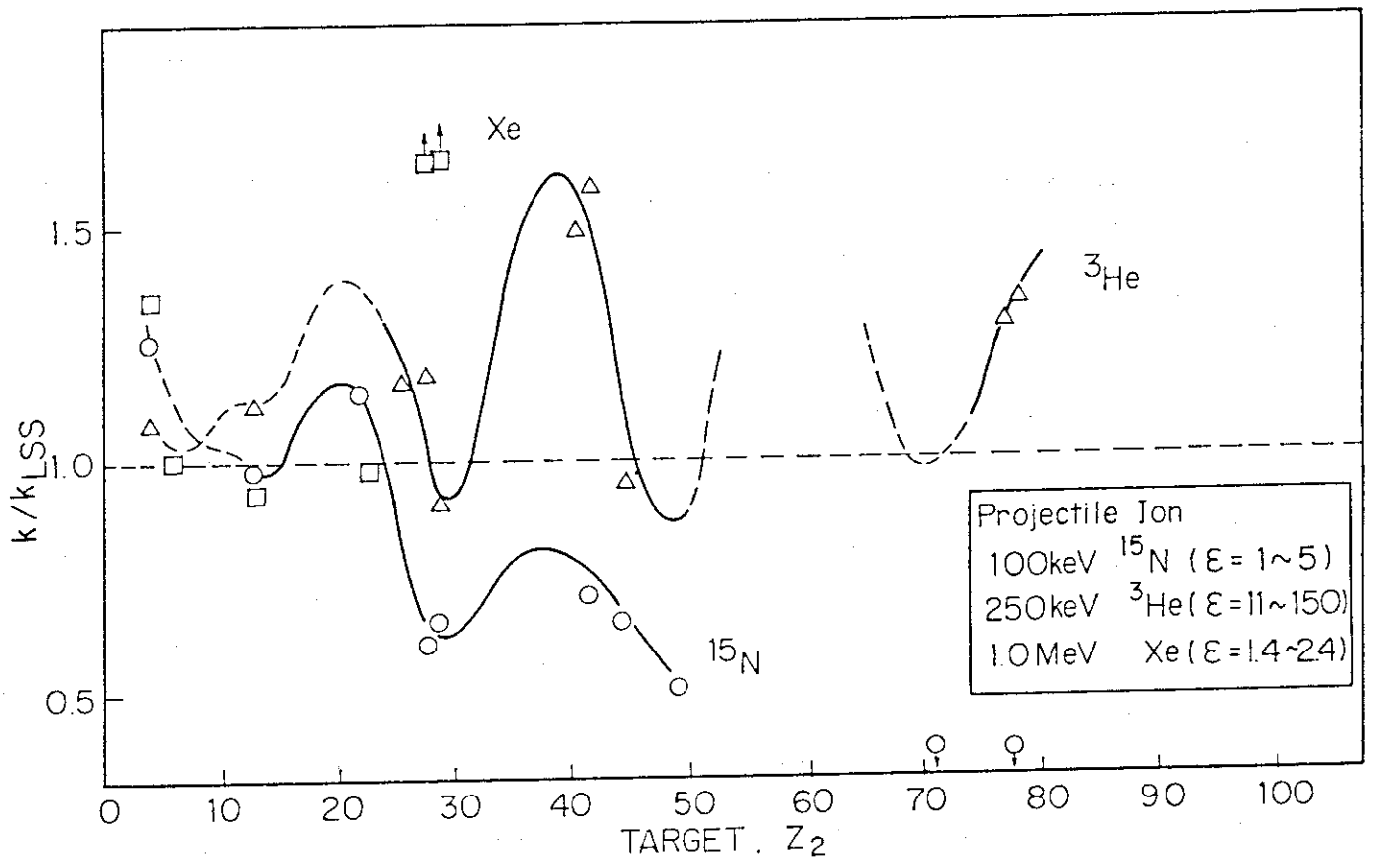

Fig. 11 The value of k/k_{LSS} in projected range as a function of target atomic number.

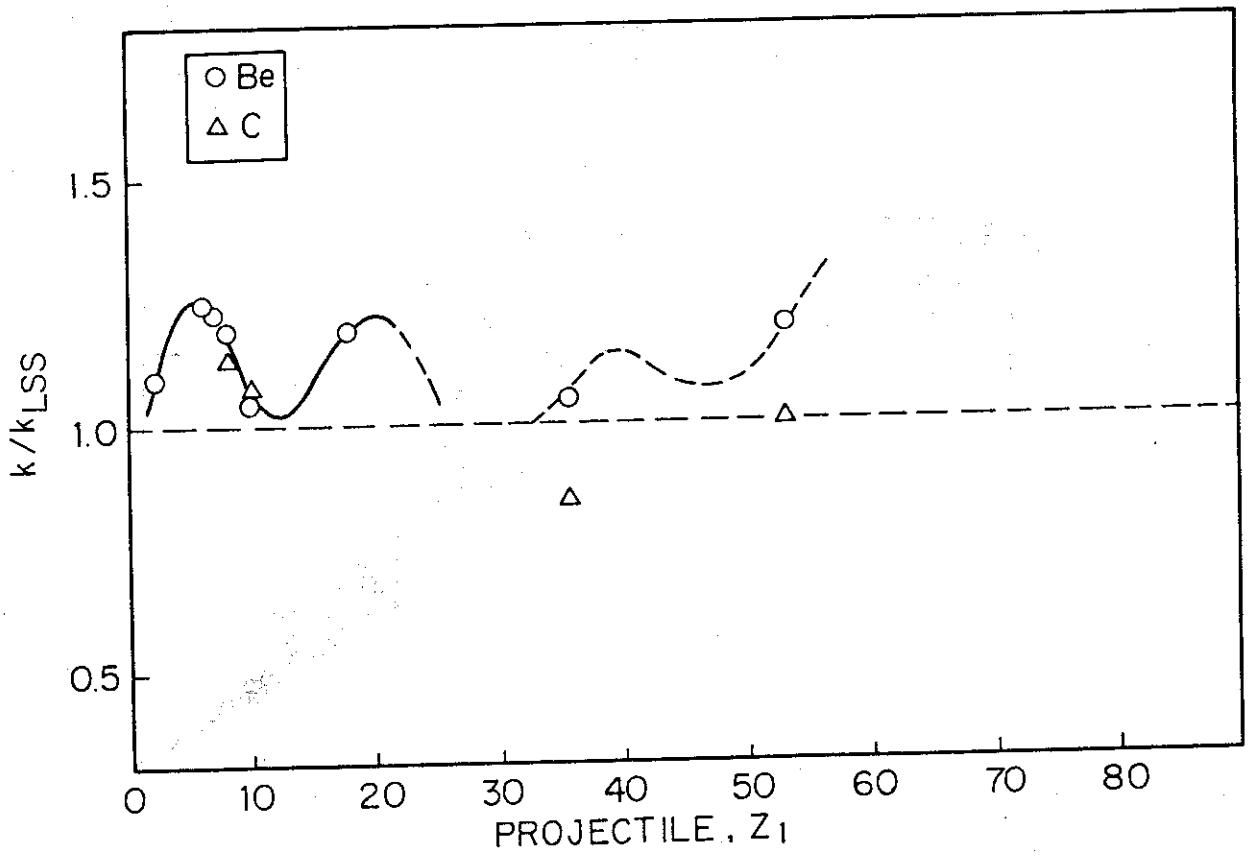

Fig. 12 The value of k/k_{LSS} in projected range as a function of projectile atomic number.

the straggling data show broad scattering. (See Fig. WA-1 to Fig. WA-4 in Appendix 3) Fig. 13 shows the relative range straggling as a function of the projectile energy. In addition to the observed data, the LSS calculations are shown taking ν as a parameter. Although the calculation seems to show general trend of the straggling, there is a difficulty in educing a definite conclusion due to the broad data scattering. Fig. 14 is another example showing the range straggling comparison between the observed data and the LSS theory in energies $\varepsilon \gtrsim 1.0$, showing that agreement is good in high energies, while discrepancy appears and increases with decrease in energy. Further development in the theory is required.

6. CONCLUSION

The experimental data with respect to the depth distribution of void, swelling, and point defects and their clusters induced by ion bombardment, and the projected range and straggling of ion-implanted atoms have been accumulated recently. In this work, the data are collected and compared with the LSS theoretical calculation using the E-DEP-1 computer code.

It is recognized in general that the experimentally observed damage peak is deeper than that E-DEP-1 calculated using the LSS electronic stopping parameter, k_{LSS}. Agreement between the observation and calculation can be obtained using a modified electronic stopping parameter $k = 0.8 - 0.9\ k_{LSS}$. With regard to the deposited atoms by ion bombardment, the peak of the observed distribution is deeper in some cases and shallower in other cases than that calculated by E-DEP-1, indicating that the modified electronic stopping parameter k is oscillating relative to k_{LSS}. This oscillatory behavior is not recognized in the damage distribution. It is suggested that future work should be made to determine the distribution of ion-induced damage in relation to that of the deposited atoms, since the defect evolution may directly be related to the implanted atoms.

the straggling data show broad scattering. (See Fig. WA-1 to Fig. WA-4 in Appendix 3) Fig. 13 shows the relative range straggling as a function of the projectile energy. In addition to the observed data, the LSS calculations are shown taking ν as a parameter. Although the calculation seems to show general trend of the straggling, there is a difficulty in educing a definite conclusion due to the broad data scattering. Fig. 14 is another example showing the range straggling comparison between the observed data and the LSS theory in energies $\varepsilon \gtrsim 1.0$, showing that agreement is good in high energies, while discrepancy appears and increases with decrease in energy. Further development in the theory is required.

6. CONCLUSION

The experimental data with respect to the depth distribution of void, swelling, and point defects and their clusters induced by ion bombardment, and the projected range and straggling of ion-implanted atoms have been accumulated recently. In this work, the data are collected and compared with the LSS theoretical calculation using the E-DEP-1 computer code.

It is recognized in general that the experimentally observed damage peak is deeper than that E-DEP-1 calculated using the LSS electronic stopping parameter, k_{LSS}. Agreement between the observation and calculation can be obtained using a modified electronic stopping parameter $k = 0.8 - 0.9\ k_{LSS}$. With regard to the deposited atoms by ion bombardment, the peak of the observed distribution is deeper in some cases and shallower in other cases than that calculated by E-DEP-1, indicating that the modified electronic stopping parameter k is oscillating relative to k_{LSS}. This oscillatory behavior is not recognized in the damage distribution. It is suggested that future work should be made to determine the distribution of ion-induced damage in relation to that of the deposited atoms, since the defect evolution may directly be related to the implanted atoms.

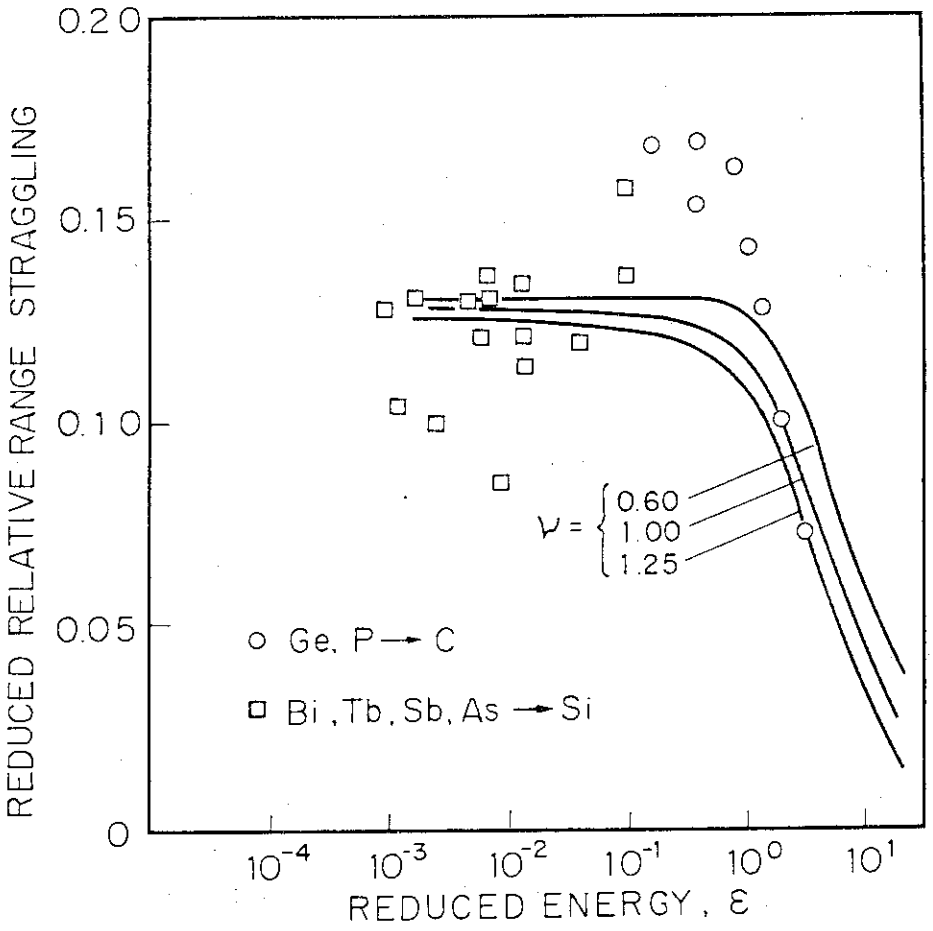

Fig. 13 Range straggling as a function of projectile energy.

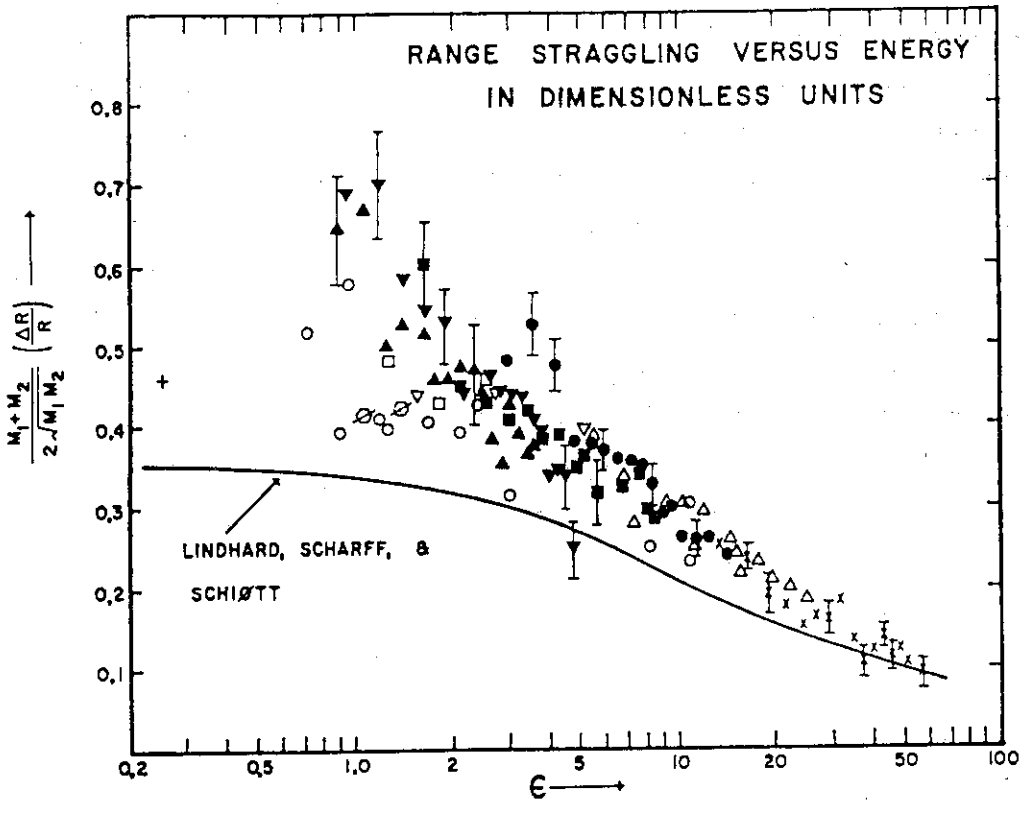

Fig. 14 Range straggling as a function of projectile energy in energies $\varepsilon \gtrsim 1.0$.
(Fron Ref. 5-91, Appendix 3)

References

1. J. Lindhard, M. Scharff and H.E. Schiøtt, Danske Videnskab. Selskab 33 No.14 (1963).
2. G.L. Kulcinski, J.J. Laidler and D.G. Doran, Radiation Effects 7 (1971) 195.
3. I. Manning and G.P. Mueller, Computer Physics Communication 7 (1974) 85-94.
4. J. Lindhard, V. Nielsen M. Scharff and P.L. Thompson, Danske Vindenskab. Selskab 33, No.10 (1963).
5. D.K. Brice, Ion Implantation Range and Energy Deposition Distributions, Vol.1 (Plenum, New York, 1975).
6. L.K. Mansur and M.H. Yoo, J. Nucl. Mater, 85 & 86 (1979) 523-532.
7. M. Luomajarvi, J. Kfinonen, M. Bister and A. Anttila, Phys. Rev. B 18 (1978) 4657.

APPENDIX 1. EXPERIMENTAL DATA AND LITERATURES CONCERNING VOID SWELLING

Table SA-1 is a list of projectile-target combinations which void swelling data are compiled. The experimental data on the void density and swelling as a function of depth are reproduced in the figures from Fig. SA-1 to Fig. SA-23. The dashed line in the figures shows damage curve calculated by the E-DEP-1 code with $k=k_{LSS}$. In the last part in this Appendix, all the literatures collected are listed.

Table SA-1

Ion	Target	Energy	Reference	Figure
Al	Nickel	8.1MeV	3-2	SA-1
Al	Nickel	8.1MeV	3-2	SA-2
Ni	Nickel	18MeV	3-1	SA-3
Ni	Nickel	14MeV	3-8	SA-4
Cu	Nickel	19MeV	3-8	SA-5
Cu	Nickel	14MeV	3-8	SA-6
C	Nickel	5MeV	3-2	SA-7
He	Nickel	500KeV	3-5,6,7	SA-8
Ni	Stainless Steel	5MeV	3-1	SA-9
Ni	Stainless Steel	5MeV	3-13	SA-10
Ni	Stainless Steel	5MeV	3-1	SA-11
Ni	Stainless Steel	4MeV	3-1	SA-12
Ni	Stainless Steel	3.5MeV	3-3	SA-13
Ni	Stainless Steel	5MeV	3-13	SA-14
Ni	Stainless Steel	4MeV	3-10	SA-15
Ni	Stainless Steel	4MeV	3-10	SA-16
Ni	Niobium	3.2MeV	3-4	SA-17
Ni	Molybdenum	5MeV	3-15,16	SA-18
Al	Aluminum	100KeV	3-12	SA-19
N	Stainless Steel	1.1MeV	3-17	SA-20, 21
C	Stainless Steel	1.0MeV	3-18	SA-22, 23

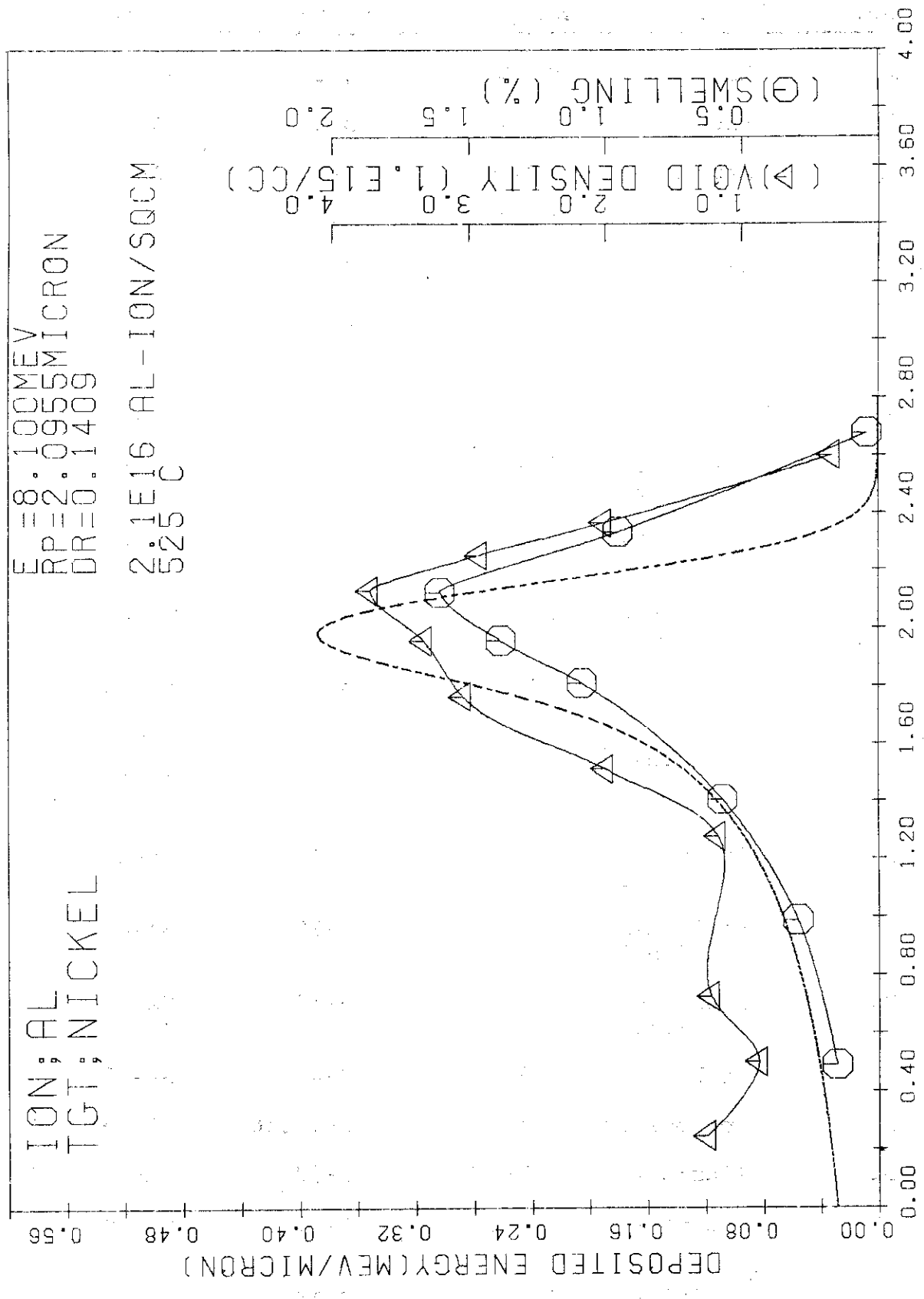
ION:AL
TGT:NICKEL
E=8.100MEV
RP=2.0955MICRON
DR=0.1409
2.1E16 AL-ION/SQCM
525 C
DEPOSITED ENERGY(MEV/MICRON)
DEPTH (MICRON)
(%) SWELLING (Δ)
(1.E15/CC) VOID DENSITY (▷)

Fig. SA-1

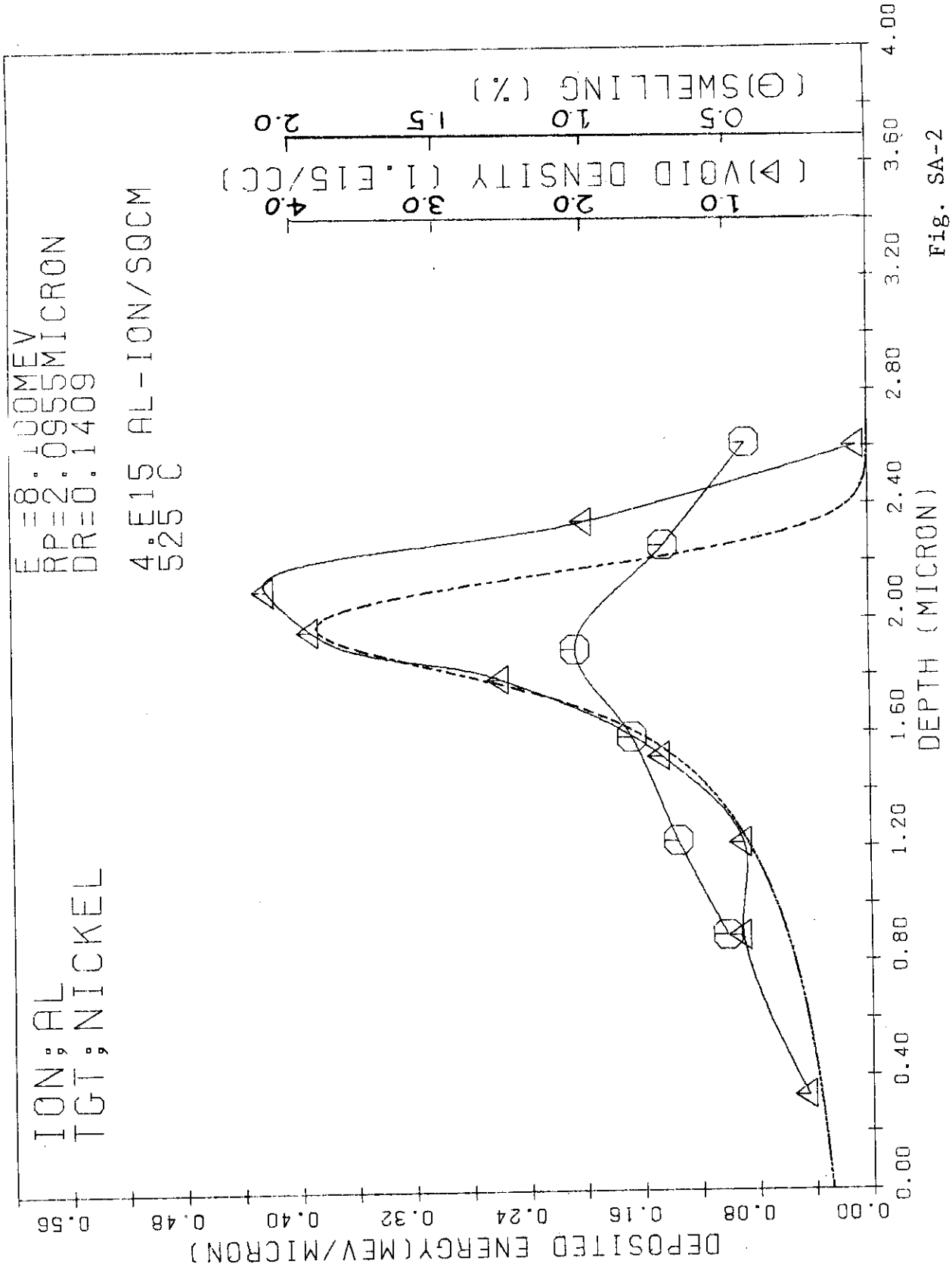
ION : AL
TGT : NICKEL
E=8.400MEV
RP=2.0959MICRON
DR=0.1409
4.E15 AL-ION/SQCM
525 C
DEPOSITED ENERGY(MEV/MICRON)
DEPTH (MICRON)
(▷)VOID DENSITY (1.E15/CC)
(⊖)SWELLING (%)

Fig. SA-2

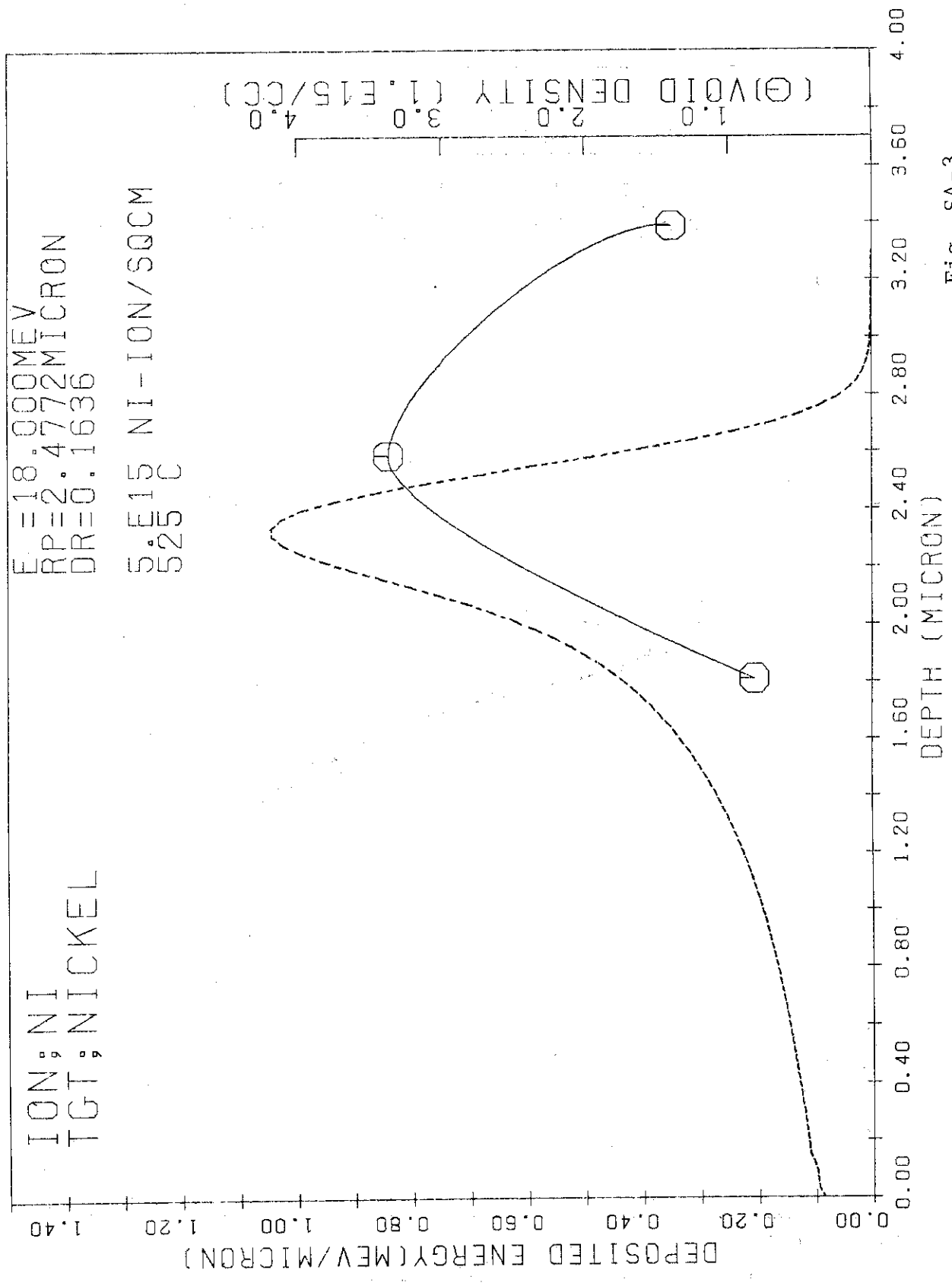
ION: NI
TGT: NICKEL
E=18.000MEV
RP=2.4772MICRON
DR=0.1636
5.E15 NI-ION/SQCM
525 C
DEPOSITED ENERGY(MEV/MICRON)
DEPTH (MICRON)
(Θ)VOID DENSITY (1.E15/CC)

Fig. SA-3

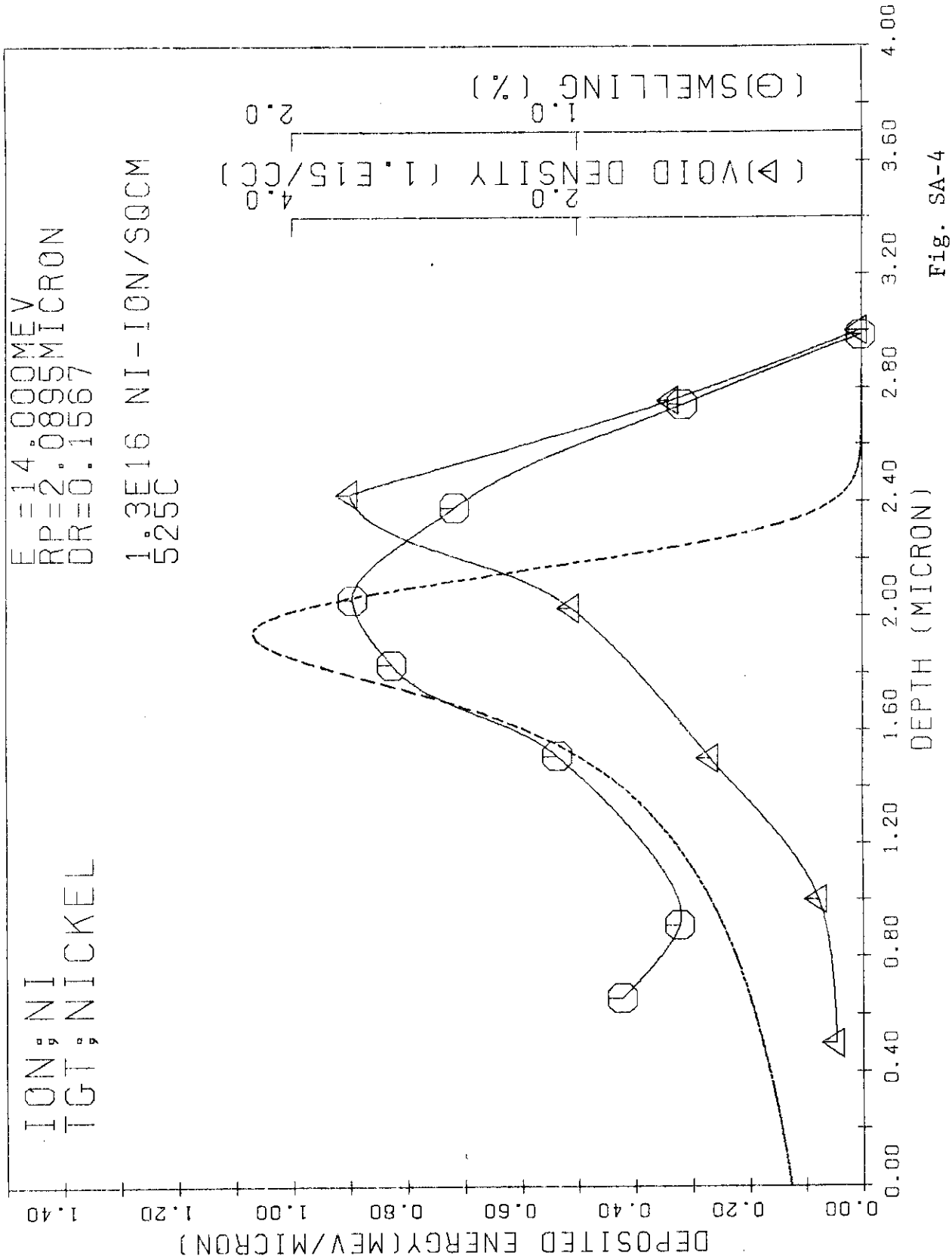
ION=NI
TGT=NICKEL
E=14.000MEV
RP=2.08957
DR=0.1567
1.3E16 NI-ION/SQCM
525C
(▽)VOID DENSITY (1.E15/CC)
(○)SWELLING (%)
DEPTH (MICRON)
DEPOSITED ENERGY(MEV/MICRON)

Fig. SA-4

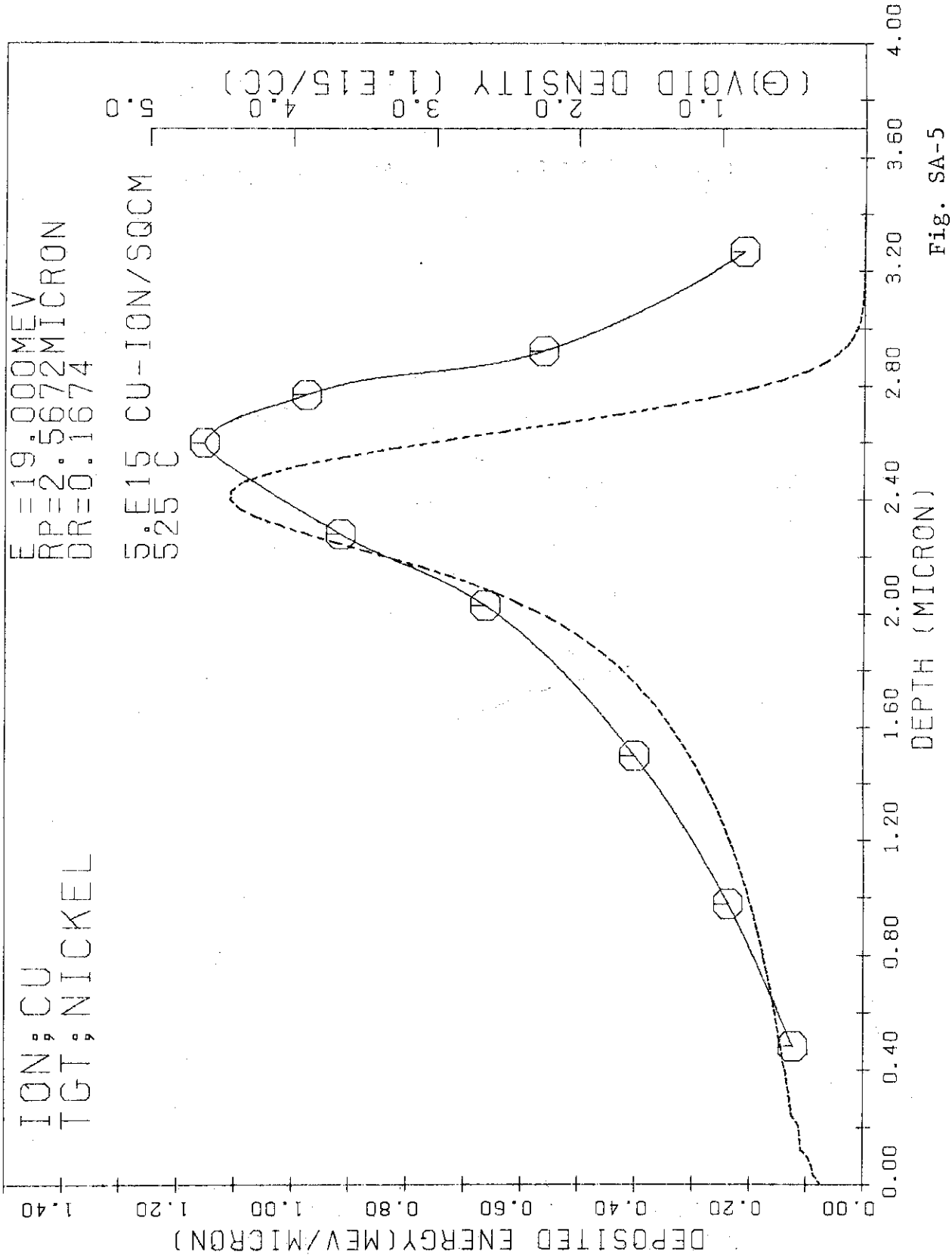
ION=CU
TGT=NICKEL
E=19.000MEV
RP=2.5672MICRON
DR=0.1674
5.E15 CU-ION/SQCM
525 C
DEPOSITED ENERGY(MEV/MICRON)
(Θ)VOID DENSITY (1.E15/CC)
DEPTH (MICRON)
0.00
0.20
0.40
0.60
0.80
1.00
1.20
1.40
1.0
2.0
3.0
4.0
5.0
0.00
0.40
0.80
1.20
1.60
2.00
2.40
2.80
3.20
3.60
4.00

Fig. SA-5

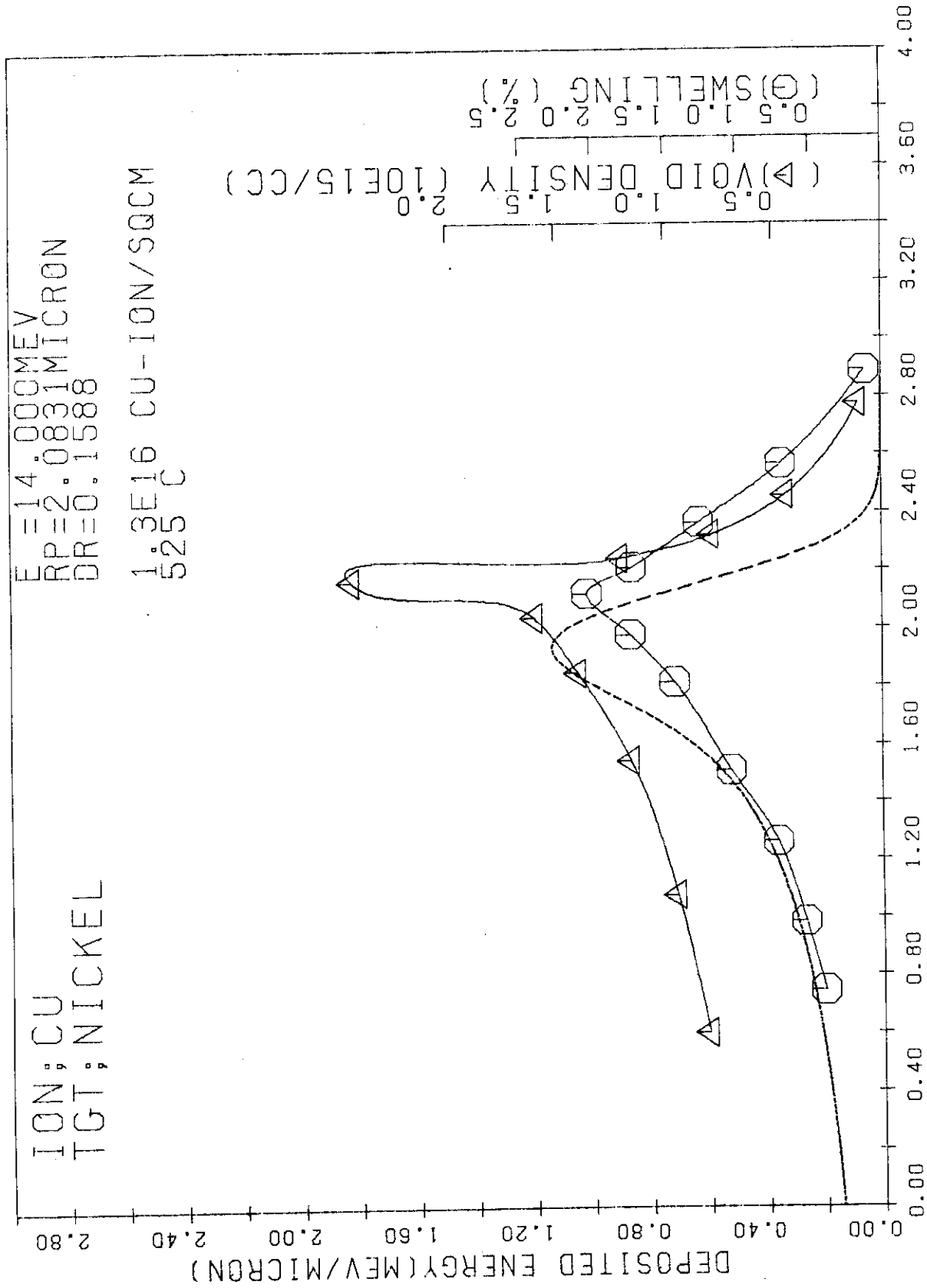
ION:CU
TGT:NICKEL
E=14.000MEV
RP=2.08831MICRON
DR=0.15588
1.3E16 CU-ION/SQCM
525 C
(▷)VOID DENSITY (10E15/CC)
0.5 1.0 1.5 2.0
(Θ)SWELLING (%)
0.5 1.0 1.5 2.0 2.5
DEPOSITED ENERGY(MEV/MICRON)
0.00 0.40 0.80 1.20 1.60 2.00 2.40 2.80
DEPTH (MICRON)
0.00 0.40 0.80 1.20 1.60 2.00 2.40 2.80 3.20 3.60 4.00

Fig. SA-6

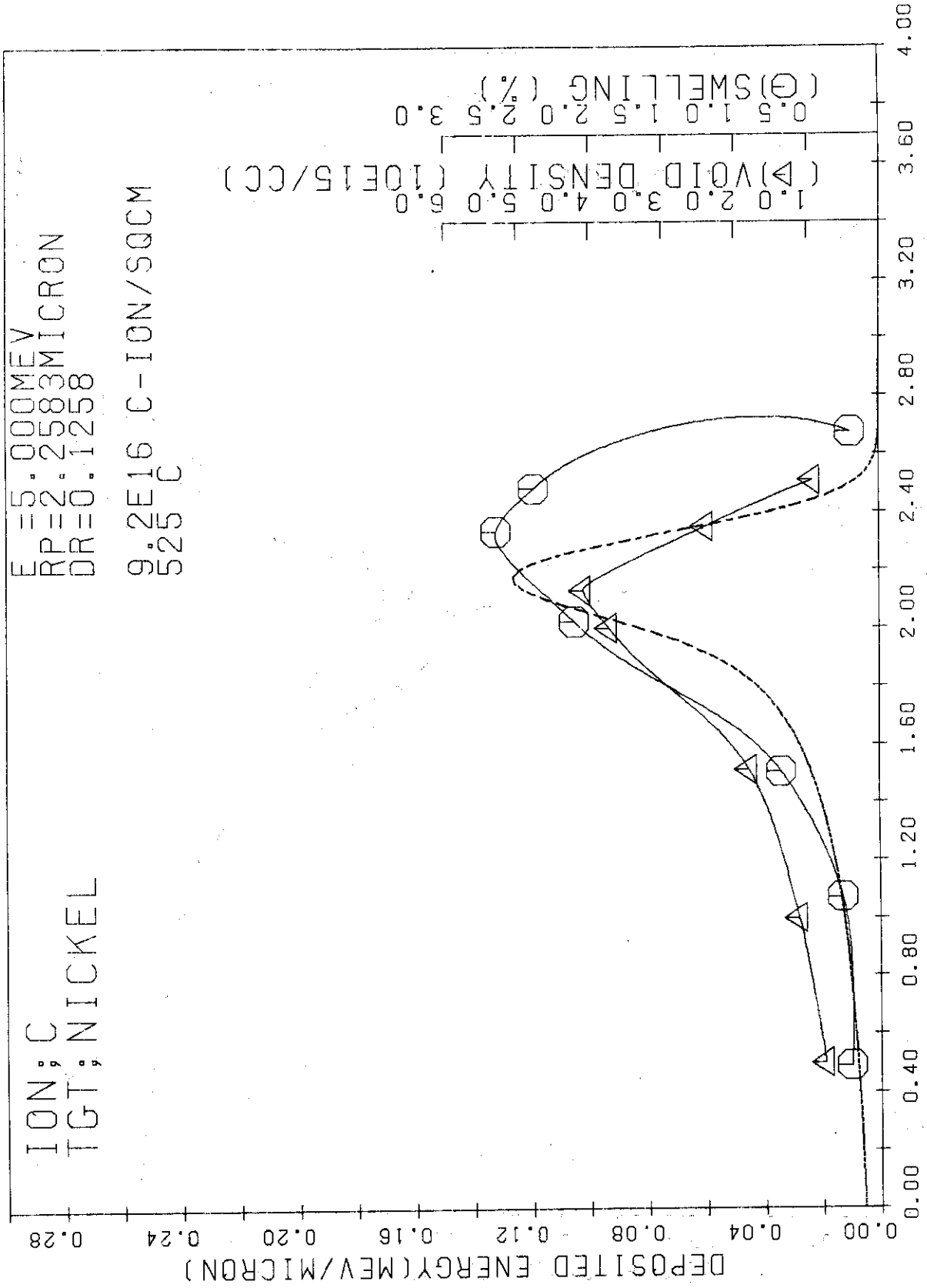
ION: C
TGT: NICKEL
E =5.000MEV
RP=2.2583MICRON
DR=0.1258
9.2E16 C-ION/SQCM
525 C
(▽)VOID DENSITY (10E15/CC)
1.0 2.0 3.0 4.0 5.0 6.0
(○)SWELLING (%)
0.5 1.0 1.5 2.0 2.5 3.0
DEPOSITED ENERGY(MEV/MICRON)
0.00 0.04 0.08 0.12 0.16 0.20 0.24 0.28
DEPTH (MICRON)
0.00 0.40 0.80 1.20 1.60 2.00 2.40 2.80 3.20 3.60 4.00

Fig. SA-7

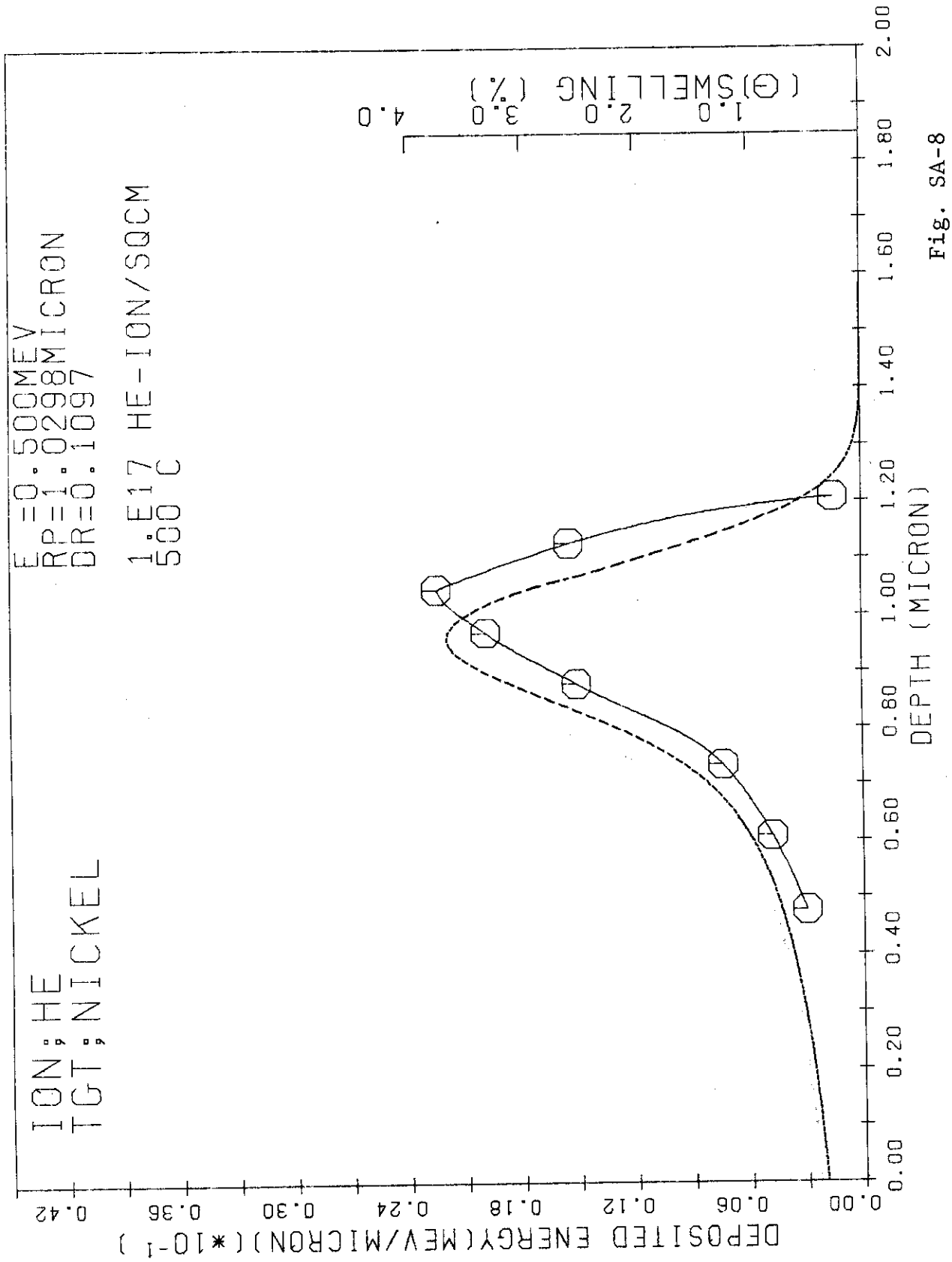
ION:HE
TGT:NICKEL
E =0.500MEV
RP=1.02298MICRON
DR=0.1097
1.E17 HE-ION/SQCM
500 C
DEPOSITED ENERGY(MEV/MICRON)(*10-1)
DEPTH (MICRON)
(%) SWELLING (Θ)

Fig. SA-8

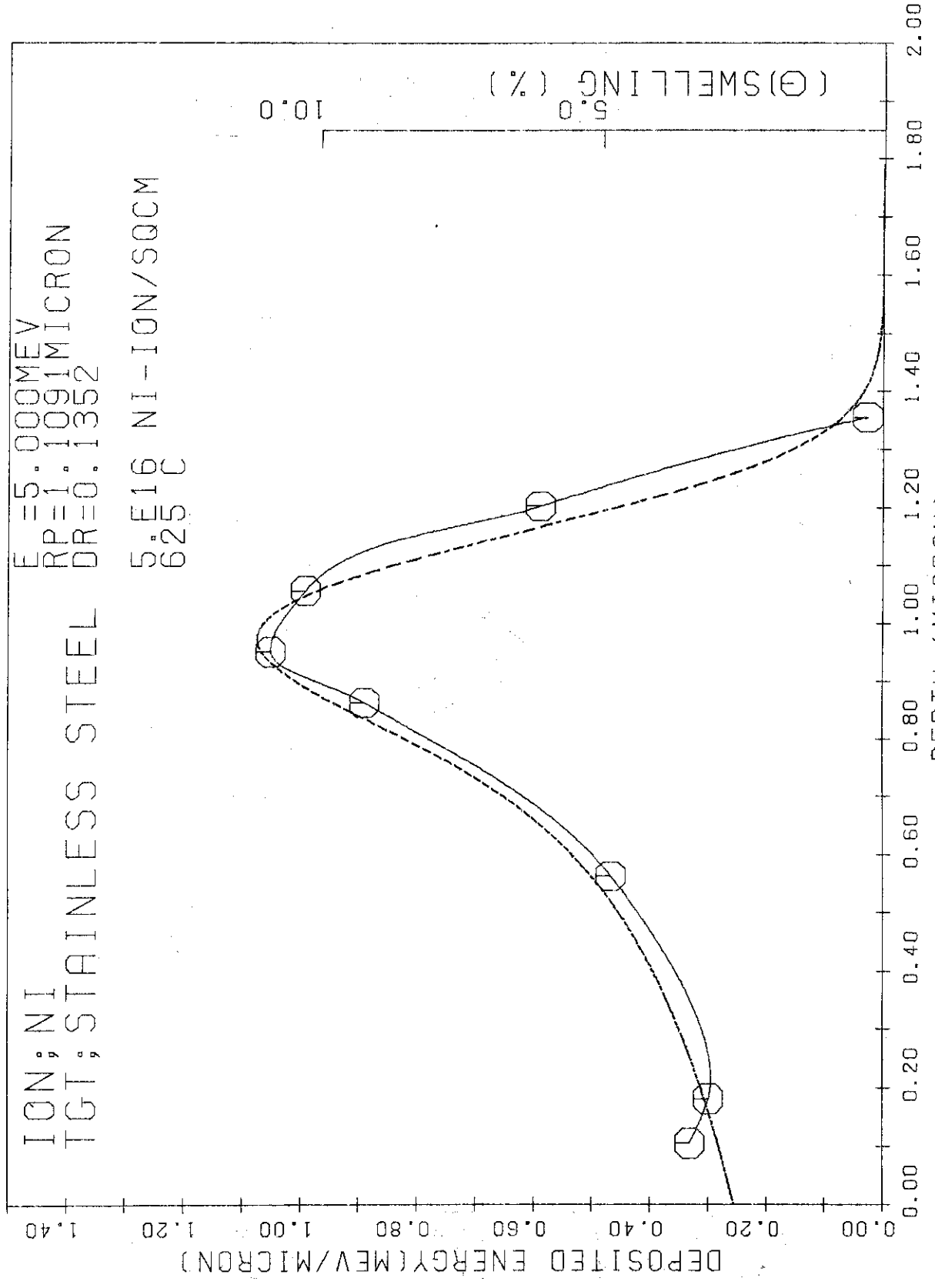
ION: NI
TGT: STAINLESS STEEL
E=5.000MEV
RP=1.1091MICRON
DR=0.1352
5.E16 NI-ION/SQCM
625 C
DEPOSITED ENERGY(MEV/MICRON)
DEPTH (MICRON)
(%) SWELLING
0.00
0.20
0.40
0.60
0.80
1.00
1.20
1.40
1.60
1.80
2.00
5.0
10.0

Fig. SA-9

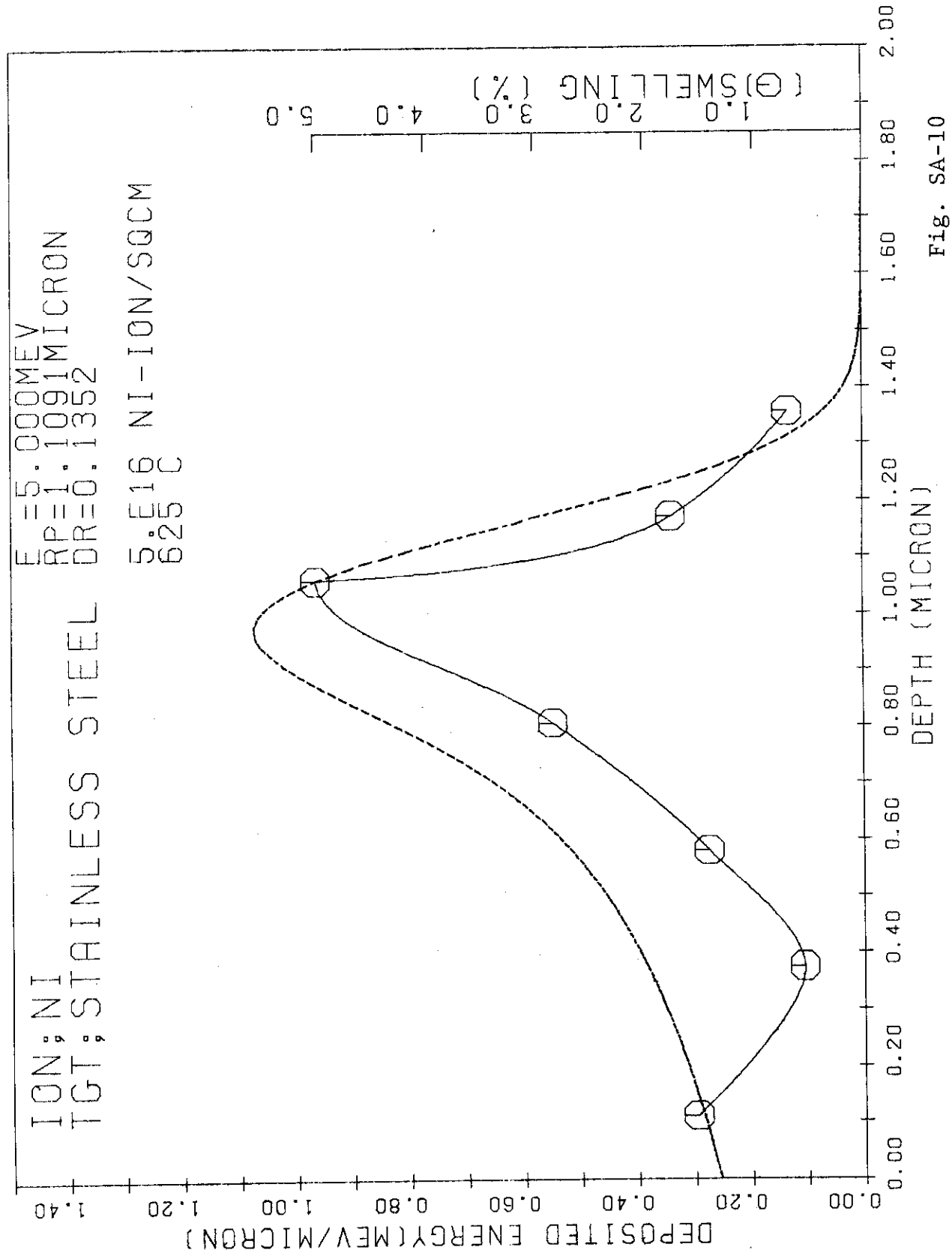
ION:NI
TGT:STAINLESS STEEL
E=5.000MEV
RP=1.1091MICRON
DR=0.13352
5.E16 NI-ION/SQCM
625 C
DEPOSITED ENERGY(MEV/MICRON)
DEPTH (MICRON)
(%) SWELLING (%)
0.00
0.20
0.40
0.60
0.80
1.00
1.20
1.40
1.60
1.80
2.00
1.0
2.0
3.0
4.0
5.0

Fig. SA-10

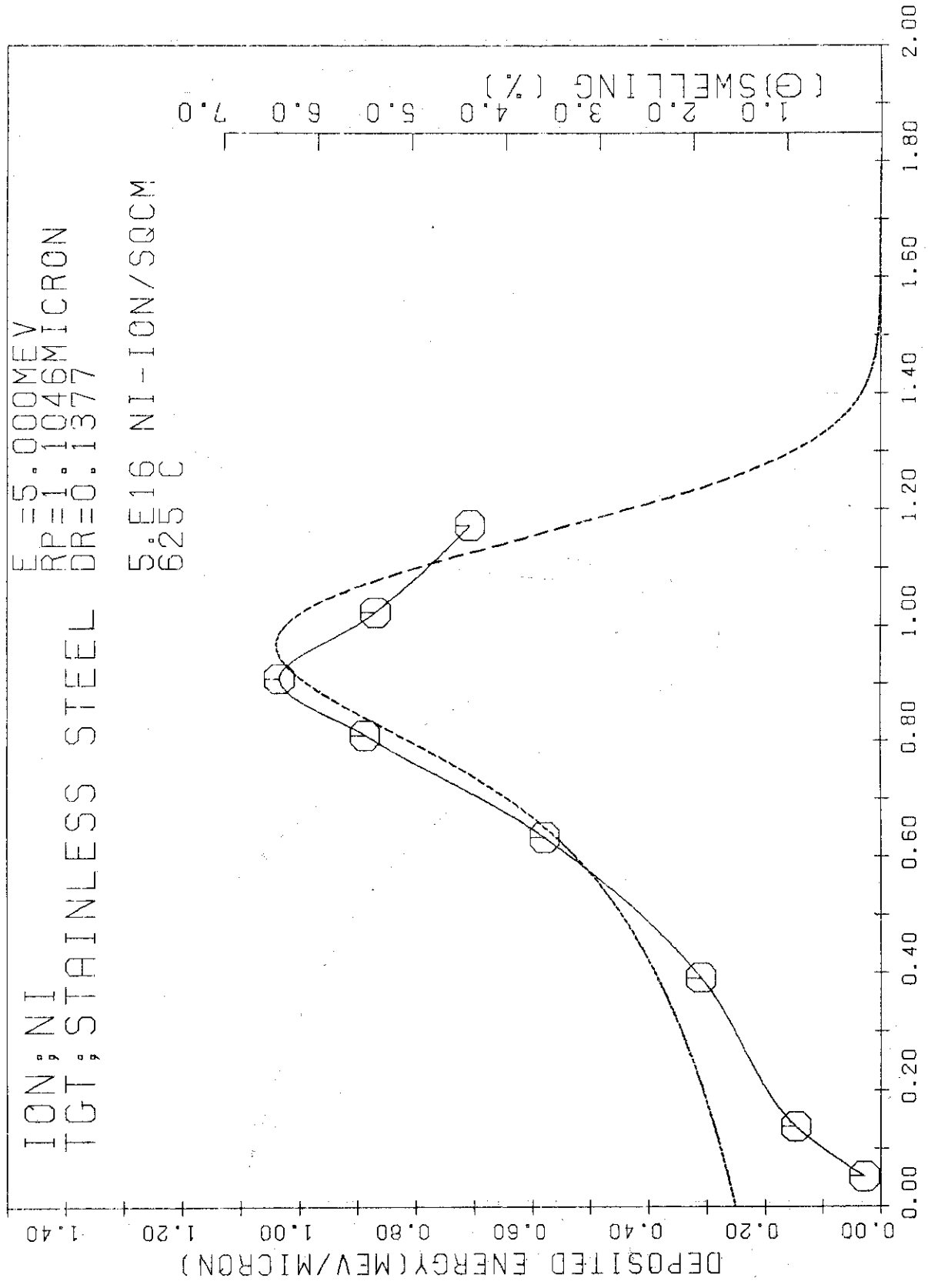
ION: NI
TGT: STAINLESS STEEL
E =5.000MEV
RP=1.1046MICRON
DR=0.1377
5.E16 NI-ION/SQCM
625 C
DEPOSITED ENERGY(MEV/MICRON)
DEPTH (MICRON)
(%) SWELLING

Fig. SA-11

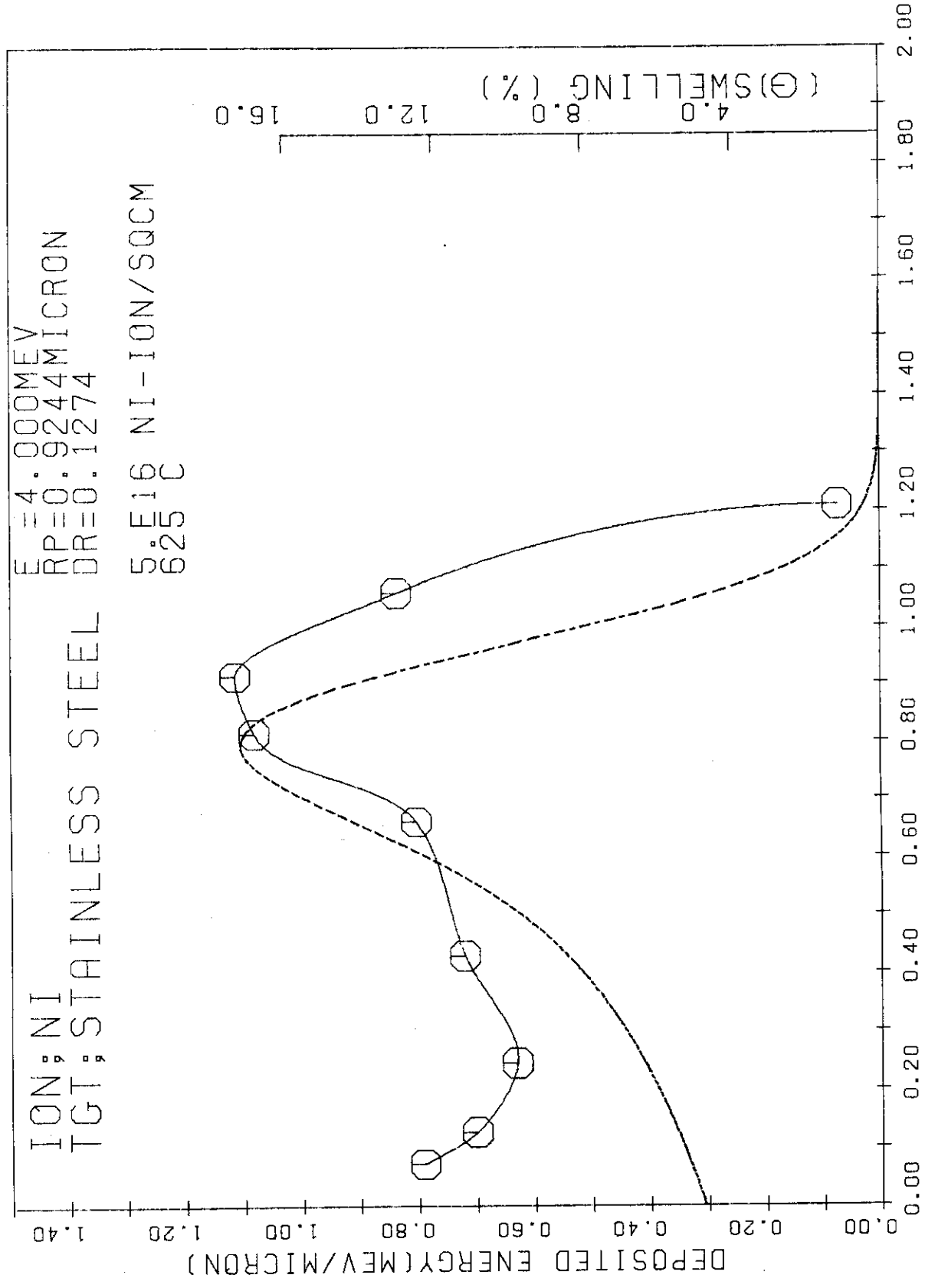
ION:NI
TGT:STAINLESS STEEL
E =4.000MEV
RP=0.92444MICRON
DR=0.12274
5.E16 NI-ION/SQCM
625 C
DEPOSITED ENERGY(MEV/MICRON)
DEPTH (MICRON)
(%) SWELLING (%)
0.00
0.20
0.40
0.60
0.80
1.00
1.20
1.40
1.60
1.80
2.00
4.0
8.0
12.0
16.0

Fig. SA-12

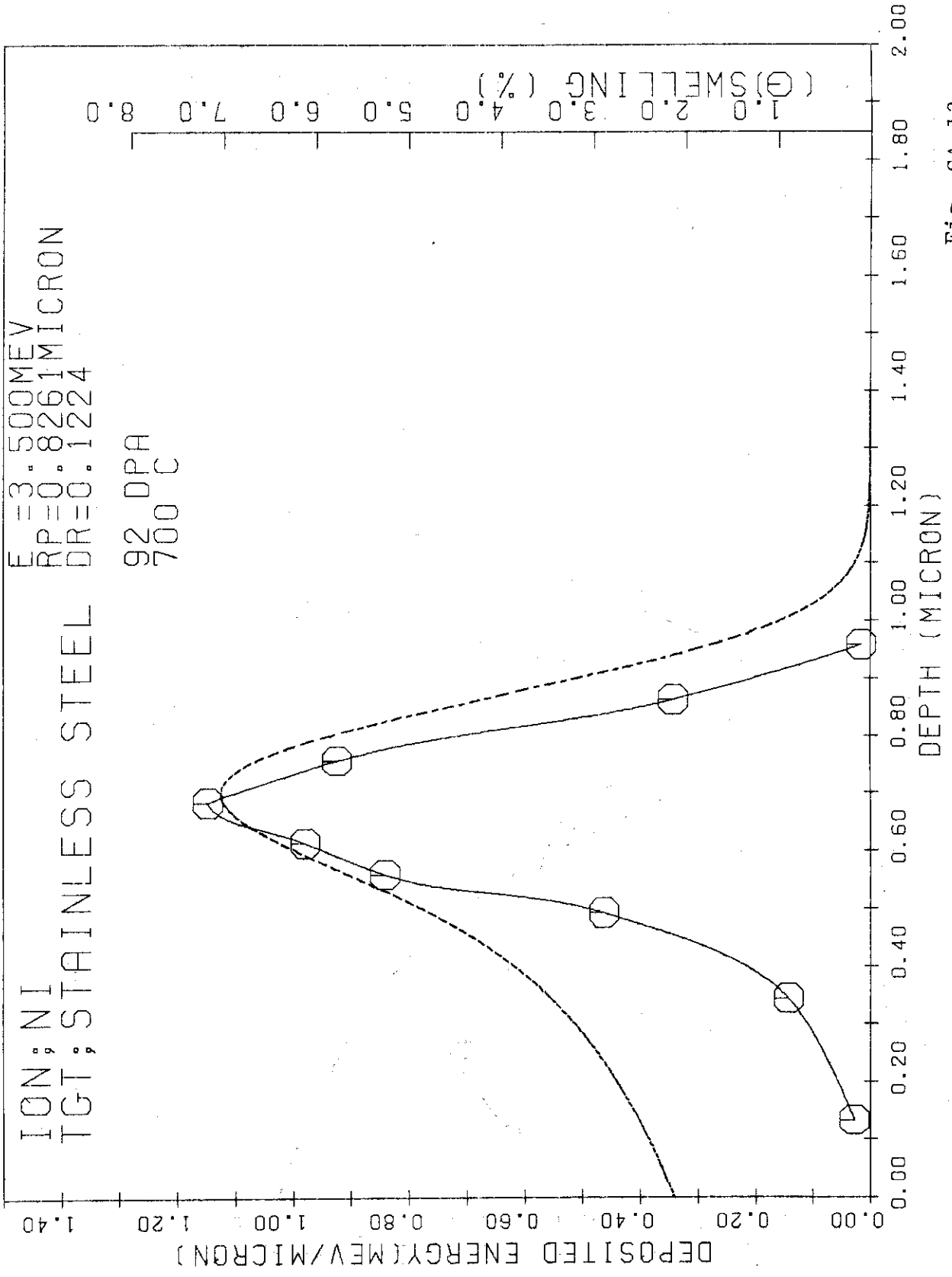
ION: NI
TGT: STAINLESS STEEL
E=3.500MEV
RP=0.8261MICRON
DR=0.1224
92 DPA
700 C
DEPOSITED ENERGY(MEV/MICRON)
DEPTH (MICRON)
(%) SWELLING

Fig. SA-13

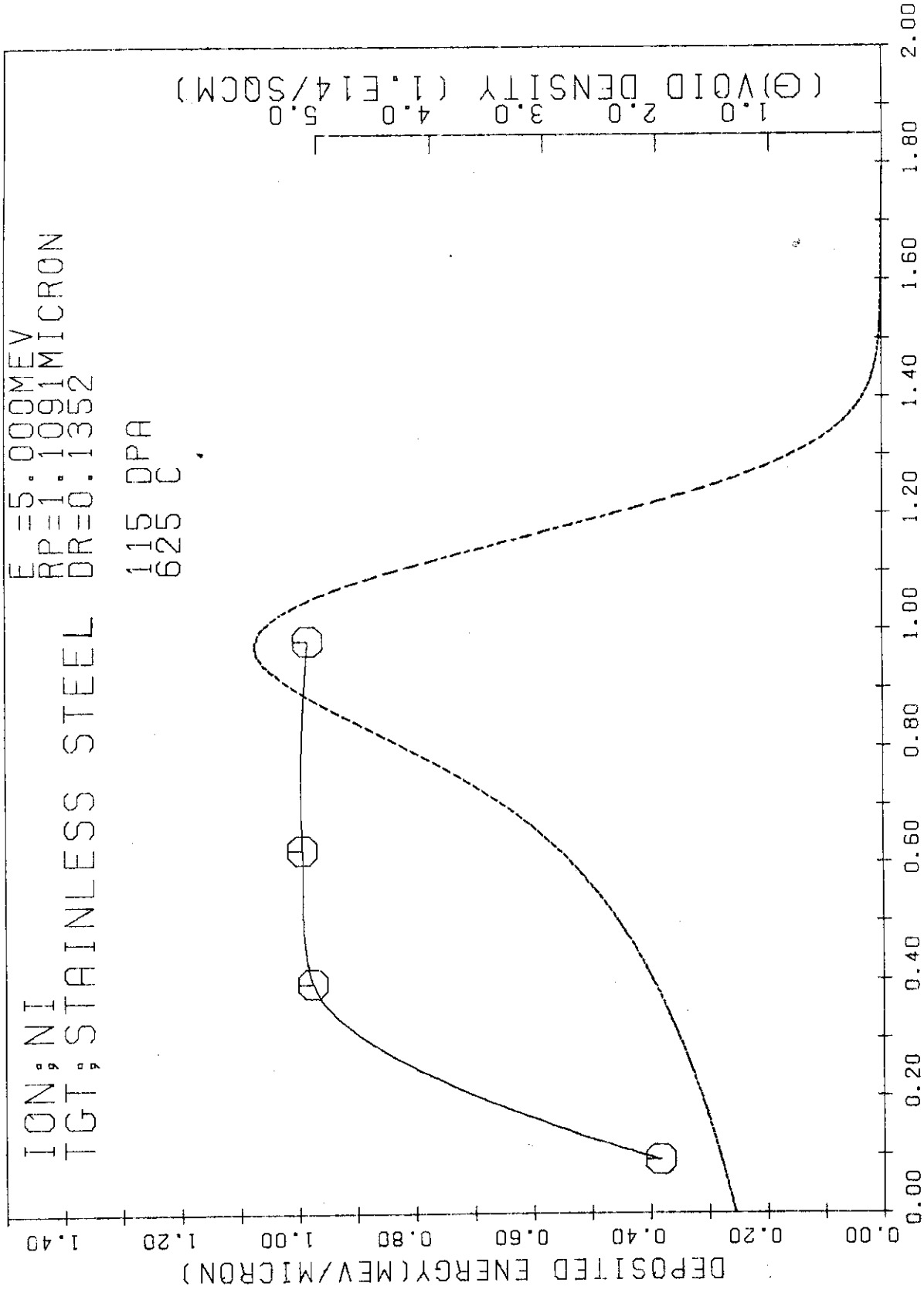
ION : NI
TGT : STAINLESS STEEL
E =5.000MEV
RP=1.1091MICRON
DR=0.13352
115 DPA
625 C
DEPOSITED ENERGY(MEV/MICRON)
DEPTH (MICRON)
(Θ)VOID DENSITY (1.E14/SQCM)
0.00
0.20
0.40
0.60
0.80
1.00
1.20
1.40
1.60
1.80
2.00
1.0
2.0
3.0
4.0
5.0

Fig. SA-14

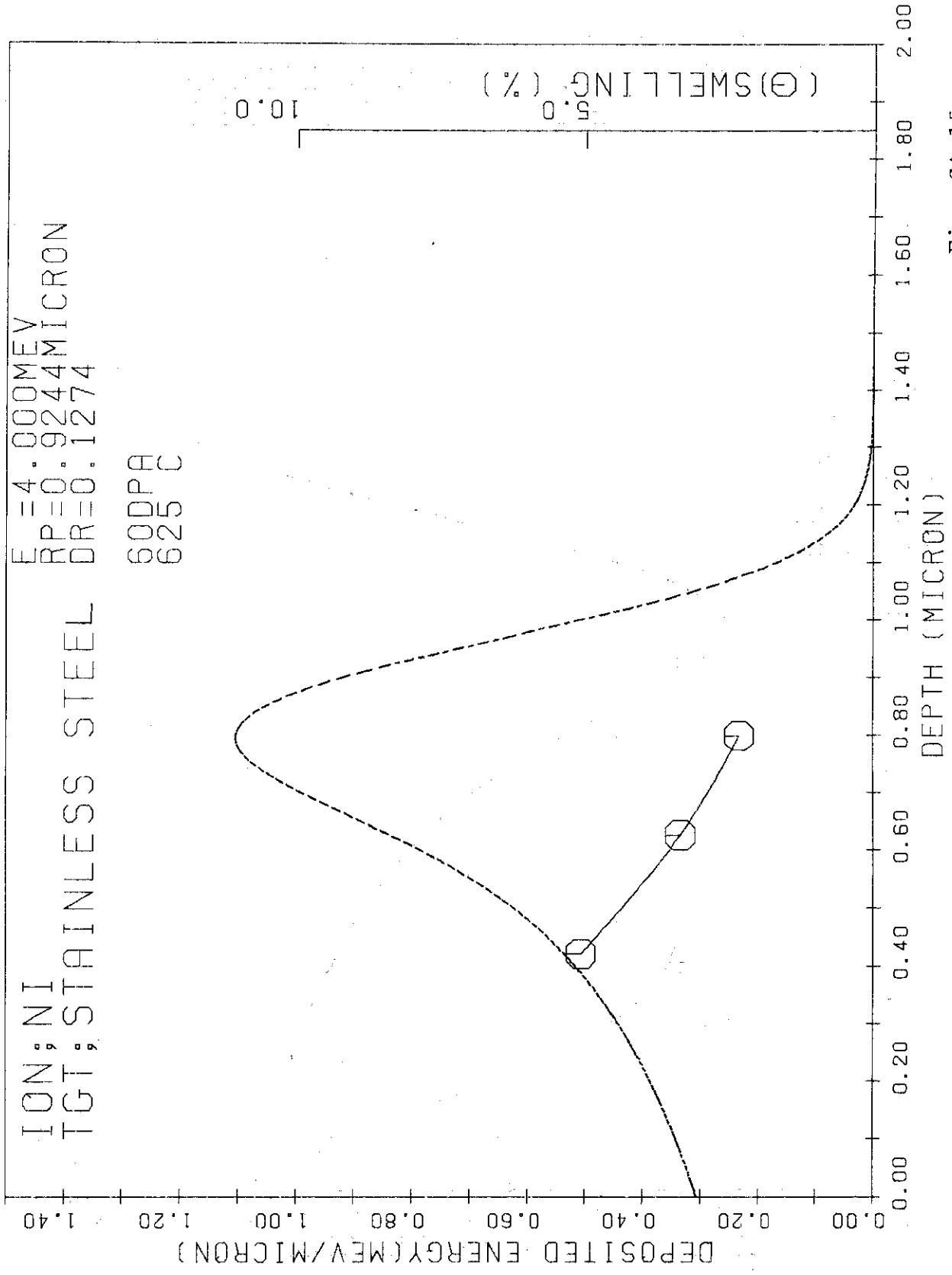
ION: NI
TGT: STAINLESS STEEL
E =4.000MEV
RP=0.9244MICRON
DR=0.1274
60DPA
625 C
(%) SWELLING
5.0
10.0
DEPTH (MICRON)
0.00
0.20
0.40
0.60
0.80
1.00
1.20
1.40
1.60
1.80
2.00
DEPOSITED ENERGY(MEV/MICRON)
0.00
0.20
0.40
0.60
0.80
1.00
1.20
1.40

Fig. SA-15

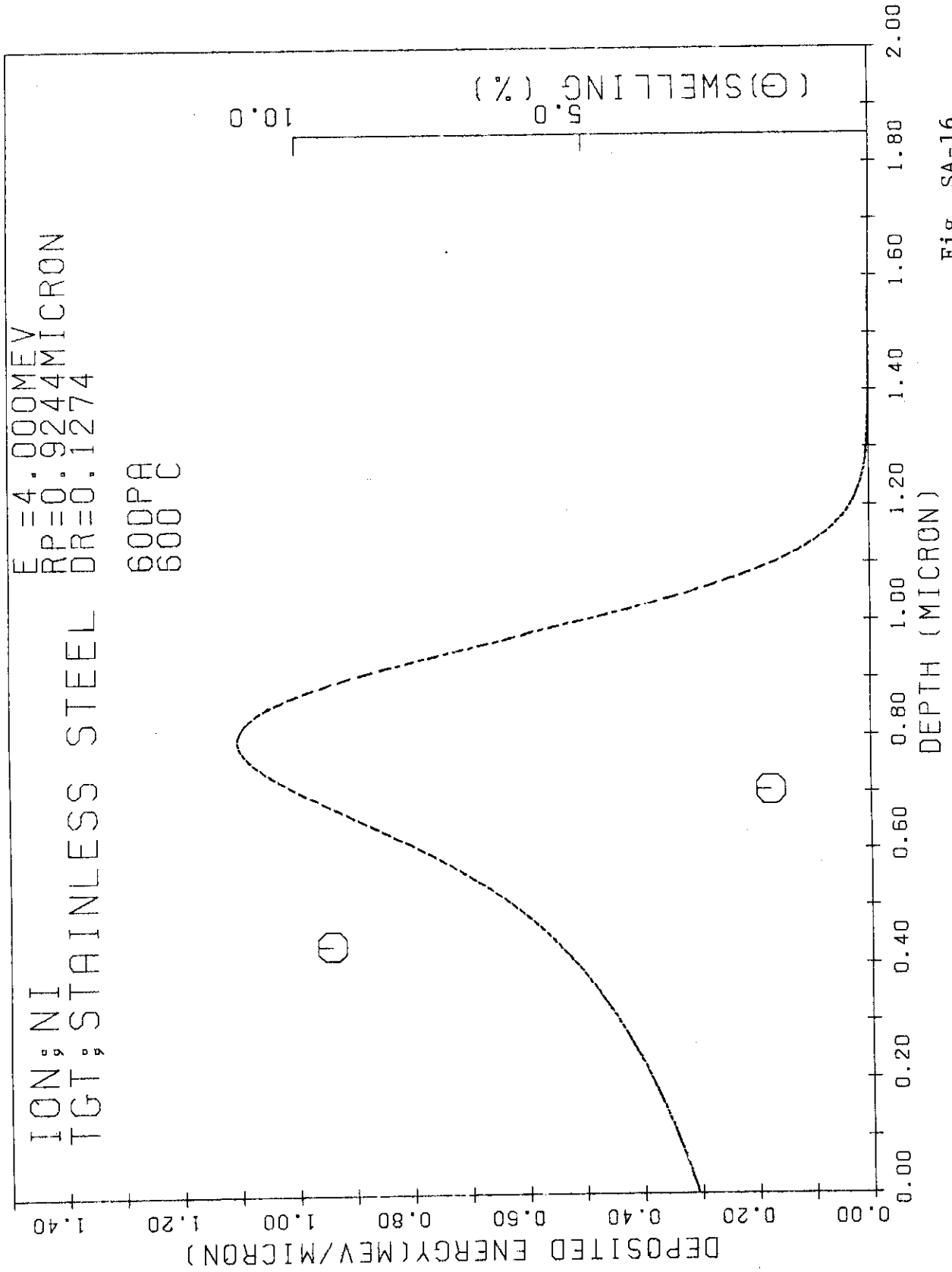
ION=NI
TGT=STAINLESS STEEL
E=4.000MEV
RP=0.9244MICRON
DR=0.1274
600PA
600°C
DEPOSITED ENERGY(MEV/MICRON)
DEPTH (MICRON)
(%) SWELLING (%)
0.00
0.20
0.40
0.60
0.80
1.00
1.20
1.40
1.60
1.80
2.00
5.0
10.0

Fig. SA-16

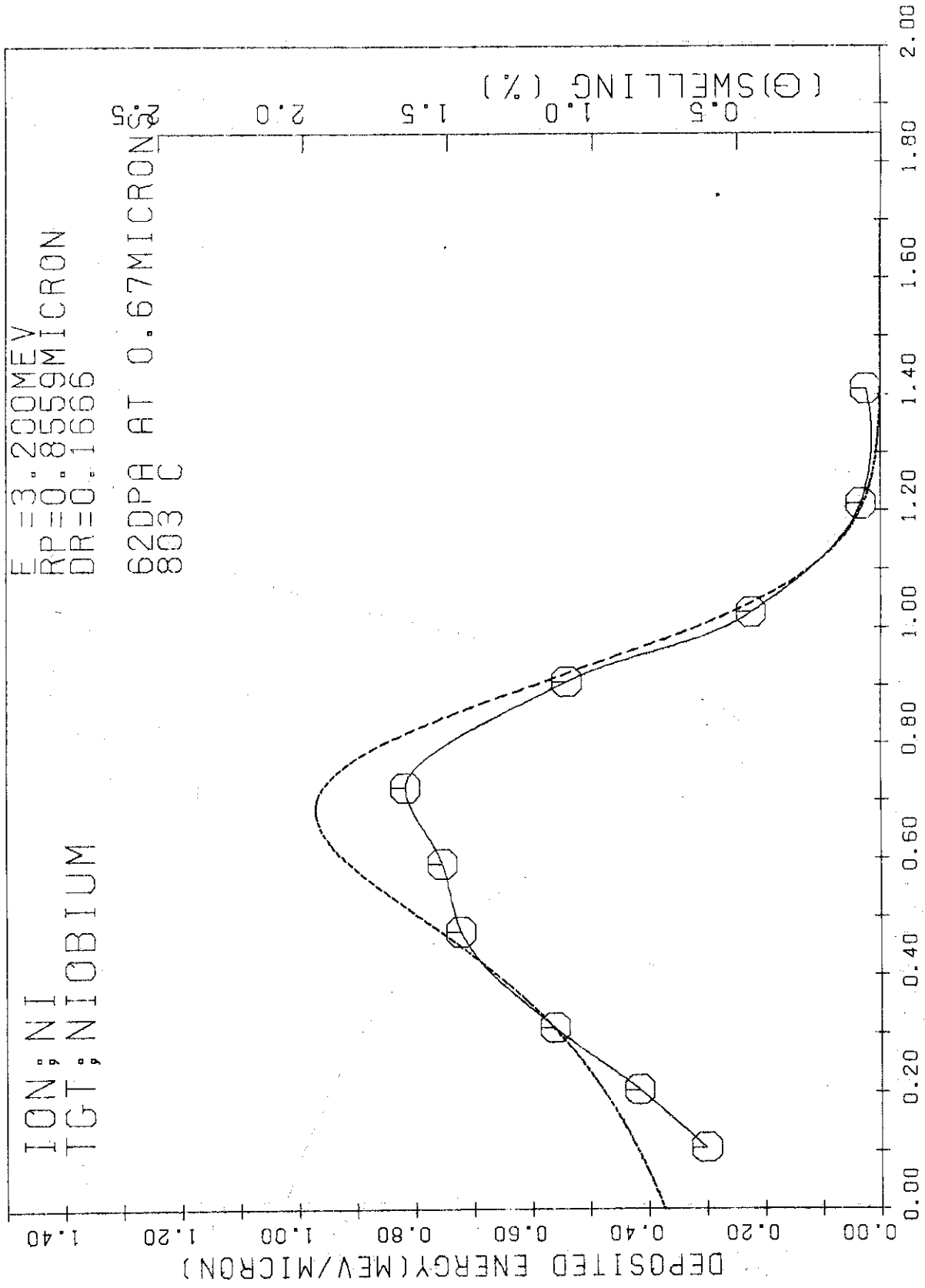
ION : NI
TGT : NIOBIUM
E =3.200MEV
RP=0.8559MICRON
DR=0.1666
62DPA AT 0.67MICRON
803 C
DEPOSITED ENERGY(MEV/MICRON)
DEPTH (MICRON)
(%) SWELLING

Fig. SA-17

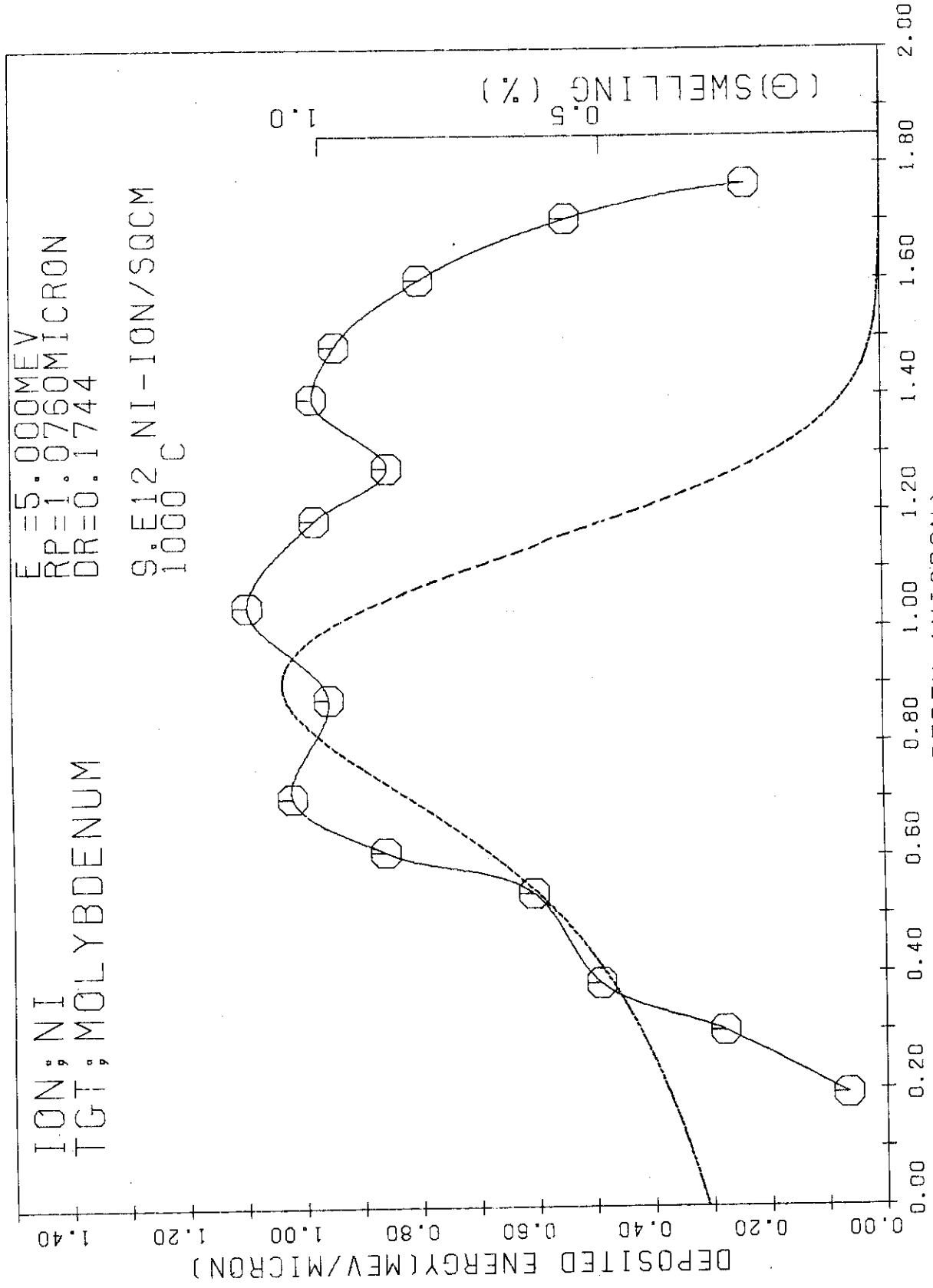
ION : NI
TGT : MOLYBDENUM
E =5.000MEV
RP=1.0760MICRON
DR=0.1744
5.E12 NI-ION/SQCM
1000 C
DEPOSITED ENERGY(MEV/MICRON)
DEPTH (MICRON)
SWELLING (%)
0.00
0.20
0.40
0.60
0.80
1.00
1.20
1.40
1.60
1.80
2.00
0.5
1.0

Fig. SA-18

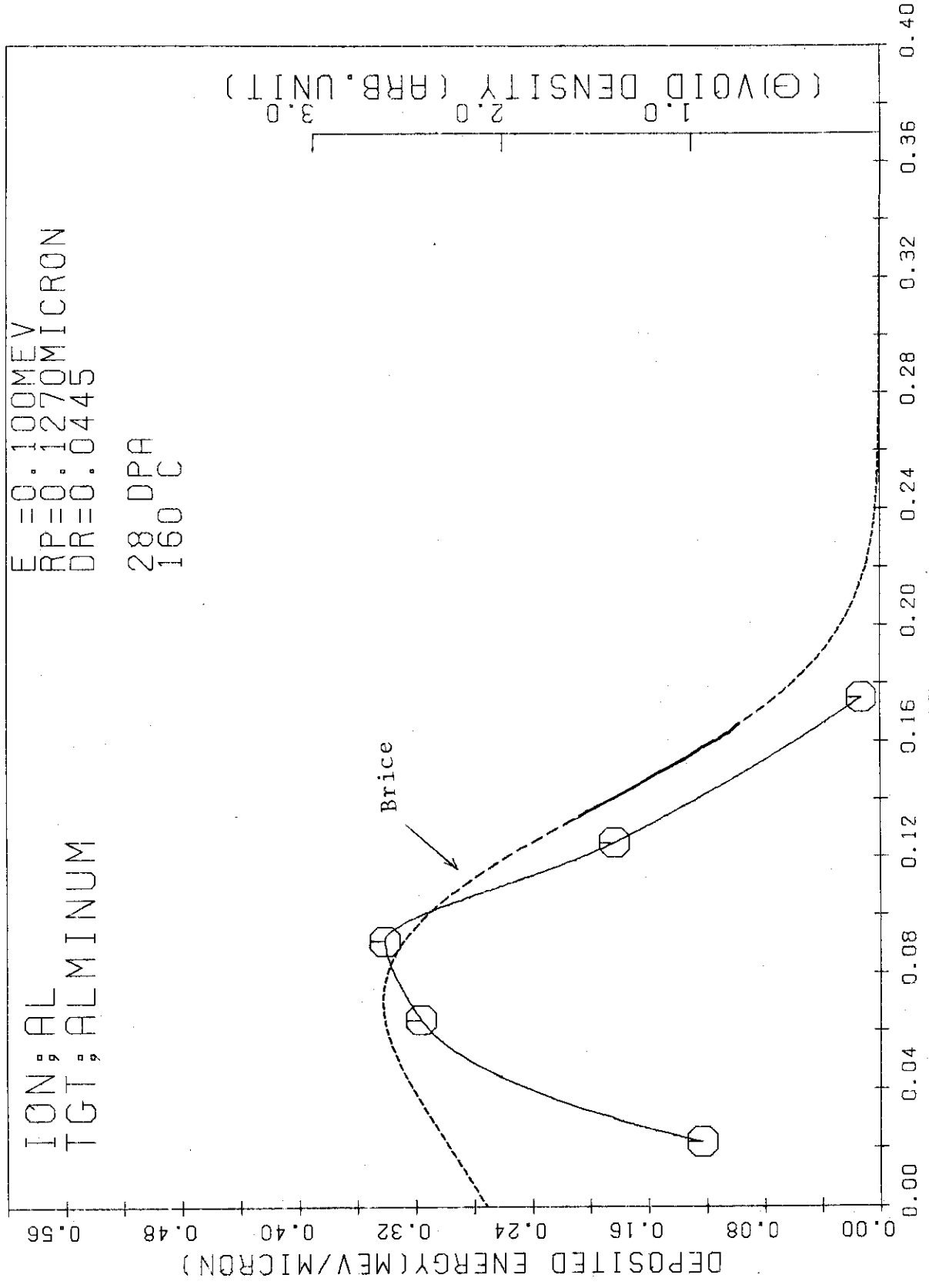
ION: AL
TGT: ALMINUM
E =0.100MEV
RP=0.1270MICRON
DR=0.0445
28 DPA
160 C
Brice
DEPTH (MICRON)
DEPOSITED ENERGY(MEV/MICRON)
(Θ)VOID DENSITY (ARB.UNIT)
0.00
0.04
0.08
0.12
0.16
0.20
0.24
0.28
0.32
0.36
0.40
0.56
0.48
0.40
0.32
0.24
0.16
0.08
0.00
1.0
2.0
3.0

Fig. SA-19

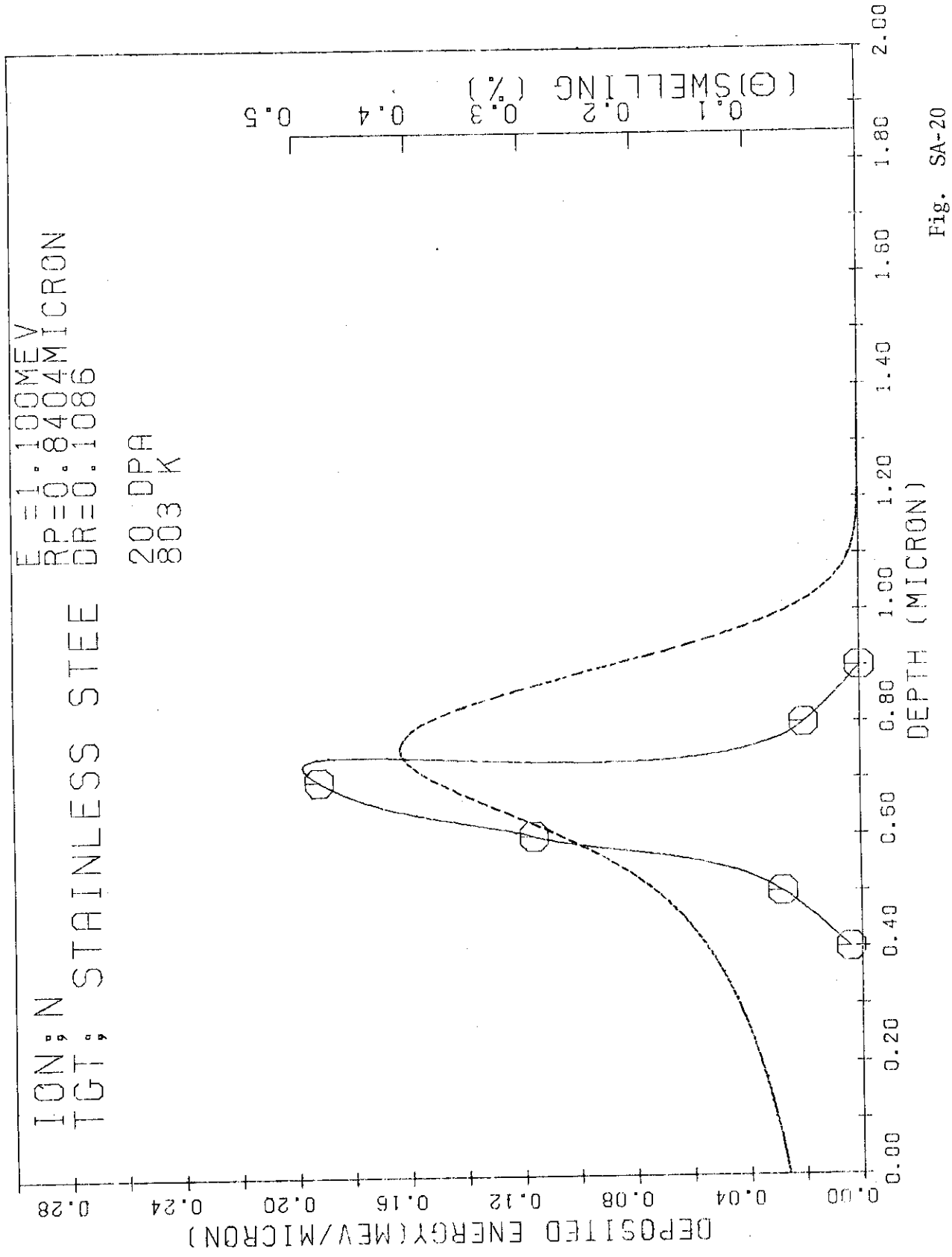
ION : N
TGT : STAINLESS STEE
E =1.100MEV
RP=0.8404MICRON
DR=0.1086
20 DPA
803 K
DEPOSITED ENERGY(MEV/MICRON)
DEPTH (MICRON)
(%) SWELLING

Fig. SA-20

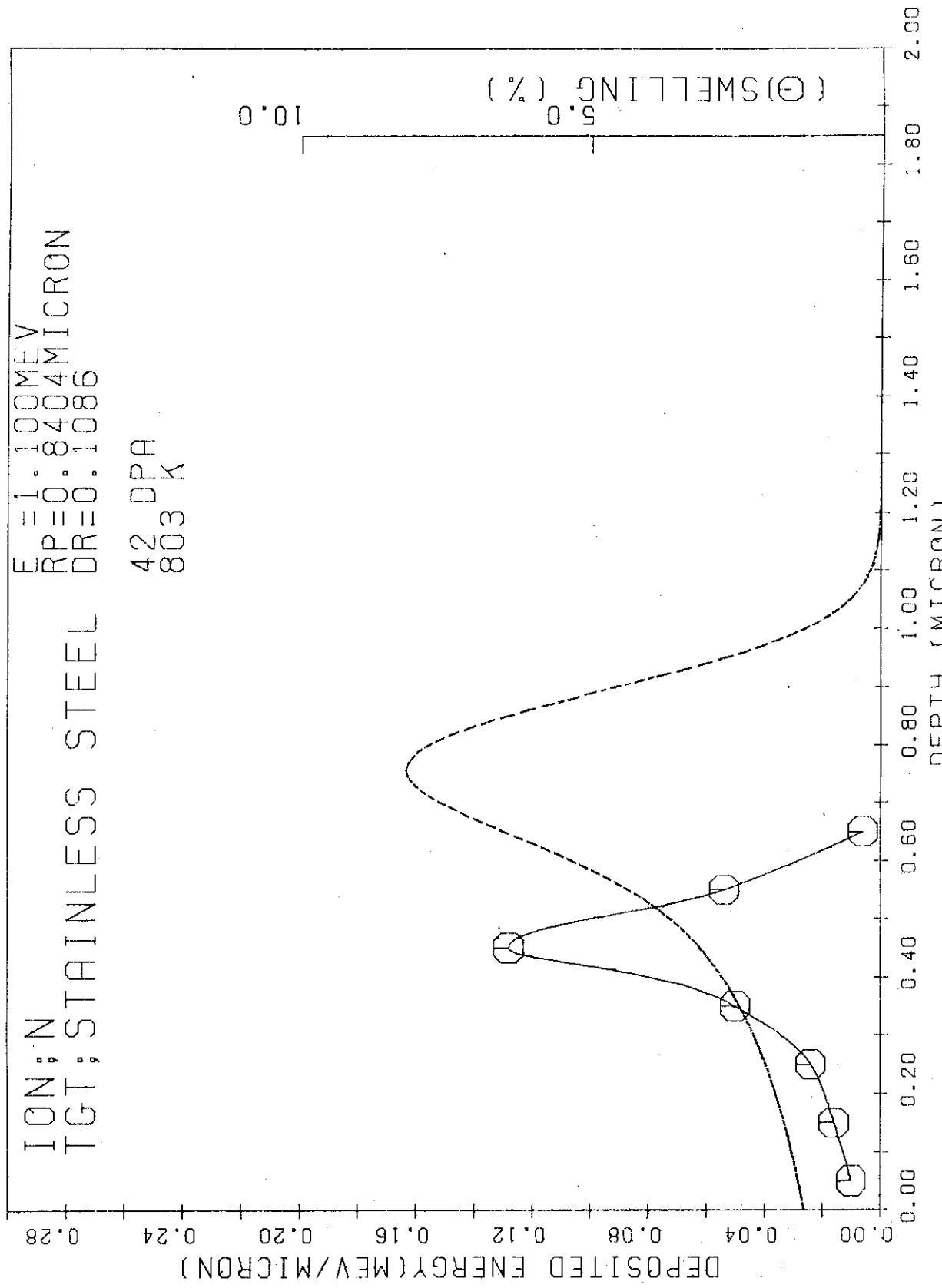
ION:N
TGT:STAINLESS STEEL
E=1.100MEV
RP=0.8404MICRON
DR=0.1086
42 DPA
803 K
DEPOSITED ENERGY(MEV/MICRON)
DEPTH (MICRON)
(%) SWELLING (%)
0.00
0.04
0.08
0.12
0.16
0.20
0.24
0.28
0.00
0.20
0.40
0.60
0.80
1.00
1.20
1.40
1.60
1.80
2.00
5.0
10.0

Fig. SA-21

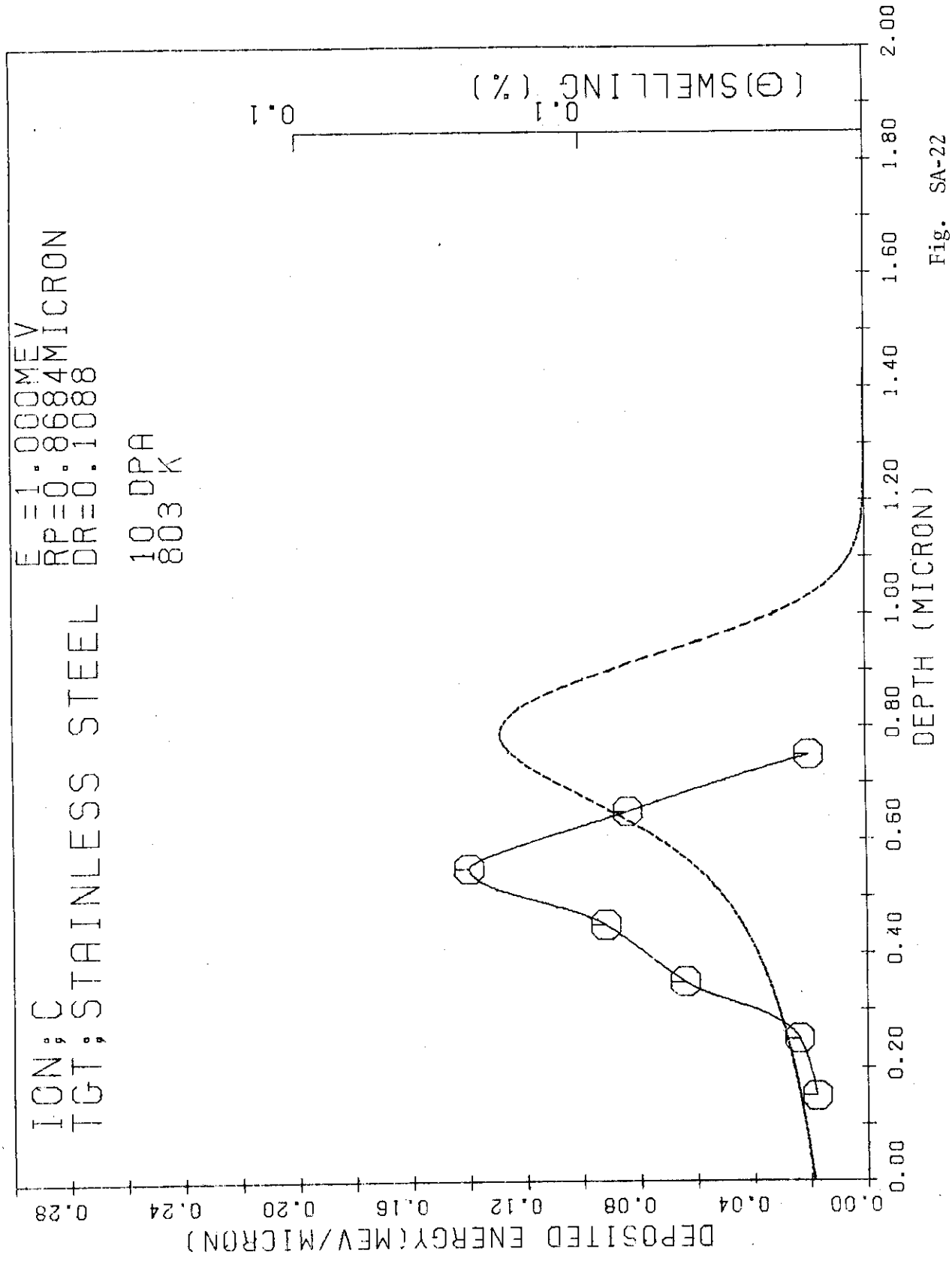
ION:C
TGT:STAINLESS STEEL
E=1.000MEV
RP=0.8684MICRON
DR=0.1088
10 DPA
803 K
DEPOSITED ENERGY(MEV/MICRON)
DEPTH (MICRON)
0.00
0.20
0.40
0.60
0.80
1.00
1.20
1.40
1.60
1.80
2.00
0.04
0.08
0.12
0.16
0.20
0.24
0.28
SWELLING (%)
0.1

Fig. SA-22

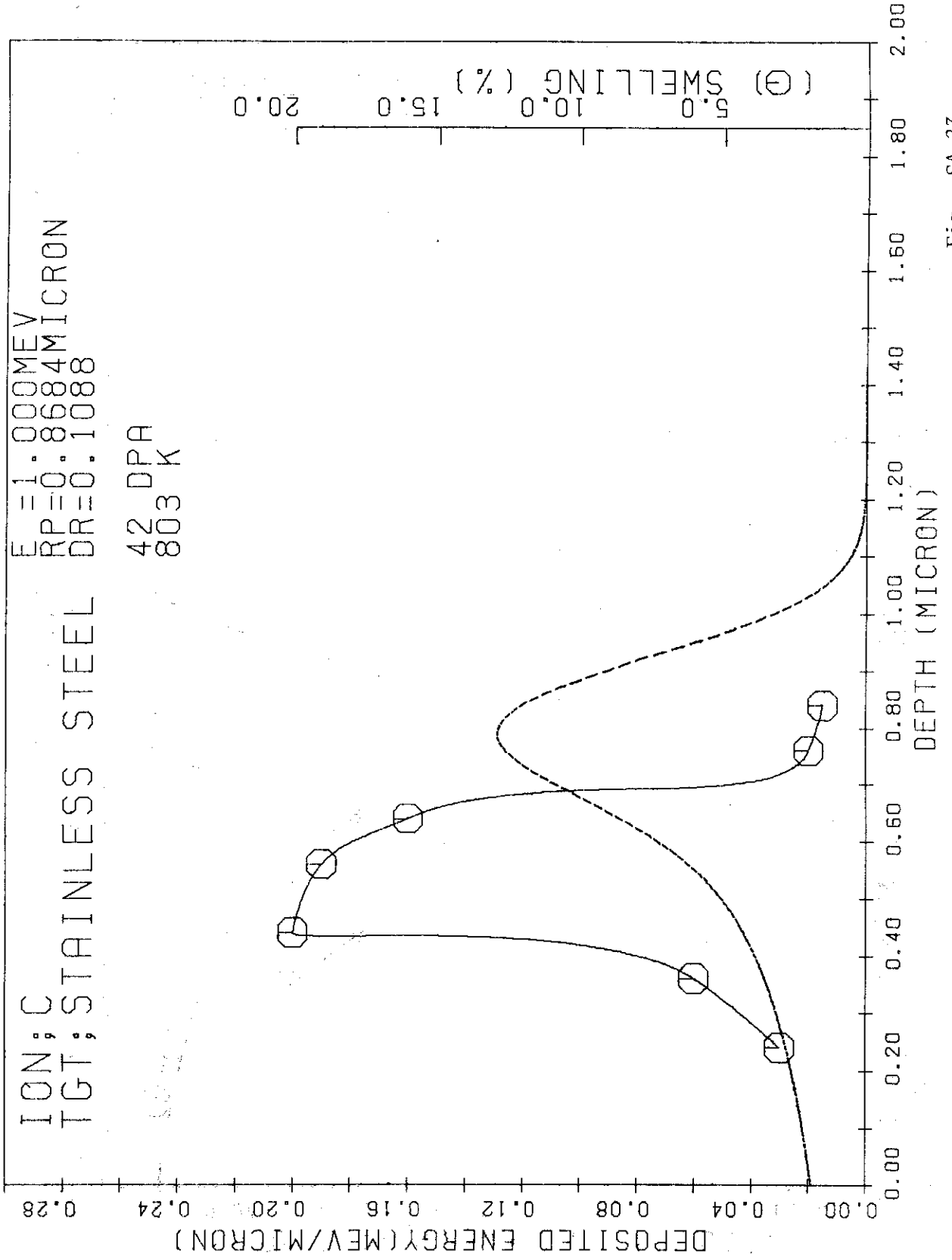
ION:C
TGT:STAINLESS STEEL
E =1.000MEV
RP=0.86884MICRON
DR=0.1088
42 DPA
803 K
DEPOSITED ENERGY(MEV/MICRON)
DEPTH (MICRON)
(%) SWELLING (%)

Fig. SA-23

Literatures

3-1. W. G. Johnston, W. G. Morris and A. M. Turkalo:
Proc. Int. Conf. Radiation Effects in Breeder Reactor Structural Materials, Scottsdale 1977, 421-430

3-2. J. B. Whitley, G. L. Kulcinski, G. L. Smith, Jr. and P. Wilkes:
UWFDM-252

3-3. S. Diamond, M. L. Bleiberg, I. M. Baron, R. Bajaj and R. W. Chickering:
Proc. Int. Conf. Radiation Effects and Tritium Technology for Fusion Reactor, ORNL 1976, 1-207-1-229

3-4. B. A. Loomis, A. Taylor and S. B. Gerber:
ibid, 1-93-1-105

3-5. G. Fenske, S. K. Das and M. Kaminsky:
J. Nucl. Mater. 85&86, 707-711 (1979)

3-6. G. Fenske, S. K. Das and M. Kaminsky:
J. Nucl. Mater. 80, 373-378 (1979)

3-7. G. Fenske, S. K. Das, M. Kaminsky and G. H. Miley:
J. Nucl. Mater. 76&77, 247-248 (1978)

3-8. J. B. Whitley, G. L. Kulcinski, P. Wilkes and H. V. Smith, Jr.:
J. Nucl. Mater. 79, 159-169 (1979)

3-9. J. B. Whitley, G. L. Kulcinski, P. Wilkes and J. Billen:
J. Nucl. Mater. 85&86, 701-706 (1979)

3-10. E. H. Lee, K. Mansur and M. H. Yoo:
J. Nucl. Mater. 85&86, 577-581 (1979)

3-11. G. Fenske, S. K. Das, M. Kaminsky and G. H. Miley:
Trans. Am. Nucl. Soc., 28,196-197 (1978)

3-12. K. L. Rusbridge:
J. Nucl. Inst. and Meth., 182/183, 521-529 (1981)

3-13. T. Lauritzen, G. M. Konze, W. L. Bell and W. K. Appleby:
Journal of Microscopy, 116, Pt 1, 65-76 (1979)

3-14. G. Fenske, S. K. Das, M. Kaminsky and G. Miley:
J. Nucl. Inst. and Meth., 170, 465-470 (1980)

3-15. J. L. Brimhall and C. H. Henager, Jr.:
Trans. Am. Nucl. Soc., 26,179 (1977)

3-16. E. R. Bradley and J. L. Brimhall:
Trans. Am. Nucl. Soc., 26,179-180 (1977)

3-15. K. Shiraishi, T. Aruga and Y. Katano:
J. Nucl. Mater., 103 & 104,1053-1058 (1981)

3-18 T. Aruga, Y. Katano and K. Shiraishi:
J. Nucl. Mater., in press (1984)

APPENDIX 2. EXPERIMENTAL DATA AND LITERATURES CONCERING POINT DEFECTS AND THEIR CLUSTERS

Table DA-1 is a list of projectile-target combinations which damage data are compiled. The experimental data on the point defects or their clusters as a function of depth are reproduced in the figures from DA-1 to DA-7. The dashed line in the figures shows damage curve calculated by the E-DEP-1 code with $k=k_{LSS}$. In the last part in this Appendix 2, all the literatures collected are listed.

Table DA-1

Ion	Target	Energy	Reference	Figure
Ni	Nickel	4MeV	4-6	DA-1
N	Molybdenum	2MeV	4-14	DA-2
Ni	Aluminum	150KeV	4-9	DA-3
He	Copper	1MeV	4-7	DA-4
Si	Silicon	2MeV	4-4	DA-5
N	Silicon	50KeV	4-5	DA-6
N	Silicon	220KeV	4-10	DA-7
N	Silicon	300KeV	4-8	DA-8
He	Silicon	30KeV	4-13	DA-9
Li	Silicon	30KeV	4-13	DA-10
C	Silicon	40KeV	4-13	DA-11
O	Silicon	60KeV	4-13	DA-12
Ne	Silicon	80KeV	4-2	DA-13
Ne	Silicon	220KeV	4-10	DA-14
Xe	Silicon	300KeV	4-3	DA-15
P	Silicon (111)	200KeV	4-9	DA-16
P	Silicon (110)	300KeV	4-12	DA-17

Table DA－1 (Continued)

Ion	Target	Energy	Reference
He	Gold	2MeV	4-15
Kr	Gold	150KeV	4-16
Xe	Gold	150KeV	4-16
Rb	Gold	50KeV	4-16
Kr	Gold	150KeV	4-16
Fe	Gold	50KeV	4-16
K	Gold	80KeV	4-16
Rb	Gold	150KeV	4-16
Kr	Gold	50KeV	4-16
He/H	Molybdenum	50/100KeV	4-17
Au	Gold	80KeV	4-19
Hg	Gold	150KeV	4-19
Au,Cu	Copper	150KeV	4-19
Hg	Nickel	150KeV	4-19
Pb	Silicon	80KeV	4-18
In	Silicon	30KeV	4-22
N	Silicon	40KeV	4-22
N	GaAs	40KeV	4-21
Cl	Silicon	30KeV	4-23
Ar	Silicon	30KeV	4-23

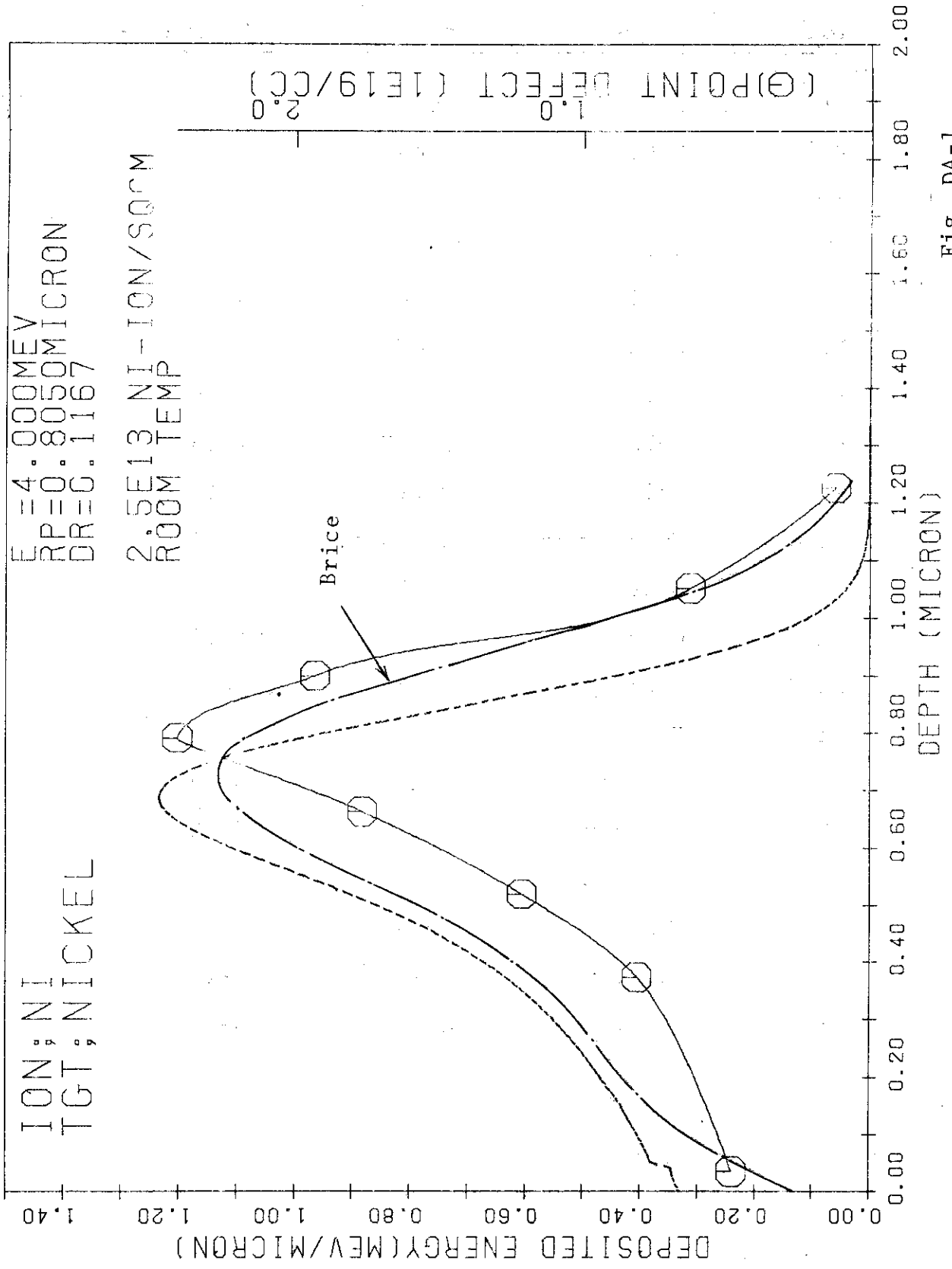
ION:NI
TGT:NICKEL
E=4.000MEV
RP=0.8050MICRON
DR=0.1167
2.5E13 NI-ION/SQCM
ROOM TEMP
Brice
DEPOSITED ENERGY(MEV/MICRON)
DEPTH (MICRON)
(Θ)POINT DEFECT (1E19/CC)

Fig. DA-1

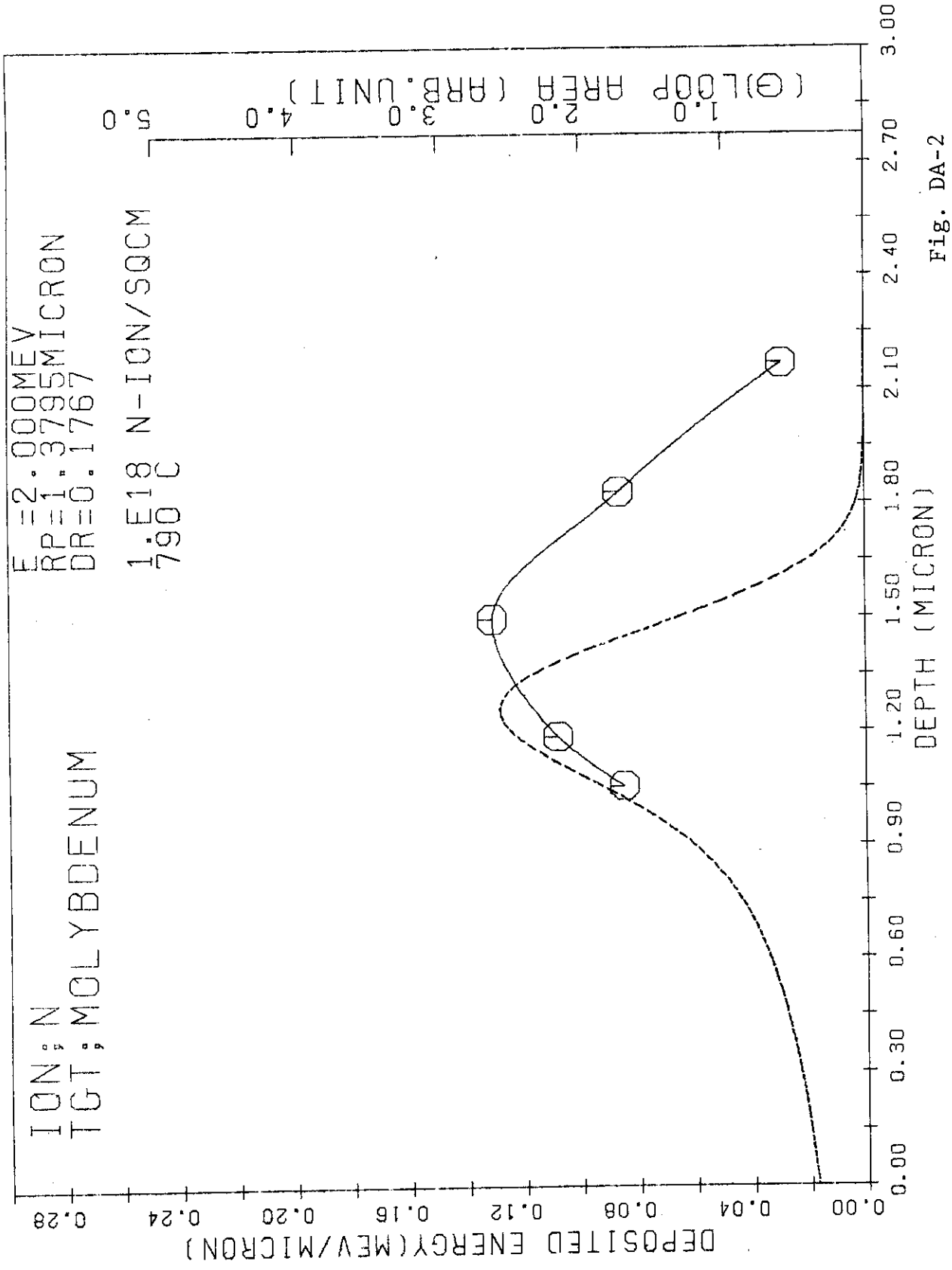
ION:N
TGT:MOLYBDENUM
E=2.000MEV
RP=1.3795MICRON
DR=0.1767
1.E18 N-ION/SQCM
790 C
DEPOSITED ENERGY(MEV/MICRON)
DEPTH (MICRON)
(G)LOOP AREA (ARB.UNIT)

Fig. DA-2

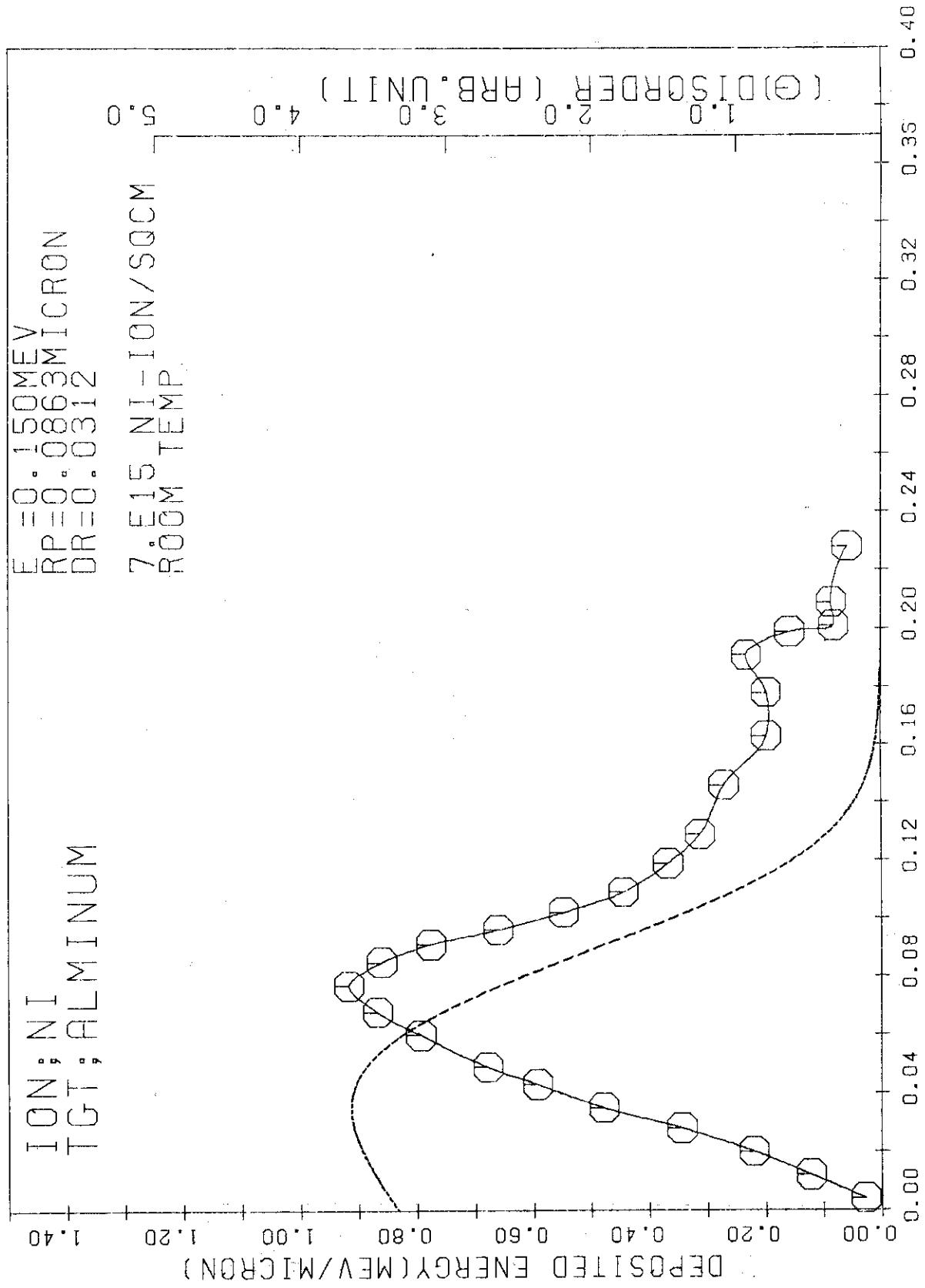
ION:NI
TGT:ALMINUM
E=0.150MEV
RP=0.0863MICRON
DR=0.0312
7.E15 NI-ION/SQCM
ROOM TEMP
DEPOSITED ENERGY(MEV/MICRON)
DEPTH (MICRON)
(Θ)DISORDER (ARB.UNIT)
0.00
0.20
0.40
0.60
0.80
1.00
1.20
1.40
0.00
0.04
0.08
0.12
0.16
0.20
0.24
0.28
0.32
0.35
0.40
1.0
2.0
3.0
4.0
5.0

Fig. DA-3

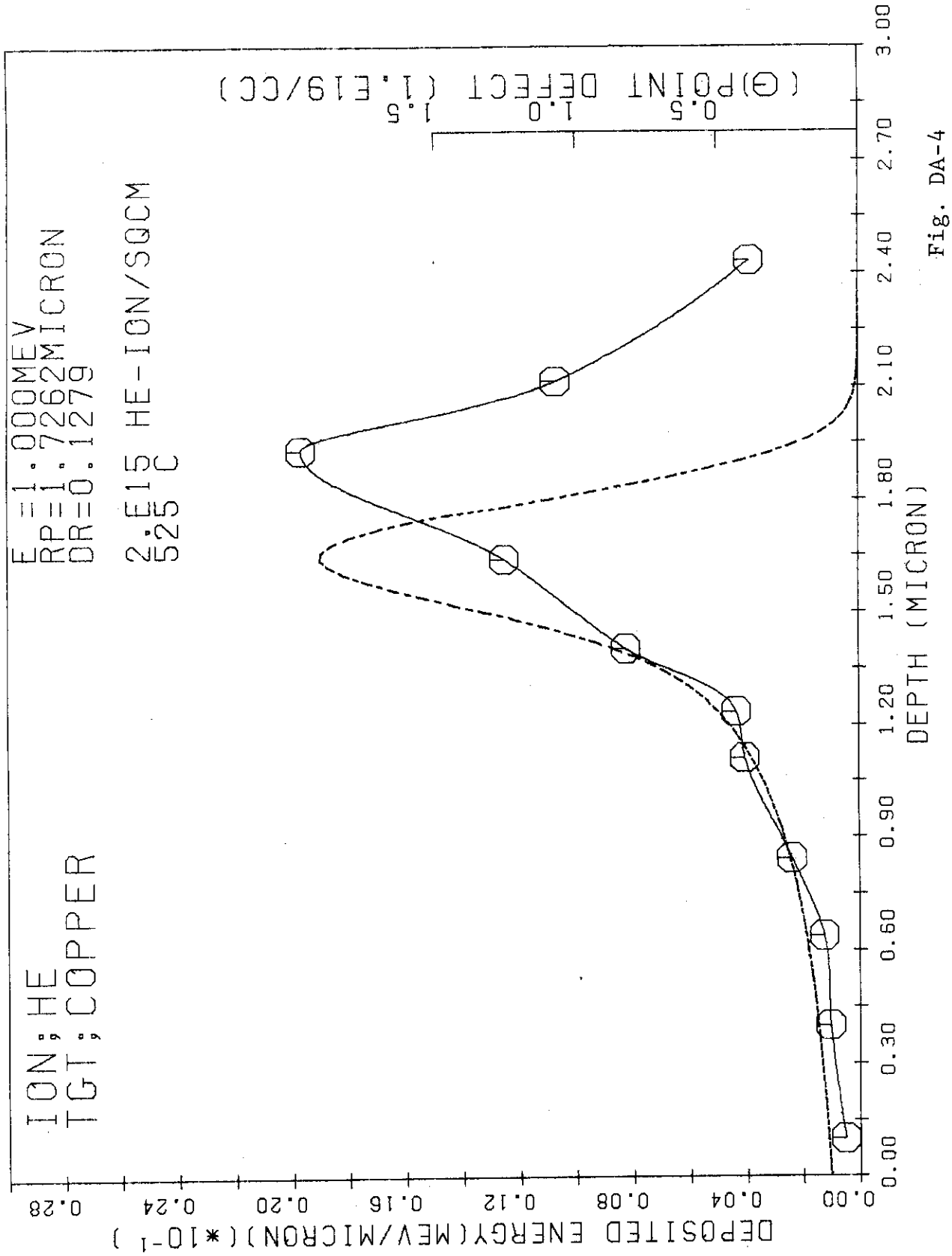
ION : HE
TGT : COPPER
E =1.000MEV
RP=1.7262MICRON
DR=0.1279
2.E15 HE-ION/SQCM
525 C
DEPOSITED ENERGY(MEV/MICRON)(*10-1)
DEPTH (MICRON)
(Q)POINT DEFECT (1.E19/CC)

Fig. DA-4

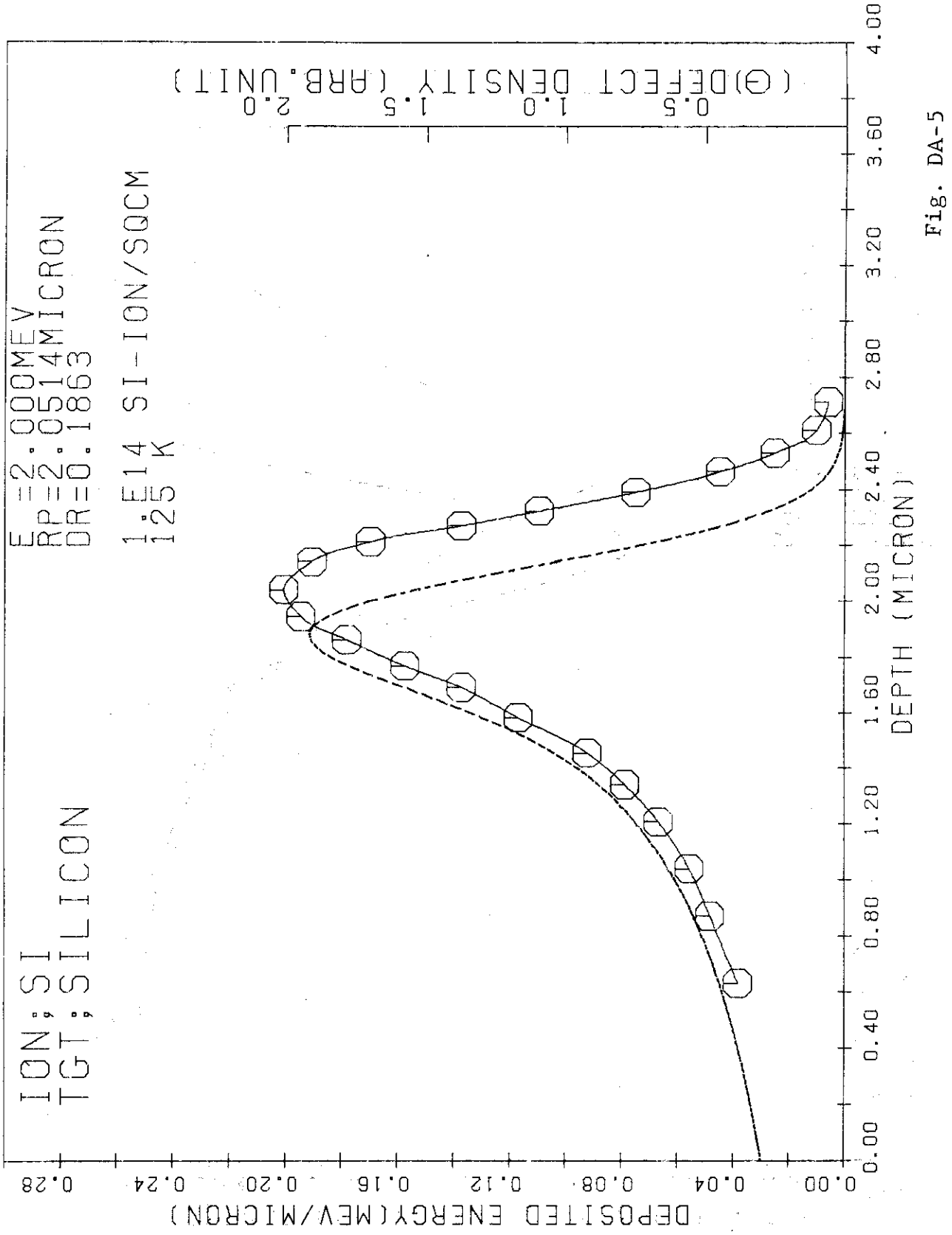
ION : SI
TGT : SILICON
E =2.000MEV
RP =2.0514MICRON
DR =0.1863
1.E14 SI-ION/SQCM
125 K
DEPOSITED ENERGY(MEV/MICRON)
0.00
0.04
0.08
0.12
0.16
0.20
0.24
0.28
DEPTH (MICRON)
0.00
0.40
0.80
1.20
1.60
2.00
2.40
2.80
3.20
3.60
4.00
(Q)DEFECT DENSITY (ARB.UNIT)
0.5
1.0
1.5
2.0

Fig. DA-5

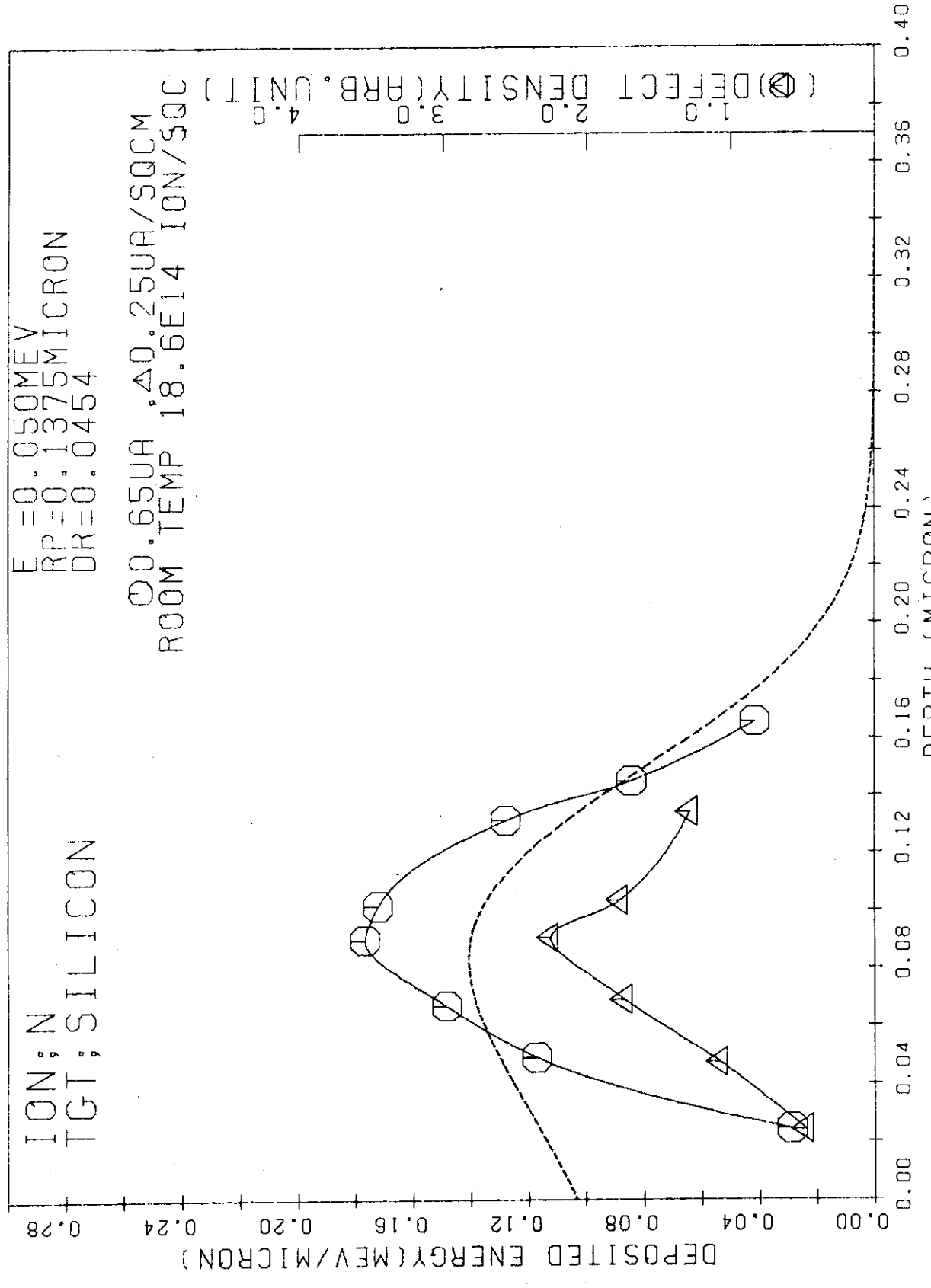
ION:N
TGT:SILICON
E=0.050MEV
RP=0.1375MICRON
DR=0.0454
Ø0.65UA ,Δ0.25UA/SQCM
ROOM TEMP 18.6E14 ION/SQC
(●)DEFECT DENSITY(ARB.UNIT)
DEPOSITED ENERGY(MEV/MICRON)
DEPTH (MICRON)

Fig. DA-6

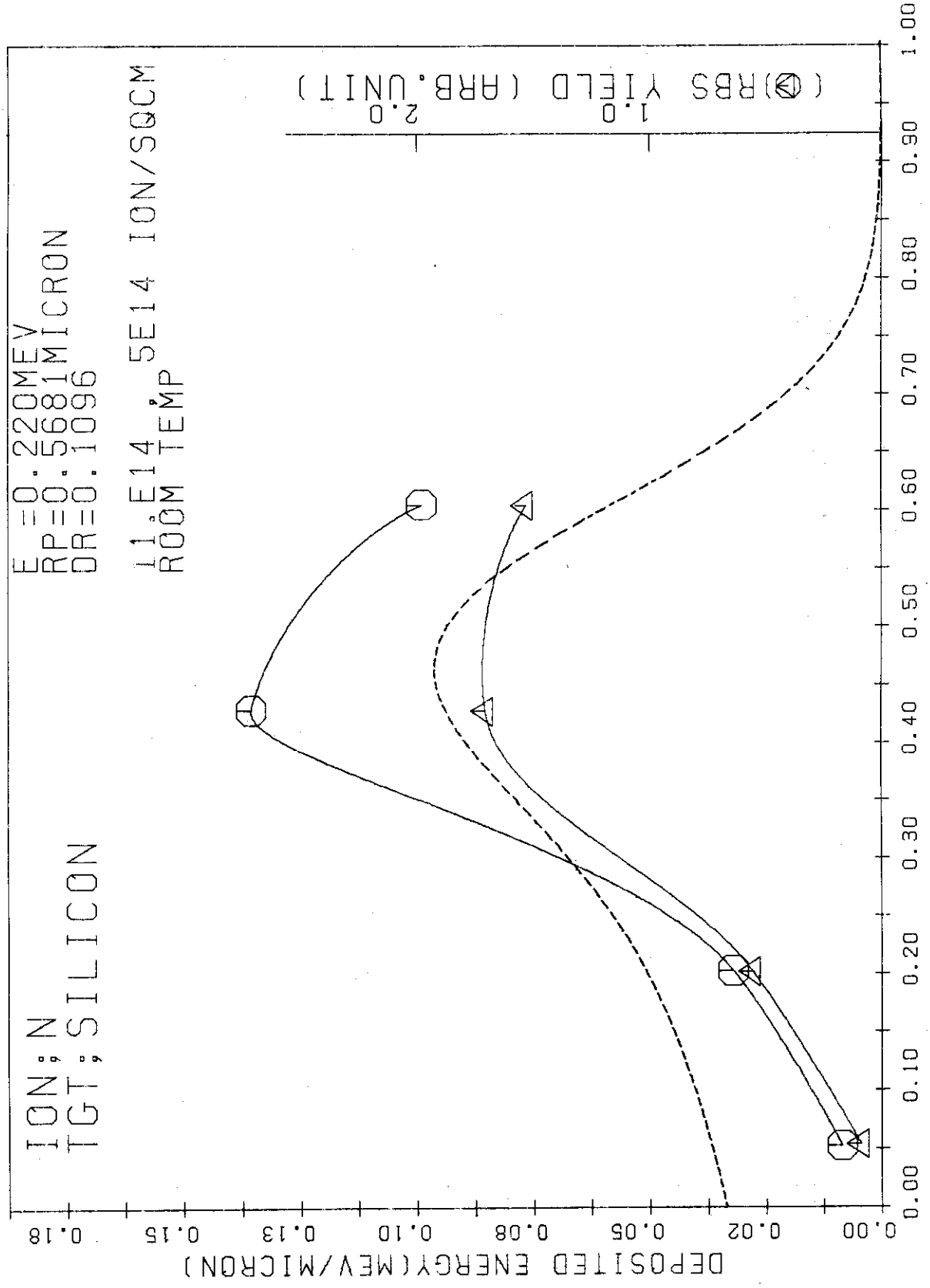
ION:N
TGT:SILICON
E=0.220MEV
RP=0.5681MICRON
DR=0.1096
1.1E14 5E14 ION/SQCM
ROOM TEMP
(●)RBS YIELD (ARB.UNIT)
1.0
2.0
DEPOSITED ENERGY(MEV/MICRON)
0.00
0.02
0.05
0.08
0.10
0.13
0.15
0.18
DEPTH (MICRON)
0.00
0.10
0.20
0.30
0.40
0.50
0.60
0.70
0.80
0.90
1.00

Fig. DA-7

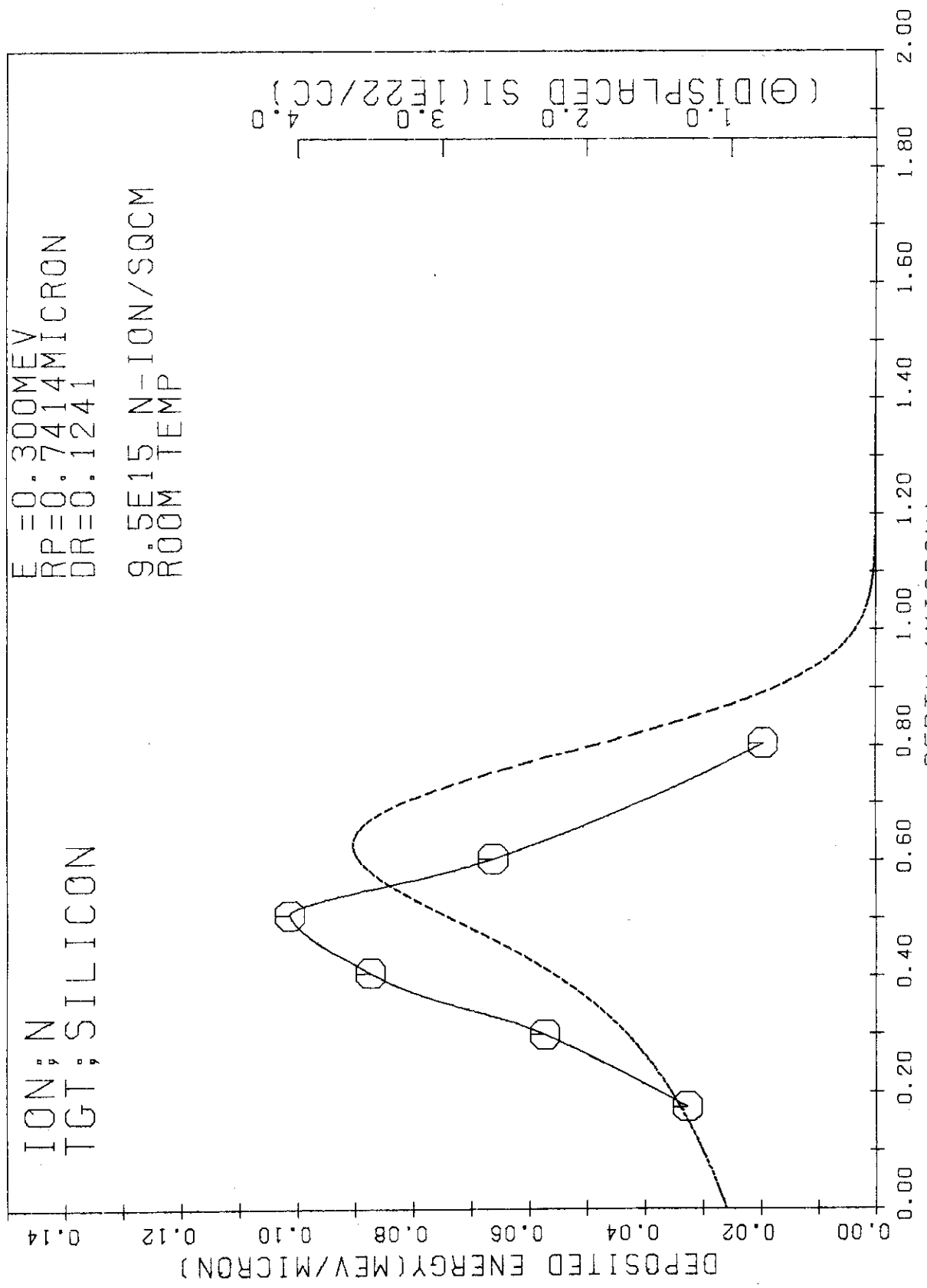
ION: N
TGT: SILICON
E =0.300MEV
RP=0.7414MICRON
DR=0.1241
9.5E15 N-ION/SQCM
ROOM TEMP
DEPOSITED ENERGY(MEV/MICRON)
DEPTH (MICRON)
(G)DISPLACED SI(1E22/CC)

Fig. DA-8

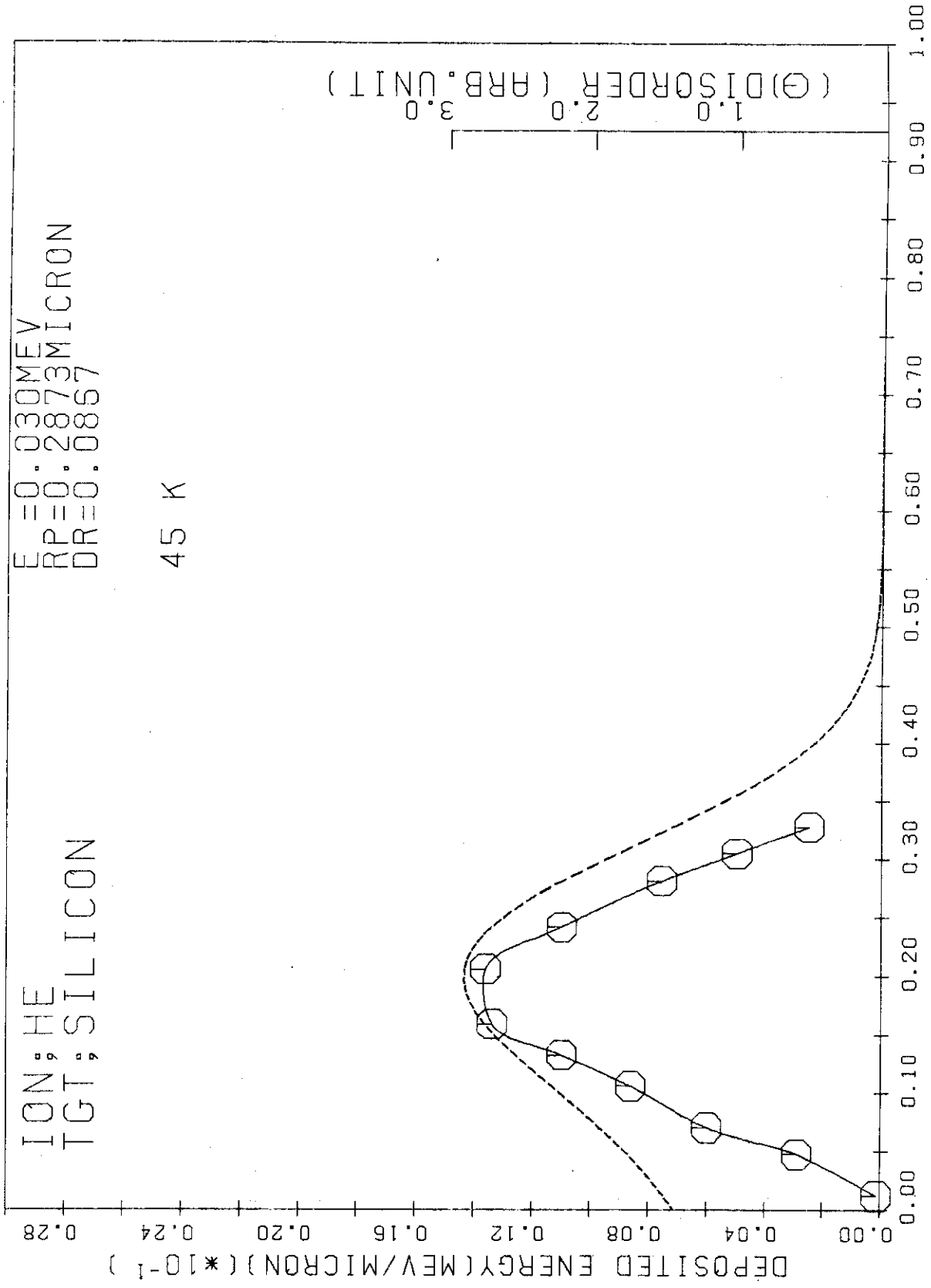
ION : HE
TGT : SILICON
E =0.030MEV
RP=0.28873MICRON
DR=0.0867
45 K
DEPOSITED ENERGY(MEV/MICRON)(*10⁻¹)
DEPTH (MICRON)
(Θ)DISORDER (ARB.UNIT)

Fig. DA-9

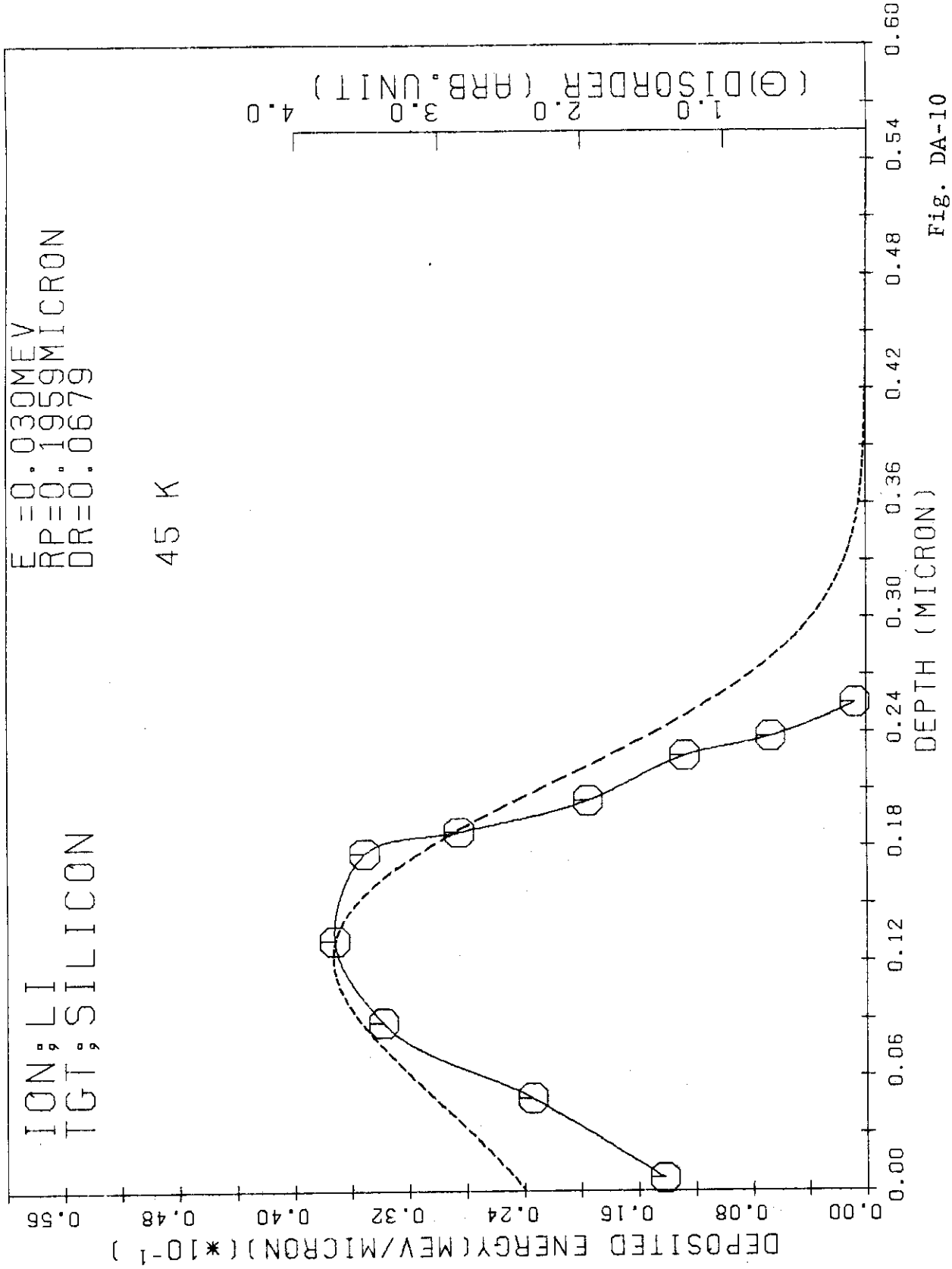
ION=LI
TGT=SILICON
E =0.030MEV
RP=0.1959MICRON
DR=0.0679
45 K
DEPOSITED ENERGY(MEV/MICRON)(*10⁻¹)
DEPTH (MICRON)
(Θ)DISORDER (ARB.UNIT)
0.00
0.08
0.16
0.24
0.32
0.40
0.48
0.56
0.00
0.06
0.12
0.18
0.24
0.30
0.36
0.42
0.48
0.54
0.60
1.0
2.0
3.0
4.0

Fig. DA-10

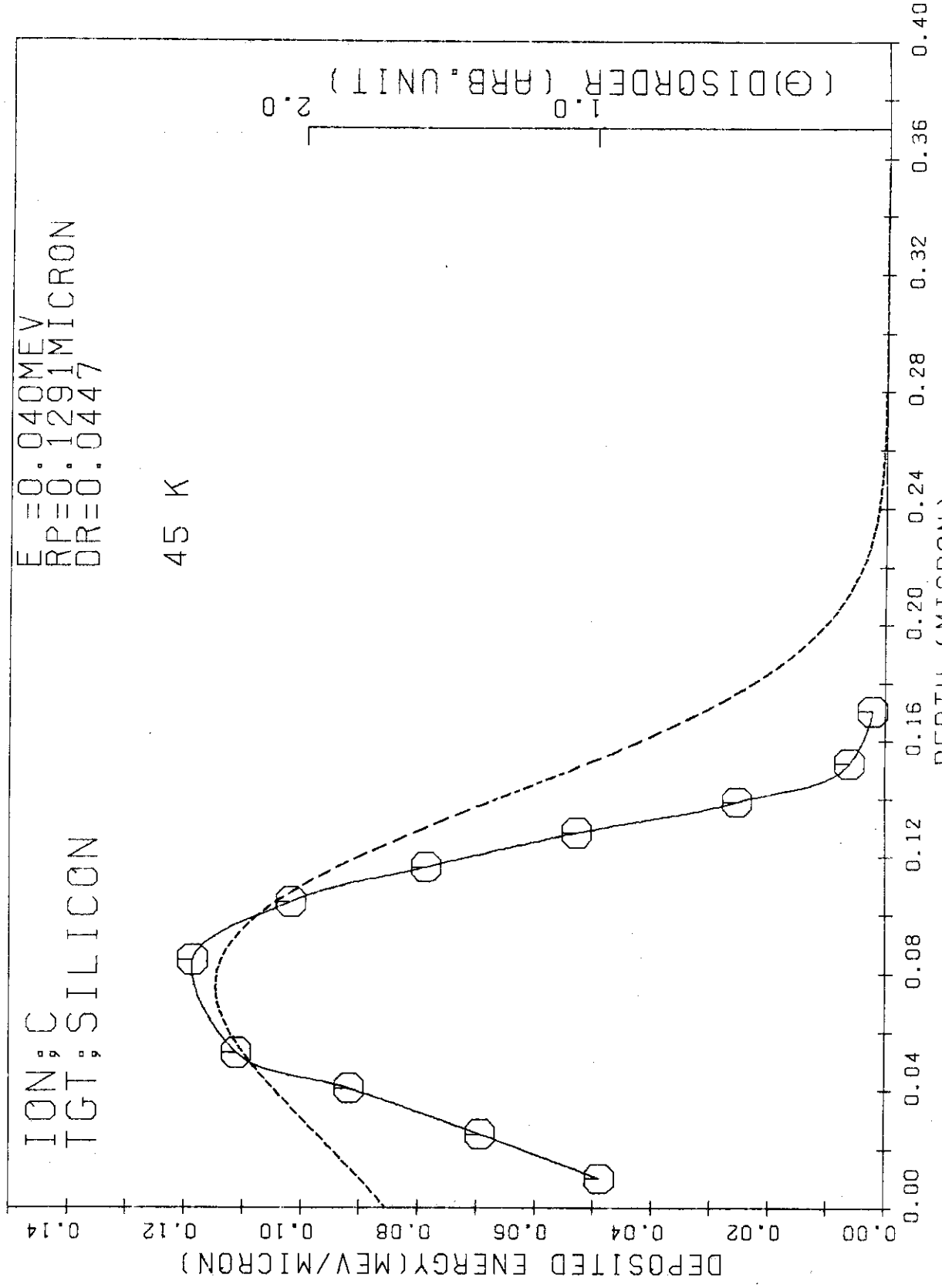
ION:C
TGT:SILICON
E =0.040MEV
RP=0.1291MICRON
DR=0.0447
45 K
DEPOSITED ENERGY(MEV/MICRON)
DEPTH (MICRON)
(Θ)DISORDER (ARB.UNIT)
0.00
0.02
0.04
0.06
0.08
0.10
0.12
0.14
0.00
0.04
0.08
0.12
0.16
0.20
0.24
0.28
0.32
0.36
0.40
1.0
2.0

Fig. DA-11

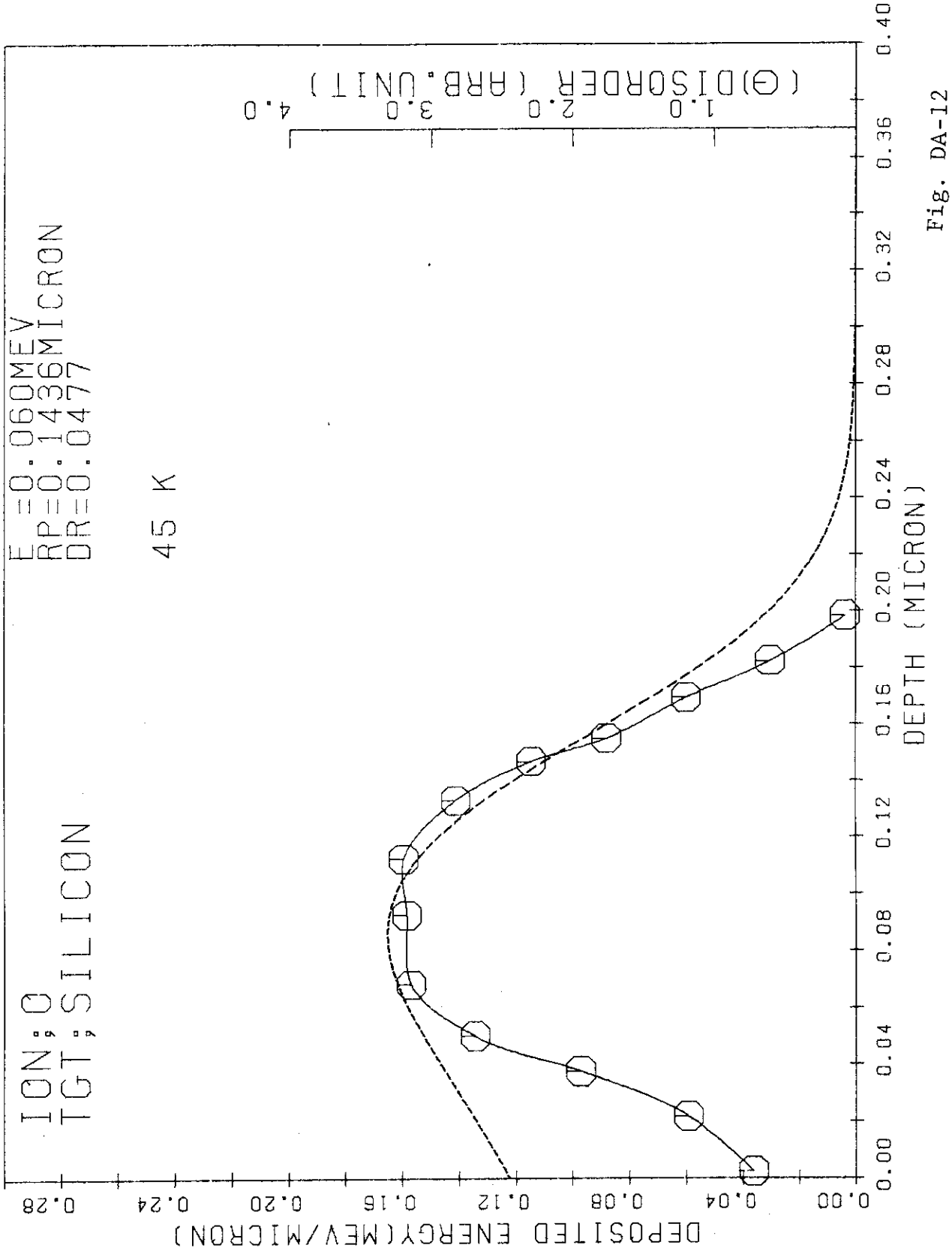
ION:C
TGT:SILICON
E =0.060MEV
RP=0.1436MICRON
DR=0.0477
45 K
DEPOSITED ENERGY(MEV/MICRON)
DEPTH (MICRON)
(G)DISORDER (ARB.UNIT)
0.00
0.04
0.08
0.12
0.16
0.20
0.24
0.28
0.32
0.36
0.40
1.0
2.0
3.0
4.0

Fig. DA-12

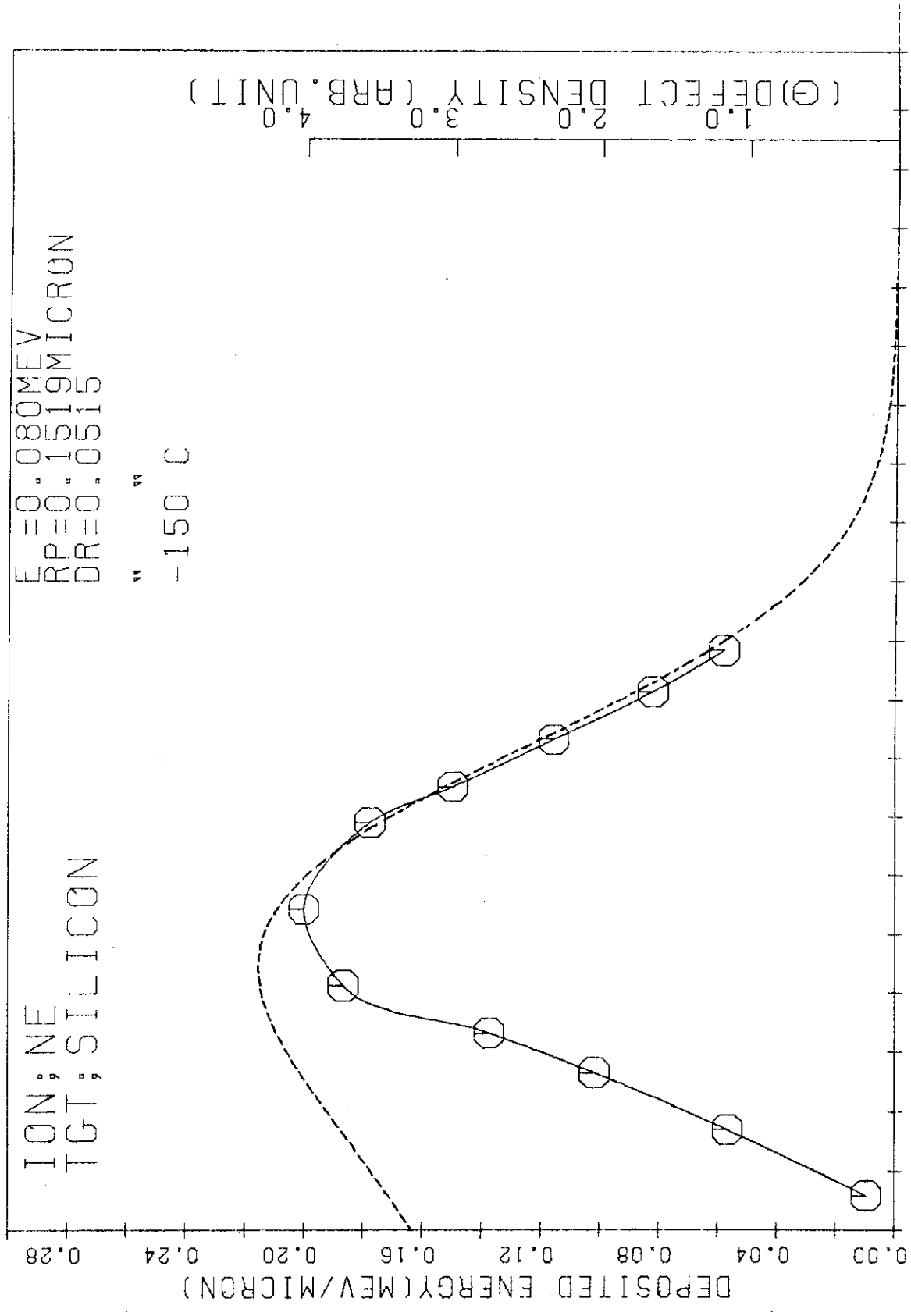
ION : NE
TGT : SILICON
E =0.080MEV
RP=0.15519MICRON
DR=0.0515
" -150 C
DEPOSITED ENERGY(MEV/MICRON)
DEPTH (MICRON)
(Θ)DEFECT DENSITY (ARB.UNIT)
0.00
0.04
0.08
0.12
0.16
0.20
0.24
0.28
0.32
0.36
0.40
1.0
2.0
3.0
4.0

Fig. DA-13

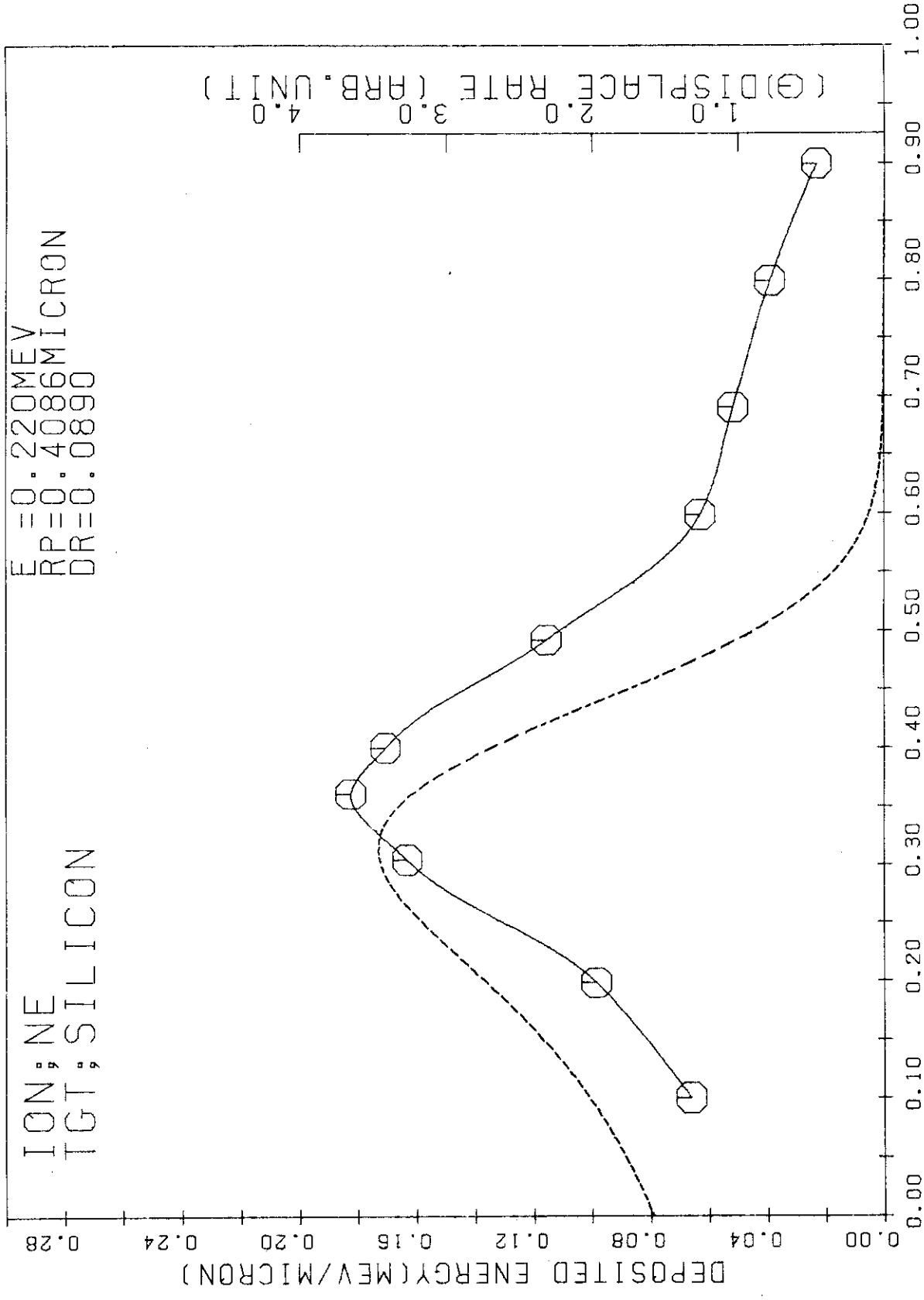
ION : NE
TGT : SILICON
E =0.220MEV
RP=0.40886MICRON
DR=0.0890
DEPOSITED ENERGY(MEV/MICRON)
DEPTH (MICRON)
(G)DISPLACE RATE (ARB.UNIT)

Fig. DA-14

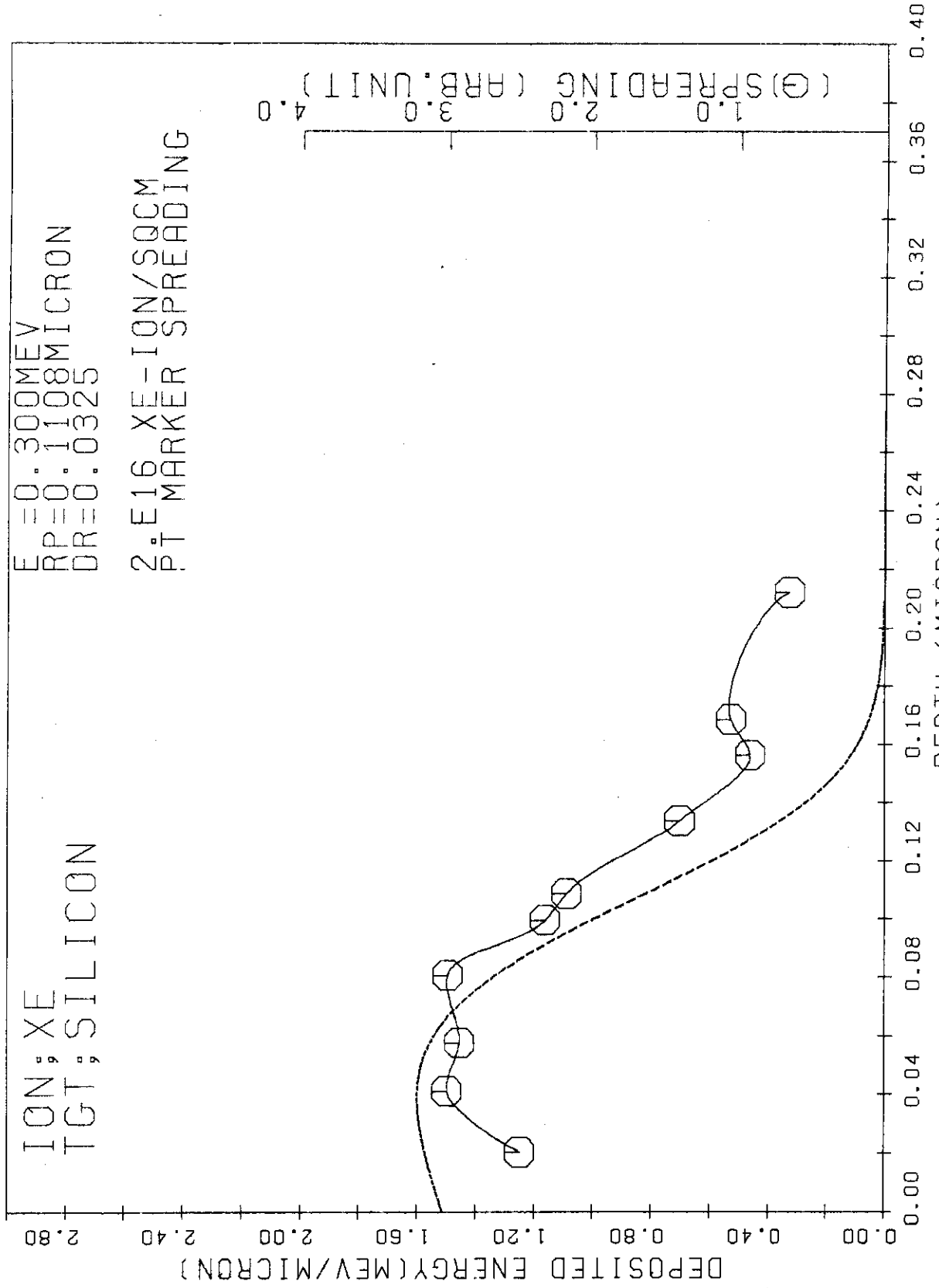
ION=XE
TGT=SILICON
E=0.300MEV
RP=0.1108MICRON
DR=0.0325
2.E16 XE-ION/SQCM
P.T MARKER SPREADING
DEPOSITED ENERGY(MEV/MICRON)
DEPTH (MICRON)
(Q)SPREADING (ARB.UNIT)
0.00
0.40
0.80
1.20
1.60
2.00
2.40
2.80
0.04
0.08
0.12
0.16
0.20
0.24
0.28
0.32
0.36
0.40
1.0
2.0
3.0
4.0

Fig. DA-15

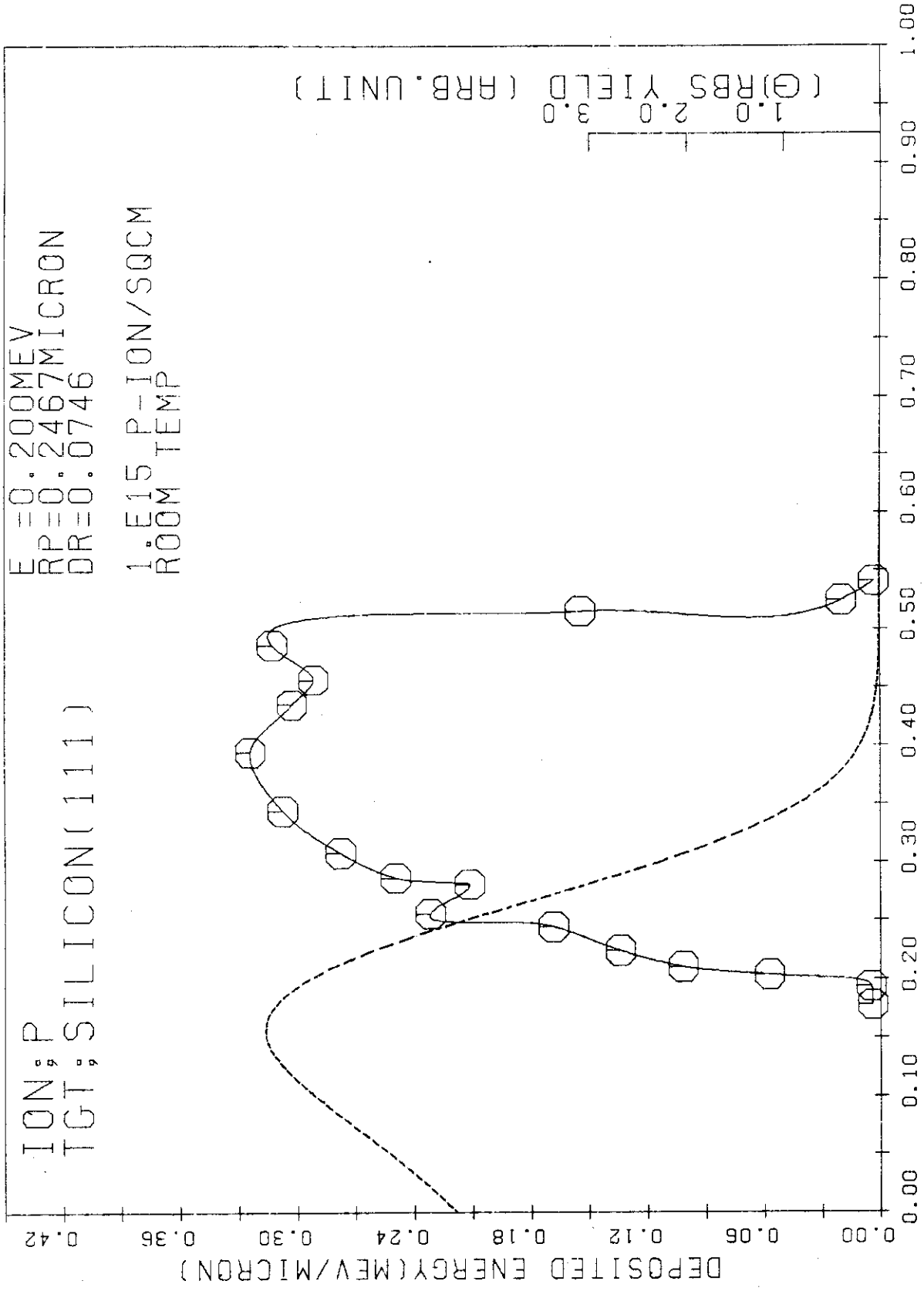
ION=P
TGT=SILICON(111)
E =0.200MEV
RP=0.2467MICRON
DR=0.0746
1.E15 P-ION/SQCM
ROOM TEMP
(Q)RBS YIELD (ARB.UNIT)
1.0 2.0 3.0
DEPTH (MICRON)
0.00 0.10 0.20 0.30 0.40 0.50 0.60 0.70 0.80 0.90 1.00
DEPOSITED ENERGY(MEV/MICRON)
0.00 0.06 0.12 0.18 0.24 0.30 0.36 0.42

Fig. DA-16

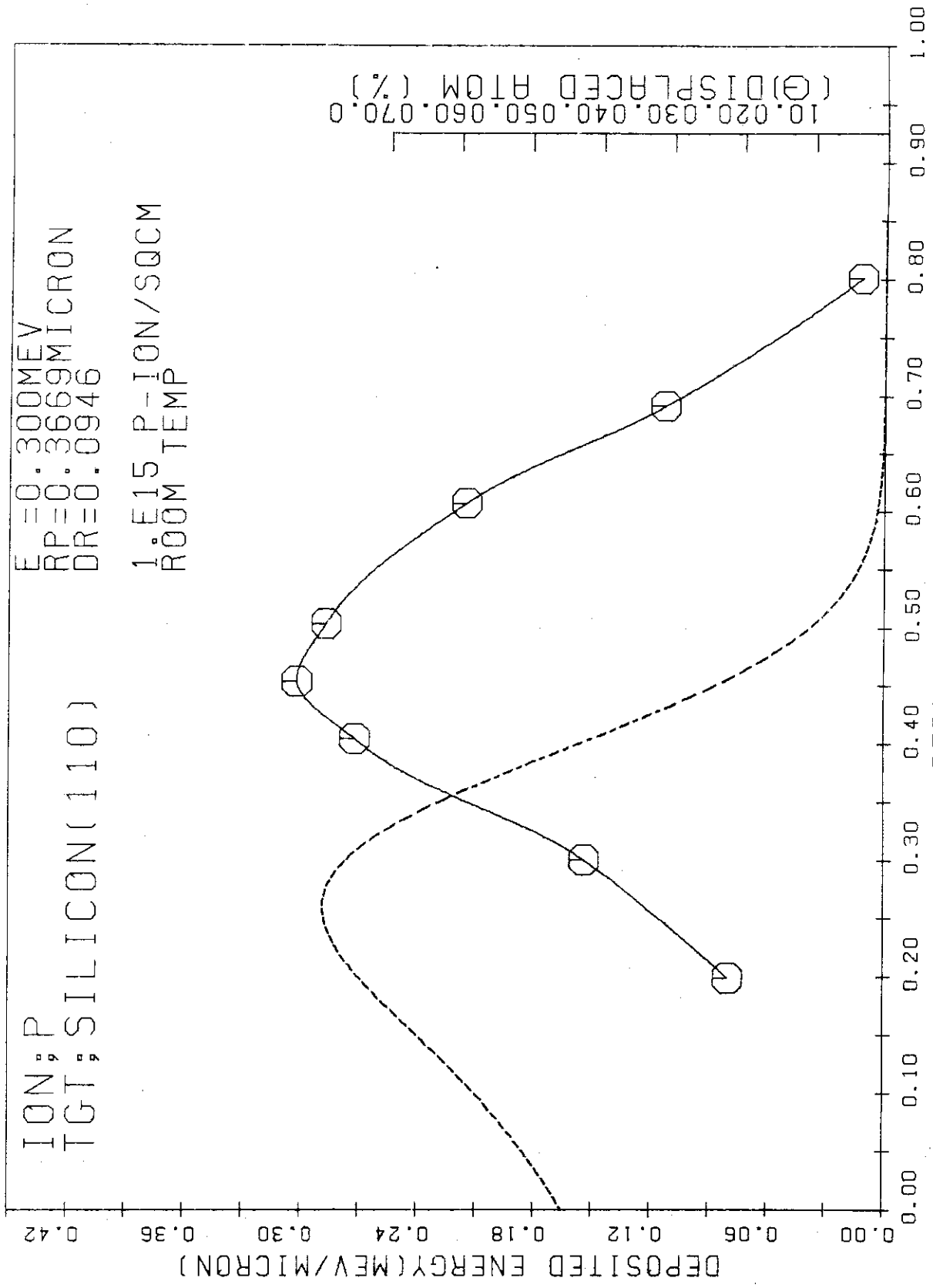
ION=P
TGT=SILICON(110)
E =0.300MEV
RP=0.3669MICRON
DR=0.0946
1.E15 P-ION/SQCM
ROOM TEMP
DEPOSITED ENERGY(MEV/MICRON)
DEPTH (MICRON)
(%) DISPLACED ATOM (%)

Fig. DA-17

Literatures

4-1. L. C. Feldman and L. C. Rodgers:
J. Appl. Phys. 41, 3776-3782 (1970)

4-2. E. K. Baranova, V. M. Gureev, Yu. V. Martynenko and K. V. Starinin:
Sov. Phys. Semicond. 13(10), 1176-1177 (1979)

4-3. B. Y. Tsaur, S. Matteson, G. Chapman, Z. L. Liau and M-A. Nicolet:
Appl. Phys. Lett. 35(10), 825-828 (1979)

4-4. K. F. Heidemann and H. F. Kappert:
Inst. Phys. Conf. Ser. No. 46, Chapter 8, 492-499 (1979)

4-5. I. A. Abroyan, N. F. Zitta, V. V. Konyshev, A. I. Titov and A. V. Khlebalkin:
Bull. Acad. Sci. USSR Phys. Ser. 40, No. 8. 170-173 (1976)

4-6 J. Narayan and O. S. Oen:
Proc. Workshop on Correlation of Neutron and Charged Particle Damage, ORNL CONF-760673, 356-368 (1976)

4-7. J. Narayan, T. S. Noggle and O. S. Oen:
ERDA-C-751006, 90-97 (1976)

4-8. P. Baeri, S. U. Campisano, G. Ciavola, G. Foti and E. Rimini:
Nucl. Inst. and Meth., 132, 237-240 (1976)

4-9. S. T. Picraux and D. M. Follstaedt, P. Baeri, S. U. Campisano, G. Foti and E. Rimini:
Rad. Eff. 49, 75-80 (1980)

4-10. H. E. Roosendaal, M. Weick, H. H. Hubbes and H. O. Lutz:
Rad. Eff. 45, 19-28 (1979)

4-11. H. F. Kappert, N. Pfannkuche, K. F. Heidemann and E. TE Kaat:
Rad. Eff. 45, 33-44 (1979)

4-12. F. Cembali, R. Galloni and F. Zignani:
Rad. Eff. 26, 161-171 (1975)

4-13. D. A. Thompson, J. E. Robinson and R. S. Walker:
Rad. Eff. 32, 169-175 (1977)

4-14. J. H. Evans:
Rad. Eff. 8, 115-120 (1971)

4-15. P. P. Pronko:
Nucl. Inst. and Meth., 132, 249-259 (1976)

4-16. M. O. Rault, H. Bernas and J. Chaumont:
Phil. Mag. A, 39,757-783 (1979)

4-17. A. Anttila, J. Hirvonen and M. Hautala:
Phys. Rev. 23, 1082-1808 (1981)

4-18. C. E. Christodoulides, N. J. Kadhim and G. Carter:
Rad. Eff. 52, 225-234 (1980)

4-19. D. I. R. Norris:
Atomic Collision Phenomena in Solids, 97-110 (1970)

4-20. S. T. Picraux, J. Bottiger and N. Rud:
Appl. Phys. Lett., 28, 179-181 (1976)

4-21. N. A. G. Ahmed, C. E. Christodoulides and G. Carter:
Rad. Eff. 52, 211-224 (1980)

4-22. D. A. Thompson, A. Golanski, K. H. Haugen and
D. V. Stevanovic:
Rad. Eff. 52, 69-84 (1980)

4-23. N. A. G. Ahmed, C. E. Christodoulides and G. Carter:
Physics Letter 69, 431-435 (1979)

APPENDIX 3. EXPERIMENTAL DATA AND LITERATURES CONCERNING IMPLANTED ATOMS

Table RA-1 is a list of projectile-target combinations which range data are compared. The experimental data on projected range as a function of projectile energy are reproduced in the figures from Fig. RA-1 to RA-6. The solid line in the figures shows the range obtained by the LSS calculation (ν=1.0). Fig. RA-7 is taken from Ref. 5-14.

In the figures from Fig. RB-1 to RB-46, the R_p data are compared with the LSS for each projectile - target combination shown in Table RB-1. The LSS calculation is performed for various ν ranging from 0.75 to 1.25 with interval of 0.05 (ν=1.0 for the original LSS theory). Fig. WA-1 to Fig. WA-4 show the range straggling as a function of the projectile energy. The experimental data are compared with the LSS calculation. In the last part of this Appendix 3, all the literatures collected are listed.

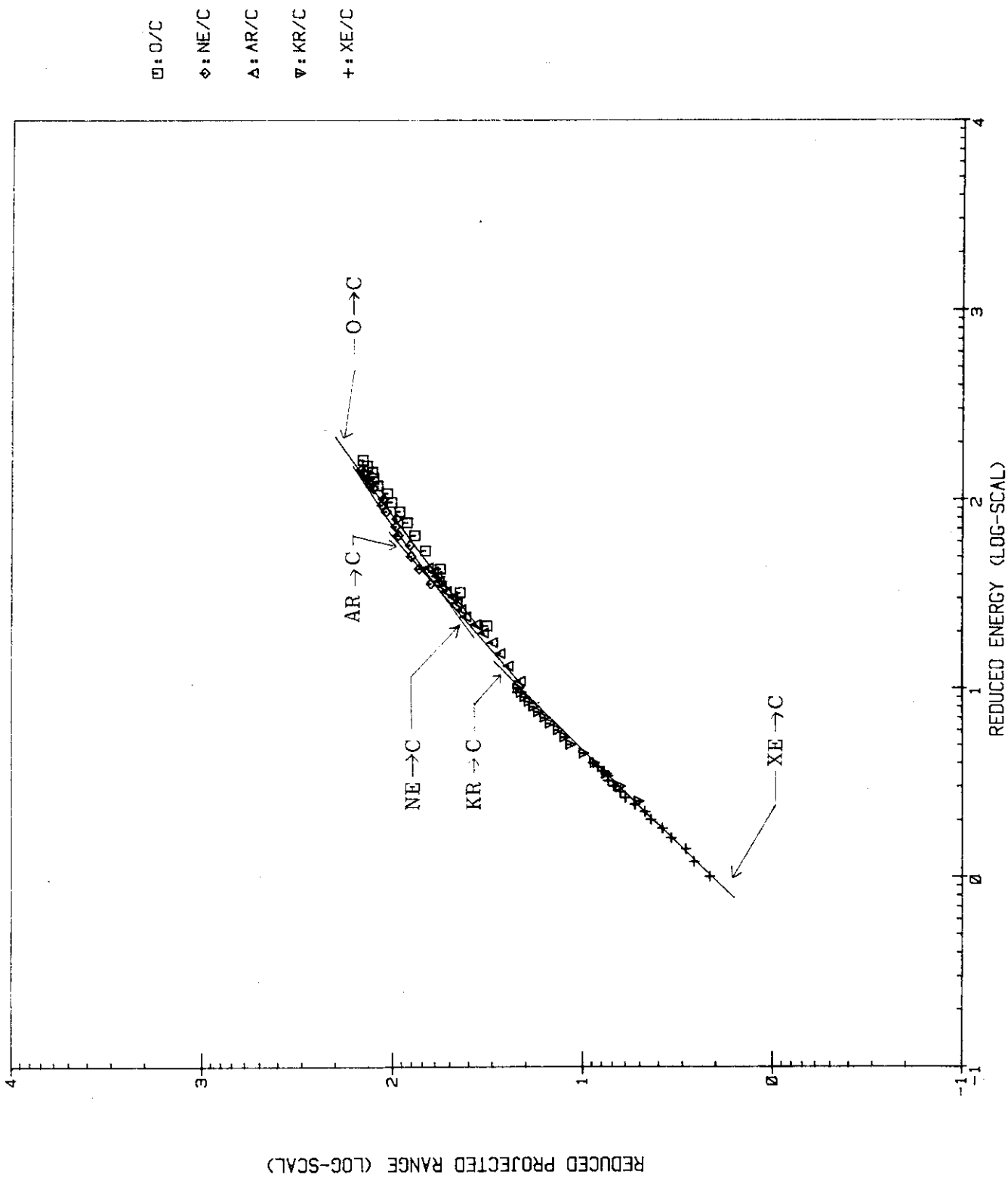
□: O/C
◇: NE/C
△: AR/C
▽: KR/C
+: XE/C
O→C
AR→C
NE→C
KR→C
XE→C
REDUCED ENERGY (LOG-SCAL)
REDUCED PROJECTED RANGE (LOG-SCAL)

Fig. RA-1

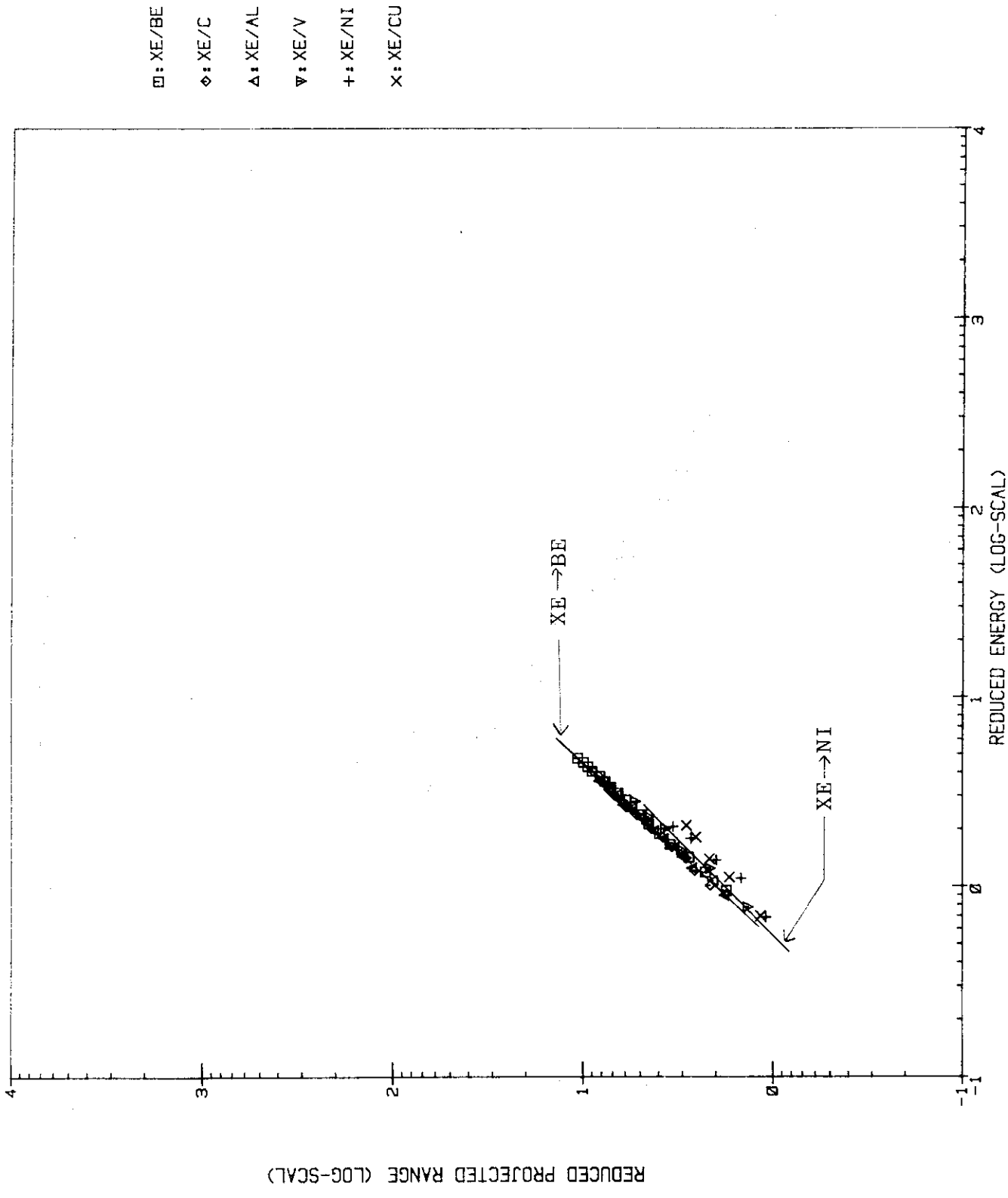
□: XE/BE
◇: XE/C
△: XE/AL
▽: XE/V
+: XE/NI
×: XE/CU
XE →BE
XE→NI
REDUCED ENERGY (LOG-SCAL)
REDUCED PROJECTED RANGE (LOG-SCAL)

Fig. RA-2

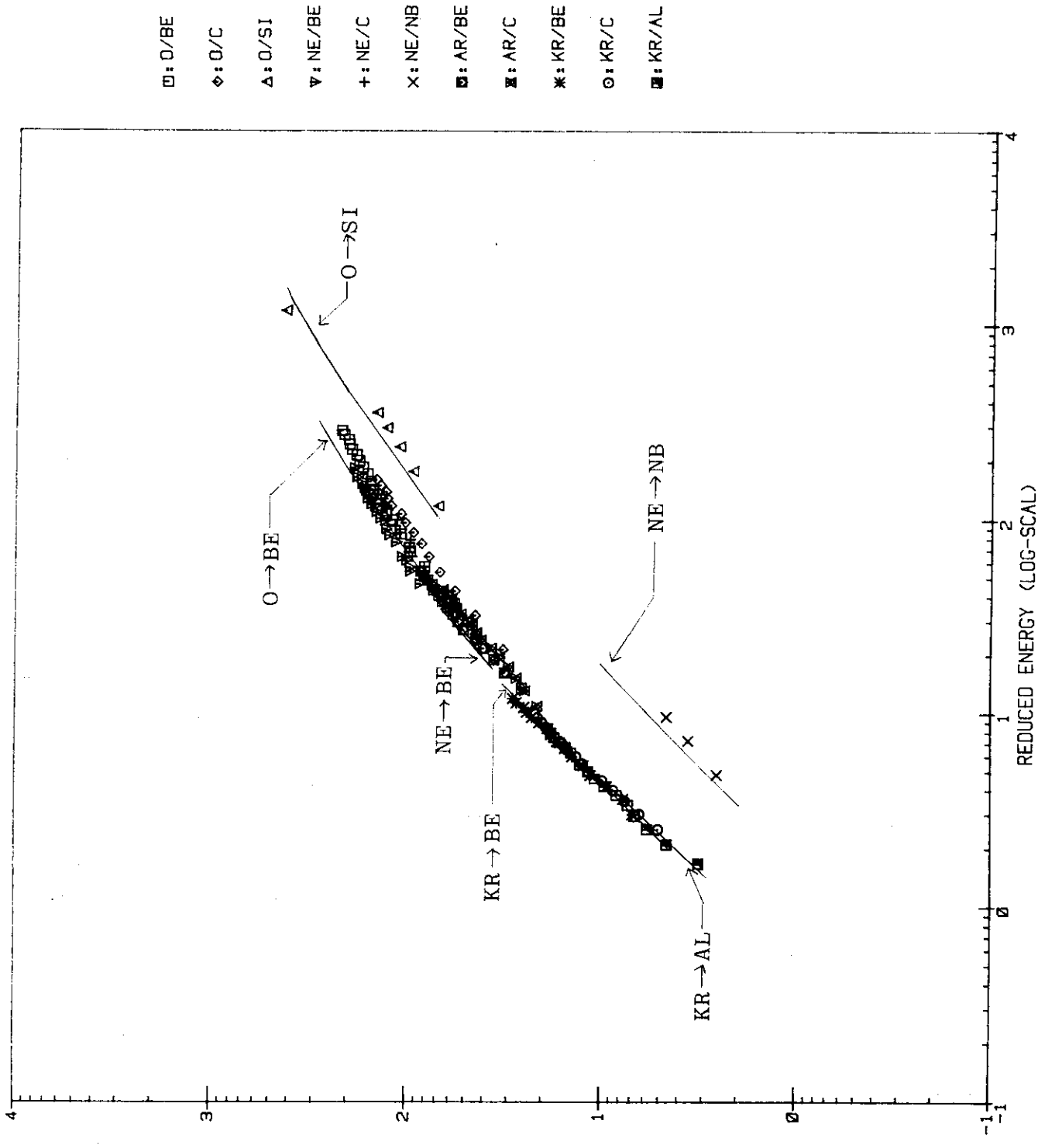
□: O/BE
◇: O/C
△: O/SI
▽: NE/BE
+: NE/C
×: NE/NB
▣: AR/BE
⧓: AR/C
✱: KR/BE
⊙: KR/C
▩: KR/AL
O→BE
O→SI
NE→BE
NE→NB
KR→BE
KR→AL
REDUCED ENERGY (LOG-SCAL)
REDUCED PROJECTED RANGE (LOG-SCAL)

Fig. RA-3

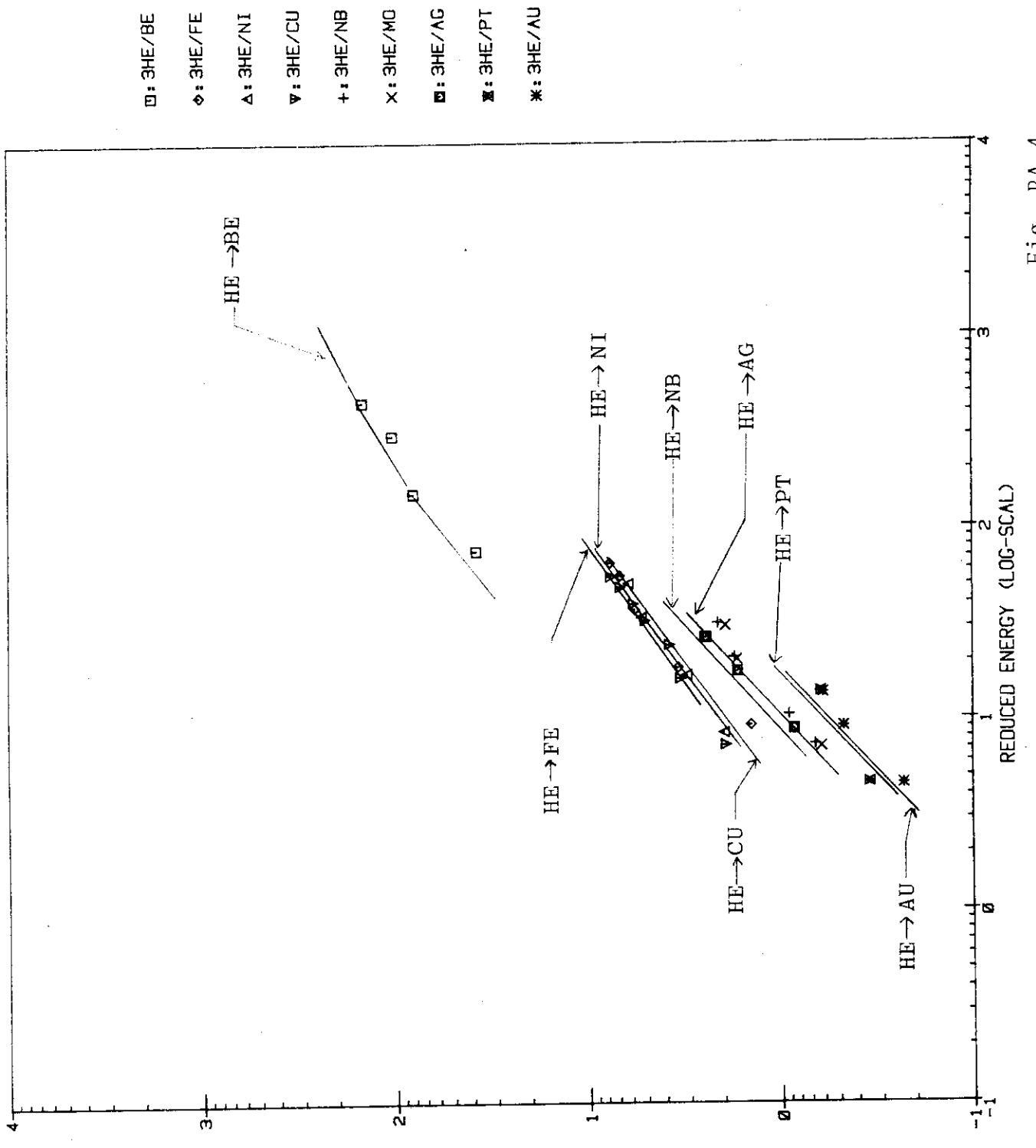
□: 3HE/BE
◇: 3HE/FE
△: 3HE/NI
Ψ: 3HE/CU
+: 3HE/NB
×: 3HE/MO
⊠: 3HE/AG
⊠: 3HE/PT
✱: 3HE/AU
HE →BE
HE→ NI
HE→NB
HE →AG
HE→PT
HE→ FE
HE→CU
HE→ AU
REDUCED ENERGY (LOG-SCAL)
REDUCED PROJECTED RANGE (LOG-SCAL)

Fig. RA-4

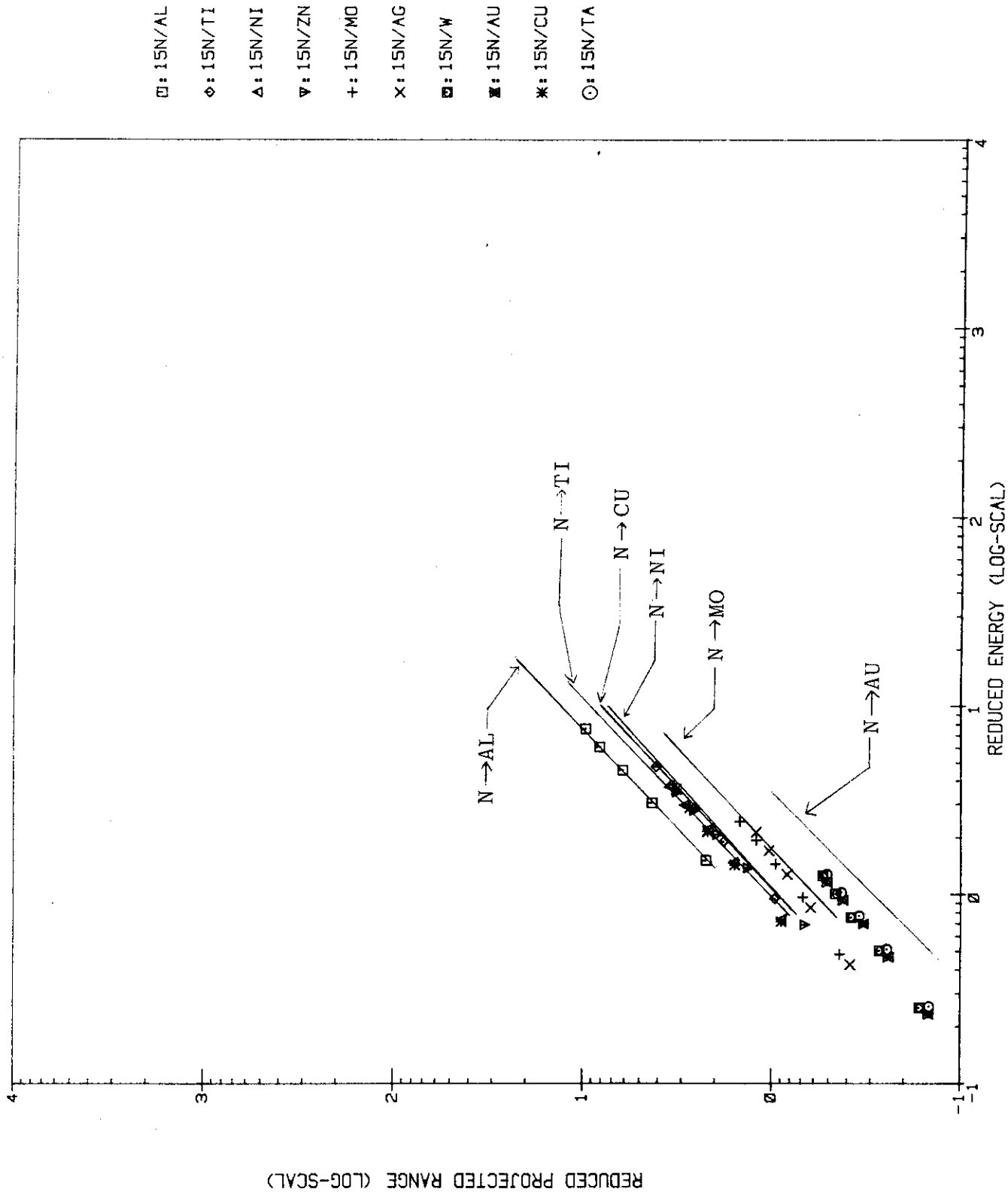
□: 15N/AL
◇: 15N/TI
△: 15N/NI
▽: 15N/ZN
+: 15N/MO
×: 15N/AG
▣: 15N/W
▣: 15N/AU
✳: 15N/CU
○: 15N/TA
N→AL
N→TI
N→CU
N→NI
N→MO
N→AU
REDUCED ENERGY (LOG-SCAL)
REDUCED PROJECTED RANGE (LOG-SCAL)

Fig. RA-5

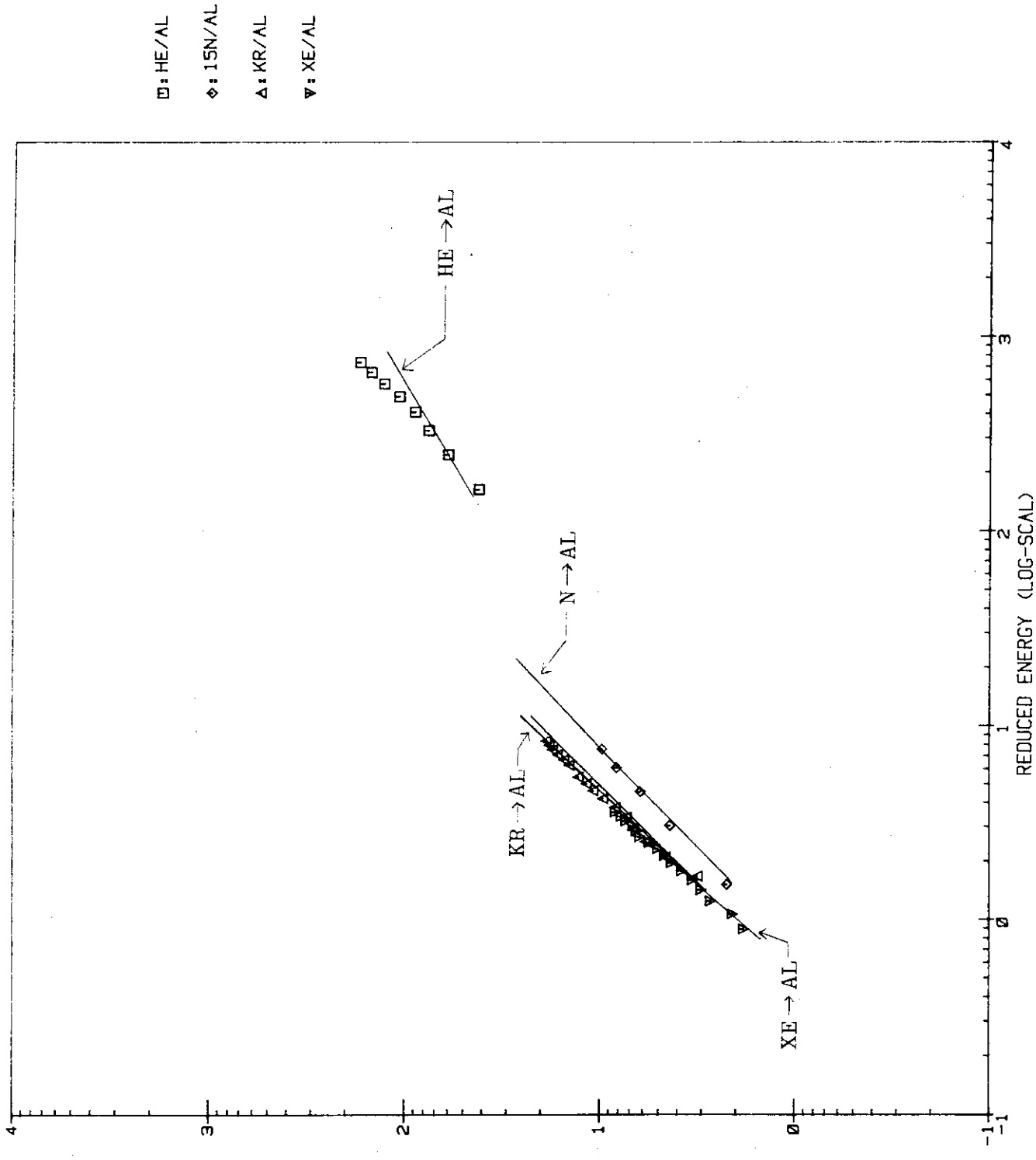
□: HE/AL
◇: 15N/AL
△: KR/AL
▽: XE/AL
HE → AL
N → AL
KR → AL
XE → AL
REDUCED ENERGY (LOG-SCAL)
REDUCED PROJECTED RANGE (LOG-SCAL)

Fig. RA-6

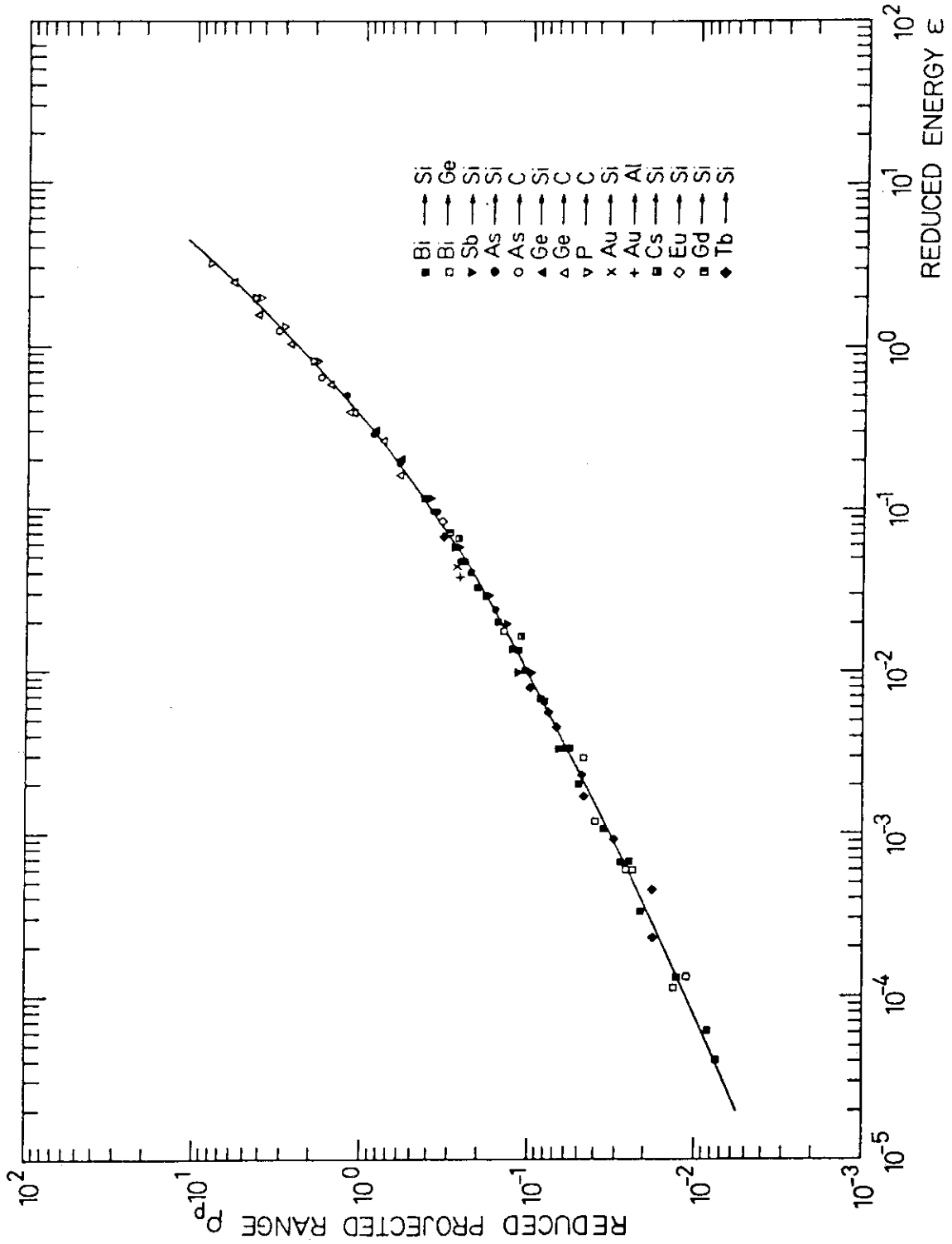

Previous and recent measurements of projected ranges in amorphous group IV materials by our laboratory.

Fig. RA-7 (From Ref.5-14)

Table RA-1

Ref.	Ion	Target	Energy	Comment
5-1.	Sb	Al	30keV	RBS Segregation effect
5-2.	O	Si	2MeV	
5-3.	H,He	Si	5-90KeV	Monte-Carlo
5-4.	Fe	Si	30KeV	AES TEM Damage density
5-5.	B	Si	10KeV	SIMS Atomic mixing
5-6.	N,As	Fe,Si	150KeV	RBS Energy loss
5-7.	B	Si	300KeV	AES Damage distribution Annealing
5-8.	Ne	Nb	300-600KeV	(p,Gamma) reaction
5-9.	Pb	Si	20-200KeV	RBS
5-10.	S,Se	GaAs	260-300KeV	SIMS Implantation Temp
5-11.	Si	GaAs	50-600KeV	C-V measurement Annealing
5-12.	B	Si	10-200KeV	(n,Alpha) reaction
5-13.	As	GaAs,Si	40-600KeV	SIMS Annealing
5-14.	As-Tb	Si,C,Ge		SIMS RBS
5-15.	He	W	0.1-1.5KeV	Field-Ion microscopy
5-16.	He	Ni	20KeV	ERD Void
5-17.	B	Si	300KeV	AES

Table RA－1 (Cont.)

Ref.	Ion	Target	Energy	Comment
5-18.	As,B	Si,SiO_2, Si_3N_4		(n,Alpha) reaction Activation analysis
5-19.	Ti,Ni	Zr		RBS Void Corrosion behaviour
5-20.	He	Ni,SUS316	8KeV	He trapping Bubble formation Surface blistering
5-21.	N	SUS304,316	400KeV	AES Damage Impurity distribution
5-22.	He	Al	150KeV	RBS
5-23.	N	Co	0.5-5KeV	AES
5-24.	B	Si		(n,Alpha) reaction Range paramerers
5-25.	P	Si	250KeV	SIMS Metallisation silicon
5-26.	B,Fe,In,P	Si		General,Review SIMS Annealing
5-27.	D	SUS304	6KeV	(^{3}He,Alpha) reaction Trapping Diffusion Damage
5-28.	B	Si		SIMS Annealing
5-29.	Ar,As	Si	130KeV	RBS Diffusion
5-30.	Cu	Si		Ion induced X-ray emission
5-31.	As,B	Si		Theoretical Monte-Carlo

Table RA－1 (Cont.)

Ref.	Ion	Target	Energy	Comment
5-32.	Cu	Ni	15MeV	Monte-Carlo E-DEP-1 Brice code Physics computing
5-33.	Li,Be,B	Si	150KeV	SIMS
5-34.	D	Ti	6.6KeV	(^{3}He,Alpha) reaction diffusion Impurity distribution
5-35.	An	Si	10-60KeV	SIMS RBS
5-36.	In	Si	30-90KeV	C-V measurement Annealing
5-37.	Be	Si	300KeV	SIMS Annealing Damage
5-38.	Be,Li	Si	Theoretical	Pearson IV distribution Range moments
5-39.	B-An	CMT	10-500KeV	(n,Alpha) reaction
5-40.	Li-Cs	Si,GaAs GaP,In,Ge	100-250KeV	SIMS
5-41.	O	Cu,Ni,Al	10-45KeV	Ion Probe Microanalyser
5-42.	O	Cu,Ni,Al	10-45KeV	Ion Probe Microanalyser
5-43.	Al	Zn	60KeV	(p,Gamma) reaction
5-44.	D	Si	0.1-5KeV	SIMS
5-45.	Ni,Cr,Ar	Fe	25KeV	Proton induced X-ray emission analysis
5-46.	B	CMT	60-400KeV	(n,Alpha) reaction

Table RA－1 (Cont.)

Ref.	Ion	Target	Energy	Comment
5-47.	H	Si	0.5-300KeV	(n,Gamma) reaction
5-48.	O	Si	2-20MeV	X-ray emission
5-49.	He	Be-Au	100-300KeV	(n,p) reaction
5-50.	N	Si	0.67-3.17MeV	RBS
5-51.	An,Sb	C(Diamond)	350KeV	(n,Gamma) reaction
5-52.	Li	C(Diamond)	30-450KeV	SIMS
5-53.	He	Nb	30,100KeV	RBS SEM Blister
5-54.	He	Ni	20KeV	TEM Bubbles
5-55.	Si-Te	GaAs,GaP	10-350KeV	Calculation
5-56.	P,As	SiO_2		SIMS
5-57.	Zn,N	SiO_2,GaAs	50-300KeV	SIMS Impurity distribution Masking effect
5-58.	N	Al-Au	20-200KeV	(p,Gamma) reaction
5-59.	H	W	300,475eV	Field ion microscopy Diffusion

Table RA－1 (Cont.)

Ref.	Ion	Target	Energy	Comment
5-60.	N	Fe,Zr,Ni,Au	~200KeV	(p,Gamma)reaction
5-61.	He	Nb,Cu,Be,Al	~25KeV	ERD Monte-Calro
5-62.	He	Al	.4-1.8MeV	(p,Gamma)reaction
5-63.	He	Ni,Nb	30KeV	(p,p),(D,Alpha) reaction
5-64.	Ne	Ti,Si		(p,Gamma) reaction
5-65.	D	Zr	10-30KeV	(^{3}He,Alpha) reaction Temp-dependent Annealing
5-66.	D	C,Al,Ni,Zr	10-30KeV	(^{3}He,Alpha) reaction
5-67.	O,Si	Si	2MeV	RBS Damage TEM
5-68.	B	Si	100,150KeV	SIMS Sputtered surface
5-69.	^{3}He	C,Al,Si,V Ni,Zr	20-60KeV	(D,Alpha) reaction
5-70.	Ar	LiO_2	300,450KeV	RBS
5-71.	He	Ge	1MeV	Comparison of range Codes
5-72.	Havey ion	Ni,Ta,Au	~50Mev	Gamma-ray spectroscopy Radioactive evaporation

Table RA－1 (Cont.)

Ref.	Ion	Target	Energy	Comment
5-73.	B	Si	20-40KeV	(n,Alpha) reaction
5-74.	He	Cu	25Kev	ERD Blistering
5-75.	Li	Nb	8MeV	(p,N) reaction Annealing
5-76.	As,Si	SiO_2,Si_3N_4	50-500keV	Neutron activation
5-77.	T	Ti		Neutron spectra Time-of-flight specroscopy
5-78.	C,Na,Mg Al,S,Si	Ta,Al	20-100KeV	(p,Gamma) reaction
5-79.	B	Si		(n,Alpha) reaction
5-80.	B	Si	150KeV	Theoretical Monte-calro
5-81.	P	Si	50KeV	Neutron activation analysis
5-82.	B	Si	80KeV	C-V measurement
5-83.	As	SiO_2	100-350KeV	RBS
5-84.	Bi,Xe,Kr,Ar	C,Al,Si	0.12-2MeV	RBS
5-85.	D	Al,Au	20KeV	
5-86.	Cu,Au	Cu,Au	1-100KeV	Monte-calro

Table RA－1 (Cont.)

Ref.	Ion	Target	Energy	Comment
5-87.	C,N,O,F,Ne	Be,C	.5-2MeV	RBS Stopping power
5-88.	B,P,As	Si	.1-1.8MeV	
5-89.	Rb,Cs	Cu,Ag,Au		Energy straggling
	H-I		20KeV	RBS
5-90.	H,He	Ar,N_2,O_2	.2-2MeV	
5-91.	Ar,Kr,Xe	Be,C,Ag	.5-2MeV	RBS
5-92.	Cs-Au	Al	100KeV	RBS

Table RB-1

Fig.	Ion	Target
RB-1	He	Aluminum
RB-2	^{3}He	Beryllium
RB-3	^{3}He	Iron
RB-4	^{3}He	Nickel
RB-5	^{3}He	Copper
RB-6	^{3}He	Niobium
RB-7	^{3}He	Molybdenum
RB-8	^{3}He	Silver
RB-9	^{3}He	Platinum
RB-10	^{3}He	Gold
RB-11	C	Beryllium
RB-12	^{13}C	Tantalum
RB-13	N	Beryllium
RB-14	N	Iron
RB-15	N	Zirconium
RB-16	N	Gold
RB-17	^{15}N	Aluminum
RB-18	^{15}N	Titanium
RB-19	^{15}N	Nickel
RB-20	^{15}N	Copper
RB-21	^{15}N	Zinc
RB-22	^{15}N	Molybdenum
RB-23	^{15}N	Silver
RB-24	^{15}N	Tungsten
RB-25	^{15}N	Gold
RB-26	O	Beryllium
RB-27	O	Carbon
RB-28	O	Silicon
RB-29	Ne	Beryllium
RB-30	Ne	Carbon
RB-31	Ne	Niobium
RB-32	Na	Tantalum
RB-33	^{26}Mg	Tantalum
RB-34	^{29}Si	Tantalum
RB-35	Al	Tantalum
RB-36	Ar	Beryllium
RB-37	Ar	Carbon
RB-38	Kr	Beryllium
RB-39	Kr	Carbon
RB-40	Kr	Aluminum
RB-41	Xe	Beryllium
RB-42	Xe	Carbon
RB-43	Xe	Aluminum
RB-44	Xe	Vanadium
RB-45	Xe	Nickel
RB-46	Xe	Copper

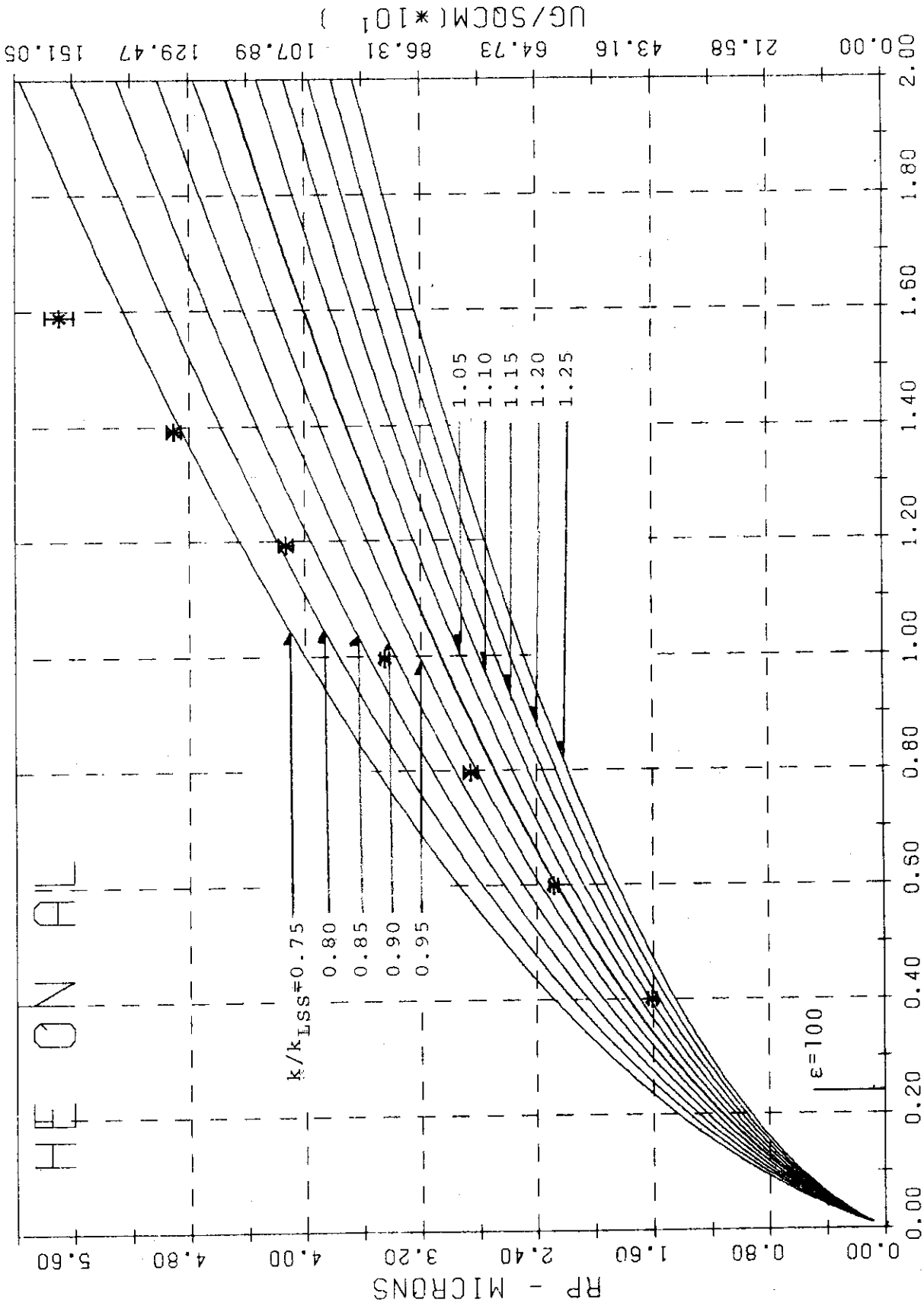

Fig. RB-1 (From Ref.5-62)

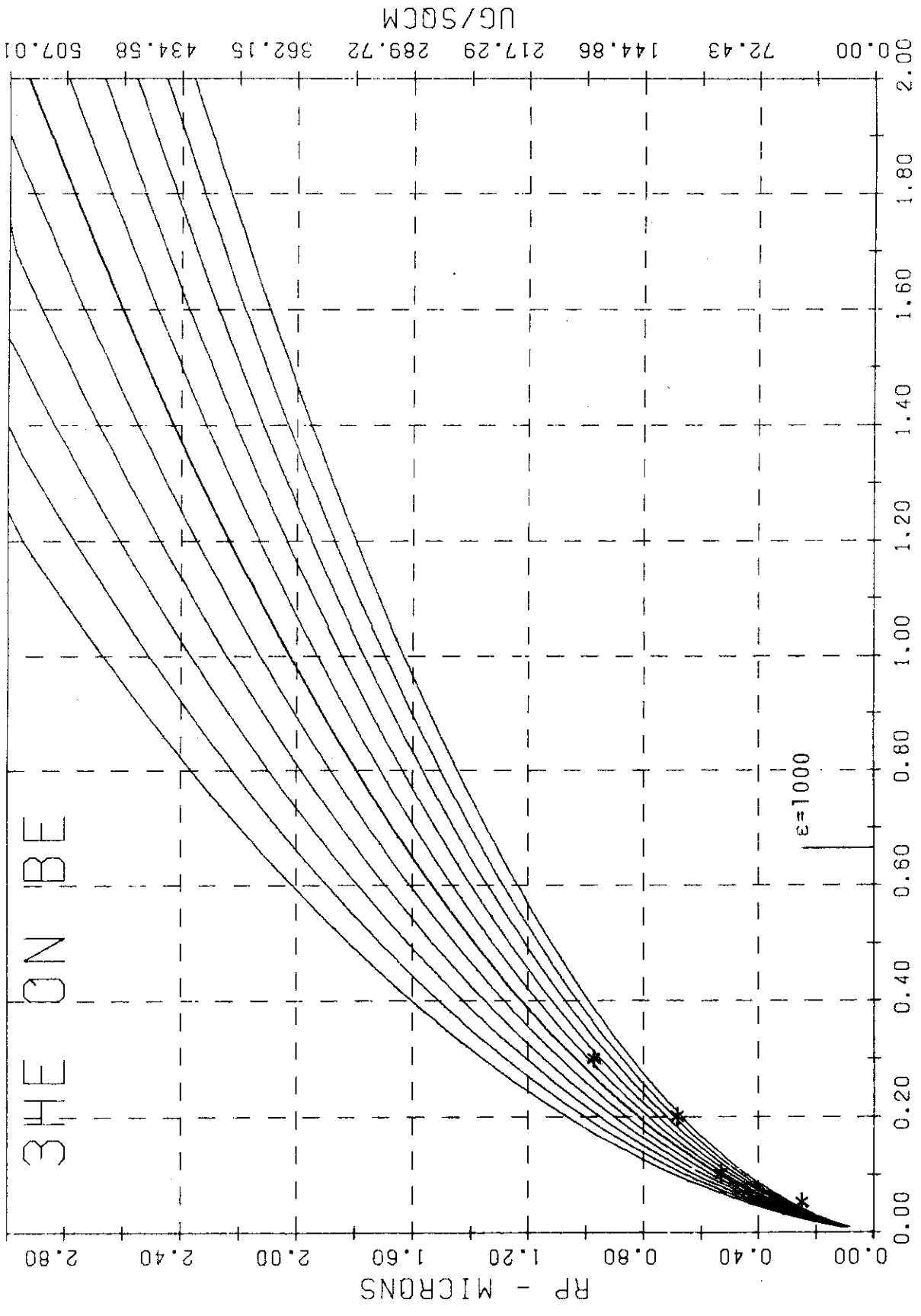

Fig. RB-2 (From Ref.5-49)

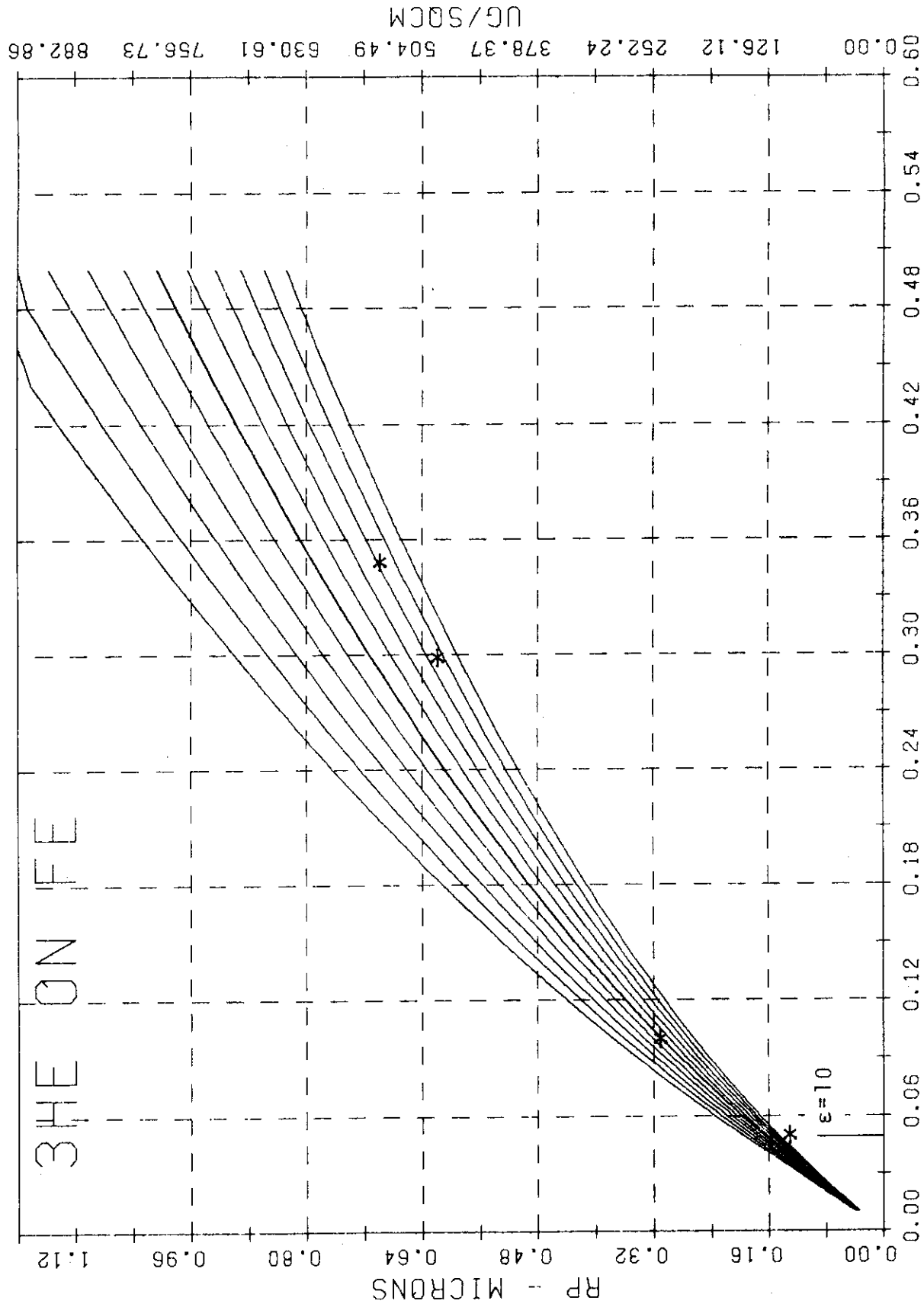

Fig. RB-3 (From Ref.5-49)

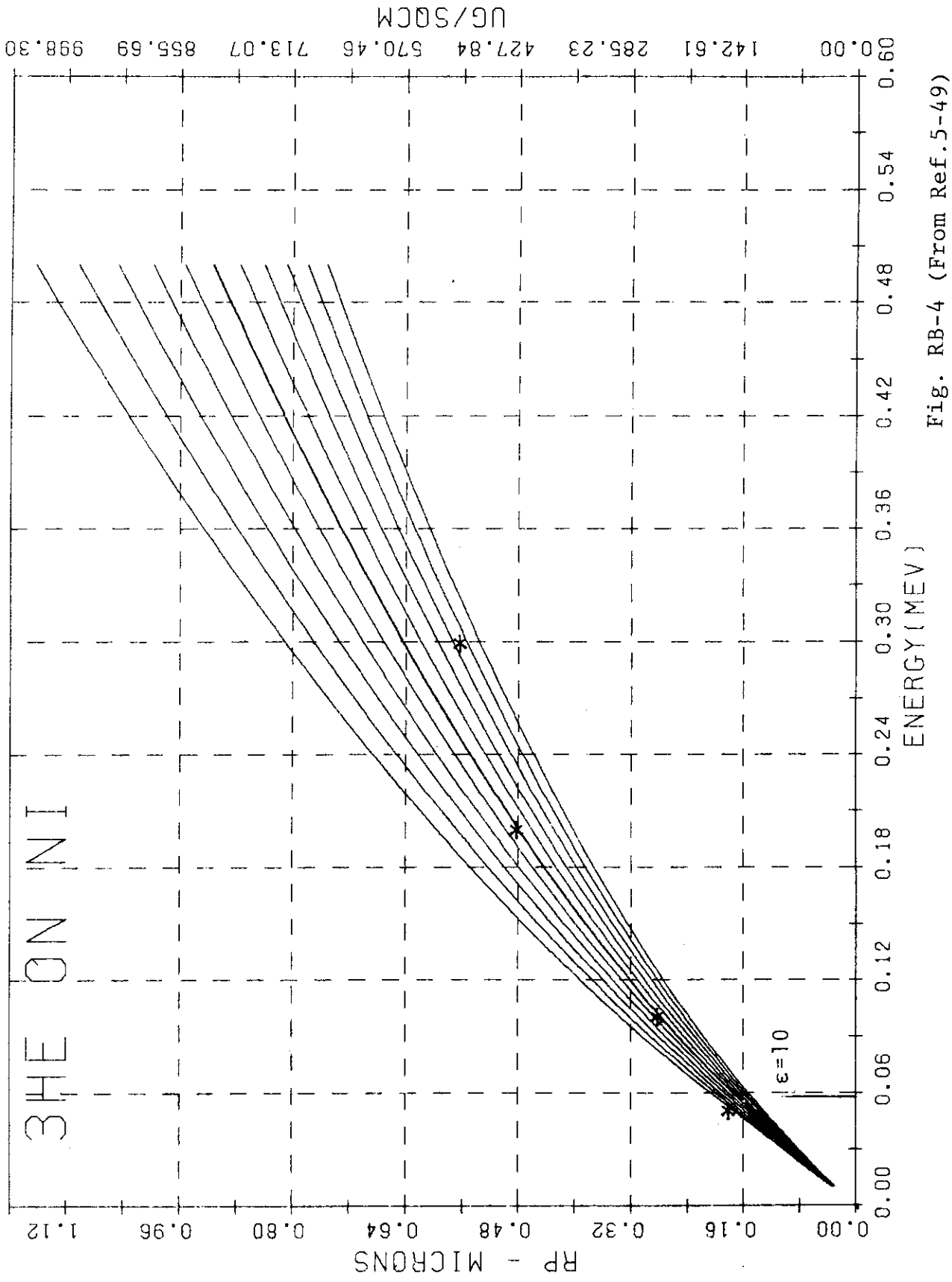

Fig. RB-4 (From Ref.5-49)

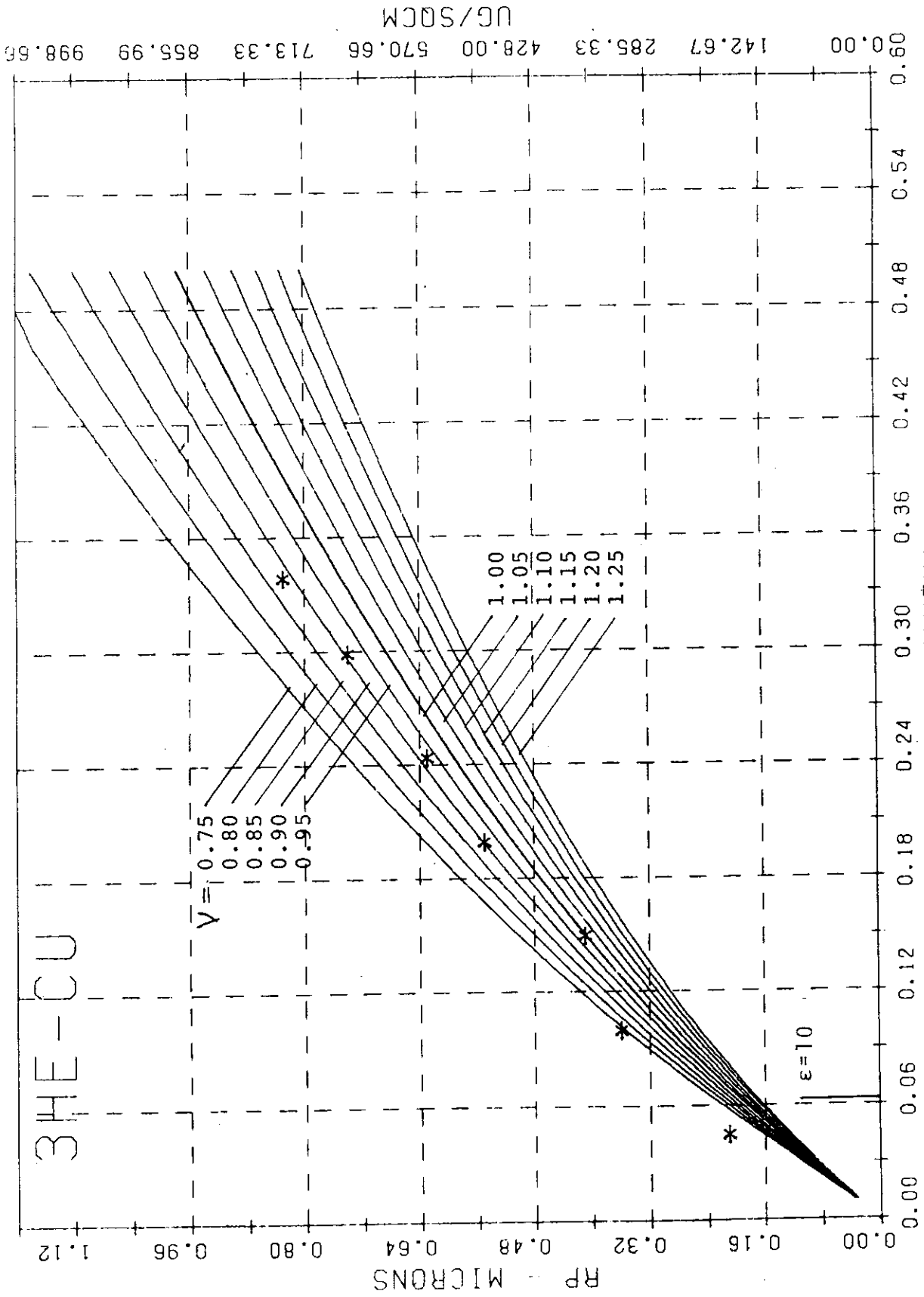

Fig. RB-5 (From Ref.5-49)

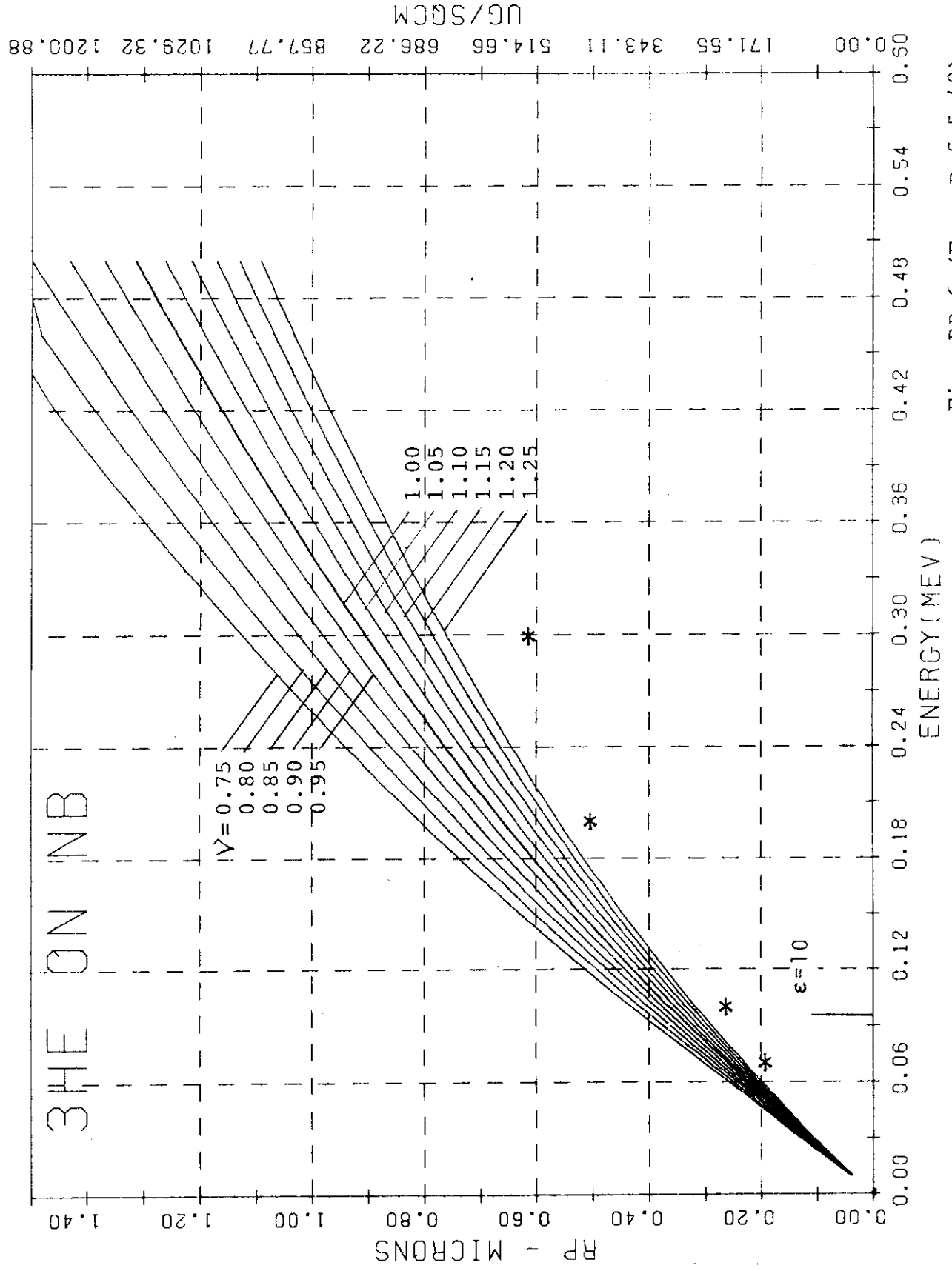

Fig. RB-6 (From Ref.5-49)

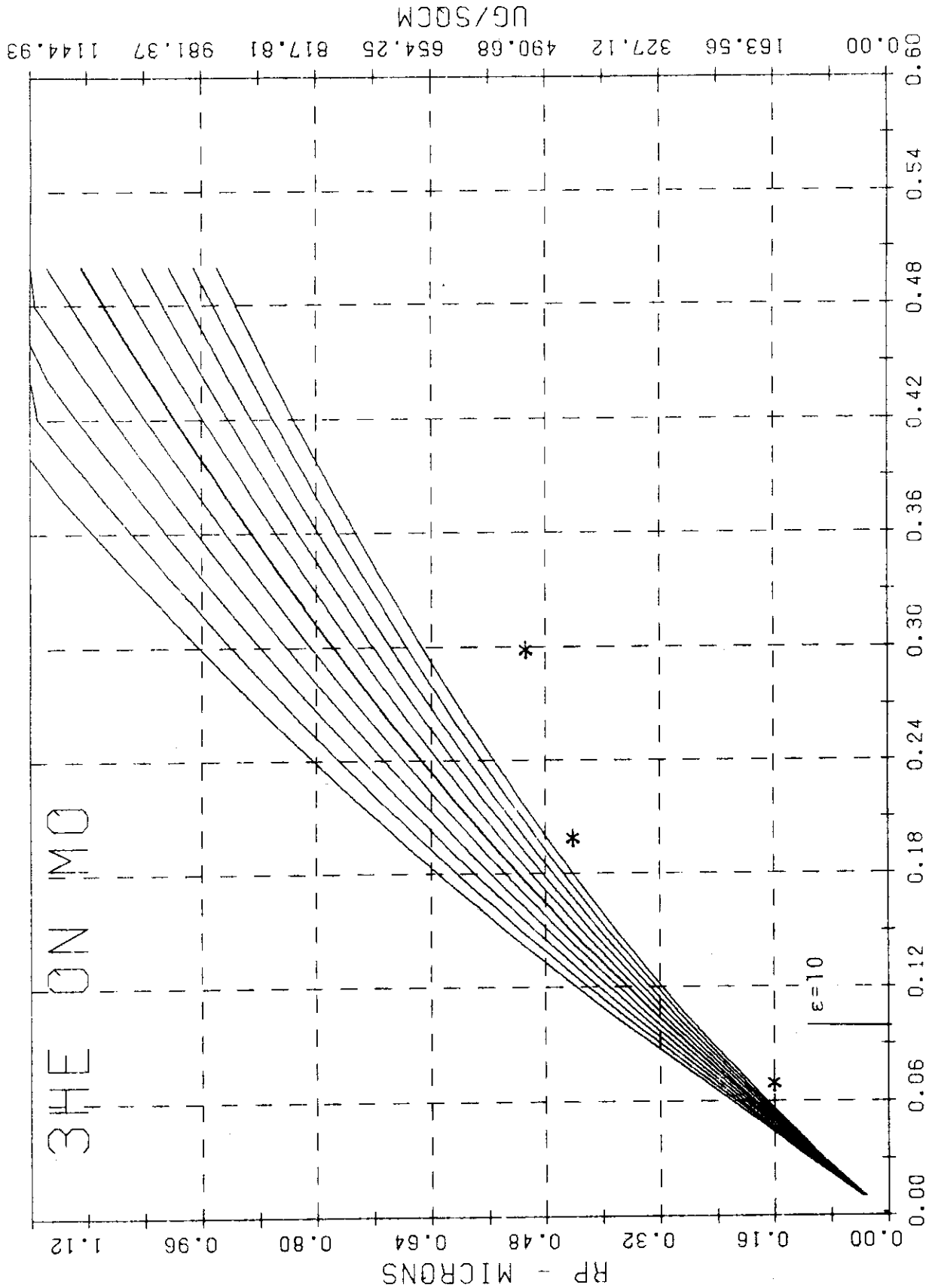

Fig. RB-7 (From Ref.5-49)

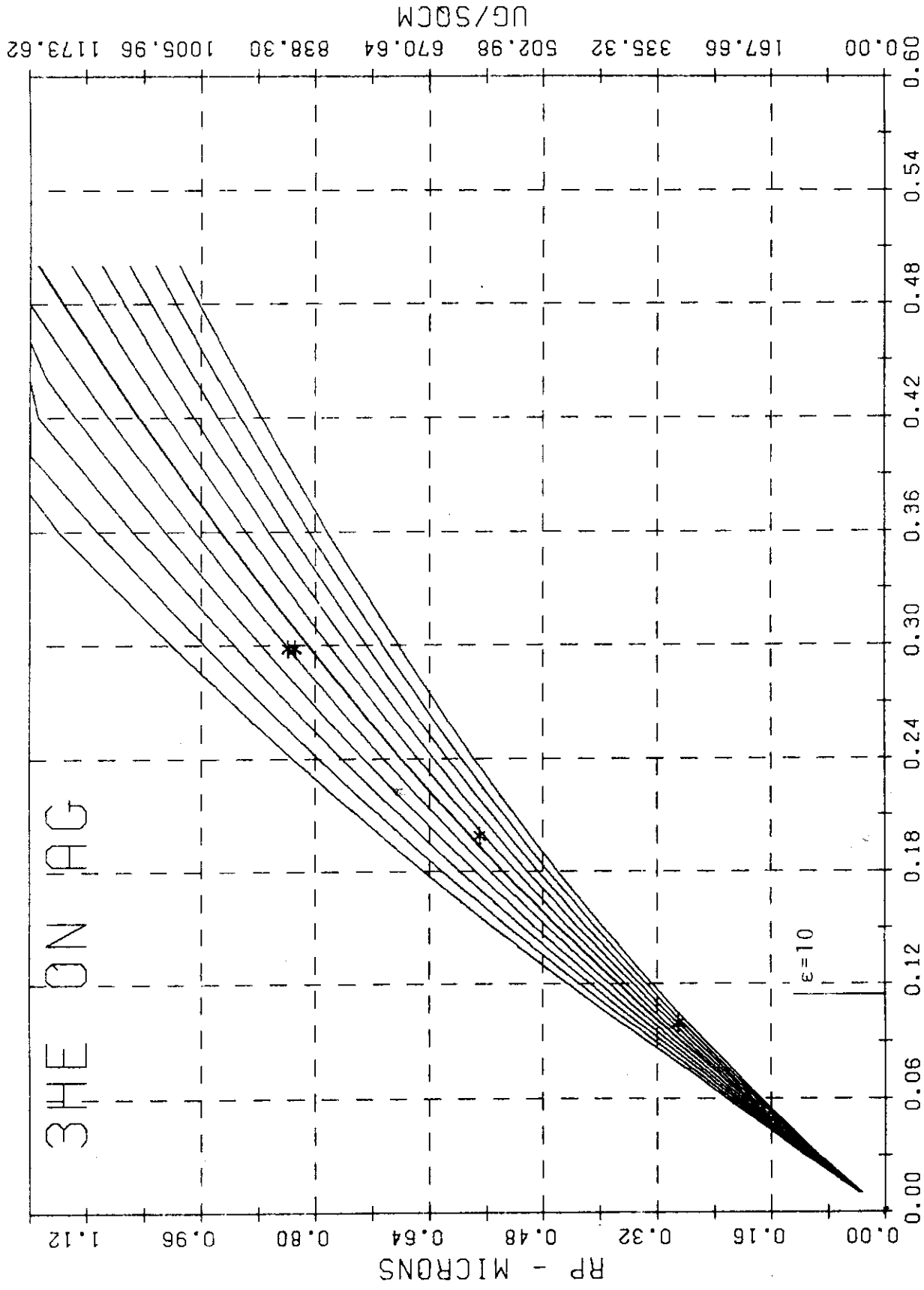

Fig. RB-8 (From Ref.5-49)

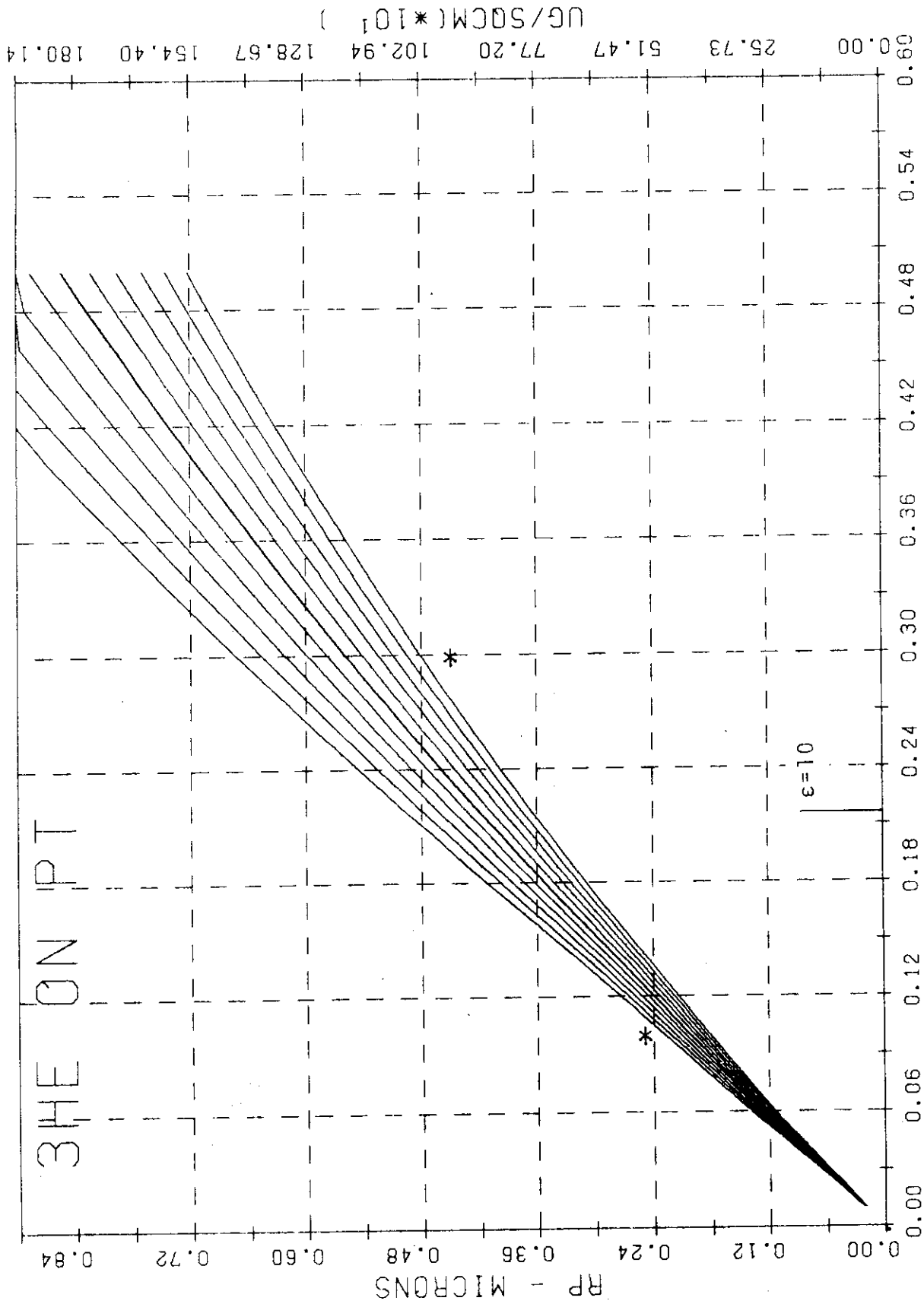

Fig. RB-9 (From Ref.5-49)

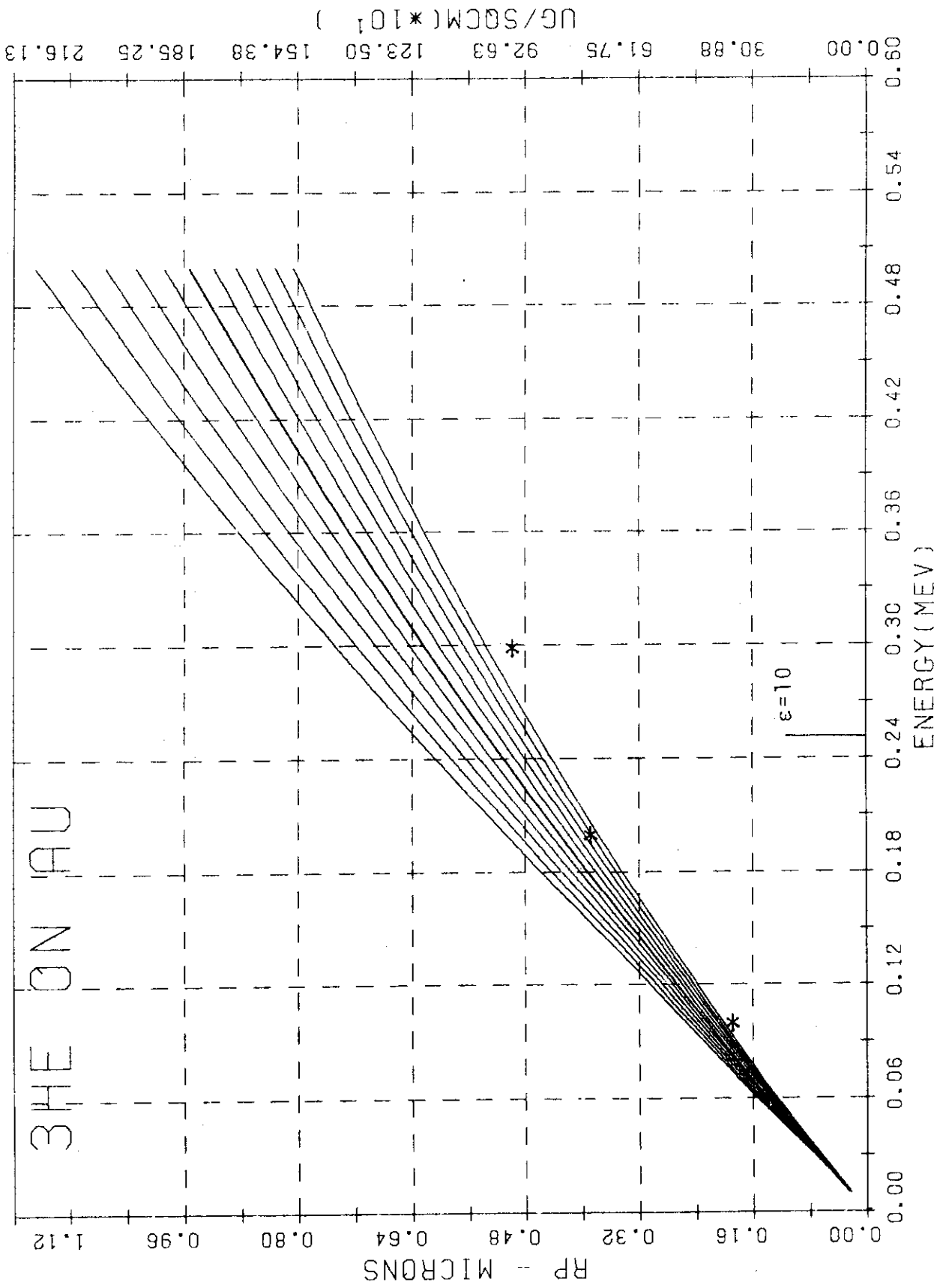

Fig. RB-10 (From Ref.5-49)

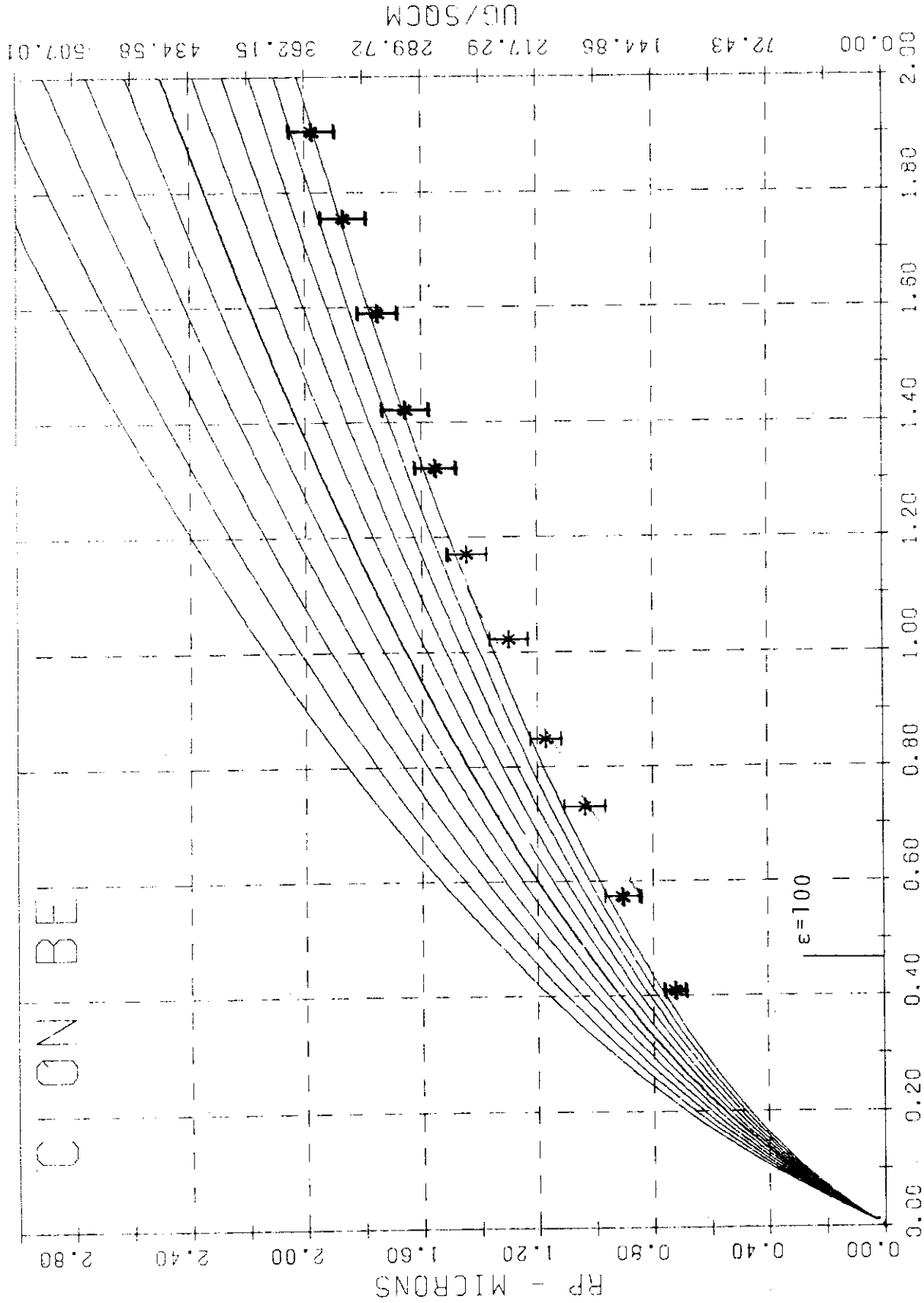

Fig. RB-11 (From Ref.5-87)

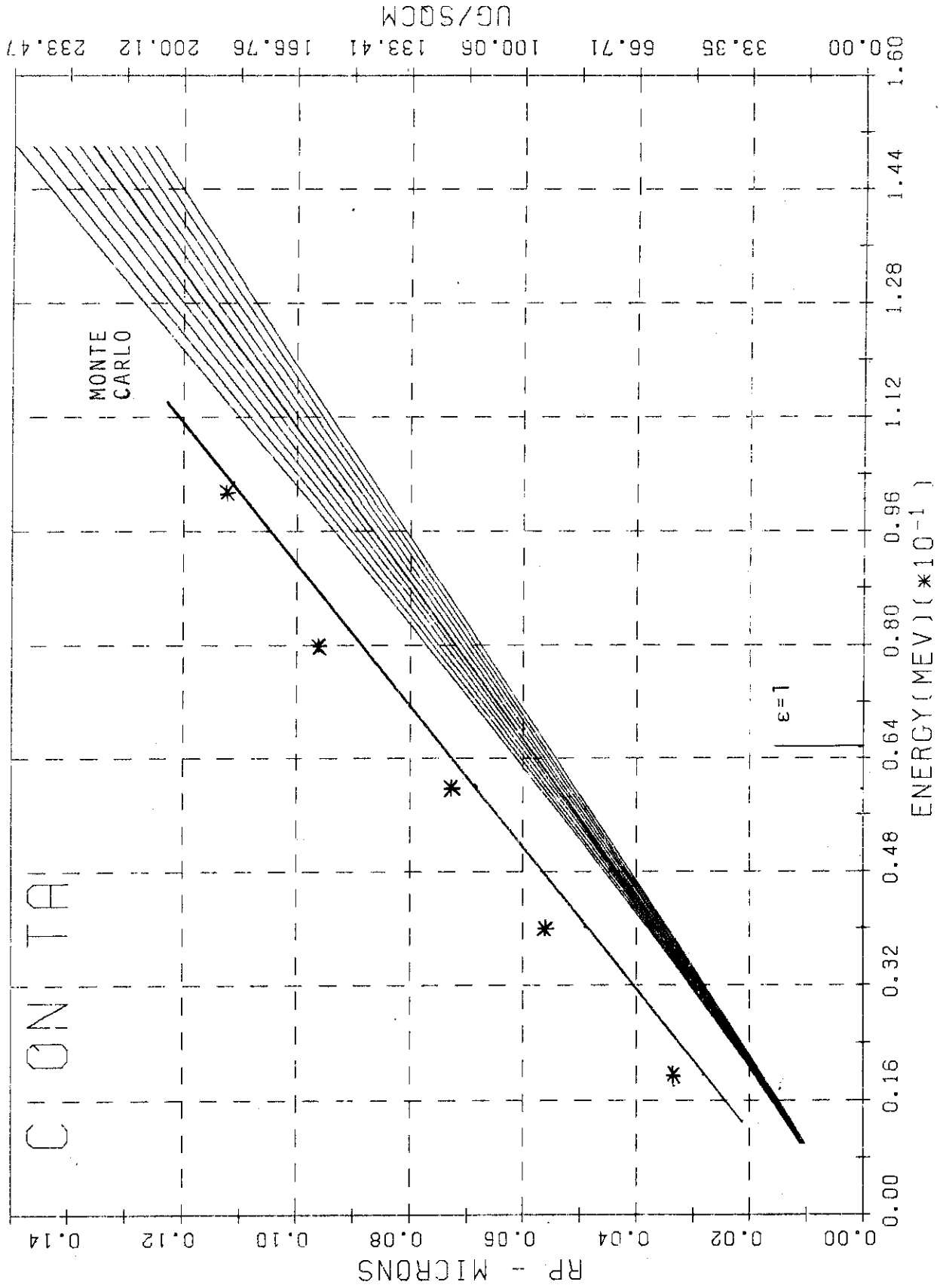

Fig. RB-12 (From Ref.5-78)

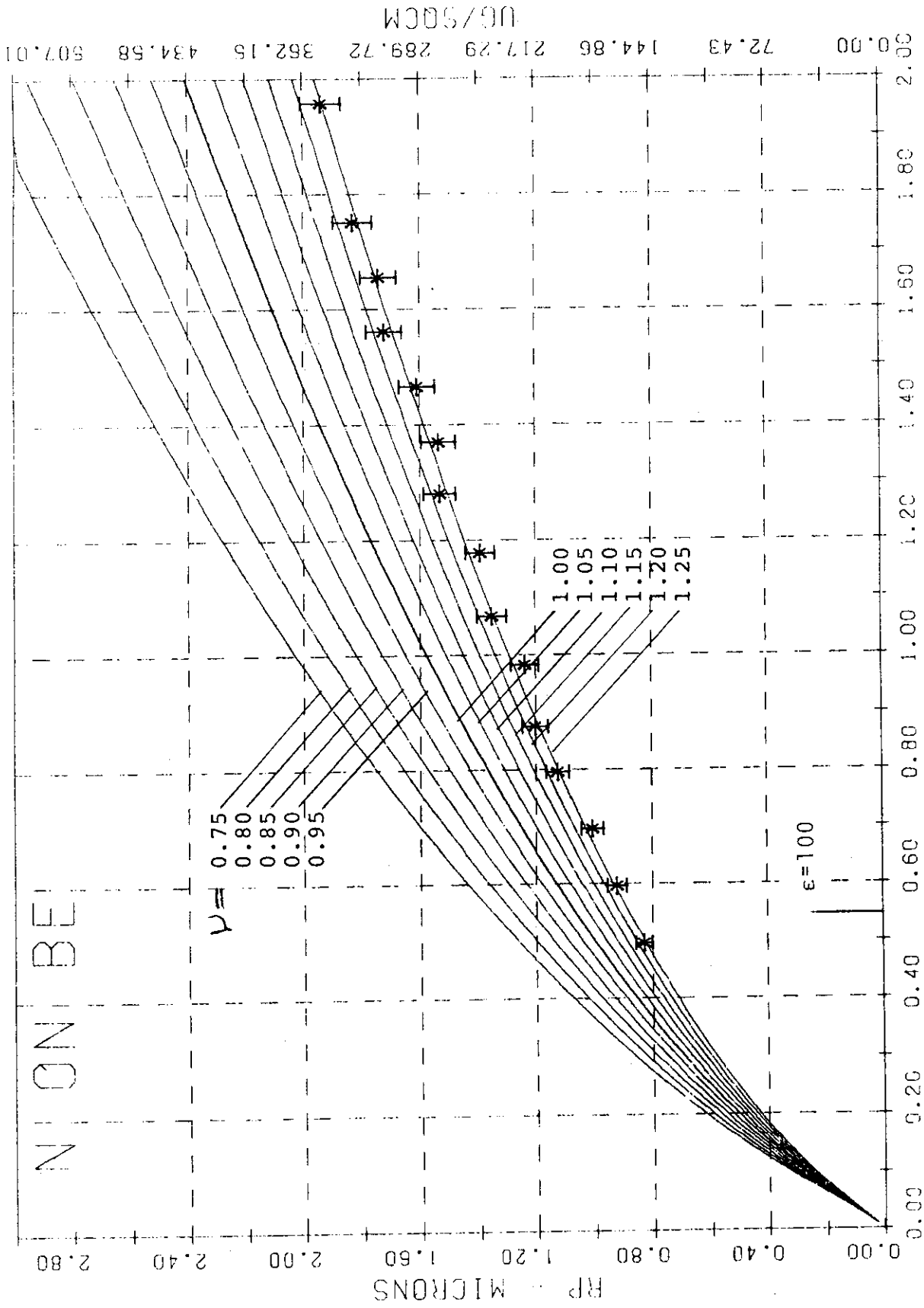

Fig. RB-13 (From Ref.5-87)

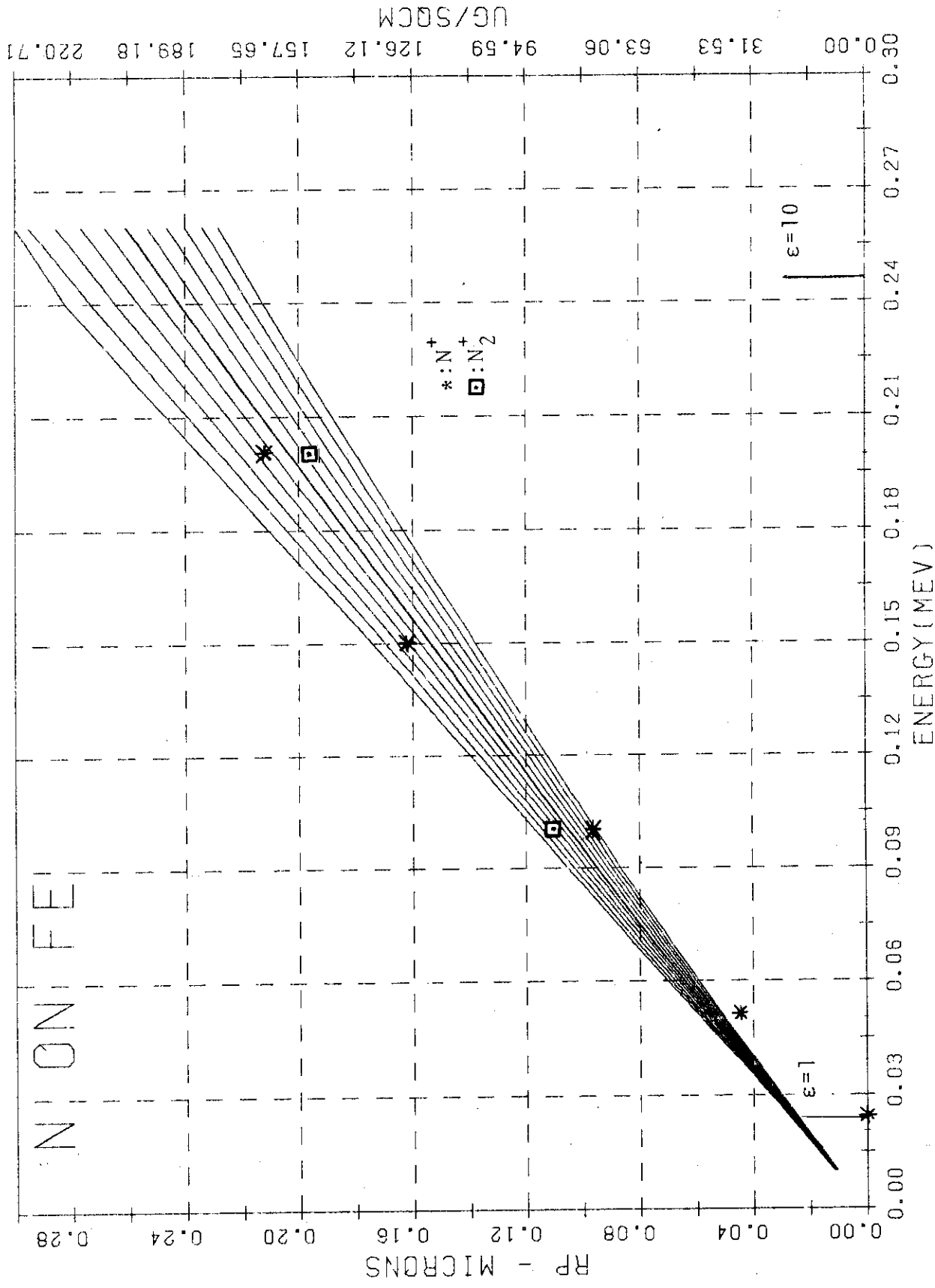

Fig. RB-14 (From Ref.5-60)

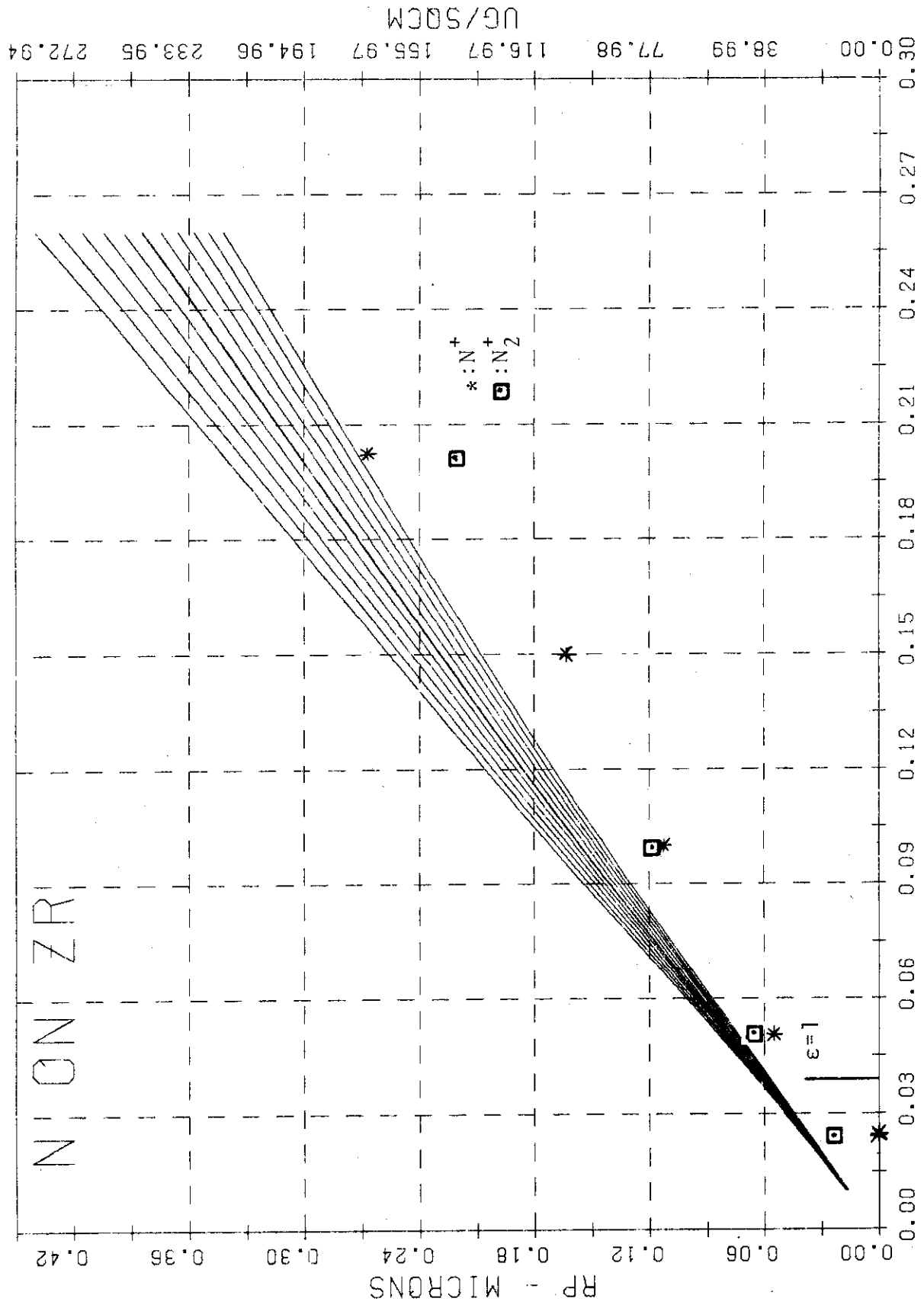

Fig. RB-15 (From Ref.5-60)

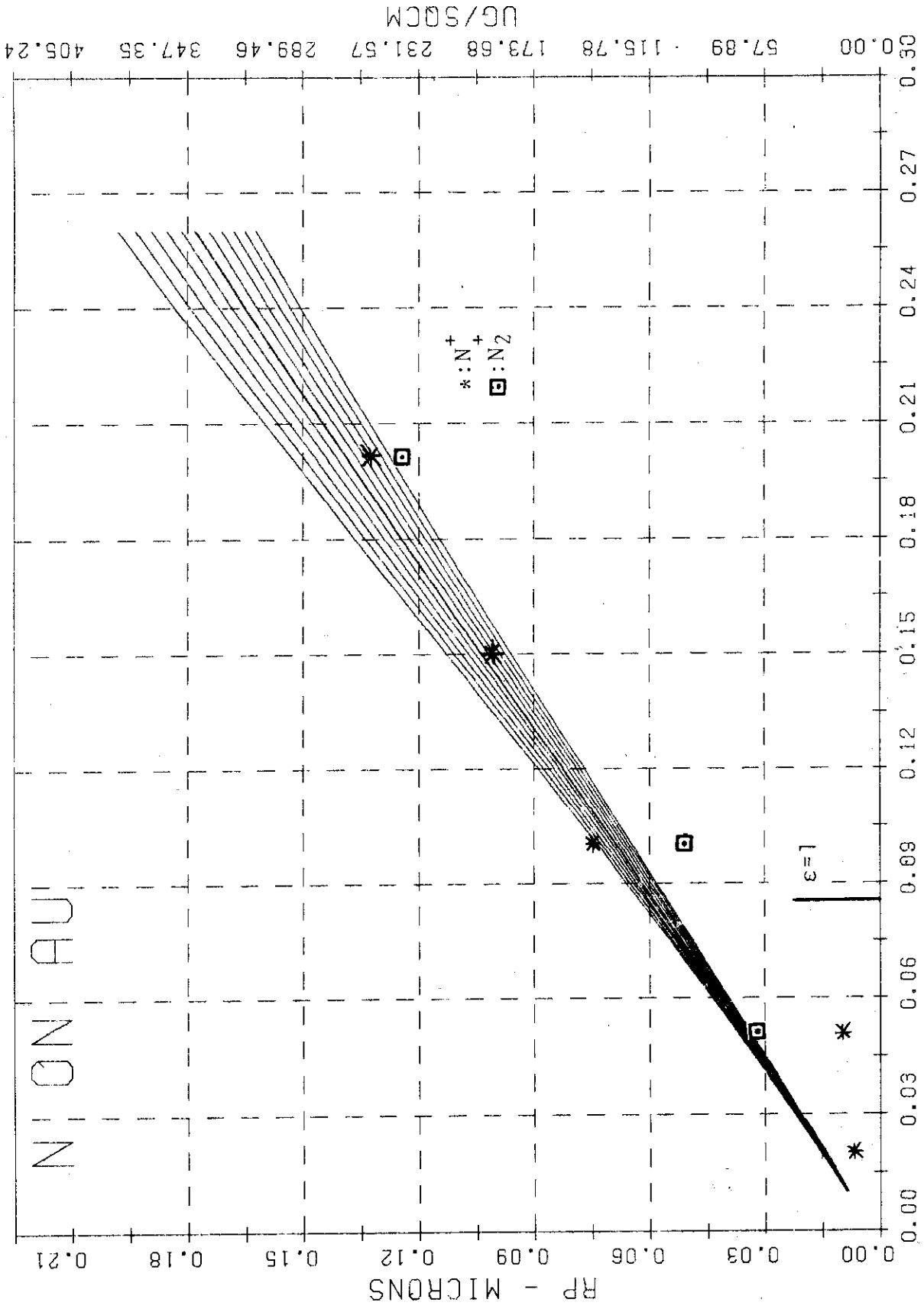

Fig. RB-16 (From Ref.5-60)

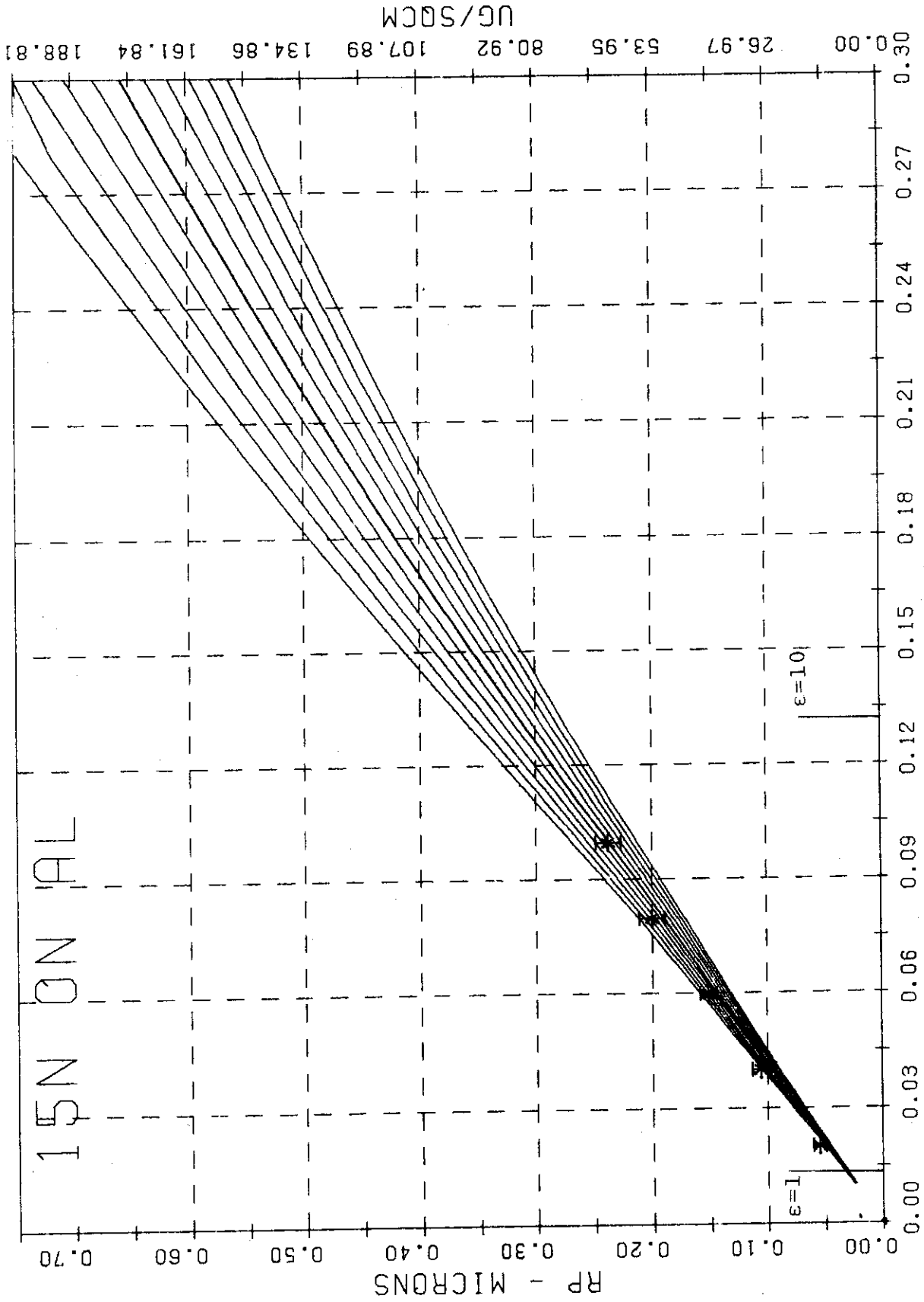

Fig. RB-17 (From Ref.5-58)

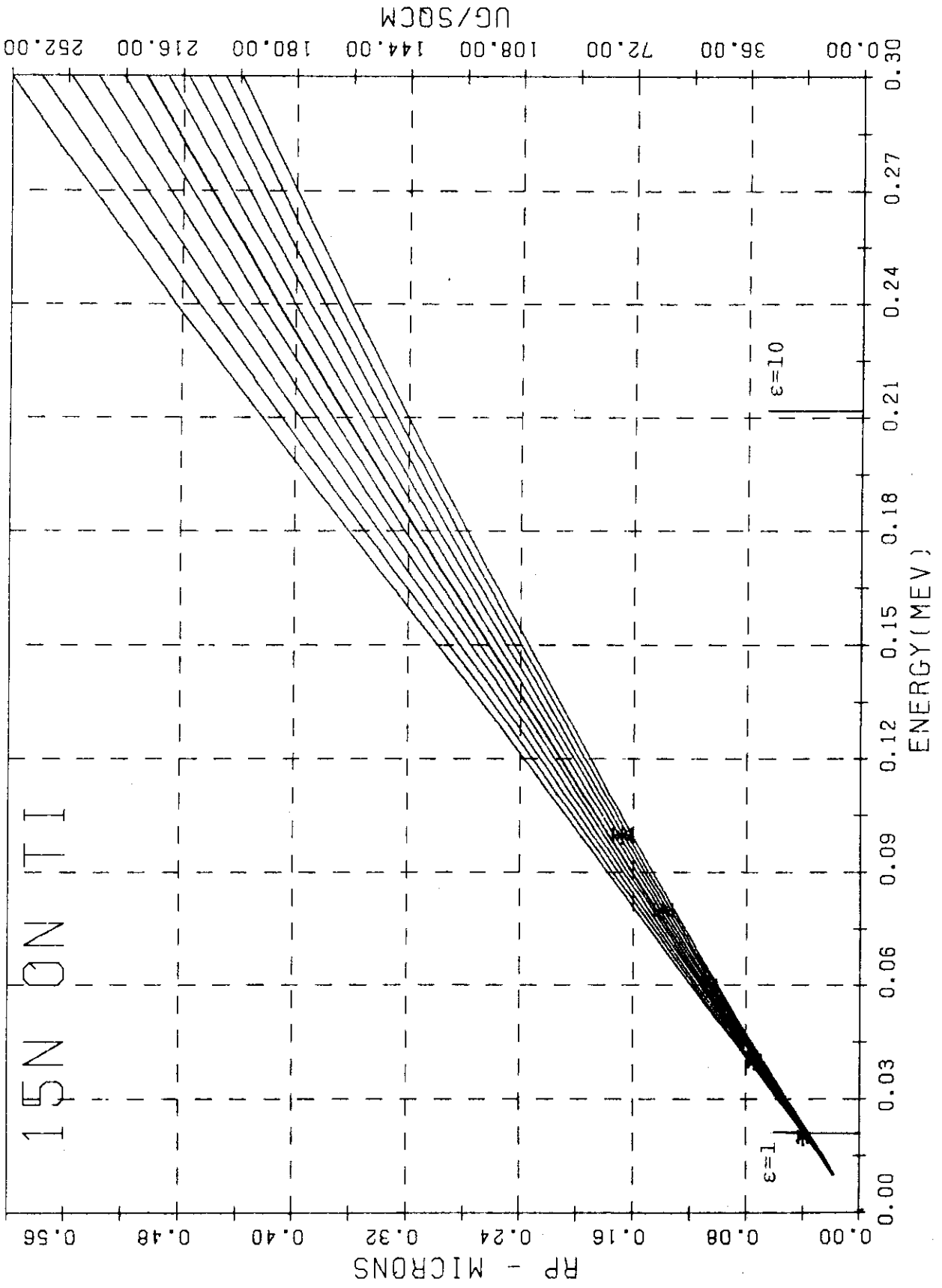

Fig. RB-18 (From Ref.5-58)

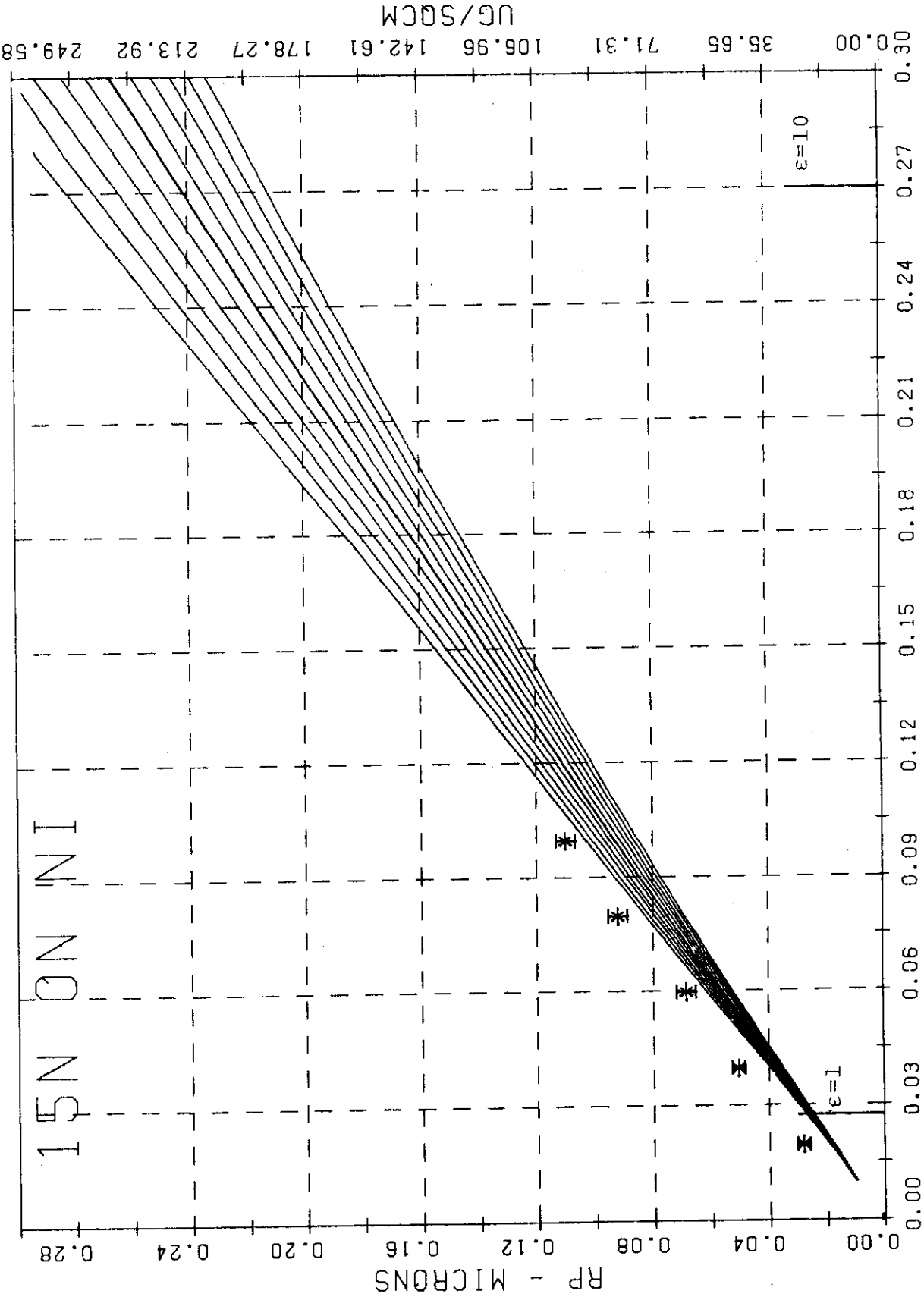

Fig. RB-19 (From Ref.5-58)

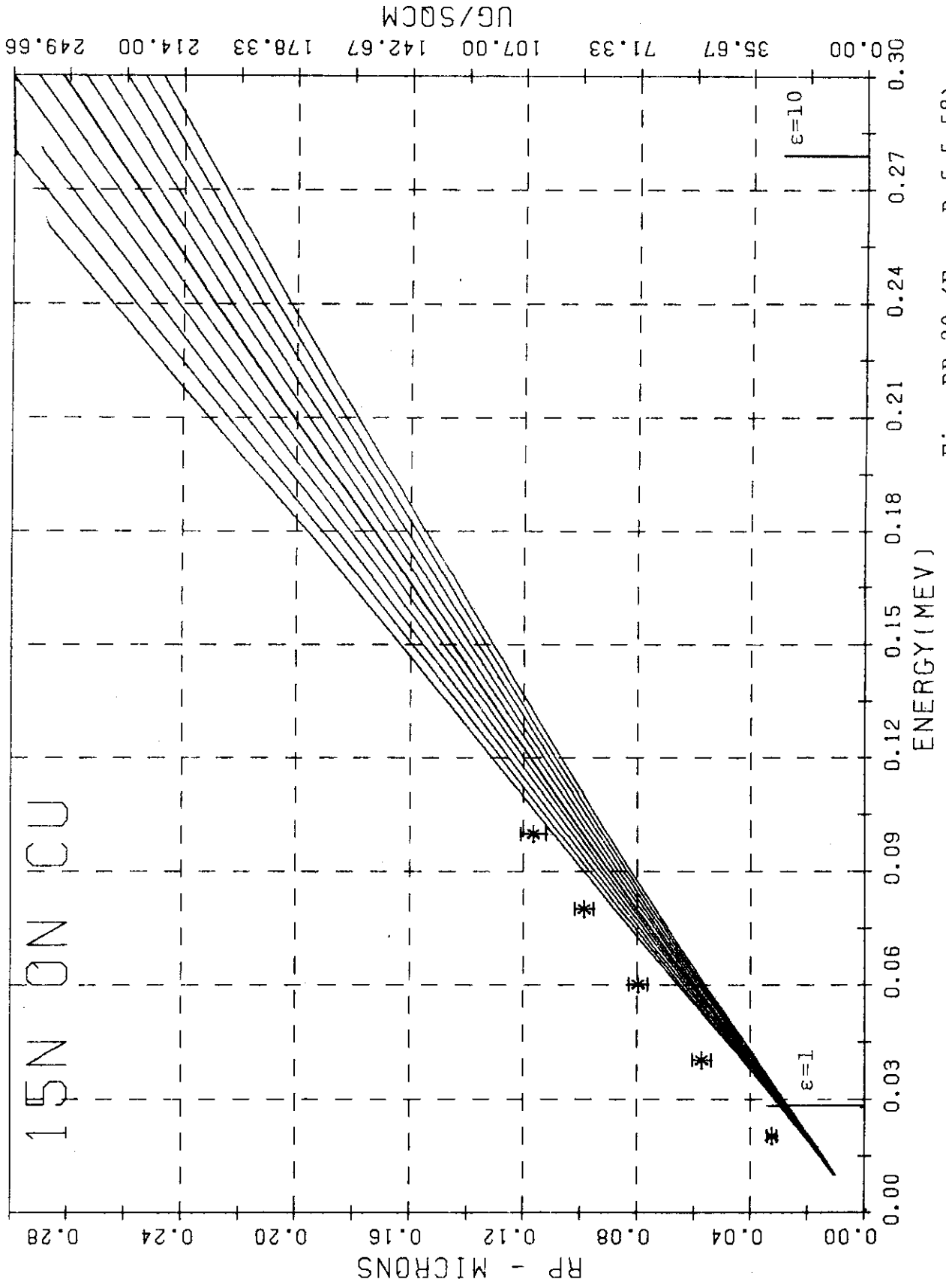

Fig. RB-20 (From Ref.5-58)

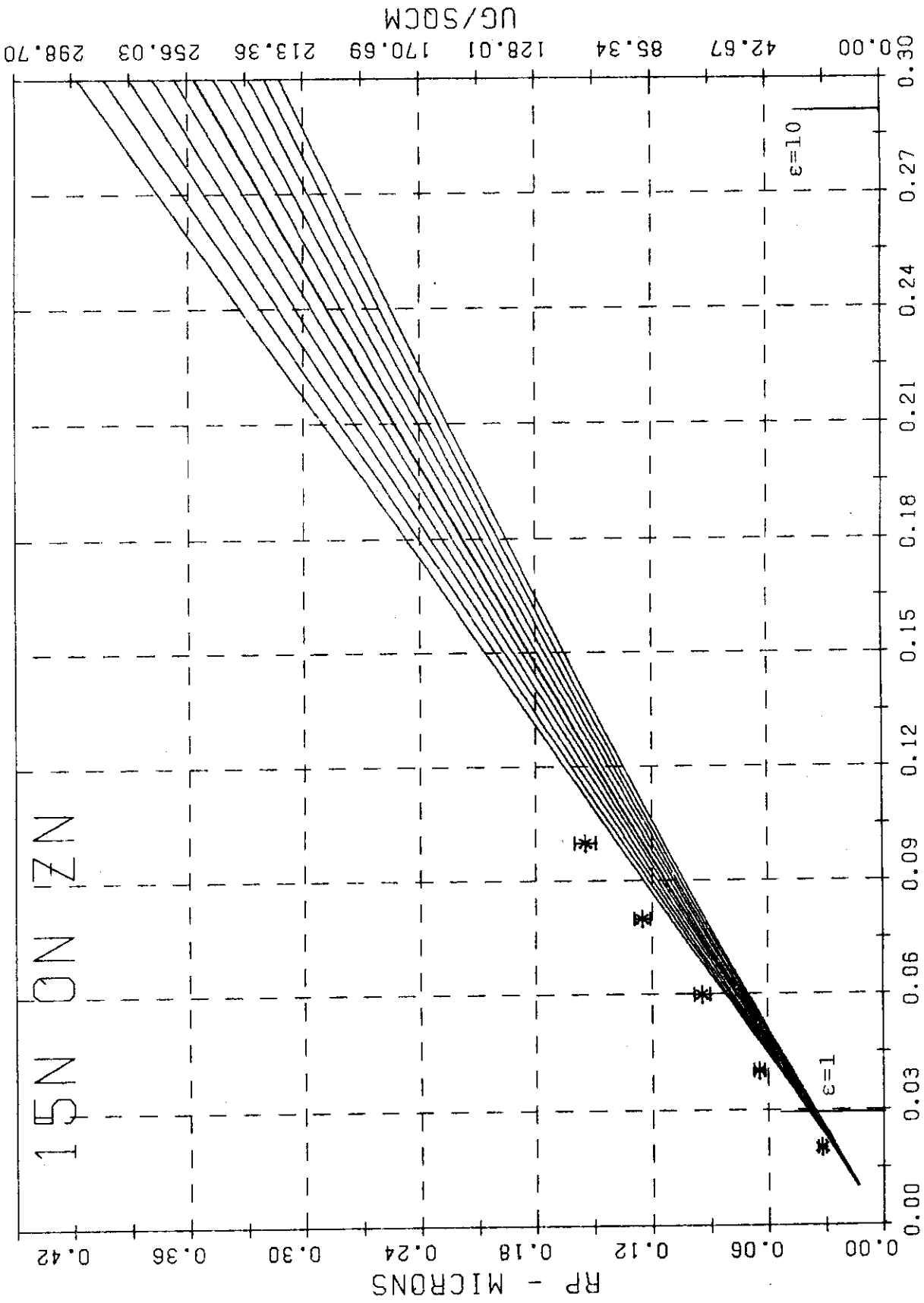

Fig. RB-21 (From Ref.5-58)

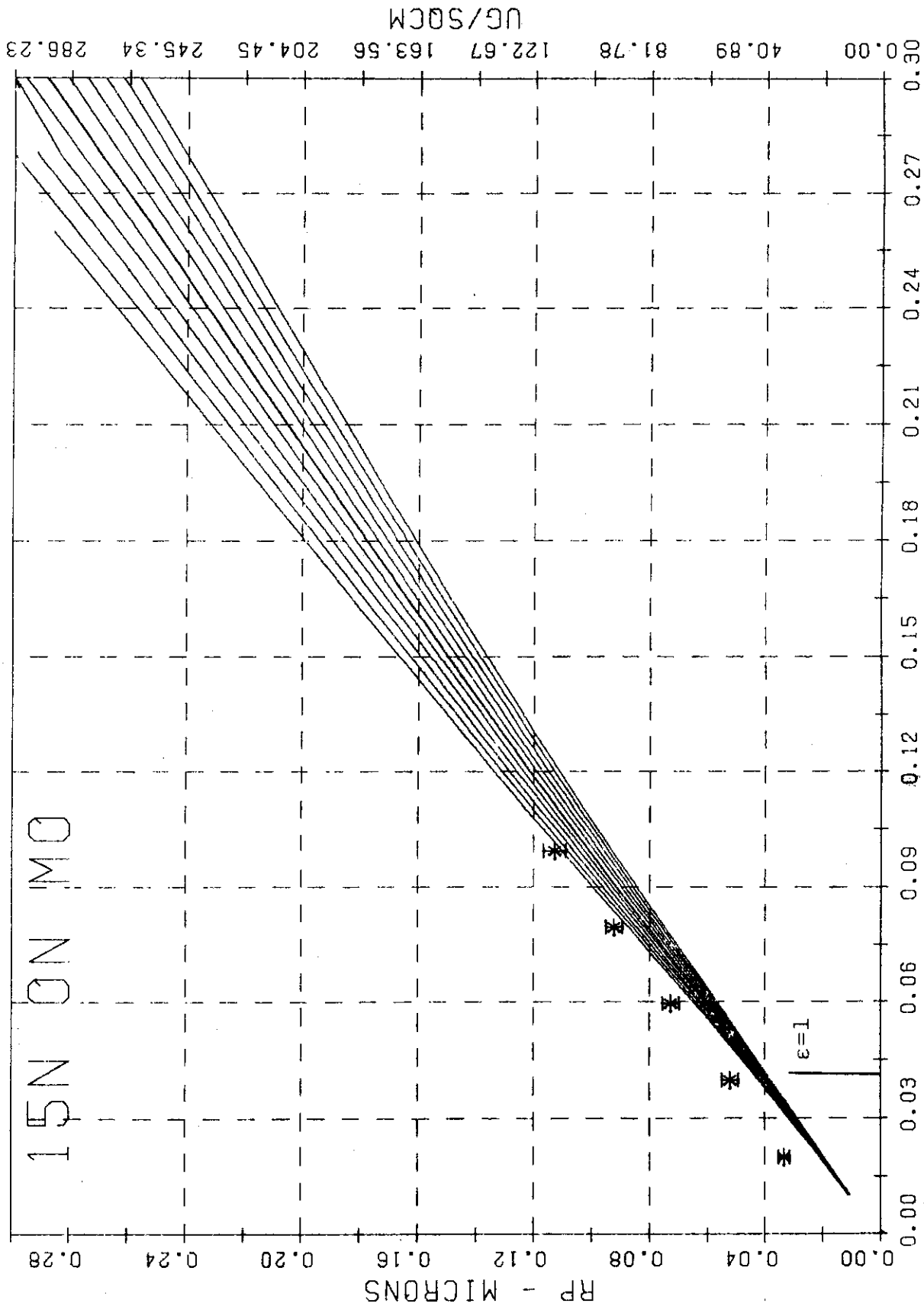

Fig. RB-22 (From Ref.5-58)

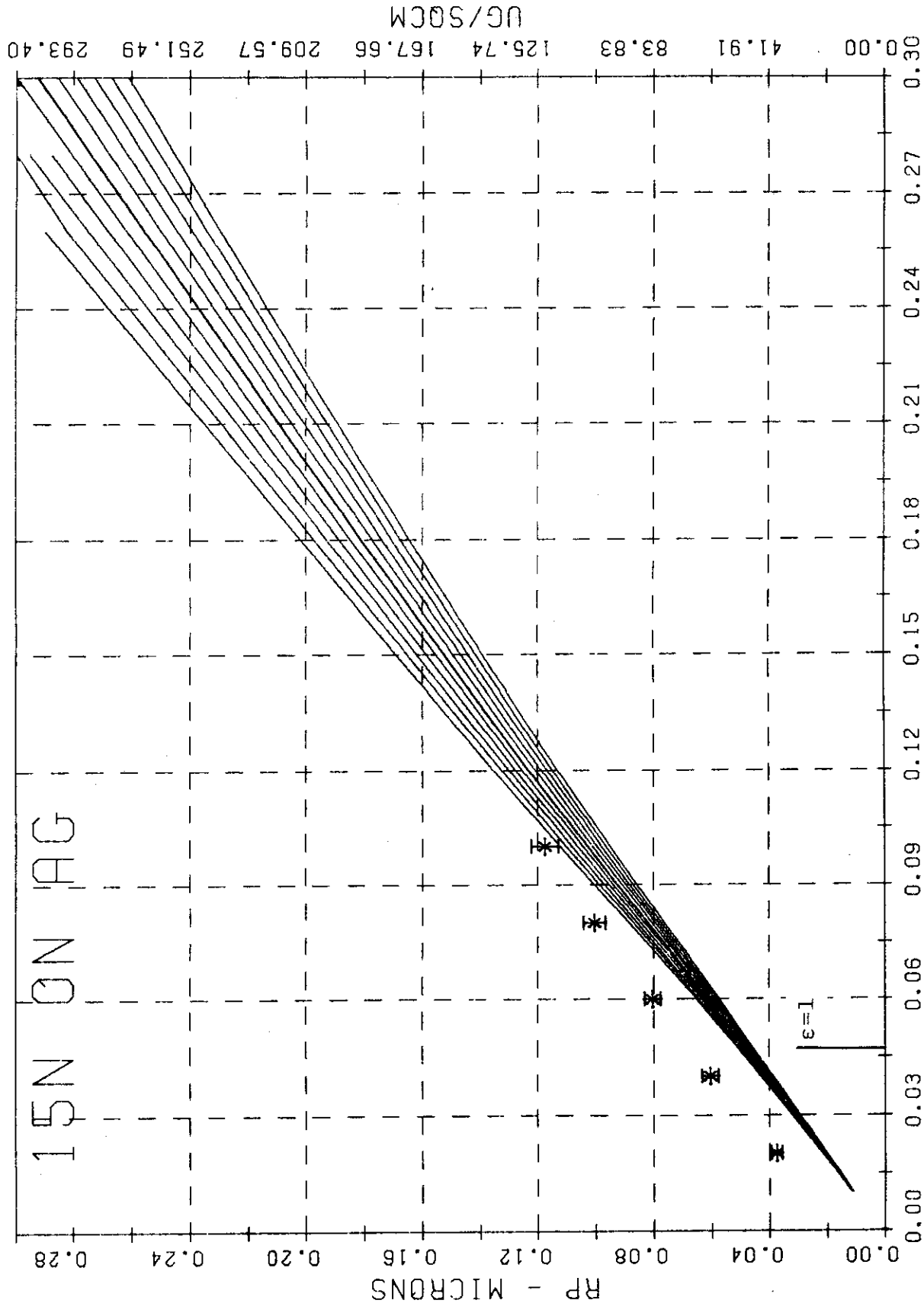

Fig. RB-23 (From Ref.5-58)

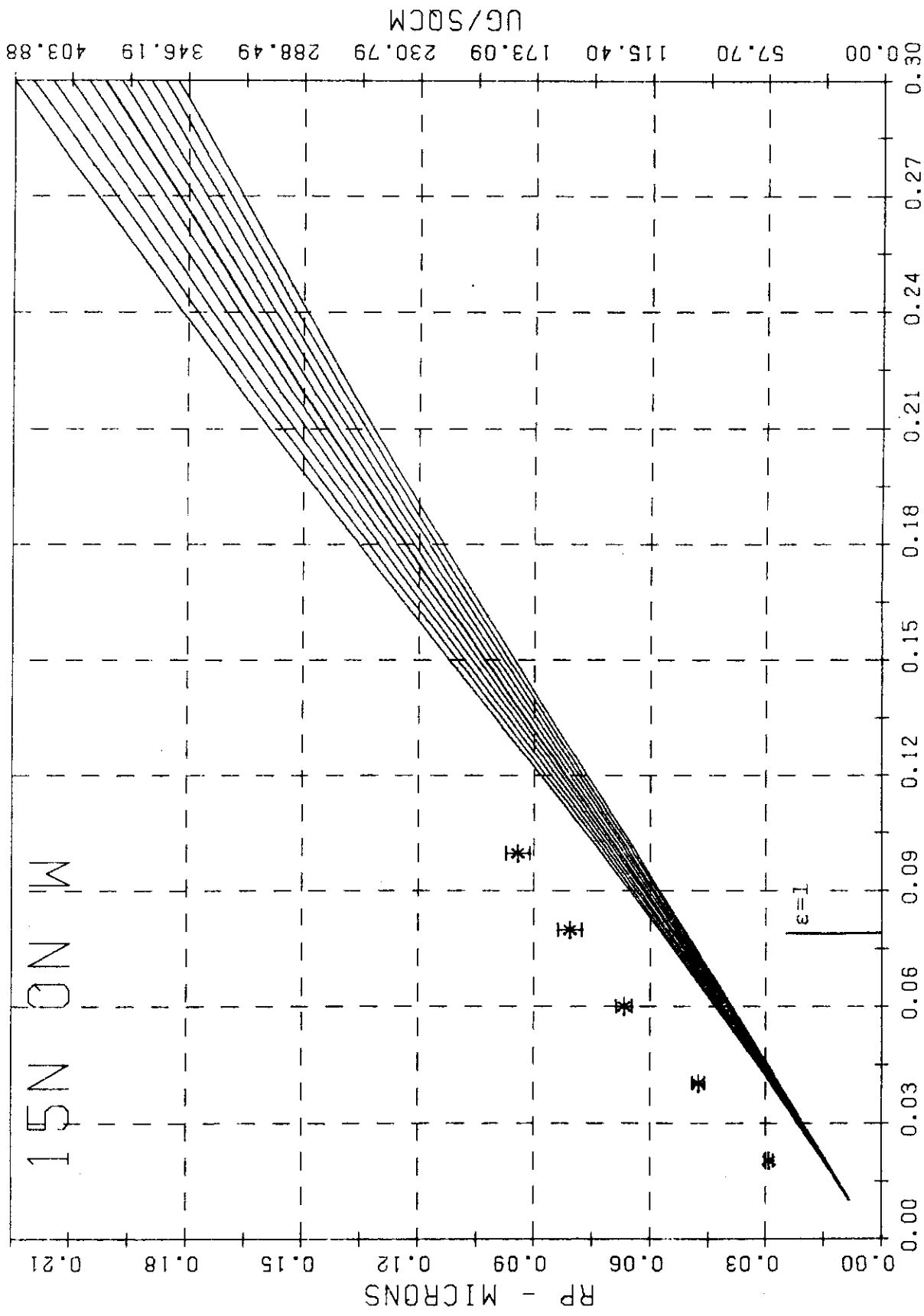

Fig. RB-24 (From Ref.5-58)

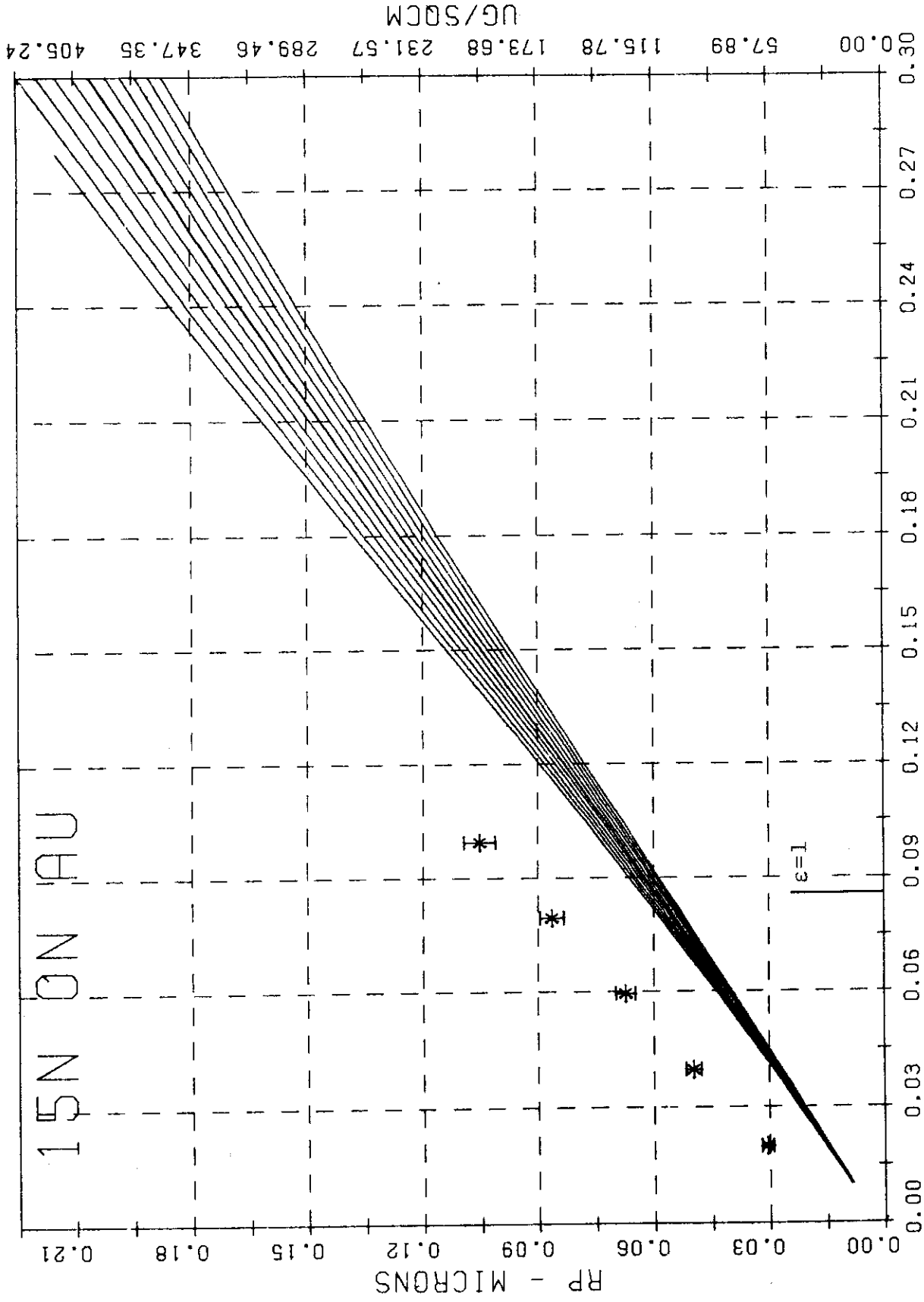

Fig. RB-25 (From Ref.5-58)

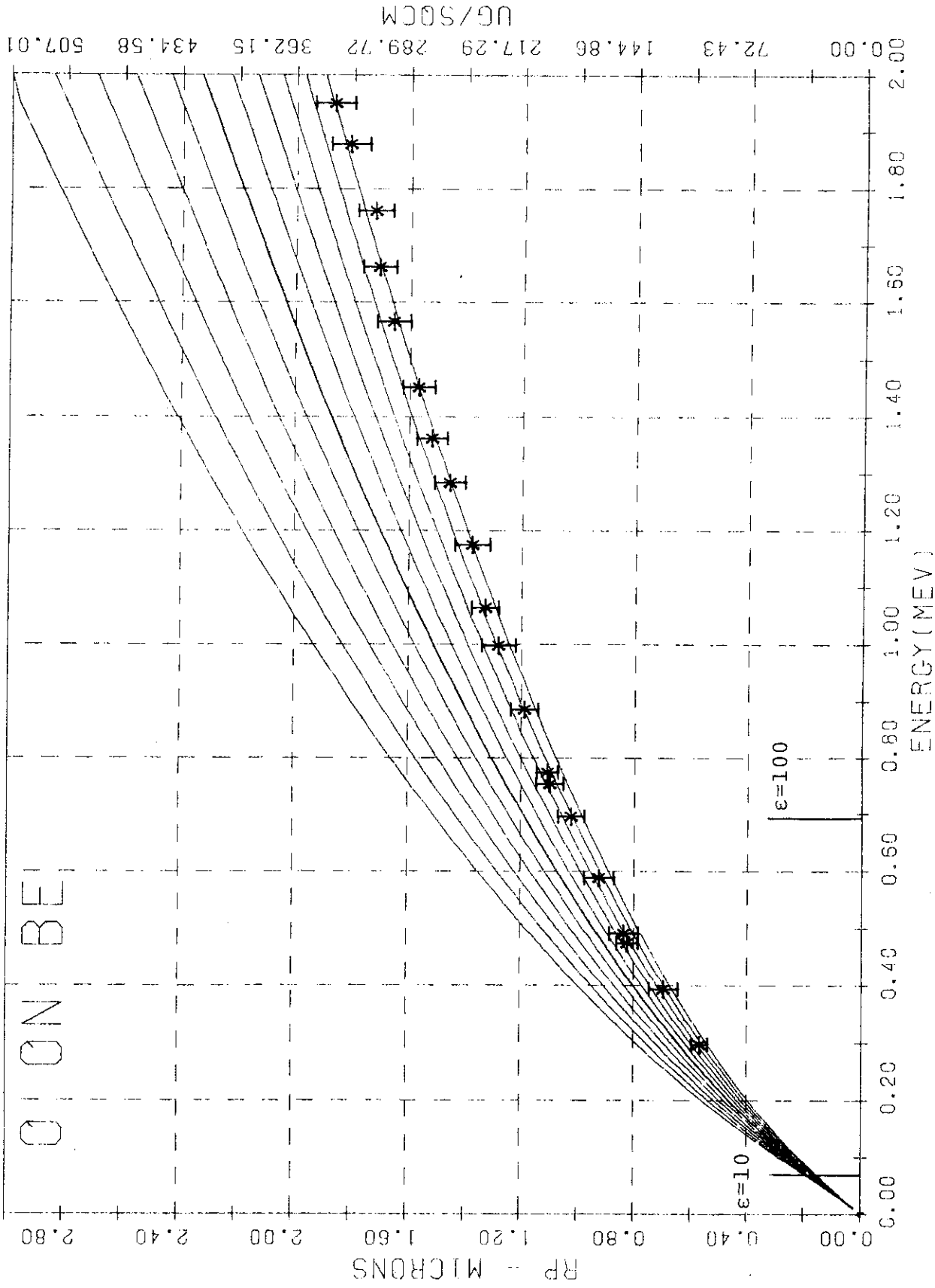

Fig. RB-26 (From Ref.5-87)

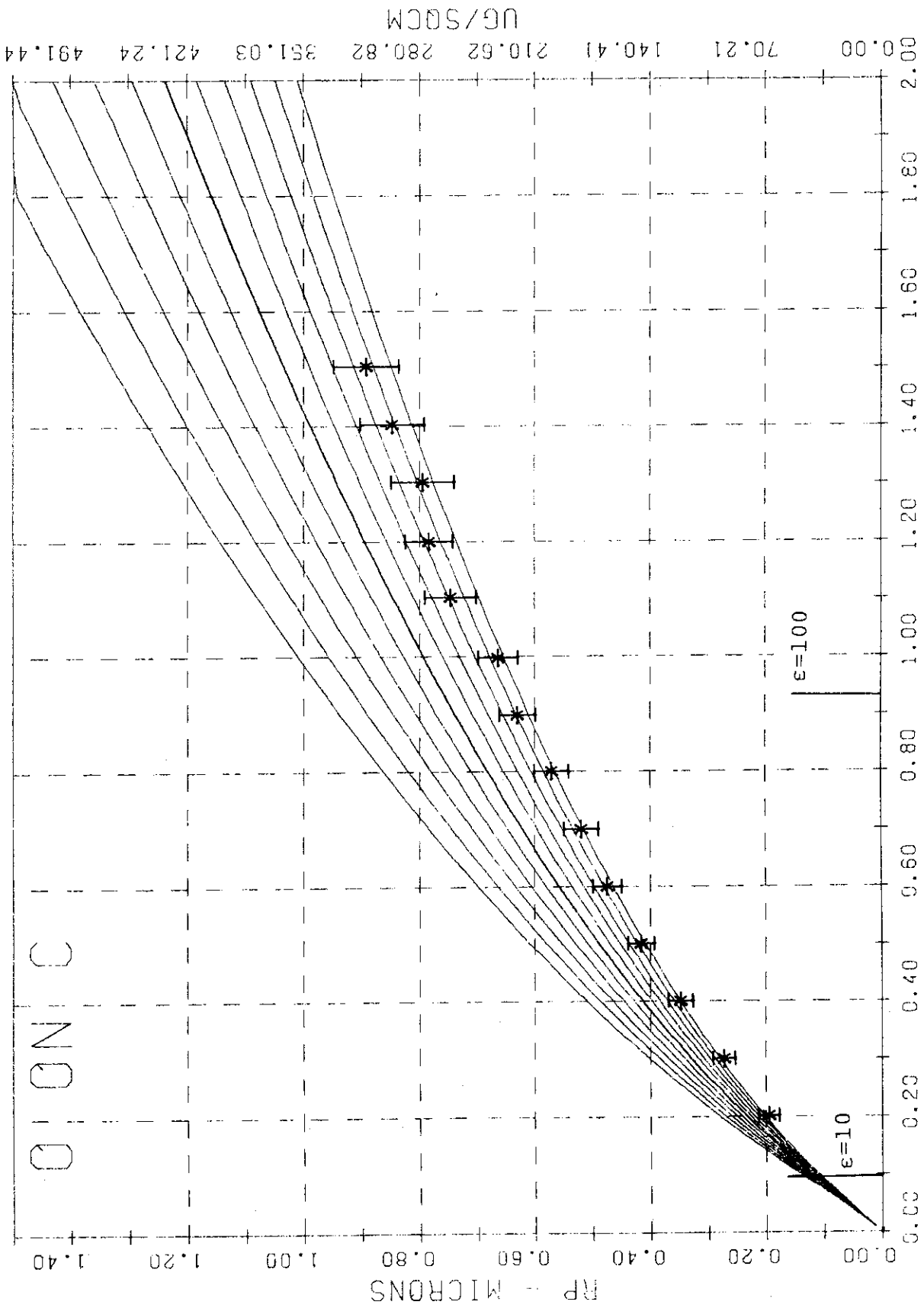

Fig. RB-27 (From Ref.5-87)

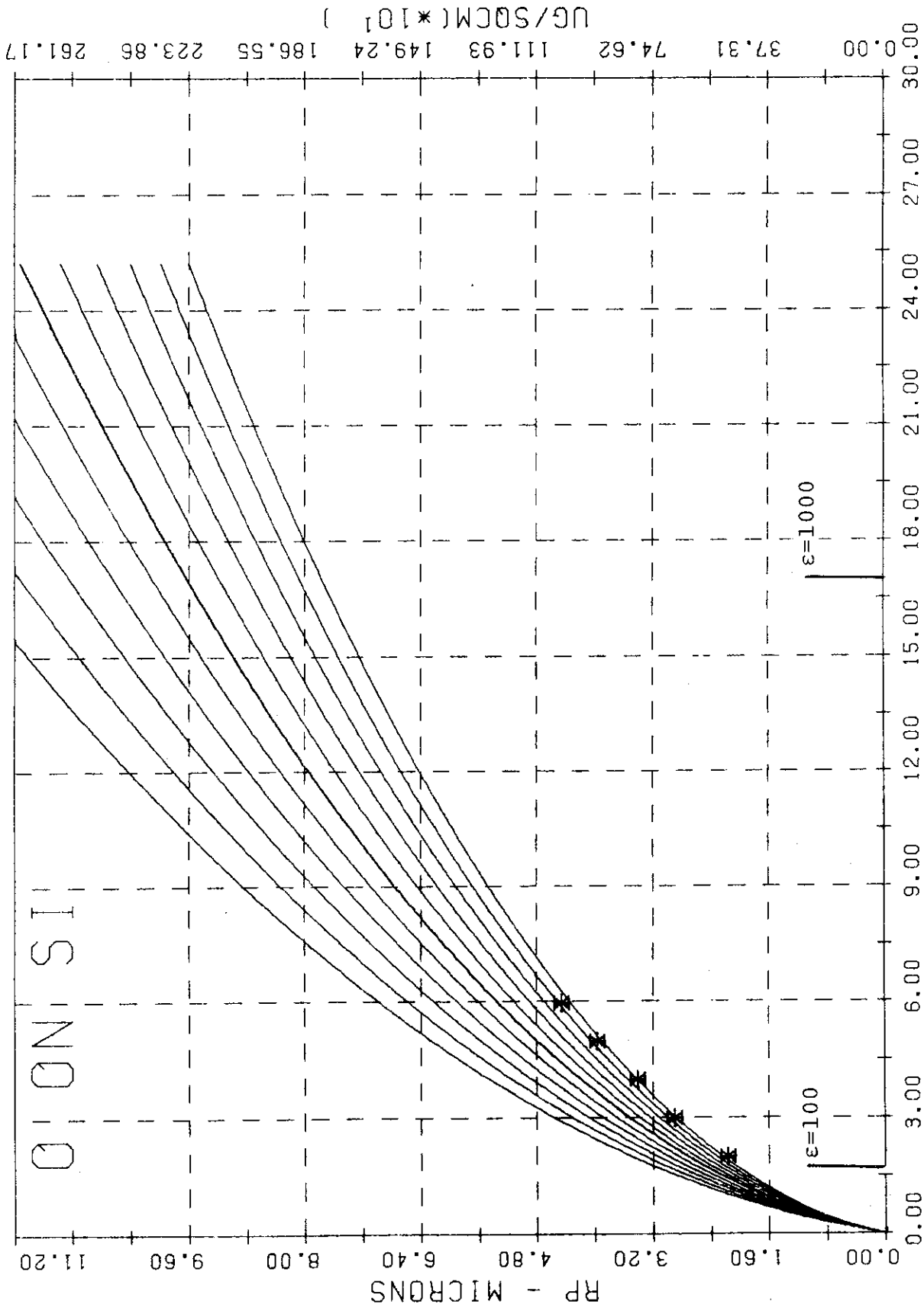

Fig. RB-28 (From Ref.5-48)

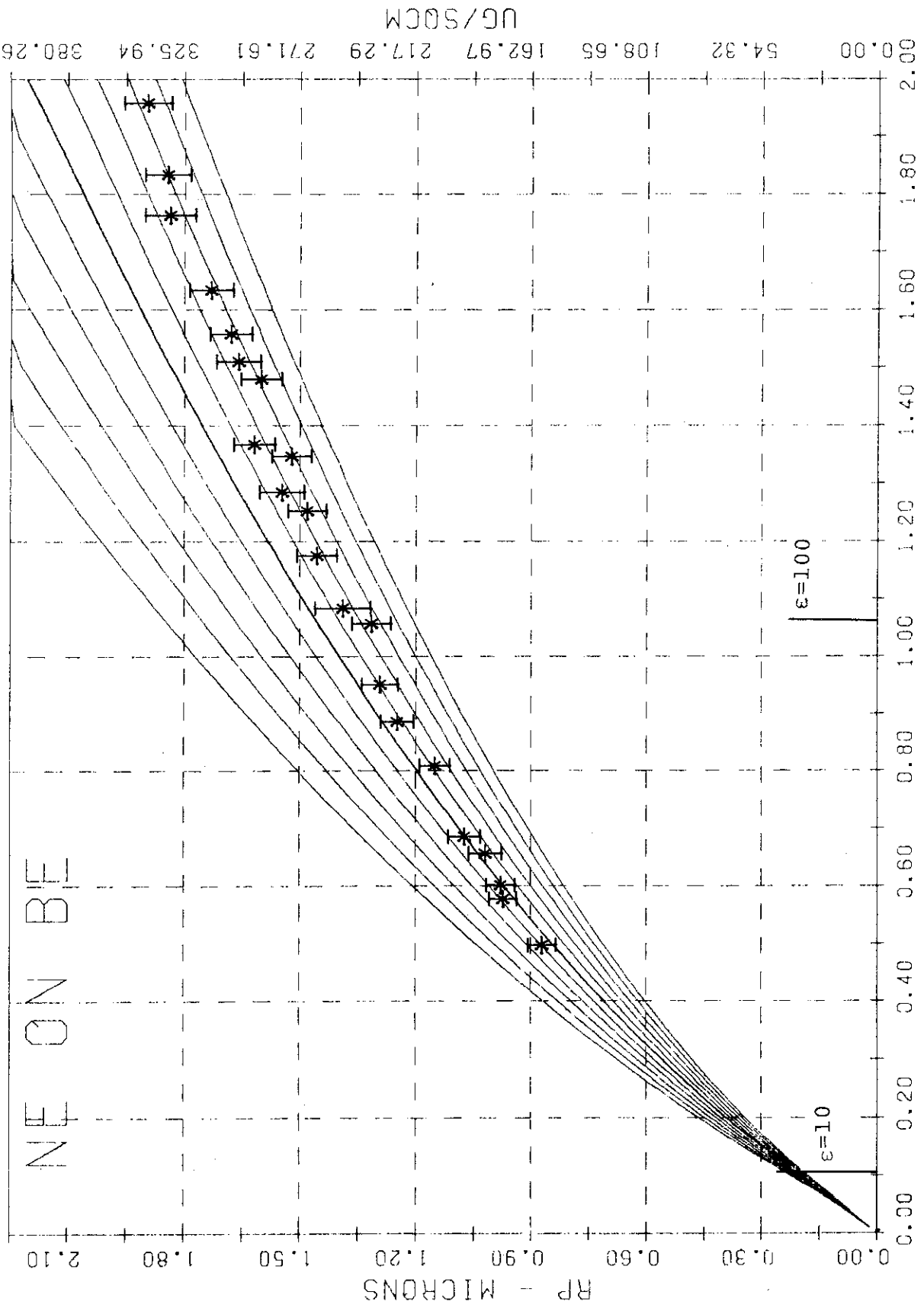

Fig. RB-29 (From Ref.5-87)

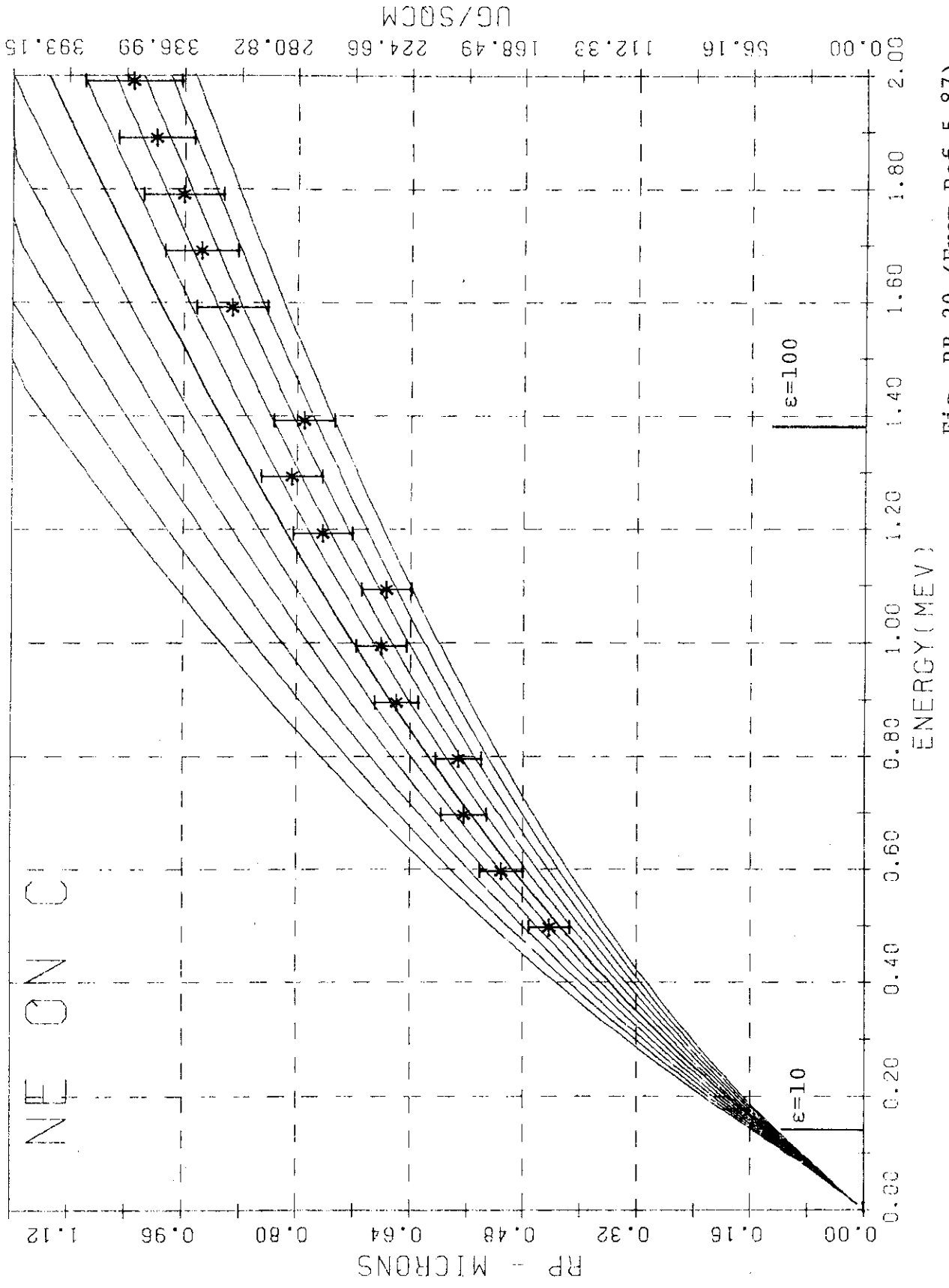

Fig. RB-30 (From Ref.5-87)

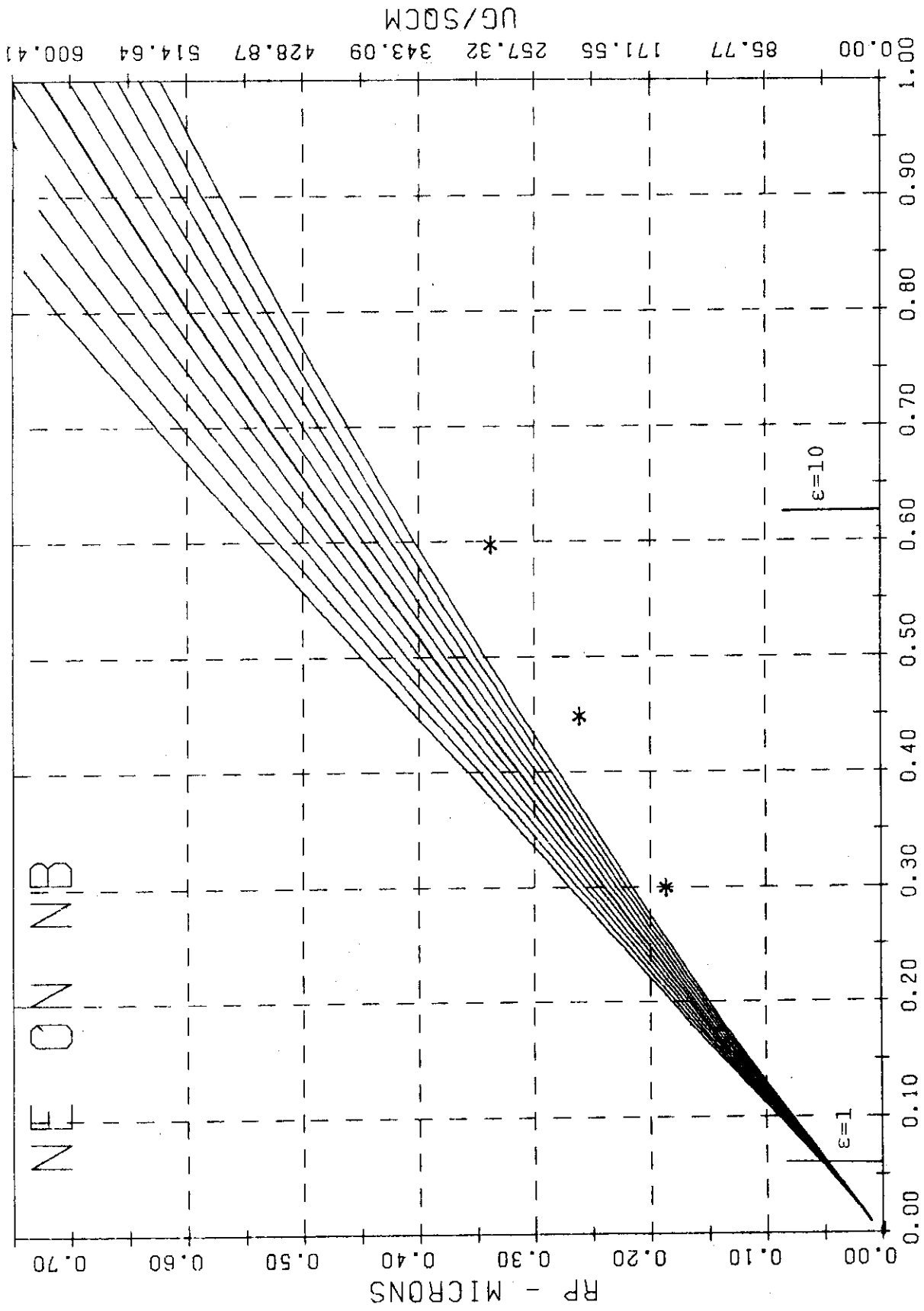

Fig. RB-31 (From Ref.5-8)

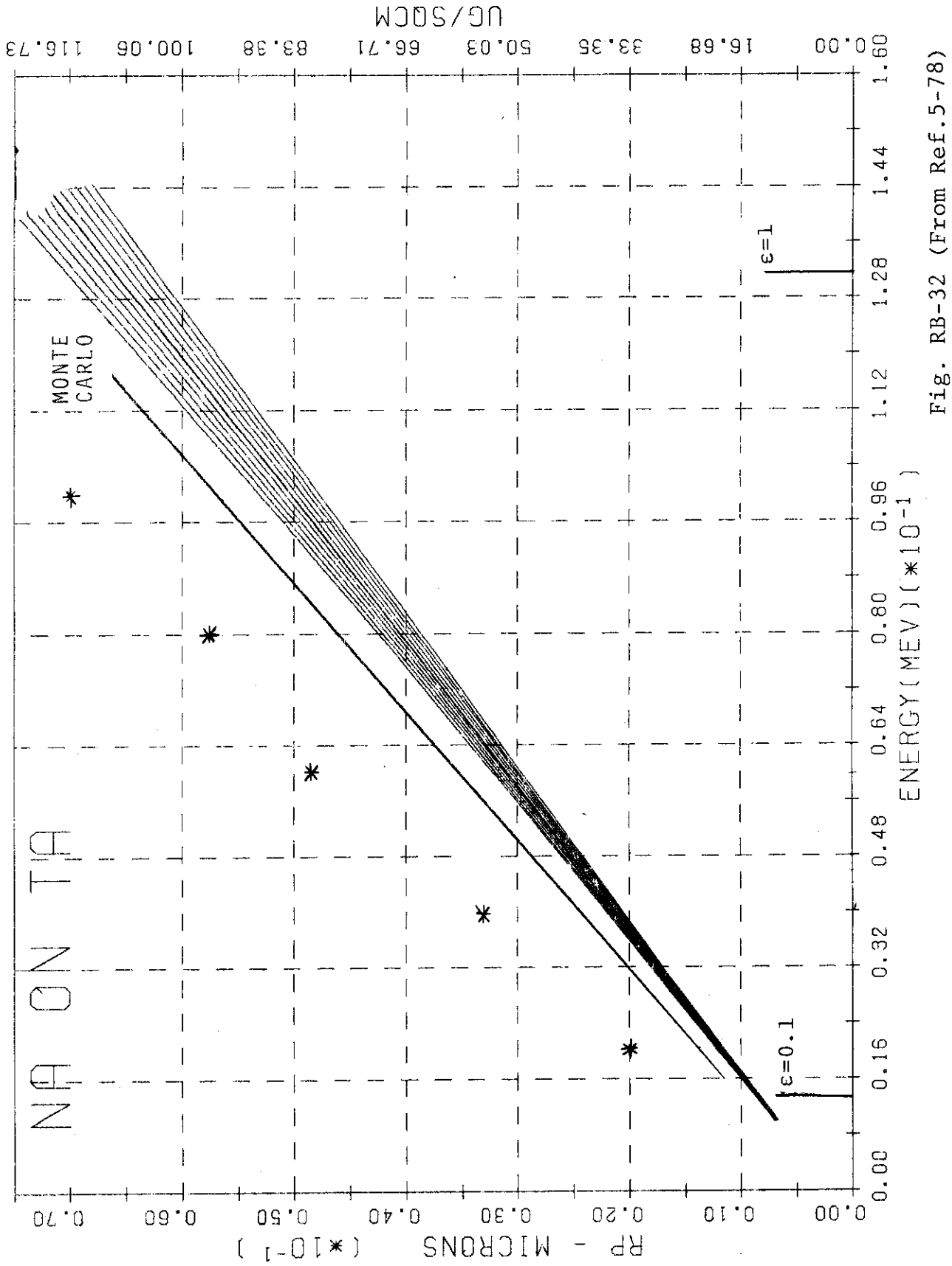

Fig. RB-32 (From Ref.5-78)

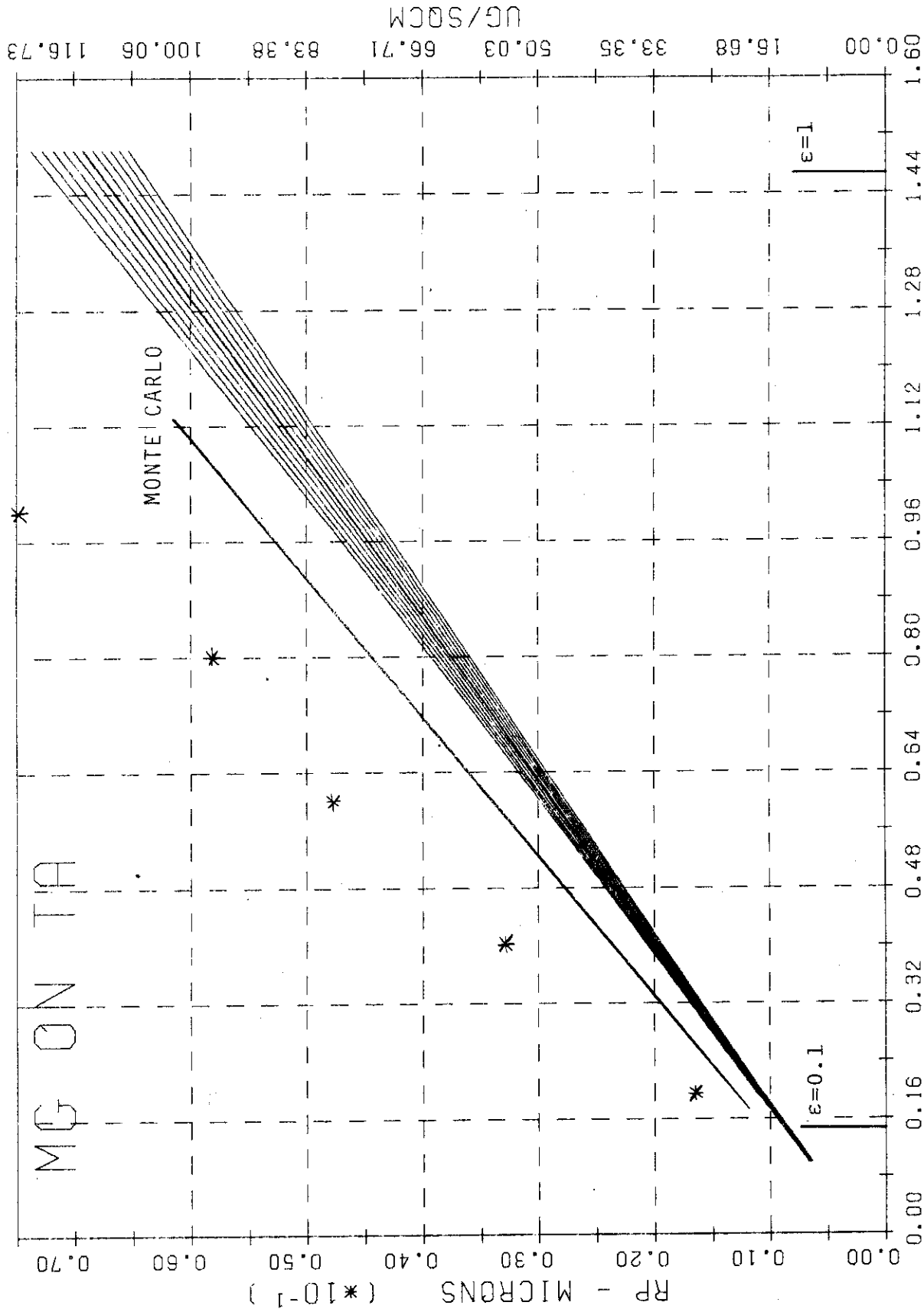

Fig. RB-33 (From Ref.5-78)

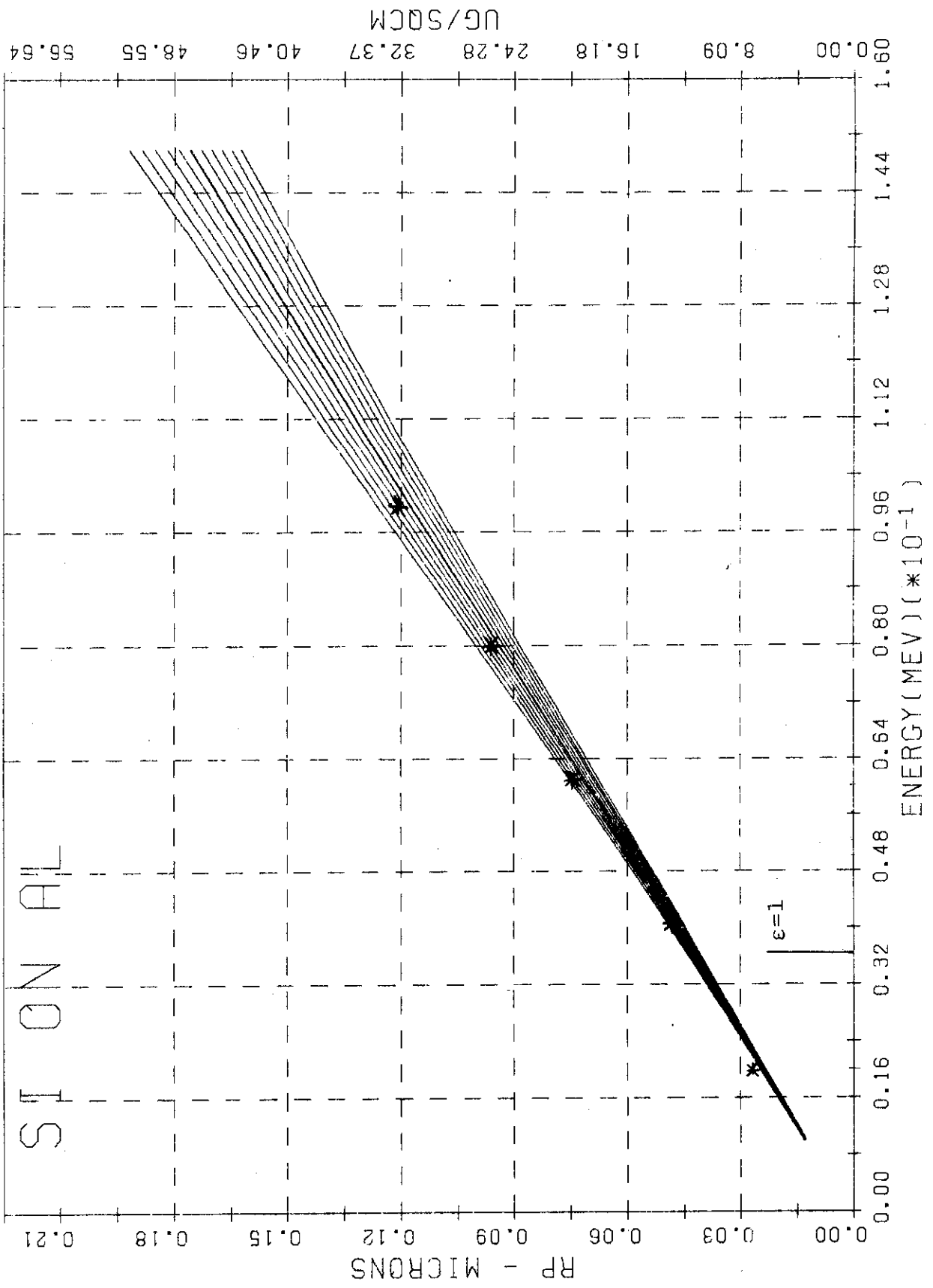

Fig. RB-34 (From Ref.5-78)

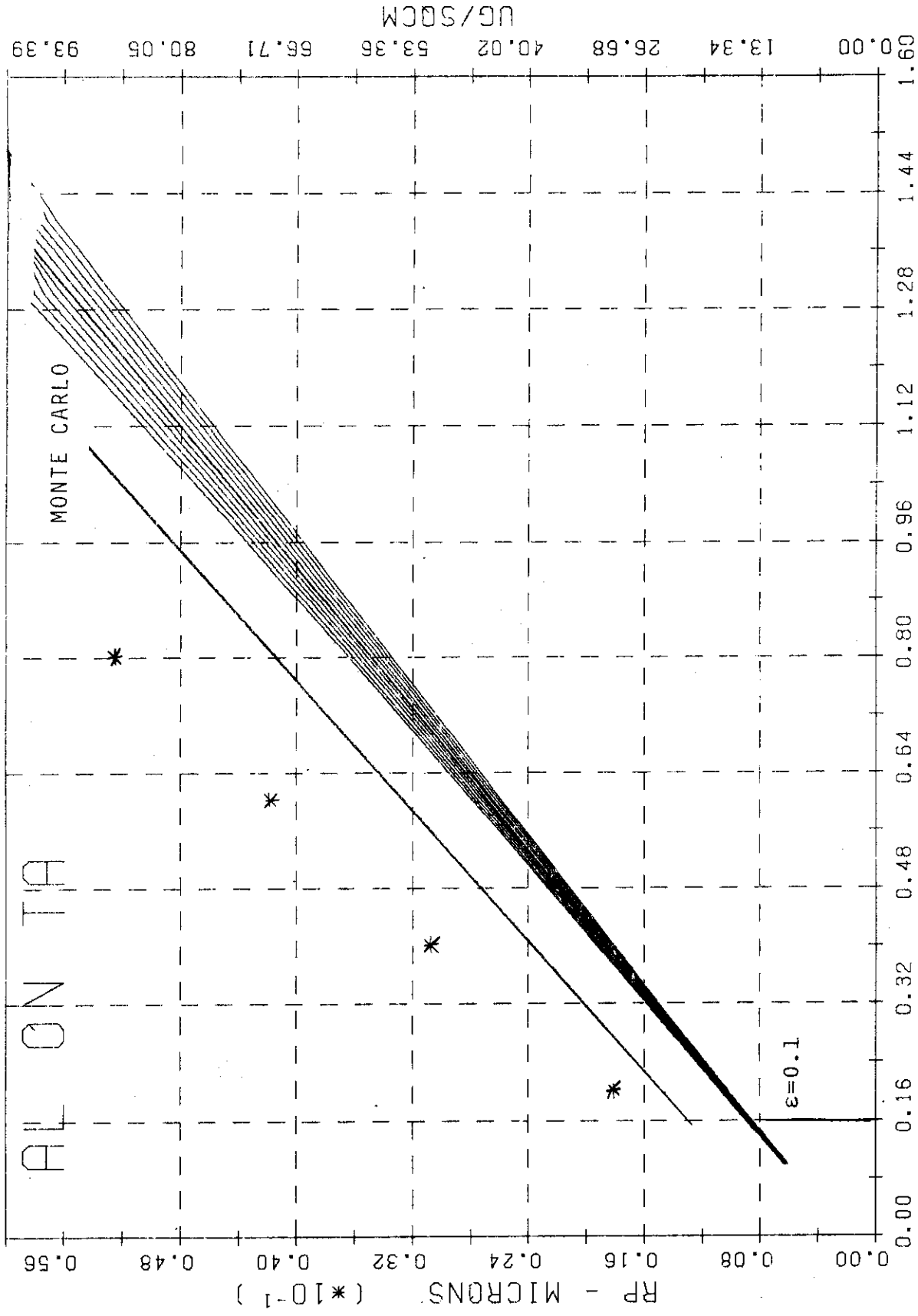

Fig. RB-35 (From Ref.5-78)

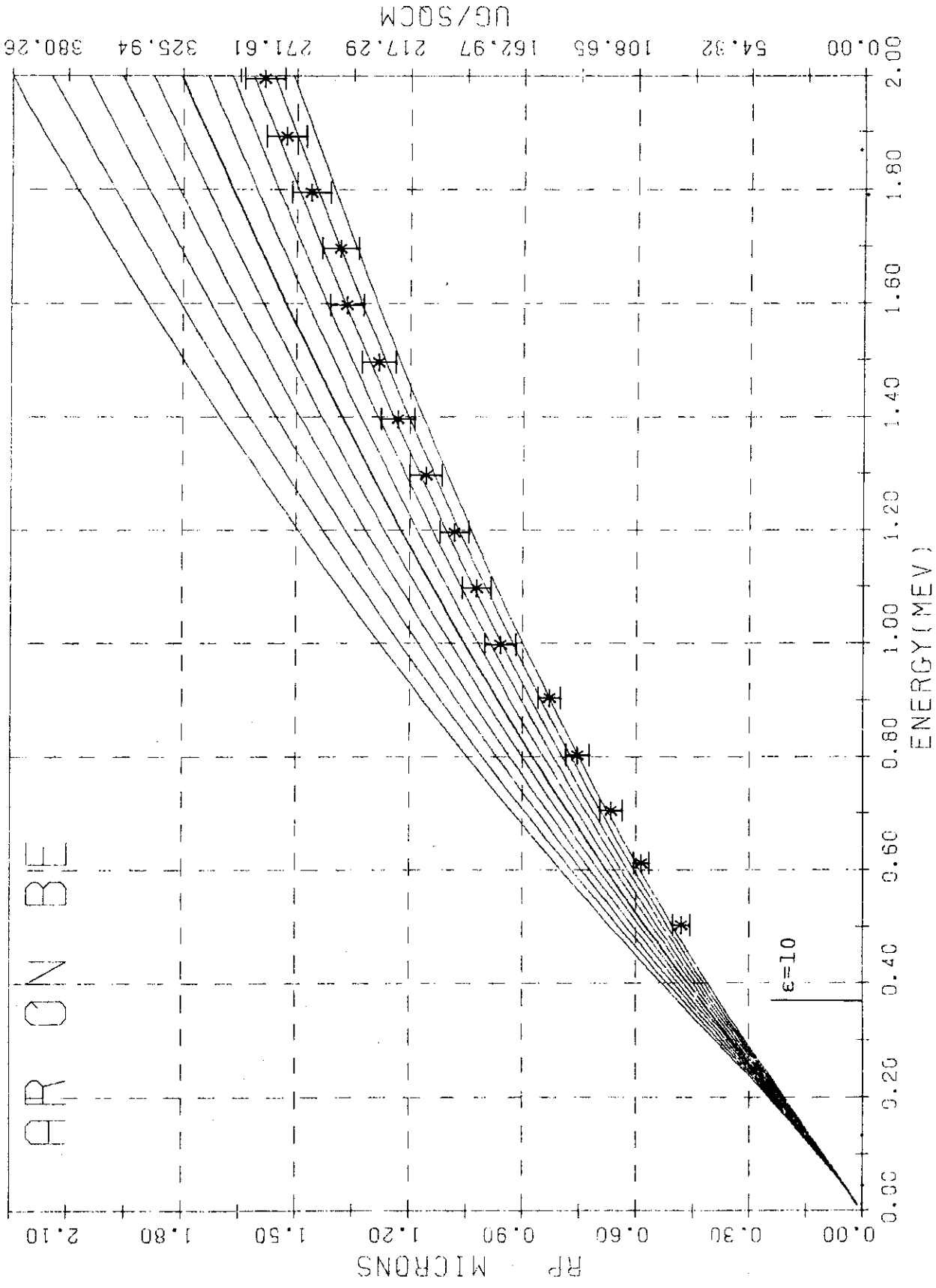

Fig. RB-36 (From Ref.5-91)

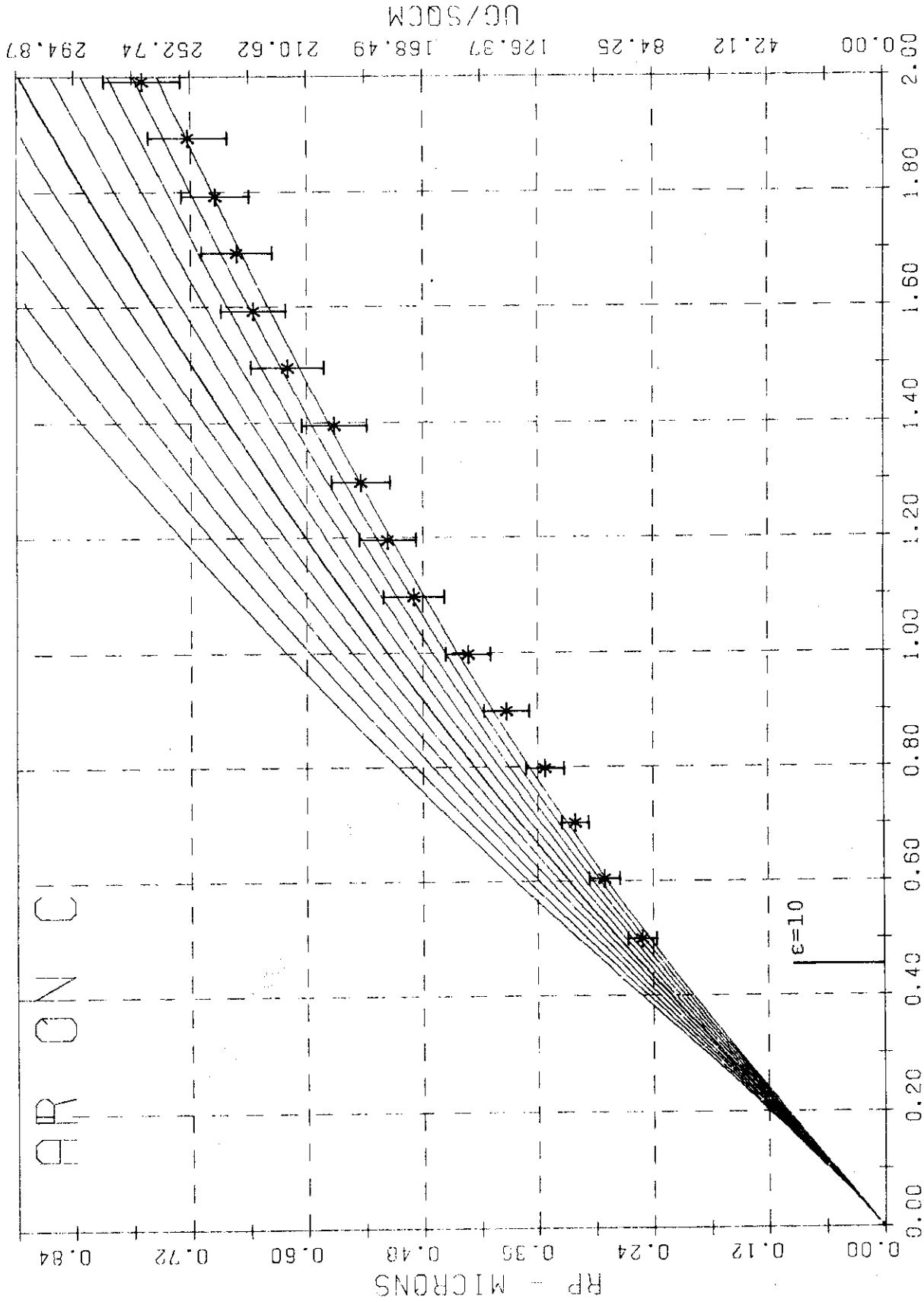

Fig. RB-37 (From Ref.5-91)

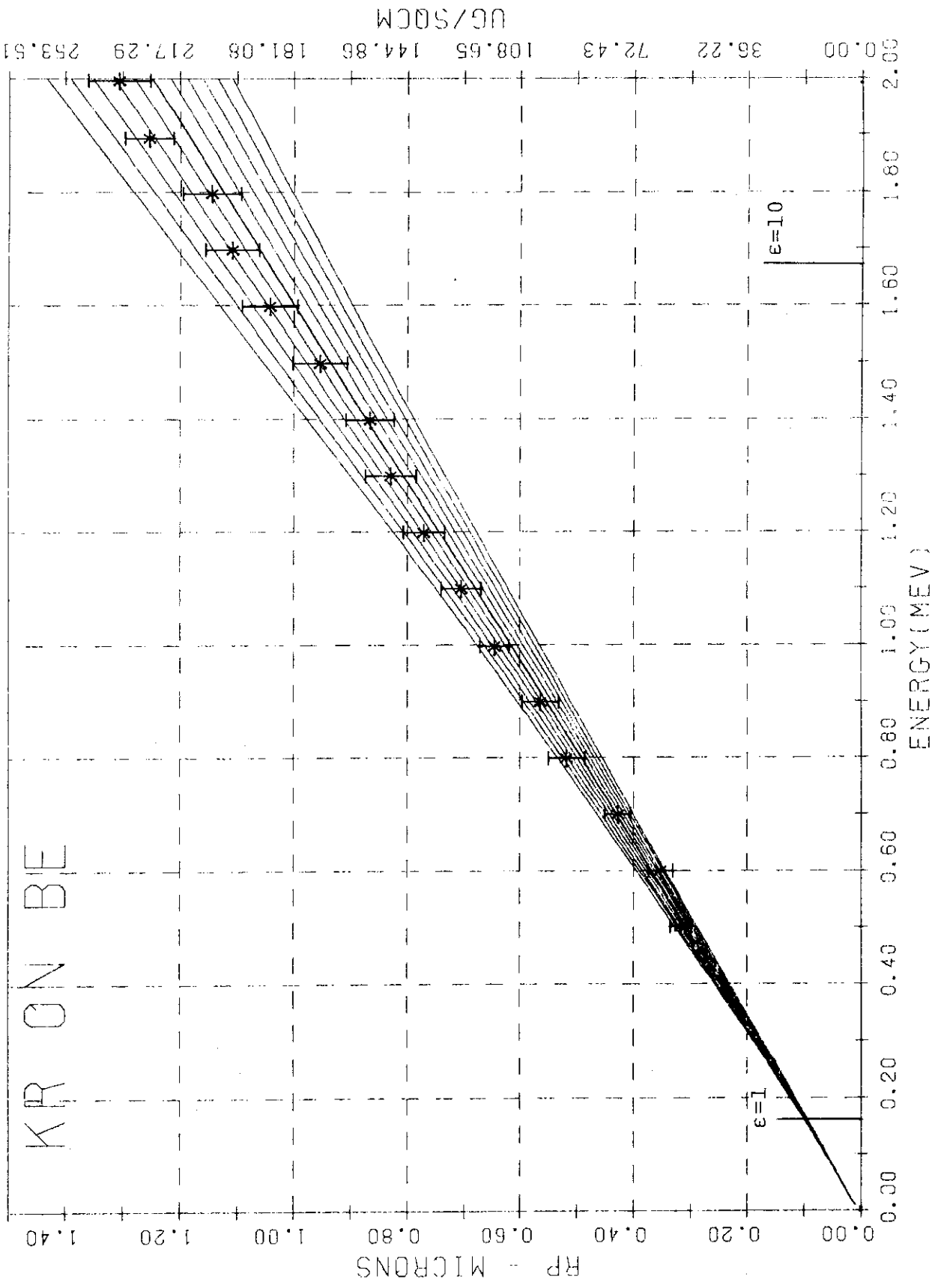

Fig. RB-38 (From Ref.5-91)

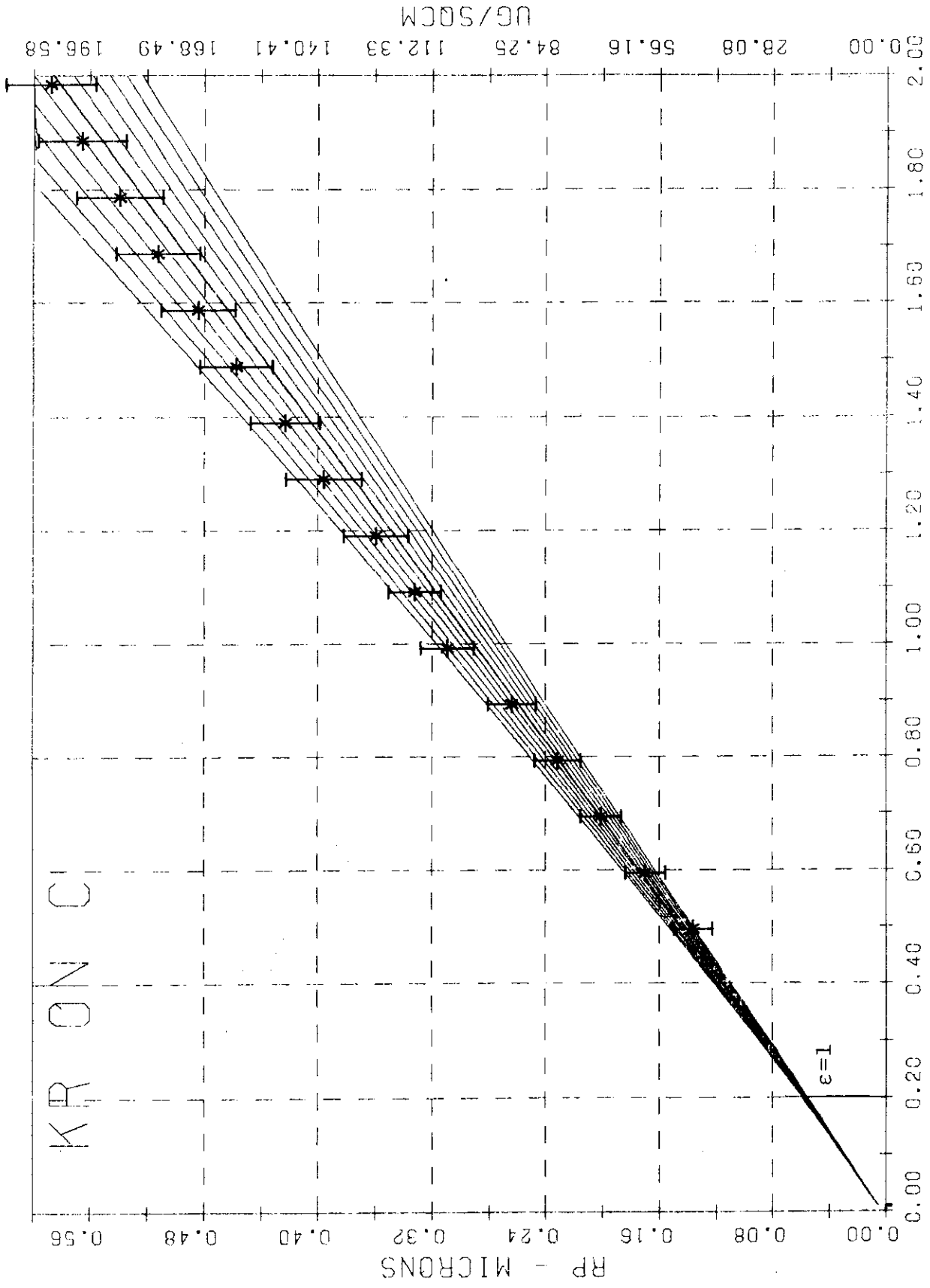

Fig. RB-39 (From Ref.5-91)

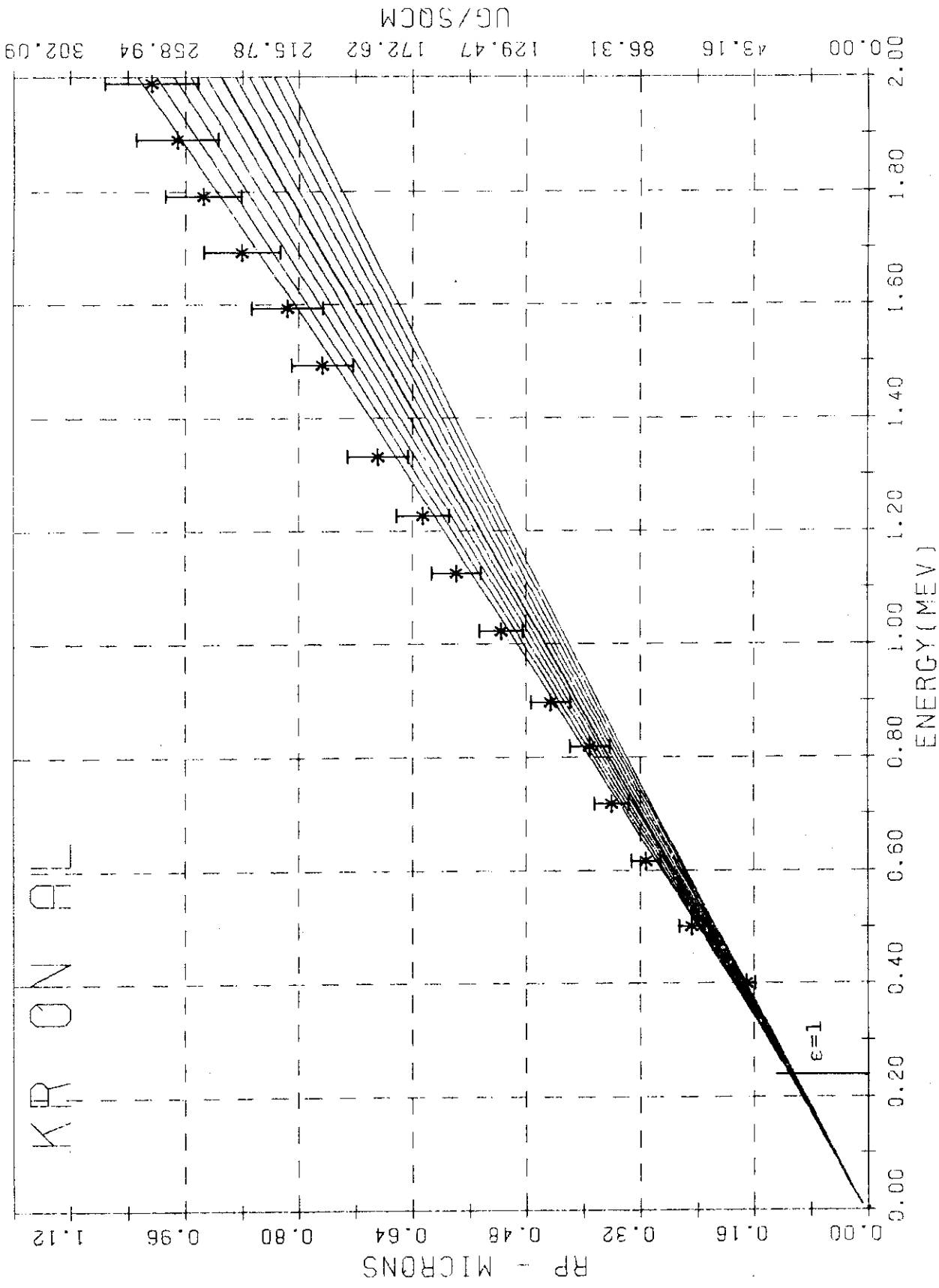

Fig. RB-40 (From Ref.5-91)

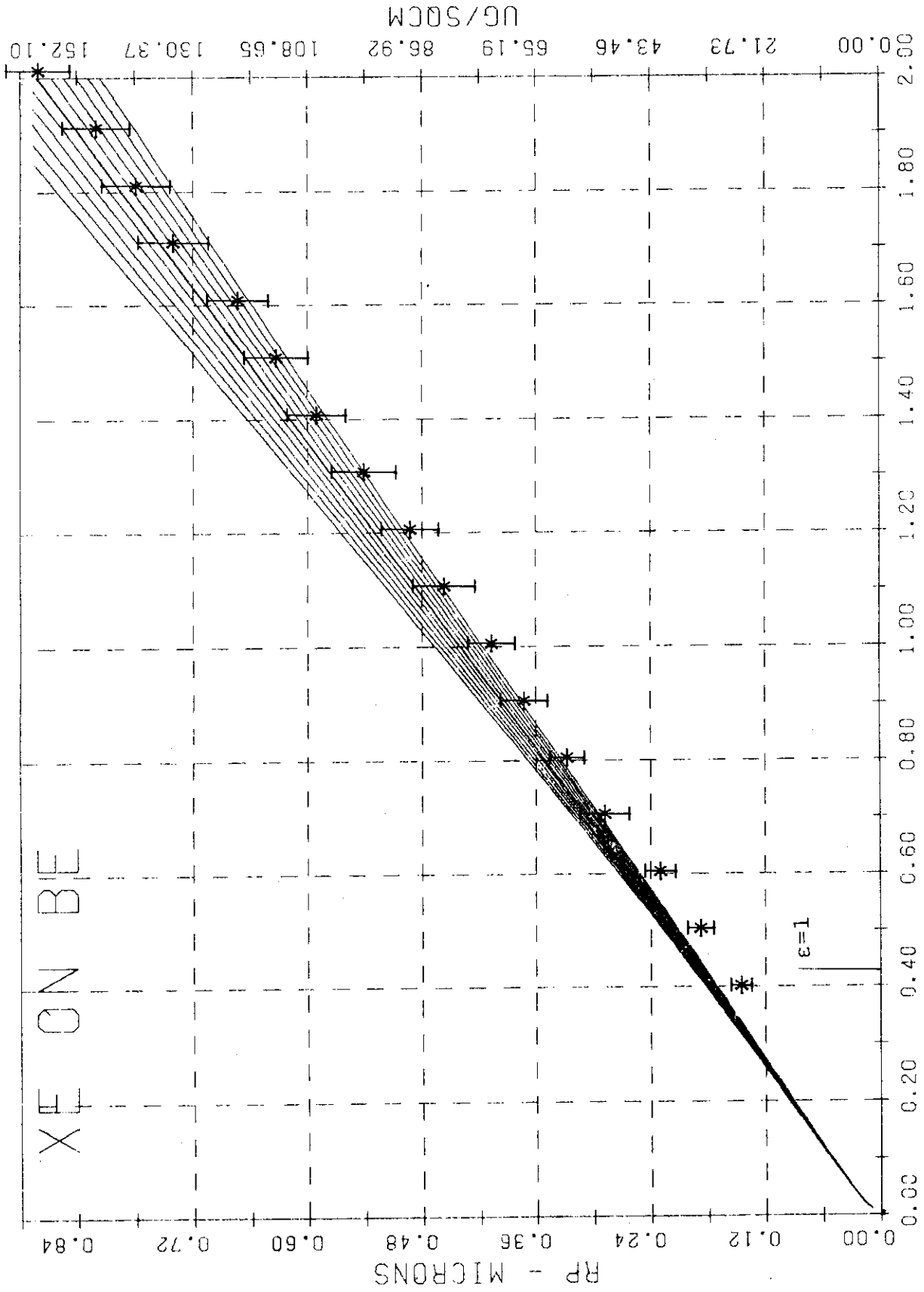

Fig. RB-41 (From Ref.5-91)

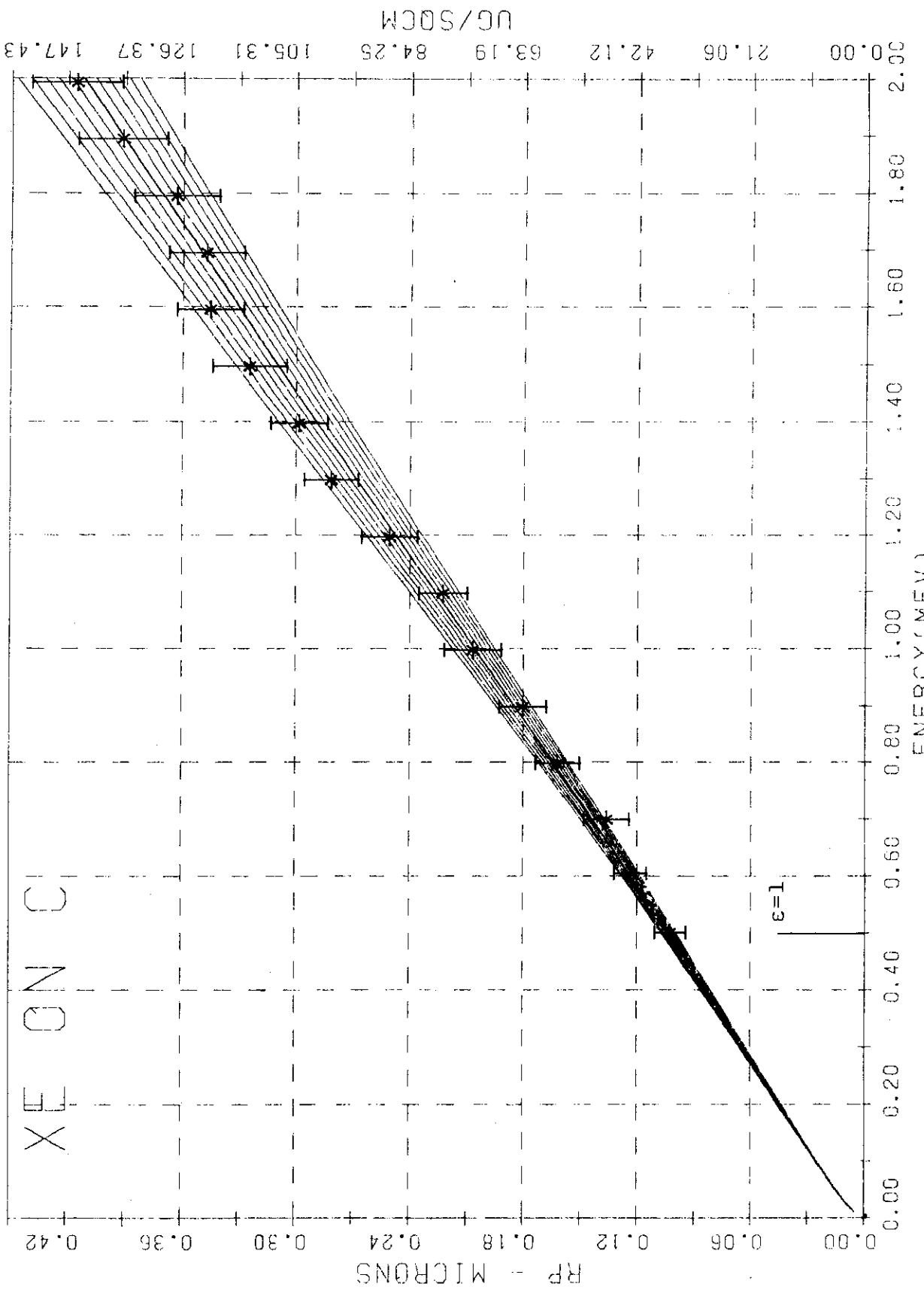

Fig. RB-42 (From Ref.5-91)

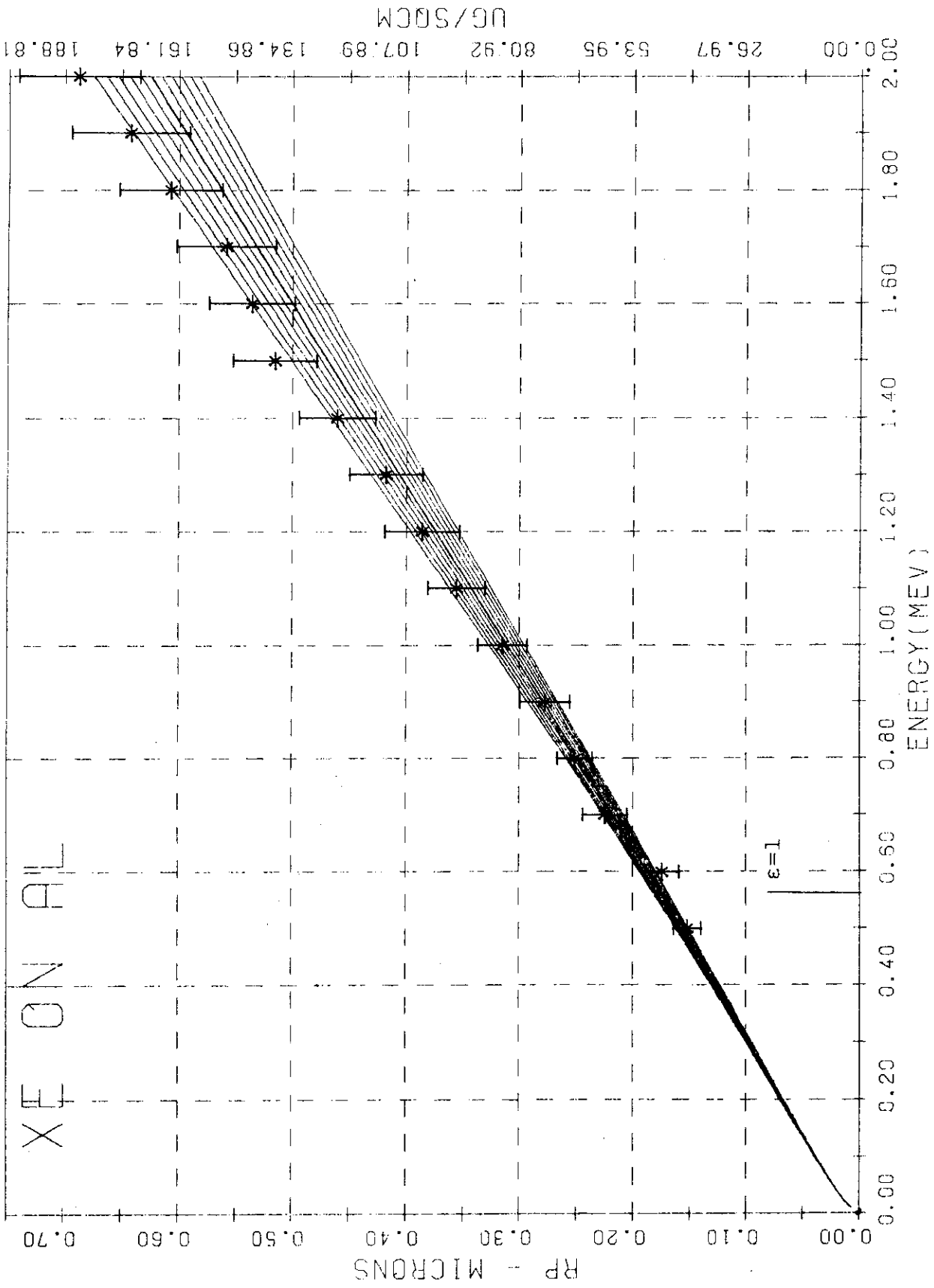

Fig. RB-43 (From Ref.5-91)

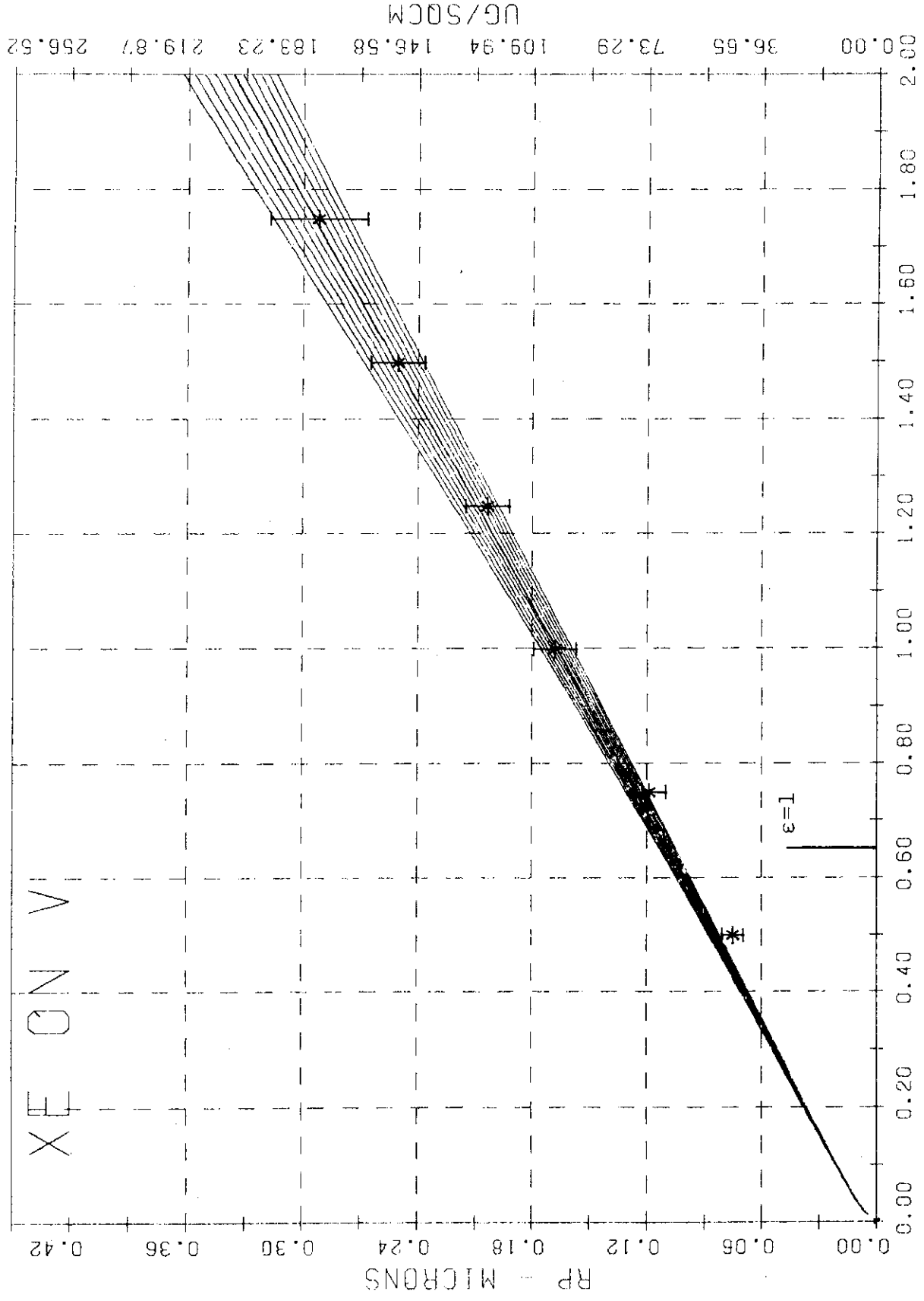

Fig. RB-44 (From Ref.5-91)

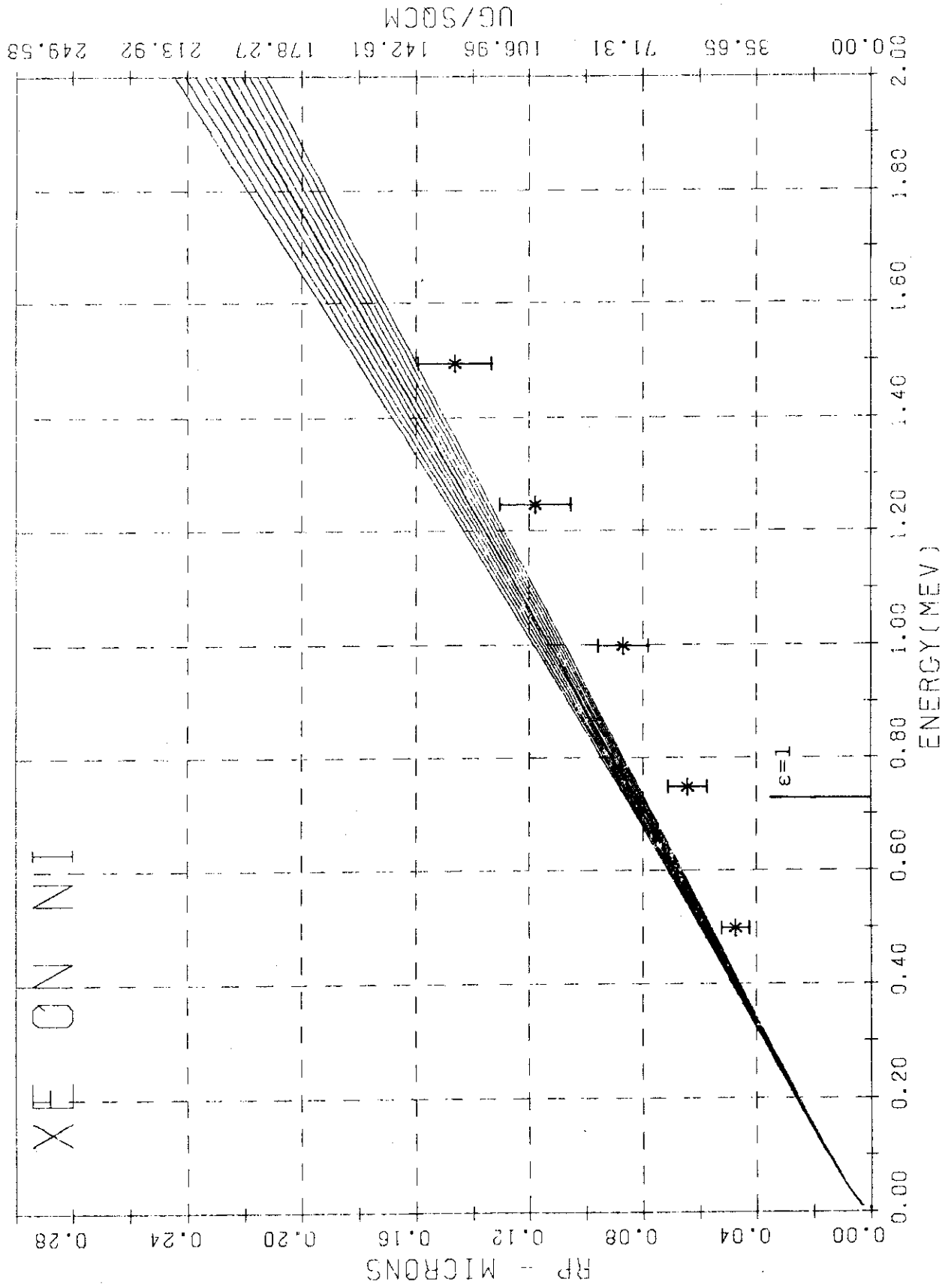

Fig. RB-45 (From Ref.5-91)

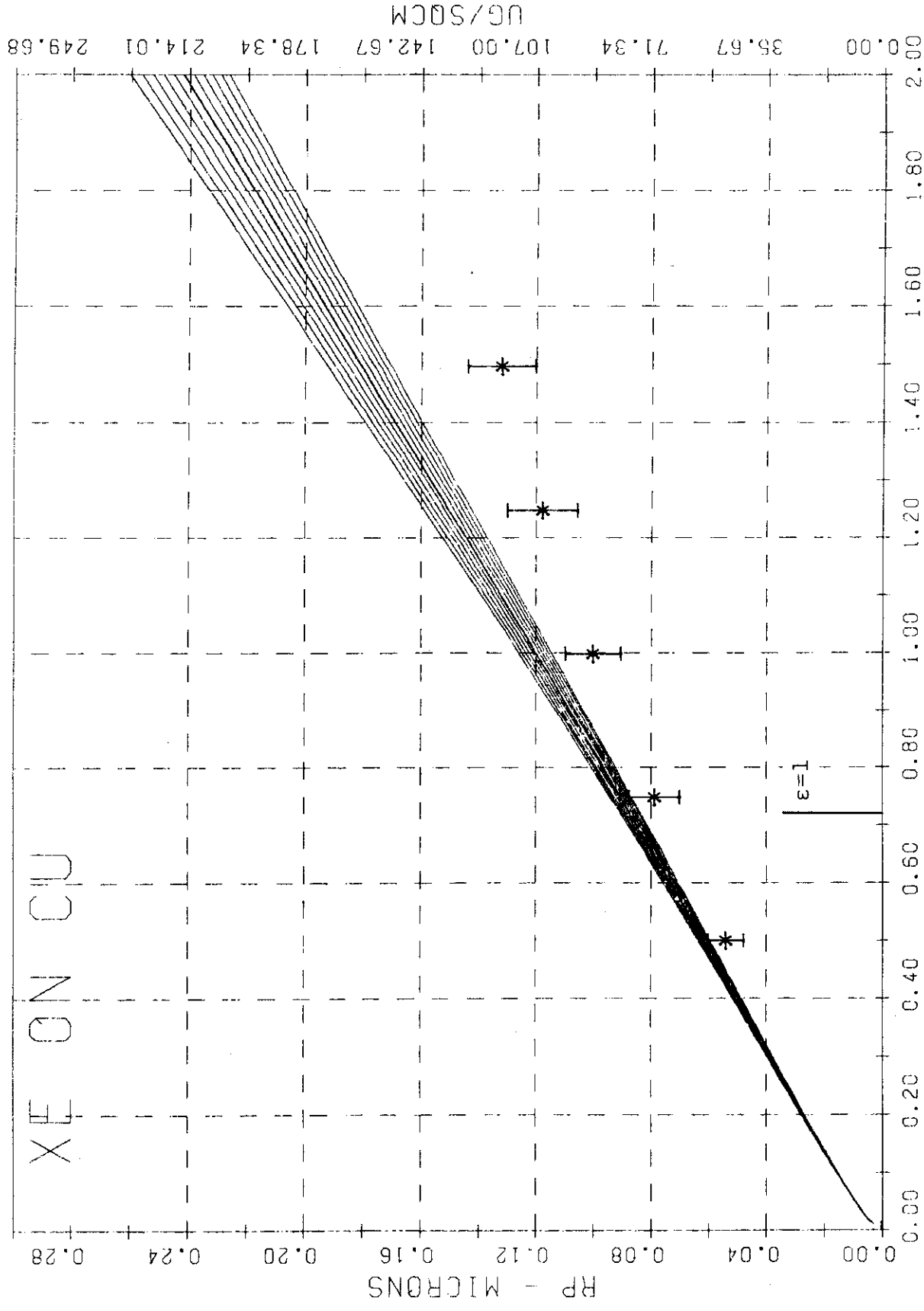

Fig. RB-46 (From Ref.5-91)

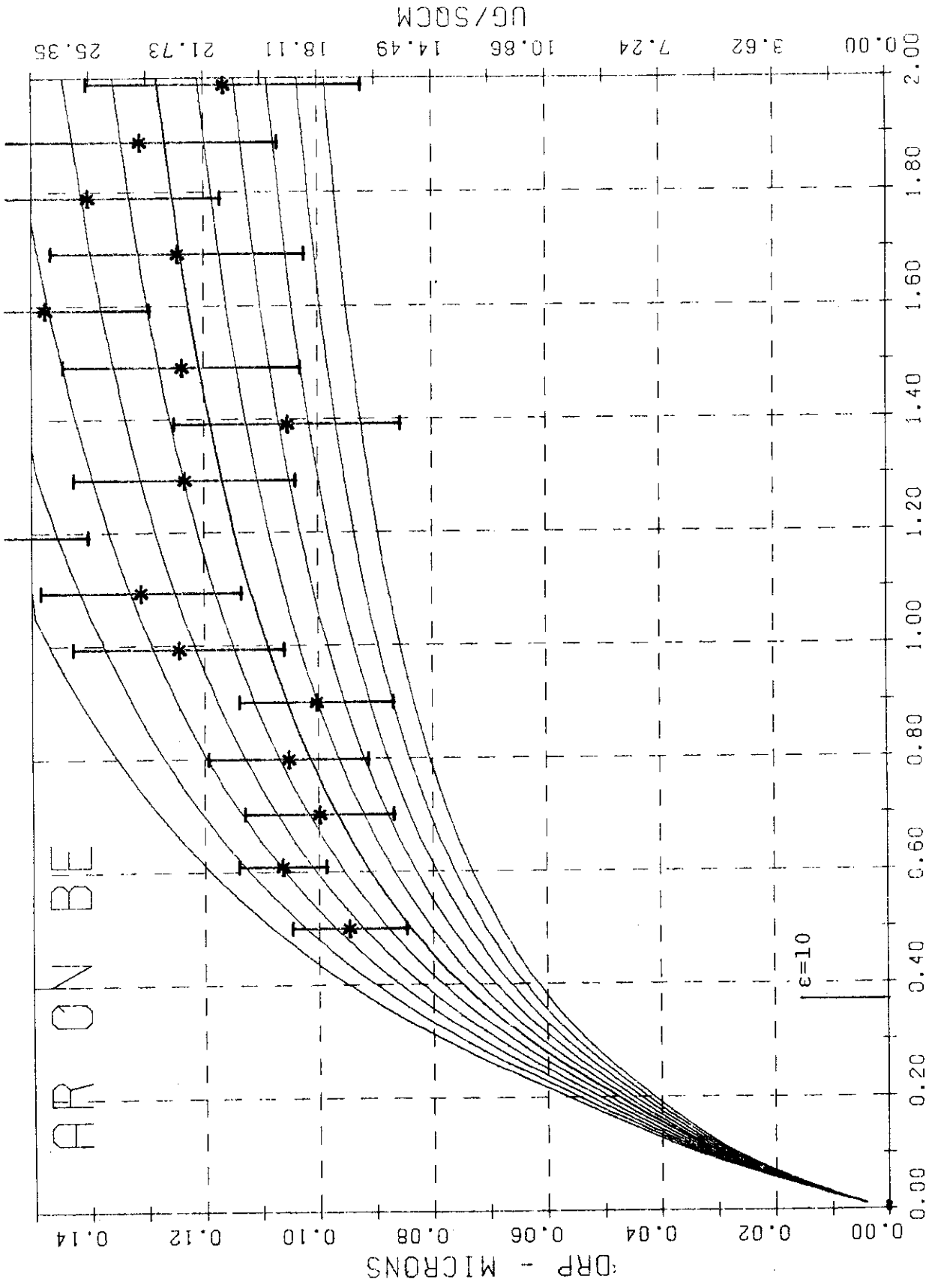

Fig. WA-1 (From Ref.5-91)

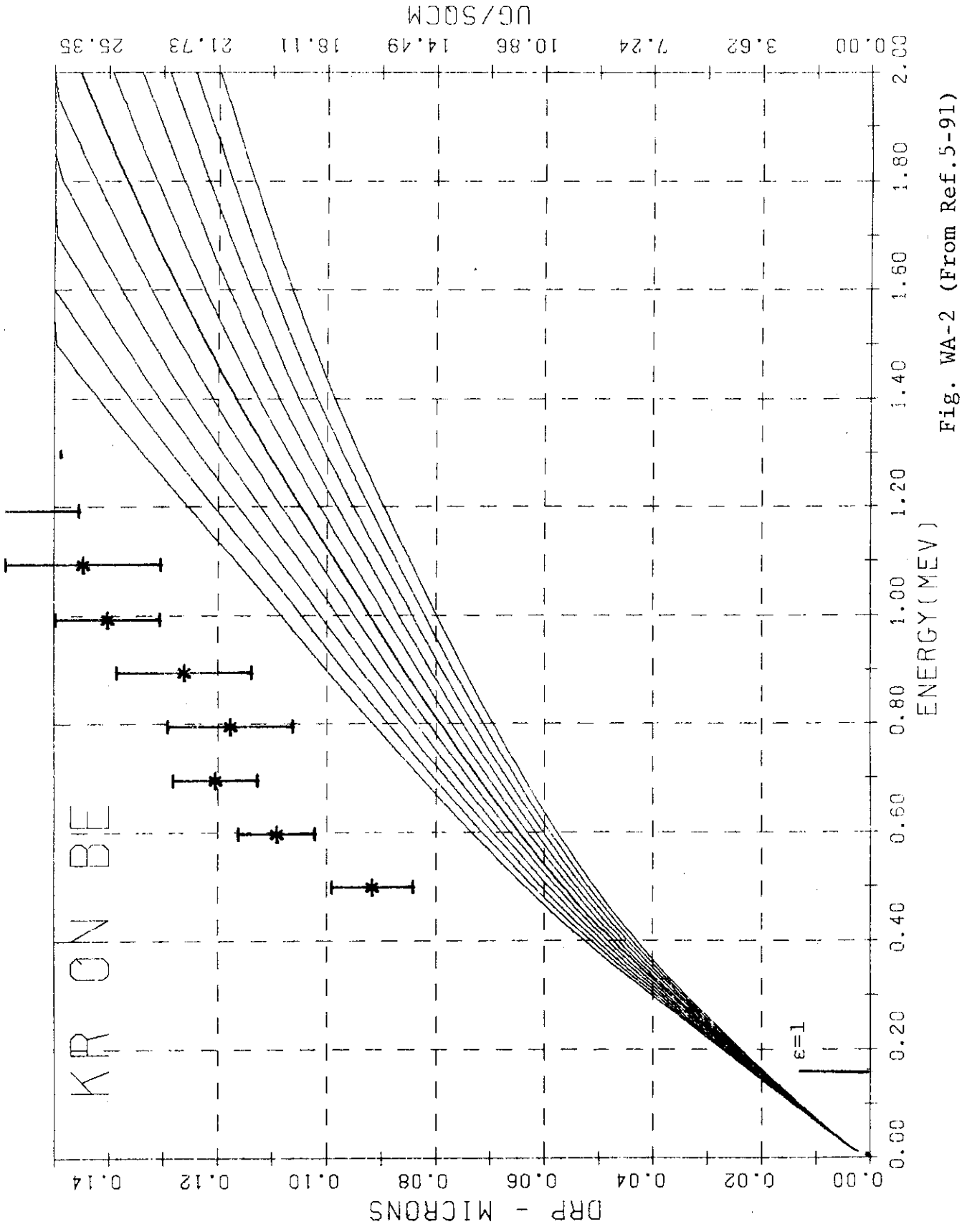

Fig. WA-2 (From Ref.5-91)

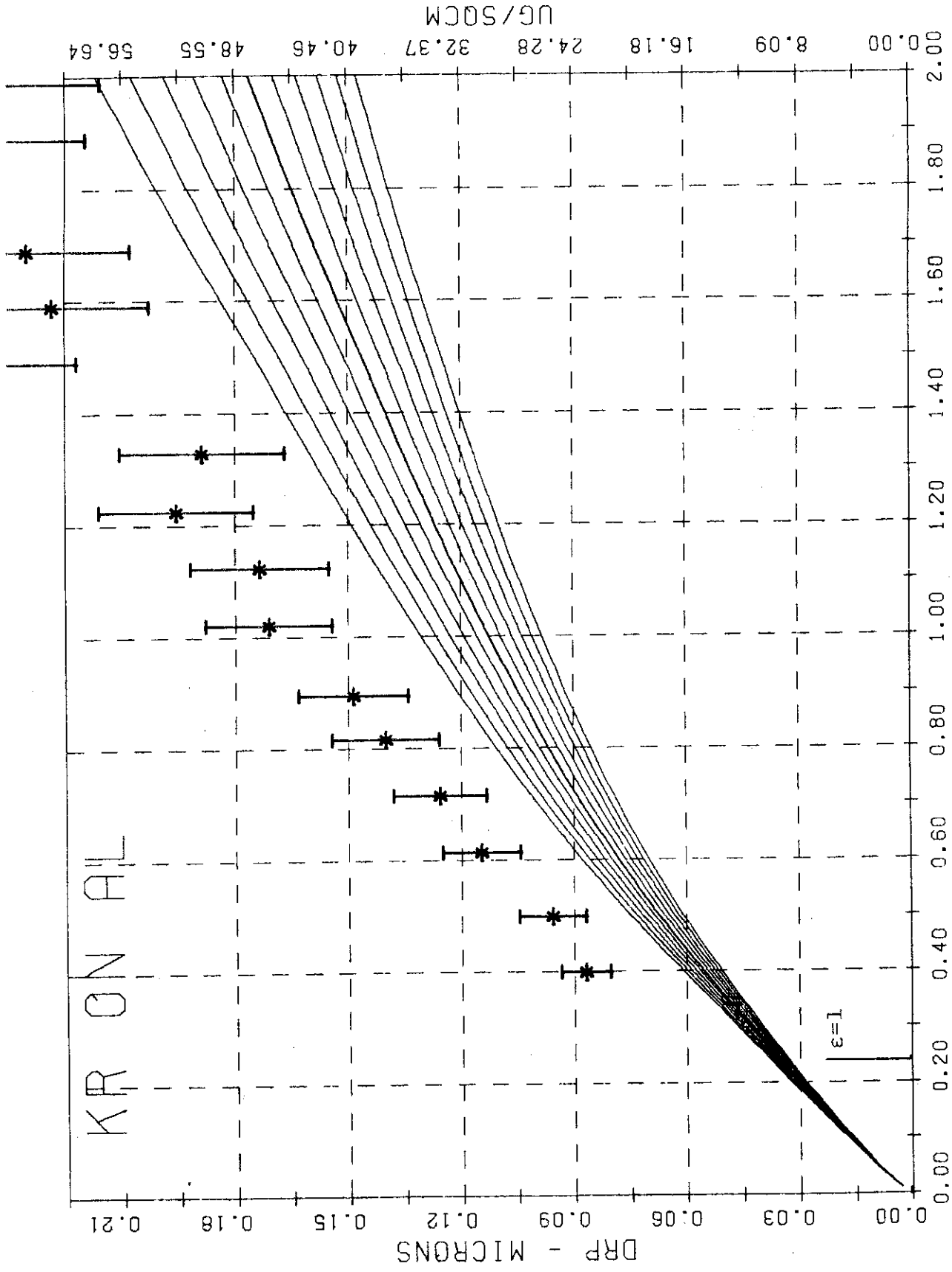

Fig. WA-3 (From Ref.5-91)

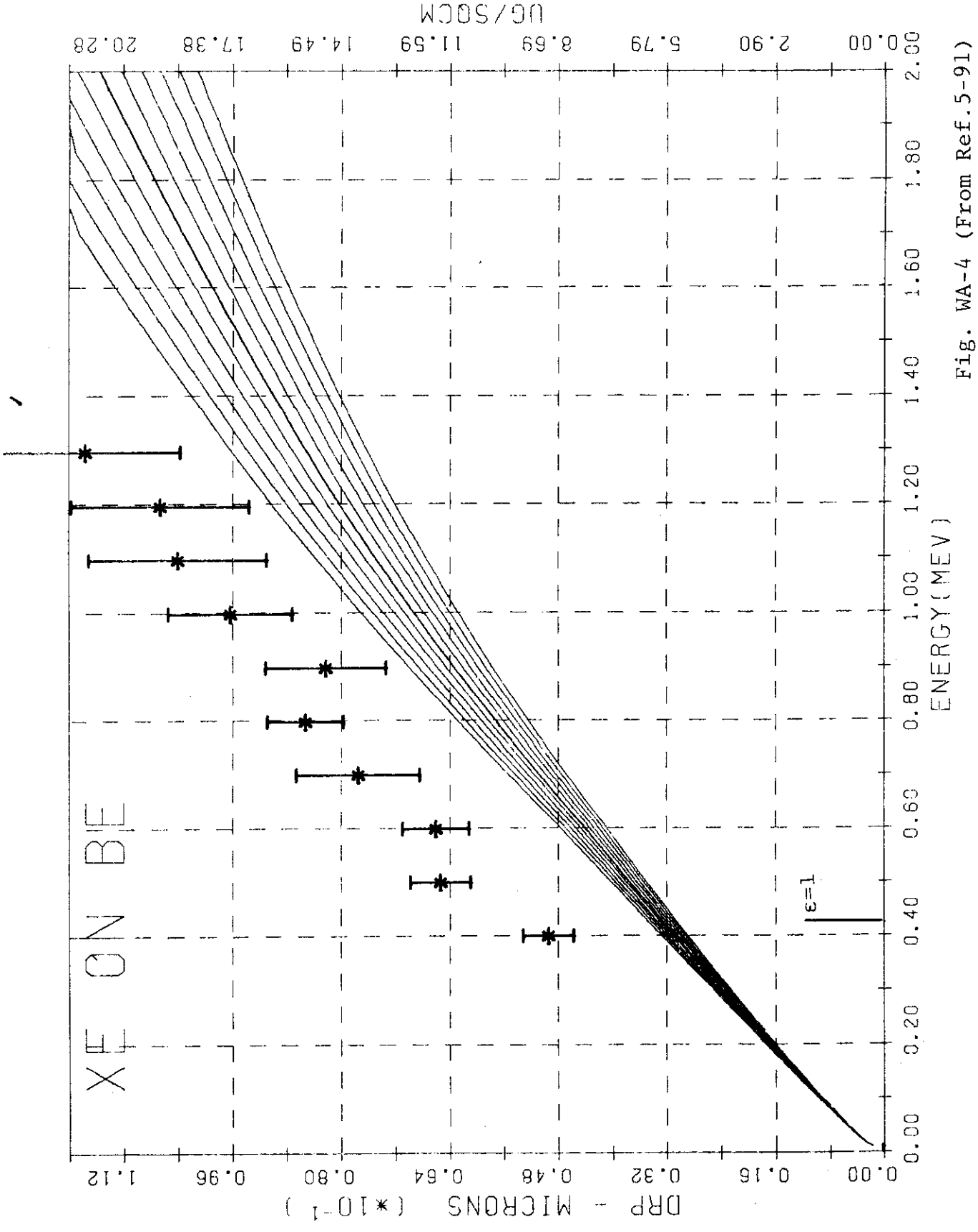

Fig. WA-4 (From Ref.5-91)

Literatures

5-1. A. K. Jain, V. N. Kulkarni and D. K. Sood:
Nucl. Instr. and Meth. 191 (1981) 151

5-2. K. F. Heidemann:
Phys. Status Solidi A 68(1981)607

5-3. A. F. Akkerman, S. A. Akkerman:
Phys. Status Solidi A68(1981)69

5-4. L. E. Tailamani and M. C. Joshi:
Nucl. Instr. and Meth. 191(1981)87

5-5. K. Wittamack and W. Wach:
Nucl. Instr. and Meth. 191(1981)327

5-6. Shi-Duan Yin, Jing-Ping Zhang, Quan Gu, Shi-Jie Liu:
Nucl. Instr. and Meth. 191(1981)147

5-7. C. A. B. Ball, F. D. Auret and H. C. Snyman:
Phys, Status Solidi A 68(545) 1981

5-8. H. Naramoto and K. Ozawa:
Nucl. Instr. and Meth. 191(1981)367

5-9. C. E. Christdoulides, N. J. Kadhim
Nucl. Instr. and Meth. 191(1981)124

5-10. R. G. Willson and D. M. Jamba:
Appl. Phys. Lett. 39(1981)715

5-11. T. Onuma, T. Hirao and T. Sugawa:
J. Appl. Phys. 52(1981)6128

5-12. J. Cervena, V. Hantowicz, J. Hoffmann, Z. Kosina
J. Kvitek, and P. Onheiser:
Nucl. Instr. and Meth. 188(1981)185

5-13. R. G. Willson:
J. Appl. Phys. 52(1981)3954

5-14. S.Kalbitzer and Oetzmann:
Rad. Effects 47(1980)57

5-15. J. Amano, A. Wargner and N. D. Seidman:
Philos. Mag. A 44(1981)177

5-16. G. Fenske, S. K. Das, M. Kaminsky, G. Mtley, B. Terreault
G. Abel and J. P. Abrif:
J. Appl. Phys. 52(1981)3618

5-17. A. G. K. Lutsch, C. A. B. Ball, F. D. Auret and
H. C. Snyman:
Microelectron. J. 12(1981)25

5-18. F. Jahnel, H. Ryssel, G. Prinke, K. Hoffmann, K. Muller, J. Riesack and R. Henkelmann:
Nucl. Instr. and Meth. 182(1981)223

5-19. M. Berti, A. Carnera, A. V. Drigo, A. Armigliato, A. Desalvo and R. Rosa:
Nucl. Instr. and Meth. 182(1981)215

5-20. W. Jager and J. Roth:
Nucl. Instr. and Meth. 182(1981)975

5-21. M. Baron, A. L. Chang, J. Schreurs and R. Kossowsky:
Nucl. Instr. and Meth. 182(1981)531

5-22. J. Greggi, W. J. Choyke, C. F. Tzeng, C. L. Chamberlain, N. J. Doyle and D. M. Matuza:
Appl. Phys. Lett. 38(1981)528

5-23. J. B. Malherbe and S. Hofmann:
Surf. and Interface Anal. 2(1980)187

5-24. H. Ryssel, G. Prinke, K. Haberger, K. Hoffmann, K. Muller and R. Henkelmann:
Appl. Phys. 24(1981)39

5-25. K. L. Wang and H. A. Storms:
Secondary Ion Mass Spectrometry Sims-II. Proceedings of the Second International Conference (1980)110

5-26. J. E. Baker, P. Williams, D. J. Wolford, J. D. Obstar and B. G. Streetman:
Secondary Ion Mass Spectrometry Simes-II. Proceedings of the Second International Conference (1980)106

5-27. J. Bohdansky, K. L. Wilson, A. E. Pontau, L. G. Haggmark and M. I. Baskes:
J. Nucl. Mater. 93-94(1980)594

5-28. W. H. Cheistie and C. W. White:
Surf. Sci. 100(1980)43

5-29. W. K. Chu, M. R. Popniak, E. T. Alessandrini and R. F. Lver:
Rad. Effects 49(1980)23

5-30. F. Bernhard, H. Kerkow and F. Kudella:
Rad. Effects 49(1980)107

5-31. H. Ryssel, K. Haberger, K. Hoffmann, G. Prinke, R. Dumcke and A. Sachs:
IEEE Trans. Electron Devices ED-27(1980)1484

5-32. H. Attaya and G. L. Kulcinski:
Trans. Am. Nucl. Soc. 34(1980)224

5-33. J. Comas, and R. G. Wilson:
J. Appl. Phys. 51(1980)3697

5-34. J. Roth, W. Eckstein and J. Bohdansky:
Rad. Effects 48(1980)91

5-35. W. K. Chu, R. H. Kastl and P. C. Murley:
Rad. Effects 47(1980)73

5-36. I. Brylowska, M. Subotowics, K. Paprocki and H. Derewiecki:
Rad. Effects 47(1980)137

5-37. R. G. Wilson and J. Comas:
Rad. Effects 47(1980)137

5-38. R. G. Wilson:
Rad. Effects 46(1980)141

5-39. H. Ryssel, G. Lang, J. P. Biersake, K. Muller and
W. Kruger:
IEEE Trans. Electron Devices Ed-27(1980)58

5-40. D. P. Leta, G. H. Morrison, G. L. Harris and C. A. Lee:
Int. J. Mass spectrom and Ion Phys 34(1980)147

5-41. M. Meyer:
J. Phys. 41(1980)409

5-42. M. Meyer, E. L. Houch and S. Barbezat:
J. Phys. 41(1980)403

5-43. J. Keinonen and A. Anttila
Appl. Phys. Lett 36(1980)271

5-44. C. W. Magee, S. A. Choen, D. E. Voss and D. K. Brice
Nucl. Instr. and Meth. 168(1980)383

5-45. A. B. Campbnell, B. D. Sartwell and P. B. Needham:
J. Appl. Phys. 51(1980)283

5-46. H. Ryssel, G. Lang, K. Muller, J. Biersack,
W. Kruger and F. Jahnel:
Phys. Status Solidi A 57(1980)619

5-47. F. J. Demond, S. Kalbitzer, H. Mannsperger
and G. Muller:
Nucl. Instr. and Meth. 168(1980)69

5-48. H. F. Kappert, K. F. Heidemann, D. Eichholz, F. Kaat
and W. Rothemund:
Appl. Phys. 21(1980)151

5-49. J. P. Biersack, D. Fink, R. A. Henkelmann. and K. Muller:
J. Nucl. Mater. 85(1979)1165

5-50. G. K. Hubler, P. R. Malmberg and T. P. Smith
J. Appl. Phys 50(1979)7147

5-51. G. Braunstein, I. Bernstein, U. Carsenty and R. Kalish:
J. Appl. Phys. 50(1979)5731

5-52. E. A. Konorova, V. F. Sergienko, S. D. Tkachenko,
V. A. Dravin and A. V. Spitsyn:
Sov. Phys.-Lebedev Inst. Rep. 4(1978)9

5-53. M. R. Risch, J. Roth and B. M. U. Scherzer:
J. Nucl. Mater. 82(1979)220

5-54. G. Fenske, S. K. Das, M. Kaminsky and G. H. Miley:
Trans. Am. Nucl. Soc. 28(1978)196

5-55. M. M. Tosic:
Fizika 10(1978)93

5-56. T. Hirao, K. Inoue, Y. Yaegashi and S. Takayanagi:
Proceedings of the Sixth Yugoslav Symposium on Physics
of Condensed Matter (1978)17

5-57. G. Mullwe, M. Trapp, R. Schimko and C. E. Richter
Phys. Status Solidi A 51(1978)87

5-58. M. Luomajarvi, J. Kfinonen, M. Bister and A. Anttila:
Phys. Rev. B 18(1978)4657

5-59. A. Wagner, and D. N. Seidman:
Phys. Rev. Lett. 42(1979)515

5-60. D. J. Land, D. G. Simons, J. G. Brennan, M. D. Brown,
J. K. Hirvonen and J. P. Biersack:
Rad. Effects 48(1980)105

5-61. G. Abel, G. Ross, B. Terreault and J. P. Labrie:
Nucl. Instr. and Meth. 170(1980)171

5-62. A. Anttila, J. Hirvonen and M. Hautala:
Rad. Effects 57(1980)41

5-63. B. M. U. Scherzer, H. L. Bay, R. Behrisch, P. Borgessen
and J. Roth:
Nucl. Instr. and Meth. 75(1978)15

5-64. Z. E. Switkowski, J. C. Overley, W. U. Shiu-chin,
C. A. Barnes. and J. Roth:
J. Nucl. Mater 78(1978)64

5-65. W. Moller, P. Borgesen and J. Bottiger:
J. Nucl. Mater 76(1978)287

5-66. P.Borgesen, J. Bottiger and W. Moller:
J. Appl. Phys. 49(1978)4401

5-67. H. F. Kappert, K. F. Heidemann, B. Grabe and E. T. Kaan:
Phys. Status Solidi A 47(1978)751

5-68. Suk Tai Kang, R. Shimizu and T. Koshikawa:
Technol. Rep. Osaka Univ. 27(1977)327

5-69. J. Bottiger, P. S. Jensen and U. Littmark:
J. Appl. Phys. 49(1978)965

5-70. S. Nasu, K. Shiozawa, T. Tanifugi, K. Noda
and K. Uchida:
J. Nucl. Mater. 73(1978)132

5-71. R. M. More and F. J. Venskytis:
Rad. Effects 35(1978)129

5-72. K. Guttner, S. Hofmann, D. Marx, G. Munzenberg and
F. Nickel:
Nucl. Instr. and Meth. 146(1977)413

5-73. A. Z. Nagy, J. Bogancs, J. Gyulai, A. Csoke, V. Nazarov,
Z. Seres, A. Szabo and YU. Yazvitsky:
J. Radional. Chem. 38(1977)19

5-74. B. Terrault, J. G. Martel, R. G. ST-Jacques, G. Veilleux,
J. Fcuyer, C. Brassard, C. Cardinal, L. Deschenes and
J. P. Labrie:
J. Nucl. Mater 68(1977)334

5-75. J. C. Overley and H. W. Lefevre:
Proceedings of the 4th Conference on the Scientific
and Industrial Applications of Small Accelerators
(1977)557

5-76. H. R. Kastl:
Electrochemical Society Fall Meeting (1976)865

5-77. H. W. Lefevre, J. D. Anderson and J. C. Davis:
Proceeding of the 4th Conference on the Scientific and
Industrial Applications of Small Accelerators (1977)13

5-78. A. Anttila, M. Bister, A. Fontell and K. B. Winterbon:
Rad. Effects 33(1977)13

5-79. H. Ryssel, H. Kranz, K. Muller, R. A. Henkelmann and
J. Biersack:
Appl. Phys. Lett. 30(1977)13

5-80. R. Shimizu, S. T. Kang, T. Koshikawa, H. Ogata, K. Kanayama, Y. Ogata, Y. Akasaka and K. Horie: J. Appl. Phys. 48(1977)1745

5-81. F. Burkhardt and C. Wagner: Phys. Status Solidi A 39(1977)63

5-82. N. G. Blamires and B. J. Smith: J. Phys. D. 10(1979)799

5-83. K. Tsukamoto, Y. Akasaka and K. Horie: Jpn. J. Appl. Phys. 16(1977)663

5-84. D. C. Santry and R. D. Werner: Nucl. Instr. and Meth. 139(1976)135

5-85. Y. Y. Chu and L. Friedman: Nucl. Instr. and Meth. 38(1965)254

5-86. O. S. Oen, D. K. Holmes and M. T. Robinson: J. Appl. Phys. 34(1963)302

5-87. W. K. Chu, P. D. Burland, K. H. Wang and D. Powers: Phys. Rev. 175(1968)342

5-88. D. E. Davies: Can. J. Phys. 47(1967)1750

5-89. E. M. Zarutskii: Sov. Phys. -Solid State 11(1969)1364

5-90. R. A. Langley: Phys. Rev. A 4(1971)1868

5-91. D. Power, W. K. Chu, P. D. Bourland: Phys. Rev. 126(1968)376

5-92. G. W. Neilson, B. W. Farmery and M. W. Thompson: Phys. Lett. 46a(1973)45